INTERROGATING HYPOXIA-MEDIATED CD8$^+$ T CELL DYSFUNCTION IN MULTIPLE MYELOMA

By Taylor Fulton-Ward

A thesis submitted to the University of Birmingham for the degree of

DOCTOR OF PHILOSOPHY

UNIVERSITY OF BIRMINGHAM

Institute of Immunology and Immunotherapy

College of Medical and Dental Sciences

University of Birmingham

June 2024

Abstract

Introduction

Multiple myeloma (MM) is an incurable plasma cell malignancy that develops in the bone marrow (BM). The BM is understood to be immunosuppressive and hypoxic, which may limit therapeutic responses to immune-directed therapies. This thesis interrogates whether the hypoxic nature of the BM environment drives $CD8^+$ T cell dysfunction.

Methods

$CD8^+$ T cells are isolated from healthy human peripheral blood and incubated overnight in normoxia (21% oxygen) or hypoxia (1% oxygen) to allow oxygen level equilibration. Cells are activated by anti-CD3/anti-CD28 antibodies and analysed for immune function, metabolism and signalling. MM patient samples, including blood and BM mononuclear cells, are analysed *ex vivo* by flow cytometry.

Results

$CD8^+$ T cells stimulated in hypoxia demonstrate impaired proliferation, CD25 expression and IFN-γ production. However, TNF-α production, granzyme-B expression and CD107a externalisation are unaffected by hypoxia. A defect in T cell signalling lies at the level of mTOR, with impact on downstream targets. Stable isotope-based metabolic tracing identifies a reduction of activation-induced glycolysis, glucose oxidation and glutaminolysis in hypoxia. Bulk RNA sequencing and flow cytometric analysis identify BNIP3 as a marker of hypoxia and potential mechanisms driving mTOR suppression in hypoxia are explored. Stimulation of $CD8^+$ T cells with a

BCMAxCD3 bispecific antibody and BCMA-expressing MM cell lines bring these findings into a therapeutic context. $CD8^+$ T cells from the BM of MM patients demonstrate impaired proliferation and expression of c-Myc compared to those from the PB.

Conclusion

Hypoxia impairs $CD8^+$ T cell signalling, activation and specific effector functions alongside activation-induced metabolic reprogramming. These intrinsic effects correlate with reduced function of MM patient $CD8^+$ T cells found in the BM compared to the PB. This work could aid understanding the limitations of response with immune-directed therapies acting within a hypoxic environment.

Acknowledgments

I would like to express my deepest gratitude to my supervisor Dr Sarah Dimeloe for her invaluable mentorship, advice and encouragement, and to Professor Daniel Tennant for his metabolism expertise and assistance throughout my PhD.

I would like to thank Dr Nancy Gudgeon for her unwavering support and all current and past members of the Dimeloe lab. Thank you for creating such a caring and encouraging group – our Thursday tea and cake sessions will be deeply missed! Dr Nancy Gudgeon, Dr Emma Bishop, Dr Victoria Stavrou, Becca Mann, Hannah Bollons, Myah Ali, and Beth Turley, you are all wonderful people and I wish you all the best for the future.

I would like to extend my sincere thanks to Professor Gary Middleton. Thank you for believing in me right from the beginning.

Thank you to Professor Guy Pratt and all the clinical staff in the Haematology units at University Hospital Birmingham for your time and expertise in the clinical aspects of this work. Thank you to the NHS Blood and Transplant Centre Birmingham for supporting our weekly leucocyte cone collection. I would like to thank all the patients and blood donors who kindly provided samples for this study, it would not have been possible without you.

I would like to thank Dr Jennie Roberts, Dr Adam Boufersaoui and Dr Bryan Marzullo for running the GC-MS samples throughout my PhD. Thank you also to Dr Heather Long and all members of the Tennant group.

I would like to offer my special thanks to all in the Fellows' Labs (Flabbies). To Dr David Bending, Dr Kendle Maslowski, Dr Alastair Copland and Dr Rebecca Drummond for your insightful suggestions and advice, and to each and every Flabbies member for your friendship.

I would like to offer my sincere thanks to Cancer Research UK Birmingham Centre for funding this PhD.

I am deeply grateful to my family and friends for your tireless belief in me, and finally, to my partner Daniel. I would not be where I am today without you, and for that I am forever grateful.

Contents

List of figures

4. Results Chapter 2: Exploring $CD8^+$ T cell signalling and metabolism in hypoxia

5. Results Chapter 3: Interrogating potential mechanisms of defective $CD8^+$ T cell function in hypoxia

List of tables

List of abbreviations

-ve C	Negative control
2-DG	2-deoxy-glucose
2-DG-6-P	2-deoxy-D-glucose-6-phosphate
4E-BP1	Eukaryotic translation initiation factor 4E-binding protein 1
A	Activated
ACC	Acetyl-CoA carboxylase
Acetyl-CoA	Acetyl-coenzyme A
ACO1/2	Aconitase 1/2
ADP	Adenosine diphosphate
AIRE	Autoimmune regulator
AKT	Protein kinase B (PKB)
α-KG	Alpha-ketoglutarate
AMP	Adenosine monophosphate
AMPK	AMP-activated protein kinase
AP-1	Activator-protein-1
APC	Antigen presenting cell
APECED	Autoimmune polyendocrinopathy candidiasis ectodermal dystrophy
ARNT	Aryl hydrocarbon receptor nuclear translocators, or HIF-1β
ATP	Adenosine triphosphate
BAD	BCL2 associated agonist of cell death
BCL-xL	B cell lymphoma-extra large
BCL-2	B cell lymphoma/leukaemia 2
BCL-10	B cell lymphoma/leukaemia 10
BiTE	Bispecific T cell engagers
BCMA	B cell maturation antigen
BM	Bone marrow
BNIP3	BCL2 Interacting Protein 3
Ca^{2+}	Calcium
CamKK2	Calmodulin-dependent protein kinase
CARMA1	Caspase recruitment domain-containing membrane-associated guanylate kinase protein-1
CAR-T cells	Chimeric antigen receptor T cells
Cas9	CRISPR associated protein 9
CBP	CREB-binding protein

CD107a	or LAMP1: Lysosomal-associated membrane protein 1
CD45	Leucocyte common antigen
CM	Central memory
c-Myc	Cellular myelocytomatosis oncogene
CO_2	Carbon dioxide
COX4	Cytochrome oxidase subunit 4
CRAC channels	Calcium-release activated calcium channels
CRBN	Cereblon
CRISPR	Clustered Regularly Interspaced Short Palindromic Repeats
CS	Citrate synthase
CSK	C-terminal SRC kinase
cTECs	Cortical thymic epithelial cells
CTL	Cytotoxic lymphocyte
CTLA4	Cytotoxic T-lymphocyte associated protein 4
CTV	Cell trace violet
Cyt C	Cytochrome C
DAG	Diacylglycerol
DDIT4	DNA-damage-inducible transcript 4 (same as REDD1)
DEGs	Differentially expressed genes
DFO	Desferrioxamine
DLL1	Delta-like 1
DMNQ	2,3-Dimethoxy-1,4-naphthoquinone
EBV	Epstein Barr Virus
ECAR	Extracellular acidification rate
EGLN1	Egl-9 family hypoxia inducible factor 1, or PHD2
EGLN2	Egl-9 family hypoxia inducible factor 2, or PHD1
EGLN3	Egl-9 family hypoxia inducible factor 3, or PHD3
Egr1	Early growth response 1
eIF2α	Eukaryotic initiation factor 2 alpha
EIF2AK3	Eukaryotic translation initiation factor 2 alpha kinase 3
ELISA	Enzyme-linked immunosorbent assay
ELISpot	Enzyme-linked immunosorbent spot
EM	Effector memory
EMRA	Terminally differentiated effector memory cells re-expressing CD45RA
ENO1	Enolase 1

ER	Endoplasmic reticulum
ERK1/2	Extracellular signal-regulated kinase 1 and 2
ETC	Electron transport chain
FA	Fatty acid
FACS	Fluorescence-activated cell sorting
FAD	Flavin adenine dinucleotide
FAO	Fatty acid oxidation
FcRγ	Fc receptor common-gamma subunit chain
FCS	Foetal calf serum
FH	Fumarate hydratase
FIH	Factor inhibiting HIF
G6P	Glucose-6-phosphate
Gads	Grb2-related adaptor downstream of Shc
GAPDH	Glyceraldehyde-3-phosphate dehydrogenase
GC-MS	Gas chromatography-mass spectrometry
GDP	Guanosine diphosphate
GEF	Guanine nucleotide exchange factor
GFP	Green fluorescent protein
GRB2	Growth factor receptor bound protein 2
GSKβ	Glycogen synthase kinase-3 beta
GTP	Guanosine triphosphate
HIF	Hypoxia-inducible factor
HIF-1α	Hypoxia-inducible factor 1-alpha
HIF-1β	Hypoxia-inducible factor 1-beta
HK	Hexokinase
HK2	Hexokinase 2
HREs	Hypoxia-responsive elements
IDH	Isocitrate dehydrogenase
IFN-γ	Interferon-gamma
IκB	Inhibitor of nuclear factor-κB
IKK	IκB kinase complex
IL-2	Interleukin-2
IL-4	Interleukin-4
IL-6	Interleukin-6
IL-10	Interleukin-10

IL-12	Interleukin-12
IMiDs	Immunomodulatory drugs
IP_3	Inositol-3-phosphate
IRF4	Interferon regulatory factor 4
ITAMs	Immunoreceptor tyrosine-based activation motifs
K^+	Potassium
Ki67	Antigen kiel 67
KO	Knockout
LAG3	Lymphocyte-activation gene 3
LAT	Linker for activation of T cells
Lck	Lymphocyte-specific protein tyrosine kinase
LC-MS	Liquid chromatography-mass spectrometry
LDHA	Lactate dehydrogenase A
LKB1	Liver kinase B1
MALT1	Mucosa-associated lymphoid tissue translocation-protein 1
MAP1LC3A	Microtubule associated protein 1 light chain 3 alpha, or LC3
MAPK	Mitogen-activated protein kinase
MCT4	Monocarboxylate transporter 4
MDH2	Malate dehydrogenase 2
MFI	Mean fluorescence intensity
MGUS	Monoclonal gammopathy of undetermined significance
MHC I/II	Major histocompatibility complex I/II
MID	Mass isotopologue distributions
MM	Multiple myeloma
mRNA	Messenger ribonucleic acid
mTECs	Medullary thymic epithelial cells
mTOR	Mammalian target of rapamycin
mTORC1/2	Mammalian target of rapamycin complex 1/2
NA	Non-activated
NAD	Nicotinamide adenine dinucleotide
NDRG1	N-myc down-regulated gene 1
NK cells	Natural killer cells
NFAT	Nuclear factor of activated T cells
NF-kβ	Nuclear factor kappa-light-chain-enhancer of activated B cells
NHSBT	National Health Service Blood and Transplant Centre

NR4A1	Nuclear receptor subfamily 4 group A member 1
NR4A3	Nuclear receptor subfamily 4 group A member 3
O_2	Oxygen
OCR	Oxygen consumption rate
OGDH	Oxoglutarate dehydrogenase complex
OXPHOS	Oxidative phosphorylation
p70S6K	Ribosomal protein S6 kinase beta-1
PB	Peripheral blood
PBS	Phosphate buffered saline
PBMC	Peripheral blood mononuclear cell
PCA	Principal component analysis
PD-1	Programmed cell death protein-1
PDC	Pyruvate dehydrogenase
PDK1	Phosphoinositide-dependent protein kinase 1
PD-L1	Programmed death-ligand 1
PFK	Phosphofructokinase
PGK1	Phosphoglycerate kinase 1
PHA	Phytohaemagglutinin P
PHDs	Prolyl hydroxylases (1,2,3)
PI3K	Phosphoinositide-3 kinase
PIP_2	Phosphatidylinositol 4,5-bisphosphate
PIP_3	Phosphatidylinositol 3,4,5-trisphosphate
PK	Pyruvate kinase
PKC	Protein kinase C
PKCθ	Protein kinase C theta
PLCγ1	Phospholipase C gamma-1 (PLCG1)
PMA	Phorbol 12-myristate 13-acetate
PPP	Pentose phosphate pathway
PTEN	Phosphatase and tensin homolog
Q	Ubiquinone
QH_2	Ubiquinol
RAG	Recombination-activating gene
RAPTOR	Regulatory associated protein of mTOR
Ras	Rat sarcoma
RASGRP	Rat sarcoma guanyl nucleotide-releasing protein

REDD1	Regulated in development and DNA damage response 1 (same as DDIT4)
Rheb	RAS homologue enriched in brain
RICTOR	Rapamycin-insensitive companion of TOR
ROS	Reactive oxygen species
SCENITH	Single Cell ENergetIc metabolism by profilIng Translation inhibition
SCID	Severe combined immunodeficiency
SCS	Succinyl-CoA synthetase
SDH	Succinate dehydrogenase
siRNA	Small interfering RNA
SLC32A1	Solute carrier family 32 member 1
SLC3A2	Solute carrier family 3 member 2
SLE	Systemic lupus erythematosus
SLP-76	Lymphocyte cytosolic protein 2
SMM	Smouldering multiple myeloma
SOC channels	Store-operated calcium channels
SREBPs	Sterol regulatory element-binding proteins
STAT3	Signal transducer and activator of transcription 3
Succinyl-CoA	Succinyl-coenzyme A
Syk	Spleen tyrosine kinase
TBX21	T-box transcription factor, T-bet
TCA cycle	Tricarboxylic acid cycle
TCR	T cell receptor
TEMPO	Timer rapidly expressed in lymphocytes
Tfh cells	T follicular helper cells
Th1 cells	T helper 1 cells
Th2 cells	T helper 2 cells
Th17 cells	T helper 17 cells
TIGIT	T cell immunoreceptor with immunoglobulin and ITIM domain
Tim-3	T cell immunoglobulin and mucin-domain containing-3
TME	Tumour microenvironment
TNF-α	Tumour necrosis factor-alpha
Tocky	Timer of cell kinetics and activity
TPI1	Triosephosphate isomerase 1
TRAF6	Tumour necrosis factor receptor-associated factor 6
Treg cells	T regulatory cells

TSC1/2	Tuberous-sclerosis 1 and 2 complex
UK	United Kingdom
ULK1	Unc-51 like autophagy activating kinase 1
VEGF	Vascular endothelial growth factor
VEGFR2	Vascular endothelial growth factor type II receptor
VHL	Von Hippel-Lindau E3 ligase protein
WT	Wildtype
Zap70	Zeta chain of T cell receptor associated protein kinase 70

1. Introduction

1. Introduction

Cancer, defined as the proliferation and invasion of abnormal cells in the body (National Cancer Institute, 2011), remains one of the most significant causes of morbidity and mortality in the United Kingdom (UK). Between 2016 to 2018, 1,000 new cancer cases were diagnosed each day, with 1 in 2 people born after 1960 receiving some cancer diagnosis in their lifetime (Cancer Research UK, 2015). Whilst cancer survival has doubled over the last 40 years, large populations still suffer its detrimental consequences (Cancer Research UK, 2015). Current research aims to treat, detect, and prevent disease occurrence.

Over the last decade, research has exemplified the importance of studying the surrounding tumour microenvironment (TME), alongside the biology of the cancer itself. Here exists a complex interplay of cell types and metabolic states, which ultimately impact the overall disease process. The immune system, which recognises and eliminates abnormal cells (National Cancer Institute, 2015), is in constant communication with the cancer and understanding how this occurs, and implications for immune cell function, is critical to harnessing these natural defence mechanisms. Additionally, surrounding immune cells and the cancer are in competition for metabolic substrates to support their own biological processes (Xia *et al.*, 2021). Understanding which substrates are key may be invaluable to destroying abnormal cancer cells. Many novel and developing therapies rely on the functions of the immune system to effectively treat cancers. For example, immune checkpoint blockade, immunomodulatory drugs, or more recently, bispecific antibodies and chimeric antigen

receptor (CAR)- T cells. Therefore, understanding the surrounding immune metabolic TME is crucial also from a therapeutic sense.

In this thesis, a specific immune cell subset, $CD8^+$ T-lymphocytes (T cells), will be explored in the context of a key metabolic characteristic of the TME, low oxygen availability. This knowledge will contribute to our understanding of the anti-tumour immune response, and how this is impacted by the TME.

1.1. T-lymphocytes and the immune system

The immune system comprises two main arms – the adaptive and innate immune systems. The innate arm forms the first-line defence against potentially harmful invaders and the adaptive arm destroys and remembers pathogens, whilst protecting the host cells. The focus on this thesis is on a specific cell type of the adaptive immune system, $CD8^+$ T-lymphocytes.

T-lymphocytes, or T cells, work alongside other lymphoid cells, such as B-cells and natural killer (NK) cells, to direct two main responses against abnormal pathogens or cells: an antibody response or a cell-mediated response (Alberts *et al.*, 2024). Generally, T cells are focused on organising a cell-mediated response, however they provide help to B cells to produce an antibody response (Alberts *et al.*, 2024). Two main families of conventional ($\alpha\beta$) T cell exist, $CD4^+$ and $CD8^+$ T cells, distinguished by co-receptors on the cell surface which work with the T cell receptor (TCR) for antigen recognition via major histocompatibility complex (MHC, I and II) on an antigen presenting cell (APC) (Miceli and Parnes, 1991). Non-conventional ($\gamma\delta$) T cells form a

small proportion of T cells (0.5-5%) (Zhao, Niu and Cui, 2018), and will not be discussed in this report.

T cells begin their development in the thymus as a common lymphoid progenitor where they differentiate into functionally distinct $CD4^+$ and $CD8^+$ T cells through rounds of positive and negative selection (Luckheeram *et al.*, 2012). T cell progenitors arrive to the thymus from the bone marrow where they commit to the T-cell lineage (Chopp *et al.*, 2023). TCR rearrangement provides a diverse TCR repertoire that can recognise essentially any peptide fragment (Chopp *et al.*, 2023). Here, recombination-activating gene (RAG) directs rearrangement of the V and J segments of the *Tcra* gene, and V, D and J segments of the *Tcrb* gene and DNA repair machinery repairs the resultant breaks (Chopp *et al.*, 2023). Positive selection is mediated by cortical thymic epithelial cells (cTECs) to remove any T cells that recognise self-MHC:peptide complexes, prior to migration to the medulla where medullary thymic epithelial cells (mTECs) determine if they react against self-peptides (Chopp *et al.*, 2023). mTECs express the transcription factor autoimmune regulator, or AIRE, which enables them to express tissue-restricted antigens and thymocytes that are self-reactive are negatively selected (Chopp *et al.*, 2023). The autoimmune disorder autoimmune polyendocrinopathy candidiasis ectodermal dystrophy (APECED) is caused by a loss-of-function mutation in AIRE, where thymocytes escape negative selection (Chopp *et al.*, 2023). MHC-II restricted thymocytes then commit to $CD4^+$ T cells under the control of ThPOK and GATA, and MHC-I restricted thymocytes to $CD8^+$ T cells under the control of RUNX3 (Chopp *et al.*, 2023). $CD4^+$ and $CD8^+$ T cells express sphingosine 1 phosphate receptor 1 (S1PR1) to promote entry into the circulation (Chopp *et al.*, 2023).

Whilst not the focus of this report, it is important to note $CD4^+$ T cells can differentiate into distinct functional subsets during an immune response, including, T helper 1 (Th1), 2 (Th2) and 17 cells (Th17), T follicular helper cells (Tfh), and T regulatory cells (Treg), each involved in controlling antibody responses by B cells, among other specific functions (Luckheeram *et al.*, 2012). $CD8^+$ T cells are cytotoxic cells which directly target virally-infected or malignantly-transformed cells, in an antigen-specific manner (Zhang and Bevan, 2011). Traditionally, $CD8^+$ T cells are thought to be the cell type responsible for anti-tumour immune responses, however it is now well known that this requires a complex interplay of cell populations to be fully effective (Gonzalez, Hagerling and Werb, 2018). Nevertheless, the majority of immune-directed cancer therapeutics are thought to rely on the functioning of $CD8^+$ T cells for an optimal response (Raskov *et al.*, 2021).

1.1.1. Function and activation of T cells – what makes an 'ideal' $CD8^+$ T cell?

$CD8^+$ T cells harness several mechanisms to elicit their cytotoxic response. This includes the production and release of cytokines, such as interferon-gamma (IFN-γ), interleukin-2 (IL-2), and tumour necrosis factor-alpha (TNF-α), which can aid T cell activation, direct responses of surrounding immune cells and increase immunogenicity of target cells by regulating antigen presentation molecule expression (Gonzalez, Hagerling and Werb, 2018). They also produce cytolytic granules, granzymes and perforin, which are released to effectively 'kill' the threatening cell (Gonzalez, Hagerling and Werb, 2018). $CD8^+$ T cells exit the thymus as naïve cells that have not yet encountered foreign antigen (Kumar, Connors and Farber, 2018). They circulate the blood and lymphatic system and are primed by professional antigen presenting cells

(Wieczorek *et al.*, 2017). Here, the contact of TCR and MHC results in TCR activation and cellular differentiation into short-lived effector cells, which produce IL-2 and are highly proliferative, for clearance of abnormal pathogen (Kumar, Connors and Farber, 2018). Whilst the majority of effector cells apoptose following resolution of the immune response, a small proportion are retained as memory cells which exist to 'remember' the antigen in case of re-exposure (Kumar, Connors and Farber, 2018). Strong TCR stimulation preferentially favours short-lived effector cells, whilst weaker TCR stimulation favours memory precursor cells (Gräbnitz *et al.*, 2023). Importantly, with increasing strength of TCR stimulation, the frequency of cells undergoing asymmetric cell division increases (Gräbnitz *et al.*, 2023). Asymmetric cell division results in colonies of both effector and memory precursor cells, whilst with weak TCR stimulation colonies of cells of either effector or memory precursor cells are formed (Gräbnitz *et al.*, 2023). A population of terminally differentiated effector cells (terminally differentiated effector cells re-expressing CD45RA, EMRA $CD8^+$ T cells) also persist in the circulation (Kumar, Connors and Farber, 2018). The proportion of EMRA $CD8^+$ T cells increases with age and are characterised by high IFN-γ and TNF-α production but low proliferation (Larbi and Fulop, 2014; Di Benedetto *et al.*, 2015). Memory $CD8^+$ T cells can be further differentiated into central memory (CM) and effector memory (EM) $CD8^+$ T cells (Kumar, Connors and Farber, 2018). Whilst both subsets produce IL-2, CM are highly proliferative and capable of migration to lymphoid organs and EM produce greater quantities of effector cytokines (Sallusto, Geginat and Lanzavecchia, 2004; Willinger *et al.*, 2005). The surface expression of an isoform of the tyrosine phosphatase leucocyte common antigen (CD45), CD45RA, is associated with naïve T cells (Tian *et al.*, 2017; Michie *et al.*, 1992). CD62L and CCR7 are homing receptors

which enable T cell migration into lymph nodes (Sallusto *et al.*, 1999). Importantly, these surface markers can be used to define individual subsets of $CD8^+$ T cells. Naïve $CD8^+$ T cells are defined as $CD45RA^+$ $CCR7^+$ and can migrate into lymphoid tissues (Michie *et al.*, 1992; Sallusto *et al.*, 1999; Sallusto, Geginat and Lanzavecchia, 2004). Memory subset CM $CD8^+$ T cells are defined as $CD45RA^-$ $CCR7^+$ as they no longer possess naïve characteristics but are still able to migrate around lymphoid tissues, whilst EM $CD8^+$ T cells are defined as $CD45RA^-$ $CCR7^-$ and tend to rather recirculate peripheral tissues (Michie *et al.*, 1992; Sallusto *et al.*, 1999; Sallusto, Geginat and Lanzavecchia, 2004). EMRA $CD8^+$ T cells are well characterised to re-express CD45RA and are therefore defined as $CD45RA^+$ $CCR7^-$ (Michie *et al.*, 1992; Sallusto *et al.*, 1999; Sallusto, Geginat and Lanzavecchia, 2004). CD62L may also be used in replacement of CCR7 to define the same subsets (Sallusto, Geginat and Lanzavecchia, 2004). These definitions will be used throughout this thesis.

For optimal downstream function of $CD8^+$ T cells, various activation requirements need to be met. Initially, $CD8^+$ T cells see antigen presented by APCs via MHC I which is recognised by the TCR and $CD8^+$ co-receptor to form an immunological synapse (Dustin, 2014). The TCR is a heterodimer comprised of TCRα and TCRβ isoforms which complex with CD3 chains to allow TCR localisation to the membranal surface (Shah *et al.*, 2021). The CD3 chains contain immunoreceptor tyrosine-based activation motifs (ITAMs) (Courtney, Lo and Weiss, 2018). The TCR-CD3 is associated with the $CD8^+$ co-receptor, which can exist as a hetero- or homo-dimer (Leahy, 1995), and association of peptide antigen with this complex stimulates downstream TCR signalling (Courtney, Lo and Weiss, 2018). However, for complete activation, and to prevent

anergy, the $CD8^+$ T cell must receive a co-stimulatory signal (Raskov *et al.*, 2021). For example, CD28 interacts with CD80 or CD86 on the APC and helps to lower the stimulation threshold of the T cell (Zumerle, Molon and Viola, 2017). Alongside the two direct contacts of the T cell with an APC, the T cell must receive appropriate and cytokine signals for full activation and differentiation (e.g., interleukin-12 (IL-12) or type I interferons), which are also released by APCs as well as other cells, such as $CD4^+$ T cells (Keppler *et al.*, 2012). For example, when $CD8^+$ T cells are activated in the absence of IL-12 they are able to proliferate but become anergic and are unable to upregulate effector functions (Curtsinger, Lins and Mescher, 2003). Recent work has also suggested that a fourth signal, T cell metabolism and the surrounding metabolic microenvironment, is required for sufficient T cell activation (Giles *et al.*, 2023). These include the required fuels and nutrients for T cell function and differentiation (Giles *et al.*, 2023). Once a $CD8^+$ T cell has been optimally activated, the conditions in which it resides, and the competence of its signalling machinery, may also play a role in the downstream effector function it provides. The next section will focus on ideal signalling and metabolism and discuss how dysfunction may impact $CD8^+$ T cell function.

1.1.2. $CD8^+$ T cell signalling and consequences of dysfunction

Even with sufficient activation delivered by signals through the TCR, co-stimulation and surrounding cytokines, if downstream signalling is aberrant, T cell function is likely to be impaired. However, before looking at dysfunctional signalling, it is important to outline the most current understanding of T cell signalling. These pathways can be split into those that are provided by the TCR and those that originate from co-stimulatory signals. Whilst other signals exist, for this thesis, I will focus on CD28 co-stimulation.

1.1.2.1. Initial CD8⁺ T cell TCR signalling events

Lymphocyte-specific protein tyrosine kinase, or Lck, is a member of the SRC family kinase group and is closely associated with the CD3-TCR multiprotein complex (Shah *et al.*, 2021). Phosphorylation from C-terminal SRC kinase (CSK) usually keeps Lck in an inactive form, however the protein tyrosine phosphatase CD45 dephosphorylates Lck and leads to its activation (Bommhardt, Schraven and Simeoni, 2019). Through its dephosphorylation activity on Lck, CD45 regulates the strength of TCR signalling (McNeill *et al.*, 2007). Upon antigen engagement with the TCR, the CD8 co-receptor recruits Lck to the membrane to phosphorylate ITAM motifs and ultimately create binding sites for the kinase zeta chain of T cell receptor associated protein kinase 70 (Zap70) to dock and activate (Iwashima *et al.*, 1994; Isakov *et al.*, 1995; Palacios and Weiss, 2004). Zap70 phosphorylates linker for activation of T cells (LAT), and finalises the proximal signalling that forms a scaffold for downstream signalling pathways to emerge (Wange *et al.*, 2000). Initial signalling events are summarised in **Figure 1.1A.** A complex of the adaptor proteins LAT, Grb2-related adaptor downstream of Shc (Gads), and lymphocyte cytosolic protein 2 (SLP-76), is recruited to the membrane to activate phospholipase C gamma-1 (PLCγ1) (Beach *et al.*, 2007). Activated PLCγ1 hydrolyses phosphatidylinositol 4,5-bisphosphate (PIP_2), into the secondary messengers, diacylglycerol (DAG) and inositol-3-phosphate (IP_3) (Zhong *et al.*, 2008; Berridge, 2009). DAG subsequently activates the protein kinase C (PKC) theta (PKCθ) and nuclear-factor kappa-light-chain-enhancer of activated B cells (NF-kβ) pathway, whilst IP_3 initiates the calcium (Ca^{2+})-calcineurin-nuclear factor of activated T cells (NFAT) pathway (Zhong *et al.*, 2008; Berridge, 2009) **(Figure 1.1A)**.

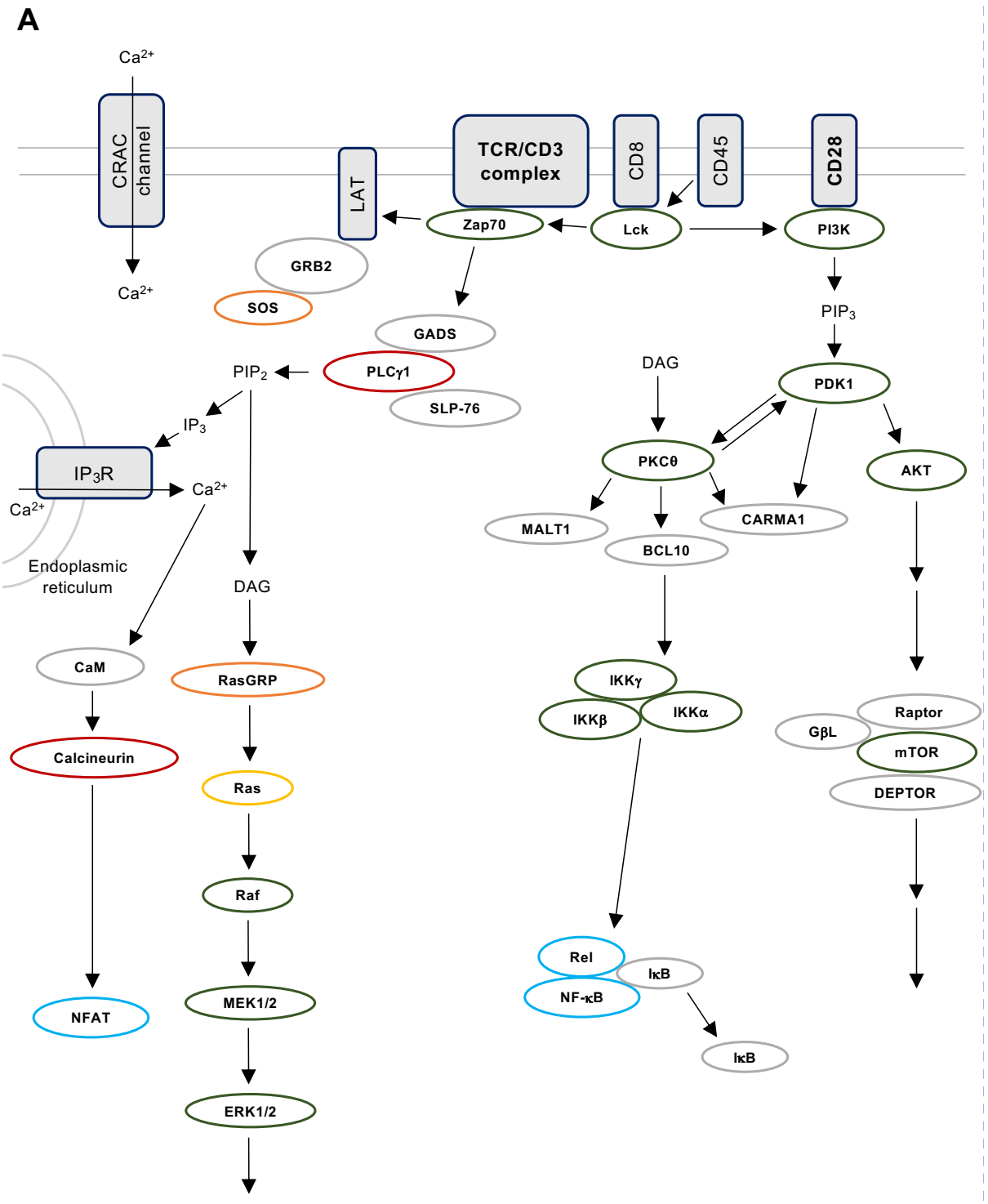

Figure 1.1. Overview of TCR and CD28 signalling pathways. A) Key proteins in the TCR and CD28 signalling pathways shown. Lck = lymphocyte-specific protein tyrosine kinase, LAT = linker for activation of T cells, GADS = Grb2-related adaptor downstream of Shc, SLP-76 = lymphocyte cytosolic protein 2, PLCγ1 = phospholipase Cγ1, PIP_2 = phosphatidylinositol 4,5-bisphosphate, PIP_3 = phosphatidylinositol 3,4,5-trisphosphate, PI3K = phosphoinositide-3 kinase, DAG = diacylglycerol, IP_3 = inositol-3-phosphate, CRAC channels = calcium-release activated calcium channels, NFAT = nuclear factor of activated T cells, CARMA1 = caspase recruitment domain-containing membrane-associated guanylate kinase protein-1, BCL10 = B cell lymphoma/leukaemia 10,

MALT1 = mucosa-associated lymphoid tissue translocation-protein 1, RASGRP = RAS guanyl nucleotide-releasing protein, mTOR = mammalian target of rapamycin, PDK1 = phosphoinositide-dependent protein kinase 1, AKT = protein kinase B (PKB), PKCθ = protein kinase C theta. Light blue = transcription factor, red = phosphatase, dark green = kinase, orange = GAP/GEF, yellow = GTPase.

1.1.2.2. Ca^{2+}-calcineurin-NFAT pathway

To initiate the Ca^{2+}-calcineurin-NFAT pathway, IP_3 binds Ca^{2+} ion channel receptors on intracellular calcium stores or the endoplasmic reticulum (ER) to stimulate release of Ca^{2+} into the cytoplasm (Kania *et al.*, 2017). The pathway is demonstrated in **Figure 1.1A.** Alternatively, when the cell senses a reduction in intracellular Ca^{2+}, an influx of extracellular Ca^{2+} is triggered through calcium-release activated calcium (CRAC) channels (Penna *et al.*, 2008; Weidinger, Shaw and Feske, 2013). As a result of the rise in intracellular Ca^{2+}, calcineurin, a protein phosphatase, is activated and dephosphorylates NFAT which promotes its translocation to the nucleus (Mulero *et al.*, 2009). NFAT is a key transcription factor which initiates production of several T cell effector molecules, such as the expression of cytokine genes (Macian, 2005).

1.1.2.3. PKCθ-IKK-NF-κB pathway

Following T cell activation, DAG binds and recruits PKCθ to the cell membrane where it phosphorylates caspase recruitment domain-containing membrane-associated guanylate kinase protein-1 (CARMA1) (Matsumoto *et al.*, 2005; Sun, 2012). CARMA1 subsequently associates with B cell lymphoma/leukaemia 10 (BCL10) (Weil and Israël, 2006). BCL10 and mucosa-associated lymphoid tissue translocation-protein 1 (MALT-1) bind and associate with tumour necrosis factor receptor-associated factor 6 (TRAF6), an E3 ubiquitin ligase, responsible for the degradation of an inhibitor of

nuclear factor-κB (IκB) kinase (IKK) complex regulatory protein, IKKγ (Zhou *et al.*, 2004; Paul and Schaefer, 2013). The degradation of IKKγ removes the inhibition placed upon IKKα and IKKβ to allow their phosphorylation and subsequent degradation of IκB (Paul and Schaefer, 2013). As a result, IκB inhibition on NF-κB is removed and NF-κB is able to translocate to the nucleus to exert its effects as a transcription factor in the regulation of genes for T cell activation and effector function, among other effects (Liu *et al.*, 2017). This pathway is demonstrated in **Figure 1.1A.**

1.1.2.4. Ras/MAPK-ERK-AP-1 pathway

Alongside PKCθ, DAG activates and recruits a RAS guanyl nucleotide-releasing protein (RASGRP1), a guanine nucleotide exchange factor (GEF), which functions to activates Ras (Ebinu *et al.*, 1998). Ras activation initiates the RAS-mitogen-activated protein kinase (MAPK) cascade, whereby Raf1 activates a MAPK kinase (e.g., MEK1/2) to activate MAPK extracellular signal-regulated kinase 1 and 2 (ERK1/2) (Chong, Vikis and Guan, 2003). The pathway is demonstrated in **Figure 1.1A.** ERK proteins have roles in sustaining the activation of the transcription factor activator-protein-1 (AP-1) which has critical roles in T cell activation (Atsaves *et al.*, 2019).

1.1.2.5. mTOR pathway

The kinase mammalian target of rapamycin (mTOR) is hugely versatile and is stimulated through various mechanisms (Zoncu, Efeyan and Sabatini, 2011). mTOR exists as two complexes: mTOR complex 1 (mTORC1) and mTOR complex 2 (mTORC2), which differ by their scaffold protein (Chi, 2012). mTORC1 contains regulatory associated protein of mTOR (RAPTOR) which is sensitive to rapamycin,

and mTORC2 contains the rapamycin-insensitive companion of TOR (RICTOR) (Chi, 2012). Upon T cell activation, the mTOR pathway is initiated through both TCR (via the DAG-Ras/MAPK-ERK-AP-1 pathway) and CD28-dependent (via the PI3K-AKT pathway) signalling (see '***1.1.2.6. CD28 co-stimulatory pathway***') (Gorentla, Wan and Zhong, 2011; Chi, 2012). The upstream signalling pathway of mTOR is demonstrated in **Figure 1.1A.** The adenosine monophosphate (AMP)-activated protein kinase (AMPK)- pathway also regulates mTOR signalling (Chapman and Chi, 2015). AMPK is activated following a reduction in available energy, which alters AMP/adenosine triphosphate (ATP) rations (Corton, Gillespie and Hardie, 1994; Hawley *et al.*, 2010; Mungai *et al.*, 2011). AMPK suppresses mTORC1 activity to limit cellular energy usage (Ma *et al.*, 2017) (see '***1.2.3.3. AMP-activated protein kinase (AMPK) pathway***').

In naïve and resting T cells, mTORC1 and its activator RAS homologue enriched in brain (Rheb) are kept inactivated by guanosine triphosphate (GTP)ase-activating activity from the tuberous-sclerosis 1 and 2 complex (TSC1-TSC2) (Chi, 2012). Following T cell activation, the TSC complex is inhibited and the inhibition on mTORC1 is lifted (Chi, 2012). This, along with activation by Rheb, enables mTORC1 signalling (Chi, 2012). mTORC1 can also be regulated via AKT and AMPK pathways (via liver kinase B1 (LKB1)) in cellular stress and calmodulin-dependent protein kinase (CamKK2) in response to Ca^{2+} signals) independently of Rheb, and by amino acids via GTPases in the recombination-activating gene (RAG) family (Chi, 2012). In contrast, mTORC2 signalling enables the complete activation of AKT and the phosphorylation

of PKCθ in the NF-κB pathway (Chi, 2012). The regulation of mTORC1 and mTORC2 activity is demonstrated in **Figure 1.2A**.

Downstream, mTORC1 has vast roles in T cell effector function, activation, proliferation and metabolism (Chapman and Chi, 2015). Additionally, mTORC1 promotes the initiation of translation and protein synthesis (Chi, 2012). To direct its effects, mTORC1 signals through ribosomal protein S6 kinase beta-1 (p70S6K), suppresses eukaryotic translation initiation factor 4E-binding protein 1 (4E-BP1), and stimulates various transcription factors, including hypoxia-inducible factor 1-alpha (HIF-1α), sterol regulatory element-binding proteins (SREBPs) and cellular myelocytomatosis oncogene (c-Myc) (Chapman and Chi, 2015) **(Figure 1.2A)**.

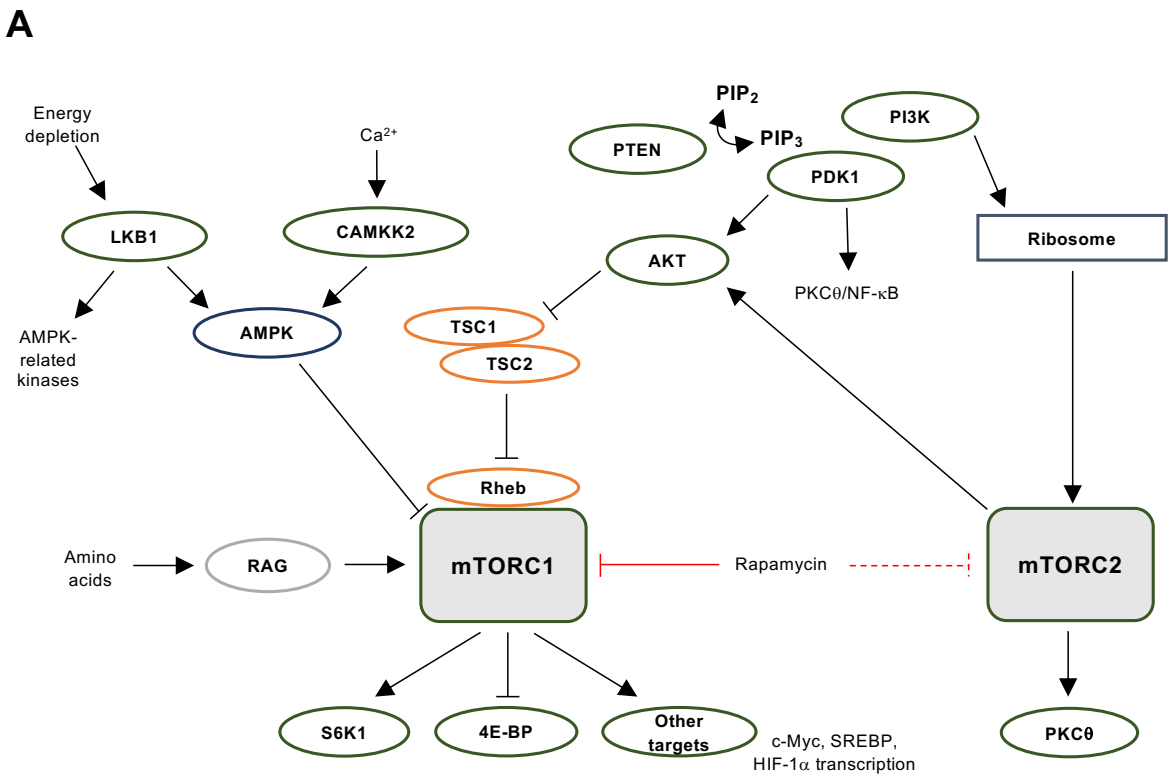

Figure 1.2. Overview of mTOR regulation. A) Key proteins in the regulation of the rapamycin sensitive mTORC1 and the rapamycin insensitive mTORC2. mTORC1/2 = mammalian target of rapamycin complex 1 or 2, LKB1 = liver kinase B1, CAMKK2 = calmodulin-dependent protein kinase, AMPK = AMP-activated protein kinase, TSC1/TSC2 = the tuberous-sclerosis 1 and 2 complex, PTEN = phosphatase and tensin homolog, PI3K = phosphoinositide-3 kinase, PDK1 = phosphoinositide-dependent protein kinase 1, AKT = protein kinase B (PKB), PKCθ = protein kinase C theta, RAG = recombination-activating gene, S6K1 = ribosomal protein S6 kinase beta-1, 4E-BP = eukaryotic translation initiation factor 4E (eIF4E)-binding protein 1.

1.1.2.6. CD28 co-stimulatory pathway

After CD28 association with CD80 and CD86, phosphoinositide 3-kinase (PI3K) is recruited to the cytoplasmic tail of CD28 to facilitate the conversion of PIP_2 to phosphatidylinositol 3,4,5-trisphosphate (PIP_3) which acts on several downstream pathways (Riha and Rudd, 2010). One of the most well characterised is the activation of phosphoinositide-dependent protein kinase 1 (PDK1) by PIP_3 which activates protein kinase B (PKB, or AKT) (Riha and Rudd, 2010). PDK1 can also activate PKCθ and p70S6K to strengthen TCR signalling pathways (Riha and Rudd, 2010). PKB (AKT) is capable of phosphorylating mTORC1 **(Figure 1.2A)**, alongside glycogen synthase kinase-3 beta (GSKβ) and B cell lymphoma/leukaemia 2 (BCL2) associated agonist of cell death (BAD) (Riha and Rudd, 2010). PKCθ also drives the inhibition of GSKβ through phosphorylation (Esensten *et al.*, 2017). The phosphorylation and inhibition of GSKβ ultimately enhances NFAT-dependent transcription, whilst the phosphorylation of BAD, alongside the upregulation of Bcl-2 and B cell lymphoma-extra large (Bcl-X_L) by PKB (AKT), is thought to regulate apoptosis, however controversy exists in this (Riha and Rudd, 2010; Esensten *et al.*, 2017). Furthermore, adaptor proteins, growth factor receptor bound protein 2 (GRB2) and GADS, bind CD28 to signal downstream to drive AP-1 transcription factor activity and IKK activation for NF-κB pathway regulation. Overall, CD28-dependent PKB (AKT) and PDK1 work together to sustain and strengthen TCR signalling and on downstream effectors (Riha and Rudd, 2010). The pathway is demonstrated in **Figure 1.1A.**

1.1.2.7. Consequences of CD8$^+$ T cell signalling dysfunction

Gaining the right balance of CD8$^+$ T cell activatory signalling is crucial to prevent disease – too little activatory signalling leads to immune deficiency, too much activatory signalling leads to autoimmunity. This section will provide some brief examples of this in context, further detail can be found elsewhere (Shah *et al.*, 2021). 'Too much' T cell signalling may lead to systemic lupus erythematosus (SLE), a chronic autoimmune disease with an unknown cause (Moulton and Tsokos, 2015). Aberrations in the TCR signalling pathway have been shown to contribute to the disease pathogenesis, for example, the replacement of the CD3ζ/Zap-70 interaction with an interaction of the homologous Fc receptor common γ subunit chain (FcRγ) and spleen tyrosine kinase (Syk) in SLE creates a stronger signal and lowering of the antigen threshold (Moulton and Tsokos, 2015). 'Too little' signalling may result in immune dysfunction, for example a deficiency of CD45 in T cells leads to severe combined immunodeficiency (SCID) and a lack of Lck may also result in immunodeficiency (Kung *et al.*, 2000; Sawabe *et al.*, 2001). It is evident that activation-induced signalling is vital for effective functioning of T cells and a defect in any aspect of the pathway may lead to downstream dysfunction, or ultimately disease.

1.1.3. CD8$^+$ T cell metabolism and consequences of metabolic limitation

Cellular metabolism involves a complex network of biochemical reactions that allow the production of energy and substrates for biomass (DeBerardinis and Thompson, 2012). These reactions can be classified as catabolic, for the breakdown of substrates to release energy; anabolic, which combine simple substrates into more complex molecules; and those for cellular waste disposal (DeBerardinis and Thompson, 2012).

T cells demonstrate distinct metabolic phenotypes across their differentiation and development, depending upon the energy and biomass requirement at each stage (Gerriets and Rathmell, 2012). Changes in metabolism also have implications for $CD8^+$ T cell function through effects on signalling, epigenetics, transcription and translation.

1.1.3.1. Oxidative phosphorylation (OXPHOS) and glycolysis

Oxidative phosphorylation (OXPHOS) partners the reduction of oxygen and the generation of ATP molecules to provide energy for the cell (Deshpande and Mohiuddin, 2023). The pathway can begin in the cytosol via glycolysis (Al-Khami, Rodriguez and Ochoa, 2017). Here, glucose entering the cell is converted via a series of 11 enzymatic reactions to pyruvate (Al-Khami, Rodriguez and Ochoa, 2017). Glycolysis also reduces nicotinamide adenine dinucleotide (NAD^+) to NADH and produces two molecules of ATP (Al-Khami, Rodriguez and Ochoa, 2017). The first intermediate of glycolysis, glucose-6-phosphate (G6P) can also be directed into the pentose phosphate pathway (PPP) to generate precursors for nucleotide synthesis (Stincone *et al.*, 2015).

Glucose-derived pyruvate can be converted into acetyl-coenzyme A (acetyl-CoA) by pyruvate dehydrogenase (PDC) and enter the mitochondria (Alabduladhem and Bordoni, 2022). Acetyl-CoA is metabolised in the tricarboxylic acid (TCA) cycle to generate NADH and flavin adenine dinucleotide (FAD) + 2 hydrogen ($FADH_2$) molecules in a series of catabolic reactions (Deshpande and Mohiuddin, 2023). The TCA cycle involves eight enzymes **(Figure 1.3A)**, three of which regulate the activity of the cycle (alpha-ketoglutarate dehydrogenase, isocitrate dehydrogenase (IDH), and citrate synthase (CS)) (Alabduladhem and Bordoni, 2022). Initially, CS combines

acetyl-CoA (2-carbons) and oxaloacetate (4-carbons) to generate citrate (6-carbons) (Arnold and Finley, 2023). Aconitase 2 (ACO2) converts citrate to isocitrate, which is decarboxylated by IDH to form alpha-ketoglutarate (α-KG, 5-carbons) and NADH (Arnold and Finley, 2023). The oxoglutarate dehydrogenase complex (OGDH) decarboxylates α-KG to generate succinyl-coenzyme A (succinyl-CoA) (4-carbons), NADH and release carbon dioxide (CO_2) (Arnold and Finley, 2023). Succinyl-CoA synthetase (SCS) converts succinyl-CoA to succinate, a substrate-level phosphorylation which generates a molecule of GTP (Arnold and Finley, 2023). Succinate dehydrogenase (SDH) converts succinate to fumarate, as well as participating in the electron transport chain (ETC) via the generation of $FADH_2$, and fumarate is converted to malate by fumarate hydratase (FH) (Arnold and Finley, 2023). Malate is finally converted to oxaloacetate by malate dehydrogenase 2 (MDH2), which also forms another NADH (Arnold and Finley, 2023). The cycle then re-starts with the combination of oxaloacetate and acetyl-CoA (Arnold and Finley, 2023). The steps involved in the TCA cycle are summarised below in **Figure 1.3A**.

NADH and $FADH_2$ generated by the TCA cycle transfer elections to the ETC which is demonstrated in **Figure 1.3B**. NADH donates electrons to complex I, and $FADH_2$ to complex II (Arnold and Finley, 2023). Electrons are passed from complex I and II to ubiquinone (Q), which drives its reduction to ubiquinol (QH_2) (Arnold and Finley, 2023). Ubiquinol transfers electrons to complex III, which re-oxidises ubiquinol to ubiquinone, and complex III passes electrons to cytochrome C (Cyt C) (Arnold and Finley, 2023). Cyt C transfers electrons to complex IV, which finally passes electrons to the highly electronegative (i.e., highly able to attract a pair of electrons) oxygen (O_2) and

generates H_2O (Arnold and Finley, 2023; Deshpande and Mohiuddin, 2023). Thus, O_2 is the final electron acceptor of the ETC (Deshpande and Mohiuddin, 2023). Throughout the transfer of electrons through the ETC, protons are pumped across the inner mitochondrial membrane by complexes I, III, and IV (Arnold and Finley, 2023). Complex V or ATP synthase uses this resultant proton gradient to generate ATP (Arnold and Finley, 2023). Electron transfer across the ETC is therefore coupled with ATP synthesis, with overall 30-32 ATP molecules being generated from the ETC (Deshpande and Mohiuddin, 2023). The ETC process is presented in **Figure 1.3B**.

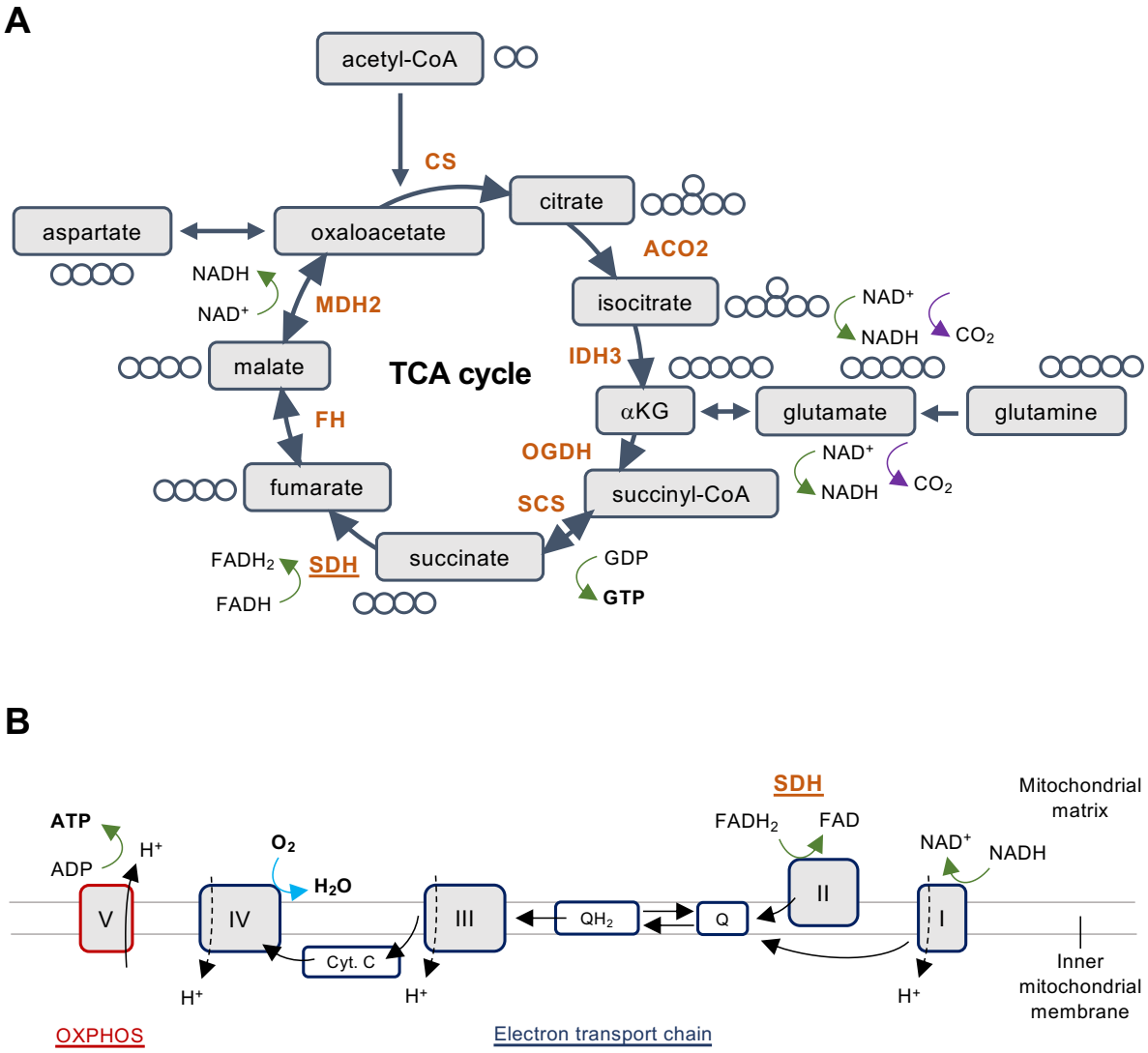

Figure 1.3. Diagram of the TCA cycle and the ETC. A) Diagram of the TCA cycle. CS combines acetyl-CoA and oxaloacetate to form citrate. ACO2 converts citrate to isocitrate. Isocitrate is decarboxylated by IDH3 to form α-KG. OGDH decarboxylates α-KG to form succinyl-CoA. Succinyl-CoA is converted to succinate by SCS, and succinate to fumarate by SDH. SDH (underlined) also participates in the ETC. FH converts fumarate to malate, and malate is converted to oxaloacetate by MDH2 to complete the cycle. Glutamine may also enter the TCA cycle by the conversion to glutamate and α-KG; B) Diagram of the ETC. From right to left: NADH donates electrons to complex I, and $FADH_2$ donates electrons to complex II. Electrons are passed from complexes I and II to ubiquinone (Q), which is reduced to ubiquinol (QH_2). QH_2 transfers electrons to complex III which re-oxidises QH_2 to Q. Complex III passes electrons to cytochrome C (Cyt. C) which transfers electrons to complex IV. Complex IV passes electrons to O_2 as the final electron acceptor and generates H_2O. Pumping of protons across the inner mitochondrial membrane by complexes I, III, and IV drives a proton gradient to generate ATP at complex V (ATP synthase). CS = citrate synthase, ACO2 = aconitase 2, IDH3 = isocitrate dehydrogenase 3, OGDH = oxoglutarate dehydrogenase complex, SCS = succinyl-CoA synthetase, SDH = succinate dehydrogenase, FH = fumarate hydratase, MDH2 = malate dehydrogenase 2. Orange = key enzymes.

Alongside glucose, many cells also utilise glutamine and fatty acids, among other nutrients, to fuel metabolic pathways (Al-Khami, Rodriguez and Ochoa, 2017). Glutamine is metabolised through glutaminolysis into glutamate and then α-KG which can enter the TCA cycle (as above, **Figure 1.3A**) (Al-Khami, Rodriguez and Ochoa, 2017). This can produce further ATP as described above, and also TCA intermediates that feed into other metabolic pathways, for example citrate which supports fatty acid synthesis (Al-Khami, Rodriguez and Ochoa, 2017). Fatty acids are metabolised through fatty acid oxidation (FAO) into acetyl-CoA which also enters the TCA cycle (Al-Khami, Rodriguez and Ochoa, 2017). The TCA cycle is therefore capable of yielding various intermediates for biomass generation, which may enter the ETC to produce ATP, but these processes do require a large input of nutrients from the external cellular environment (Al-Khami, Rodriguez and Ochoa, 2017).

1.1.3.2. Metabolic requirements across the differentiation of $CD8^+$ T cells

Resting or naïve T cells uptake low amounts of glucose and rely on the breakdown of substrates, including glucose, lipids, and amino acids, to generate the small intracellular amounts of ATP required to maintain their quiescent state (Fox, Hammerman and Thompson, 2005). They are primarily oxidative in their metabolism (Gerriets and Rathmell, 2012). Upon activation, $CD8^+$ T cells undergo massive metabolic change (known as metabolic reprogramming) to support increased biomass and protein production for their effector response (Gerriets and Rathmell, 2012). For example, increased uptake of glucose and cytoplasmic glycolysis generates macromolecules for anabolic reactions to support increased biomass and generates heightened ATP (Bauer *et al.*, 2004; Fox, Hammerman and Thompson, 2005). In this

context, where O_2 is not limiting, adoption of glycolysis is referred to as aerobic glycolysis (Bauer *et al.*, 2004; Menk *et al.*, 2018). Aerobic glycolysis is often observed in cancer cells and referred to as the Warburg Effect (Liberti and Locasale, 2016). Here, pyruvate generated through glycolysis does not enter the TCA cycle, but instead is converted into lactate and NAD^+ (Al-Khami, Rodriguez and Ochoa, 2017). Lactate is removed from the cell and NAD^+ is utilised to sustain the glycolytic flux and ATP production (Al-Khami, Rodriguez and Ochoa, 2017). The switch from oxidative metabolism is crucial as aerobic glycolysis enables continued ATP production, as well as providing the building blocks, such as nucleotides and amino acids, for biomass generation (Gerriets and Rathmell, 2012). Activated $CD8^+$ T cells also increasingly rely on amino acid metabolism, for example glutaminolysis, for their efficient function (Rivera *et al.*, 2021).

Memory $CD8^+$ T cells adopt OXPHOS and reorganise their mitochondria for the use of lipids and FAO (Rivera *et al.*, 2021). Furthermore, rather than mitochondrial fission seen in effector $CD8^+$ T cells, memory cells initiate mitochondrial fusion to protect against excess reactive oxygen species (ROS) (Rivera *et al.*, 2021). On a secondary antigenic response, memory $CD8^+$ T cells will become effector memory $CD8^+$ T cells and once again, revert to aerobic glycolysis for biomass and energy generation (Rivera *et al.*, 2021).

1.1.3.3. Relationship between CD8⁺ T cell signalling and metabolic reprogramming

As discussed in section '***1.1.2.5. mTOR pathway***', AKT dependent activation of mTOR following $CD8^+$ T cell stimulation leads to the expression of HIF-1α and c-Myc (Chapman and Chi, 2015; Gupta, Wang and Chen, 2020). Increased c-Myc expression via activation-induced AKT-dependent mTOR signalling upregulates glycolysis, glutaminolysis, and transcription of the glutamine receptors solute carrier family 32 member 1 (SLC32A1) and solute carrier family 3 member 2 (SLC3A2) (Gupta, Wang and Chen, 2020). HIF-1α, which will be covered further below (see '***1.2.3.1. Hypoxia inducible factor (HIF) proteins***'), is a known driver of glycolysis with various glycolytic enzymes and glucose transporters as targets (Dengler, Galbraith and Espinosa, 2014). However, whilst c-Myc is required, HIF-1α has not been shown to be required for activation-induced metabolic reprogramming in $CD8^+$ T cells (Wang *et al.*, 2011). Instead, HIF-1α is thought to be required for the maintenance of glycolysis following $CD8^+$ T cell entry into the cell cycle, and to enable IL-2 to sustain glucose uptake (Wang *et al.*, 2011; Finlay *et al.*, 2012). NFAT signalling is also known to induce the expression of HIF-1α and c-Myc, alongside increasing the expression of the glucose transporters GLUT1 and GLUT3 and the glycolytic enzyme hexokinase (HK) (Klein-Hessling *et al.*, 2017). Therefore, activation induced $CD8^+$ T cell signalling is crucial for the metabolic reprogramming required to increase biomass and protein production for an efficient effector response.

1.1.3.4. Consequences of $CD8^+$ T cell metabolic limitation

Metabolite deprivation is well reported to impact $CD8^+$ T cell activation and function. For example, glucose limitation, or glycolytic inhibition with 2-deoxy-glucose (2-DG) inhibits $CD8^+$ T cell IFN-γ production (Cham and Gajewski, 2005). Further work with gene array analysis determined that expression of genes for effector cytokine production, cytolytic molecule generation and cell cycle were inhibited by 2-DG in $CD8^+$ T cells (Cham *et al.*, 2008). Similarly, depletion of glutamine during $CD8^+$ T cell activation inhibits proliferation and production of cytokines (Carr *et al.*, 2010). These impacts are important in the cancer setting, as the tumour and infiltrating T cells are in continuous competition for metabolic substrates and limitation of key metabolites often occurs (Rivera *et al.*, 2021).

1.2. Hypoxia

1.2.1. Physiological hypoxia

Low oxygen (O_2) availability, or hypoxia, occurs in various pathological and physiological sites (Rocca *et al.*, 2022). Hypoxia occurs when tissue demand for O_2 exceeds the available supply (Kierans and Taylor, 2021). Atmospheric O_2 sits at 21%, the level at which most *in vitro* laboratory studies are undertaken, the bloodstream is closer to 5% O_2 and tissues range between 3-5% O_2 (Atkuri *et al.*, 2007). Therefore, the majority of cells will encounter low O_2 during their lifetime (known as 'physioxia', or physiological hypoxia) and normal processes occur at substantially lower O_2 tensions than replicated *in vitro* (Atkuri *et al.*, 2007). It has been reported that the healthy bone marrow (BM) has an O_2 tension of 7-43 mmHg, which equates to 1% - 6% O_2, and the spleen and lymph nodes can vary between 0.5-4.5% O_2 (Chow *et al.*, 2001; Harrison

et al., 2002; Spencer *et al.*, 2014; Zenewicz, 2017). Since $CD8^+$ T cells continuously flux in and out of these sites, they will encounter and function within physiological hypoxia throughout their lifespan.

1.2.2. Pathological hypoxia

Within sites of infection or malignancy, O_2 can reach pathological levels much lower than that seen in healthy tissues and organs. In fact, hypoxia is a well characterised feature of the TME, and solid tumours are often reported as anoxic (i.e., no O_2 in the environment) or harbouring O_2 levels as low as 0.3% to 4.2% (Muz *et al.*, 2015). Hypoxia arises in the TME due to several processes, including aberrant angiogenesis and the production of abnormal pro-angiogenic factors (e.g., vascular endothelial growth factor, VEGF) resulting in the formation of disrupted blood vessels which limits O_2 reaching the pathological site (Michiels, 2004; Muz *et al.*, 2015). Proliferation of malignant cells and infiltration of immune cells creates a highly dense, cellular environment, which further limits the transport of O_2 through the tissue (Li, Zhao and Li, 2021). Within these pathological sites, $CD8^+$ T cells will encounter abnormal antigen that subsequently directs their immune response hence it is important that $CD8^+$ T cells function as efficiently here as they do in other, more oxygenated sites, elsewhere in the body.

1.2.3. Cellular response to hypoxia

1.2.3.1. Hypoxia inducible factor (HIF) proteins

Hypoxia-inducible factor (HIF) proteins are the major players involved in directing the cellular response to hypoxia. They are composed of an oxygen-regulated alpha-

subunit (HIF-1α, -2α, -3α) and a beta-subunit which is constitutively expressed (HIF-1β, -2β, -3β) (Wang and Semenza, 1993). HIF-1β subunits are also known as aryl hydrocarbon receptor nuclear translocators (ARNT) (Wang *et al.*, 1995). Whilst all the HIF proteins have roles in hypoxia, the -1α and -1β subunits predominate this. In normoxia, HIF-1α subunits are hydroxylated by prolyl hydroxylases (PHDs) to be recognised by Von Hippel-Lindau (VHL) E3 ligase protein via proline hydroxylation sites and targeted for degradation (Maxwell *et al.*, 1999; Epstein *et al.*, 2001; Jaakkola *et al.*, 2001) **(Figure 1.4A)**. The oxygen-sensitive asparaginyl hydroxylase factor inhibiting HIF (FIH) also hydroxylases HIF-1α to inhibit recruitment of p300 and CREB-binding protein (CBP), transcriptional activators of HIF-1α, and inhibit transcriptional activities of HIF-1α (Ebert and Bunn, 1998; McNeill *et al.*, 2002) **(Figure 1.4A)**. In hypoxia, HIF-1α protein is not degraded and accumulates within the cell (Semenza, 2010) **(Figure 1.4A)**. It translocates to the nucleus to bind HIF-1β and form a complex, which binds hypoxia-responsive elements (HREs) on the DNA sequence 5'-RCGTG-3' (Semenza, 2010) **(Figure 1.4A)**. This recruits co-activators p300 and CBP to induce expression of target genes (Semenza, 2010) **(Figure 1.4A)**. Genes regulated through HIF-dependent mechanisms include those which reduce cellular O_2 demand and increase O_2 availability (Dengler, Galbraith and Espinosa, 2014). For example, genes involved in metabolic reprogramming, angiogenesis, apoptosis, autophagy, and homeostatic redox regulation, among others (Dengler, Galbraith and Espinosa, 2014). Notably, HIF induces expression of Egl-9 family hypoxia inducible factor 1 (Egln1, or PHD2) and Egl-9 family hypoxia inducible factor 3 (Egln3, PHD3) to create a negative feedback loop for its degradation (Metzen *et al.*, 2005; Pescador *et al.*, 2005).

Interestingly, and of importance to this report, a HIF-1α isoform, specifically isoform I.3, is stabilised and transcriptionally active upon TCR stimulation of T cells, independent of oxygen status (Nakamura *et al.*, 2005; Lukashev and Sitkovsky, 2008). Therefore, both in hypoxia and on activation, T cells stabilise HIF and induce its transcriptional effects.

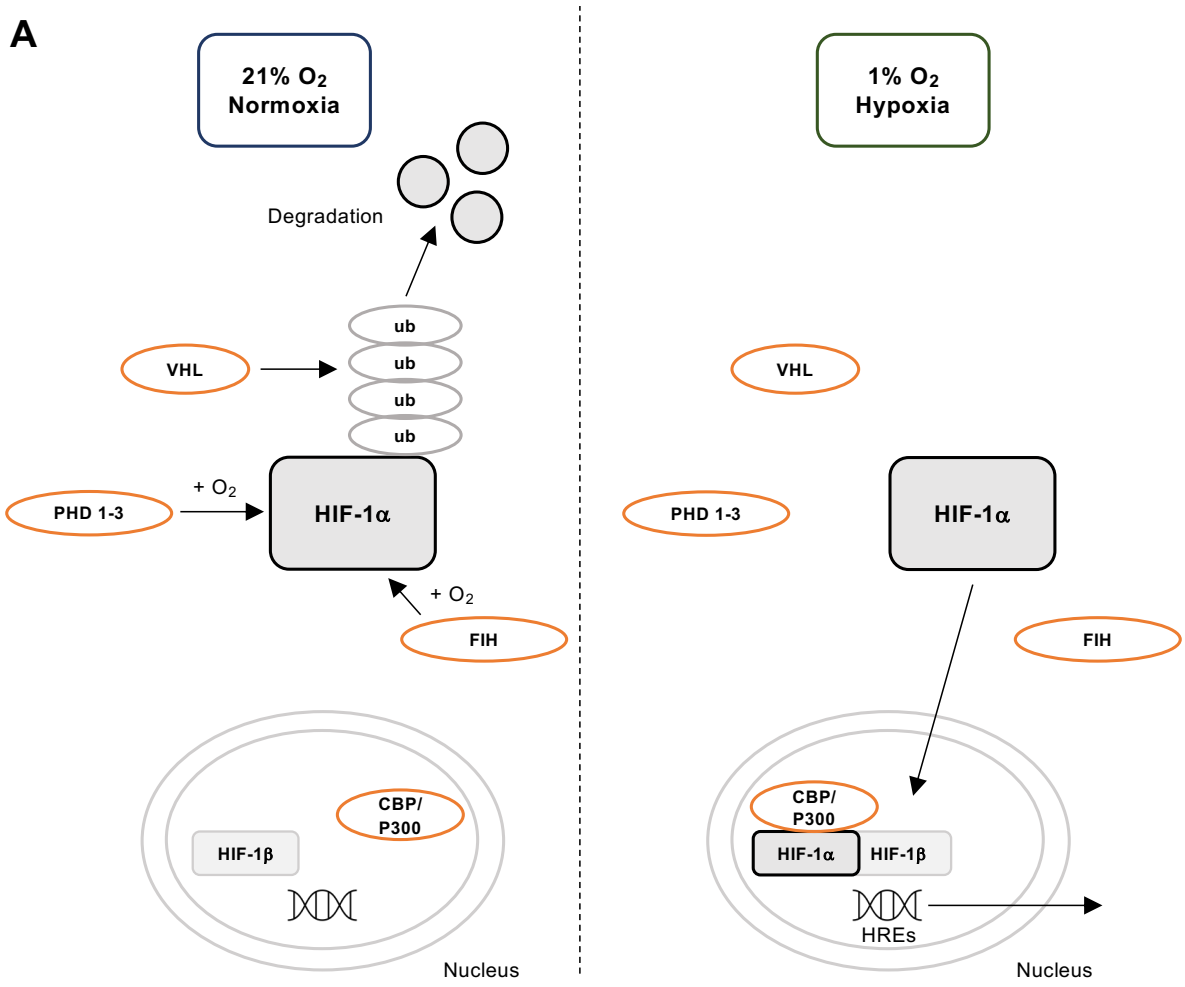

Figure 1.4. Diagram of the regulation of HIF-1α in normoxia (Left) and hypoxia (Right). A) Key proteins in the regulation of HIF-1α in normoxia and hypoxia. HIF-1α = hypoxia-inducible factor 1 alpha, HIF-1β = hypoxia-inducible factor 1 beta, PHD 1-3 = prolyl hydroxylases 1-3, VHL = Von-Hippel Lindau E3 ligase protein, FIH = factor inhibiting HIF, CBP = CREB-binding protein, HREs = hypoxia-responsive elements.

1.2.3.2. Activator protein-1 (AP-1) pathway

Whilst HIF is the primary responder to hypoxia, other mechanisms exist in parallel. In endothelial cells, hypoxia induces AP-1 mediated transcription of target genes (Bandyopadhyay, Phelan and Faller, 1995). These target genes have been identified in other reports to be downstream of MAPK signalling after T cell activation (Edmead *et al.*, 1996). AP-1 is regulated alongside NFAT proteins and their transcription factors bind composite DNA sites (Atsaves *et al.*, 2019). These DNA sites have been located on the promoter regions of various cytokine genes, including, but not limited to, *IFNG*, *TNFA*, *IL-2*, and *IL2RA* (Macián, López-Rodríguez and Rao, 2001). Absence of AP-1, or NFAT, results in T cell anergy and/or exhaustion (Macián *et al.*, 2002; Martinez *et al.*, 2015). Endogenous NFAT tends to bind sites in co-operation with AP1 to induce exhaustion (Martinez *et al.*, 2015). However, late in the immune response, it has been suggested that NFAT promotes T cell exhaustion and anergy by binding to sites in exhaustion-related genes, e.g., PD-1 and TIM3, that do not require AP-1 co-operation (Martinez *et al.*, 2015). In exhausted cells, low Ca^{2+} signalling and increased basal Ca^{2+}, may enable NFAT to enter the nucleus to maintain an exhausted state (Martinez *et al.*, 2015). Therefore, the AP-1 pathway, alongside NFAT, may have roles in T cell activation in hypoxia.

1.2.3.3. AMP-activated protein kinase (AMPK) pathway

AMPK is activated after a drop in available energy, more specifically in response to altered AMP/ATP rations (Corton, Gillespie and Hardie, 1994; Hawley *et al.*, 2010; Mungai *et al.*, 2011). For example, cellular stress arising from a lack of glucose, inhibition of mitochondrial OXPHOS or, through the induction of ROS (Corton, Gillespie

and Hardie, 1994; Hawley *et al.*, 2010; Mungai *et al.*, 2011). AMPK is activated by LKB1 in cellular stress and CamKK2 in response to Ca^{2+} signals (Woods *et al.*, 2003; Woods *et al.*, 2005; Shaw *et al.*, 2004; Hawley *et al.*, 2005). AMPK is responsible for limiting energy usage by anabolic processes, and strengthening protein transport, glycolysis and mitochondrial biogenesis (Jornayvaz and Shulman, 2010; Hardie and Ashford, 2014; Lang and Föller, 2014). Downstream targets of AMPK include the suppression of mTORC1 activity and fatty acid synthesis through acetyl-CoA carboxylase (ACC) inhibition (Ma *et al.*, 2017). AMPK phosphorylation of unc-51 like autophagy activating kinase 1 (ULK1) stimulates mitochondrial biogenesis and mitophagy (Egan *et al.*, 2011; Kim *et al.*, 2011). It has been reported that AMPK is a vital player in T cell metabolic reprogramming, especially in glutamine-dependent mitochondrial metabolism and mRNA translation, and T cell function (Blagih *et al.*, 2015; Ma *et al.*, 2017). Since hypoxia puts the cell in danger of energetic stress, AMPK-dependent mechanisms may have a role in T cells activated in hypoxia.

1.2.3.4. Nuclear-factor κB (NF-κB) pathway

NF-κB comprises a family of transcription factors which are negatively regulated by IκB (as discussed in '***1.1.2.3. PKCθ-IKK-NF-κB pathway***') (D'Ignazio and Rocha, 2016). When NF-κB accumulates in the nucleus it binds DNA to exert its transcriptional effects (D'Ignazio and Rocha, 2016). Whilst the specific mechanism is unclear, hypoxia activates NF-κB and its downstream pathways, including apoptosis repression, induction of angiogenesis, and cell motility (D'Ignazio and Rocha, 2016). It has been reported that NF-κB has roles in T cell thymic development and differentiation, survival,

and effector functions (Busuttil *et al.*, 2010; Gerondakis *et al.*, 2014; Barnes *et al.*, 2015). Therefore, the pathway may also impact T cell activity in hypoxia.

1.2.3.5. Early growth response 1 (Egr1) pathway

The early growth response 1 (Egr1) transcription factor is activated early upon hypoxic exposure (Sperandio *et al.*, 2009). Studies have linked its upregulation with the stabilisation of HIF-1α and suggest it targets HIF-1α directly (Sperandio *et al.*, 2009). Egr1 upregulates the expression of N-myc down-regulated gene 1 (NDRG1), which has been shown to be involved with T cell anergy, however contraindications to this observation also exist (Zhang, Tchou-Wong and Costa, 2007; Oh *et al.*, 2015; Hodgson *et al.*, 2022).

1.2.4. Metabolic response to hypoxia

1.2.4.1. Inhibition of OXPHOS and reliance on glycolysis in hypoxia

To maintain ATP levels in hypoxia, the majority of cells increase dependence on glycolysis rather than oxygen-dependent OXPHOS (Kierans and Taylor, 2021). In steady state conditions, ATP controls allosteric inhibition over phosphofructokinase (PFK) and pyruvate kinase (PK) (Kierans and Taylor, 2021). The inhibition of OXPHOS by O_2 limitation results in reduced ATP production and a decreased ATP/ AMP ratio (Kierans and Taylor, 2021). This reduces the allosteric inhibition of ATP over PFK and PK to encourage use of ATP to generate fructose-1,6-biphosphate, and pyruvate from phosphoenolpyruvate, respectively (Kierans and Taylor, 2021). Therefore, driving glycolytic flux (Kierans and Taylor, 2021). Following these initial events, the stabilisation of HIF transcription factors in hypoxia upregulates expression of glycolytic

enzymes and glucose transporters to support increased glycolysis (Kierans and Taylor, 2021). Once the cellular ATP/AMP ratio and O_2 balance has been restored, cells often revert back to OXPHOS, known as the Pasteur effect (Kierans and Taylor, 2021). Cancer cells are able to manipulate increased glycolytic flux even in conditions of normoxia, and a similar mechanism is observed in T cells upon activation (Warburg, 1956; Gerriets and Rathmell, 2012). This phenomenon is known as the Warburg effect (Warburg, 1956). Benefits of the Warburg effect include the regeneration of cytosolic NAD^+ for use in the conversion of glyceraldehyde-3-phosphate to 1,3-biphosphoglycerate, and therefore, sustaining glycolysis (Arnold and Finley, 2023; Finley, 2023). The Warburg effect in cancer is known to support nutrient uptake, especially in nutrient-deprived environments, increased biomass generation and protein production, transcriptional regulation and chromatin remodelling, all of which are beneficial in T cell activation (Finley, 2023).

Alongside the HIF-1α-dependent upregulation of glycolytic genes in hypoxia, HIF-1α is also able to directly suppress OXPHOS (Kierans and Taylor, 2021). HIF-1α upregulates expression of PDK1 which phosphorylates the PDC complex and prevents acetyl-CoA being produced from pyruvate, the initiation step of the TCA cycle (Kim *et al.*, 2006; Papandreou *et al.*, 2006). HIF-1α also increases expression of lactate dehydrogenase A (LDHA) (Semenza *et al.*, 1996). LDHA is responsible for converting glycolysis-derived pyruvate to lactate, oxidising the cofactor NAD^+ to allow continued glycolysis (Kierans and Taylor, 2021). Excess lactate produced by the cell in hypoxia is removed by monocarboxylate transporter 4 (MCT4) (Ullah, Davies and Halestrap, 2006).

1.2.4.2. Reactive oxygen species (ROS) in hypoxia

In hypoxia, the majority of cells experience an increase in ROS from respiratory chain complexes I, II, and III, due to the imbalance of electron flow and O_2 in the ETC (Hamanaka and Chandel, 2009). This derives from a change in rate of electron flow through the ETC and how long the electrons are present at each respiratory chain complex (known as the 'electron dwell time') (Poyton, Ball and Castello, 2009). The shorter the dwell time, the lower the chance that electrons will leak and form free radicals (Poyton, Ball and Castello, 2009). The rate of electron flow through the ETC can be determined by a change in concentration of O_2, the inner mitochondrial membrane potential, and the ability of respiratory chain complexes to transport electrons (Poyton, Ball and Castello, 2009). Hypoxia is thought to slow electron transport, increasing the dwell time, and thus, the amount of ROS produced (Poyton, Ball and Castello, 2009). ROS production from complex III is vital for the stabilisation of HIF-1α in hypoxia (Hamanaka and Chandel, 2009). Too much ROS however results in cell death and damage (Hamanaka and Chandel, 2009). HIF-1α limits ROS production in hypoxia by diverting metabolism away from OXPHOS and towards glycolysis as discussed above (Kierans and Taylor, 2021). HIF-1α also directly regulates expression of cytochrome oxidase subunit 4 (COX4) to limit ROS generation (Fukuda *et al.*, 2007).

1.2.4.3. Reductive carboxylation in hypoxia

Whilst hypoxic cells switch ATP production towards glycolysis, they still require biomass production for viability and proliferation (Eales, Hollinshead and Tennant, 2016). For this, it has been described in different cell types that they adopt reductive

carboxylation of α-KG derived from glutamine (Eales, Hollinshead and Tennant, 2016). This generates citrate, which is used for lipid synthesis in hypoxia (Metallo *et al.*, 2011; Yoo *et al.*, 2020). The process uses the enzymes IDH 1 and 2, and aconitase (ACO) 1 and 2, and can be based in the cytosol or mitochondria (Eales, Hollinshead and Tennant, 2016).

1.2.5. Effects of hypoxia on protein synthesis

Energy-intensive protein synthesis is described to be suppressed in hypoxia (Hochachka *et al.*, 1996; Liu and Simon, 2004). Initially this relates to blunted translation, however with prolonged hypoxia and dropping O_2 levels this extends to transcription (Koumenis *et al.*, 2002; Liu and Simon, 2004). Of course, several transcription factors work to increase the expression of specific genes in hypoxia, for example HIF-1α, as discussed above (Wang and Semenza, 1993). Inhibition of protein synthesis in hypoxia has been shown to be under regulation of eukaryotic initiation factor 2 alpha (eIF2α) phosphorylation but is an effect that is reversed upon re-oxygenation (Koumenis *et al.*, 2002). The phosphorylation of eIF2α is driven by eukaryotic translation initiation factor 2 alpha kinase 3 (EIF2AK3, PERK) activation upon hypoxic exposure which may be driven by ER stress and is not HIF-dependent (Koumenis *et al.*, 2002). Therefore, effects on global protein synthesis should also be considered when performing experiments in hypoxia.

1.2.6. Effects of hypoxia on cell cycle progression

Hypoxia is well known to inhibit cell cycle progression in various cell types (Ortmann, Druker and Rocha, 2014; Druker *et al.*, 2021). Mechanisms driving cell cycle inhibition

have been shown to be HIF-dependent, for example the upregulation of cell cycle inhibitors p21 and p27 (Koshiji *et al.*, 2004; Lim *et al.*, 2006), HIF-1α dependent c-Myc regulation (Koshiji *et al.*, 2004), and microRNA expression (Ortmann, Druker and Rocha, 2014). However, HIF-1α independent mechanisms have also been shown to regulate the cell cycle in hypoxia, for example the blunting of DNA replication with hypoxia (Ortmann, Druker and Rocha, 2014.

1.3. Previous literature exploring T cells exposed to hypoxia

Despite not being well defined, a fair amount of literature exploring $CD8^+$ T cells in hypoxia already exists. However, many of these studies are contradictory, and it can be difficult to extrapolate the specific effects and mechanisms. On review of the literature, it becomes clear that the specific protocol used in each study has a substantial impact on the outcome of the results. The points below state what variable in a study protocol may impact the outcome of hypoxia on $CD8^+$ T cells:

- Species of origin of $CD8^+$ T cells E.g., mouse or human
- Are $CD8^+$ T cells freshly isolated or expanded *in vitro* prior to hypoxic exposure?
- When are $CD8^+$ T cells activated? E.g., prior to or during hypoxic exposure
- How are $CD8^+$ T cells activated? E.g., anti-CD3/CD28, PMA/ionomycin

Each of these variables may reflect a specific biological question and the protocol used should be kept in mind when interpreting results. For the purpose of this thesis, protocols used have been broadly split into three (P1, P2 and P3; **Figure 1.5**).

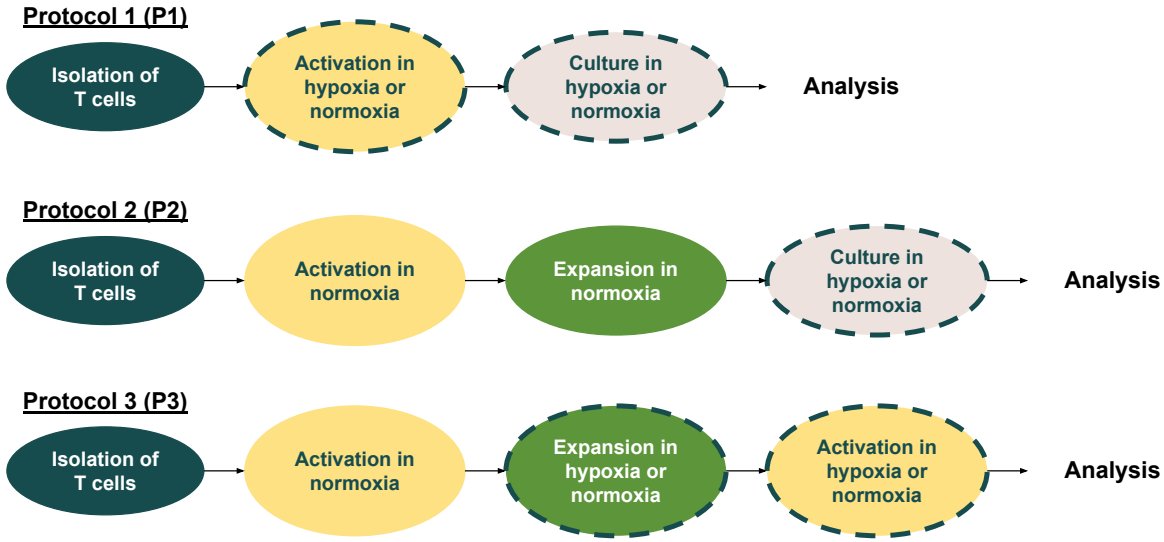

Figure 1.5. Diagram demonstrating three broad protocols typically implemented in the literature for *in vitro* experiments of T cells in hypoxia. Top = Protocol 1; Middle = Protocol 2; Bottom = Protocol 3. Blue = isolation of $CD8^+$ T cells/splenocytes. Yellow = activation of cells. Green = expansion into cytotoxic lymphocytes (CTLs) or differentiated $CD8^+$ T cells. Grey = culture of $CD8^+$ T cells/splenocytes. Dotted line = comparison of hypoxia and normoxia.

Protocol 1 (P1) reflects a situation in which a $CD8^+$ T cell is activated by its cognate antigen, or anti-CD3/CD28 antibodies, and directed to carry out its functional effect in hypoxia. The results of the experiment tell you how well the $CD8^+$ T cell has responded to activation in hypoxia and carried out its subsequent effects. To replicate this and determine the impacts of hypoxia on T cell activation and function, the $CD8^+$ T cells are cultured in hypoxia vs. normoxia immediately upon isolation. The cells are activated in hypoxia and cultured for a specific time period. As introduced in '**3. Results Chapter 1**', this is the protocol utilised in this thesis.

Protocol 2 (P2) rather reports how well a cell previously differentiated under normoxia, for example a cytotoxic lymphocyte (CTL) differentiated in the presence of IL-12, carries out its function when subsequently exposed to hypoxia. The $CD8^+$ T cells are isolated, activated and expanded in normoxia, and then once differentiated, exposed to hypoxia and analysed for functional readouts. Protocol 3 (P3) is similar, except after activation of T cells in normoxia, they are expanded in hypoxia. vs normoxia and then re-activated in the different O_2 conditions. This may reflect if a T cell is activated in the periphery but differentiates in a normoxic (P2) or hypoxic site (P3), and with or without re-activation by its antigen (P3 or P2, respectively). In order to sufficiently review the literature, studies are presented in **Table 1.1.** with their corresponding protocol and other variables used. They are then summarised below.

Table 1.1. Table presenting previous literature exploring $CD8^+$ T cells activated and cultured in hypoxia, split into three protocols (P1, P2, P3). Key findings and the overall effect of hypoxia (beneficial or inhibitory) is shown.

Study ID	Species	Protocol (Method*)	Key findings	Hypoxia beneficial or inhibitory?
Impacts of hypoxia on $CD8^+$ T cell activation				
Caldwell *et al.*, 2001	Mouse	**P1** – Isolated splenocytes and differentiated into CTLs over 5-6 days. Cultured in 20% vs 2.5% vs 1% O_2. The reducing agent 2-ME was included in media for 20% O_2 cultures, but not 2.5% or 1% O_2. NB: both $CD4^+$ and $CD8^+$ T cells included.	When differentiated in normoxia, a higher number $CD8^+$ CTLs were present and a greater number of these expressed CD25 than when differentiated at 2.5% O_2. However, activated cells at 2.5% O_2 had a higher surface density of CD25 expression.	Hypoxia may be inhibitory if observing overall activation, however, suggests CTLs differentiated at 2.5% develop more slowly with greater activation levels.
Doedens *et al*, 2013	Mouse	**P2** – Isolated $CD8^+$ T cells from splenocytes via negative selection and activated with anti-CD3/CD28 for 48 hours. Then cultured with fresh media + IL-2 +/- IL-4 for 24-48 hours to	In hypoxia, CTLs had increased expression of co-stimulatory molecules (OX40, GITR, 4-1BB0) than CTLs in normoxia. Co-inhibitory surface expression of LAG-3 and	Hypoxia beneficial

		differentiate into CTLs. Cultured in 21% or 1% O_2 for 6 hours.	CTLA-4 also increased in CTLs in hypoxia (HIF-1α dependent).	
Gropper *et al.*, 2017	Mouse	**P3** – Naïve $CD8^+$ T cells isolated from OT-I spleens, activated in normoxia, and expanded into CTLs in 20% vs 1% O_2 for 5 days. At 3 days, cells were activated with SINFEKL peptide + IL-2.	$CD8^+$ T cells expanded into CTLs in hypoxia expressed higher levels of TIM3 and LAG3, but no difference in CTLA4 and PD1.	May reflect greater activation status or higher expression of inhibitory receptors.
Hasan *et al.*, 2021	Human	**P1** – Naïve ($CD45RA^+$ $CCR7^+$) $CD8^+$ T cells isolated from PBMC and activated for 4 days in 20% vs 2% O_2. Then cultured for 2 days + TGF-β1 to form tissue-resident memory cells.	Cells differentiated to tissue-resident memory $CD8^+$ T cells in 2% O_2 increased expression of CD69, CD103, PD-1, CD101 and CXCR6, whilst no difference was observed in CD49a. Hypoxia was shown to be the main factor in increasing CD69 expression and TGF-β1 increased CD103 expression.	N/A
Liu *et al.*, 2020	Human	**P2** *(cells activated just prior to hypoxic exposure)* – Isolated T cells from peripheral blood samples of healthy donors, activated	Activated T cells exposed to hypoxia for 48 hours increased expression of CD39, PD-1,	Hypoxia beneficial to activation

		with OKT3 (anti-CD3), and then exposed to normoxia (21% O_2, normal cell culture) or hypoxia (1% O_2) for 48 hours. NB: both $CD4^+$ and $CD8^+$ T cells included.	and TIM-3 compared to those kept in normoxia.	
Palazon *et al.*, 2017	Mouse	**P2** – $CD8^+$ activated with anti-CD3/CD28 for 48 hours, expanded for 5 days + IL-2 (form CTLs). Then, cultured for 24 hrs in 21% vs 1% O_2.	Exposure of CTLs to hypoxia increased expression of co-stimulatory receptors (e.g., OX40, GITR) and checkpoint receptors.	Hypoxia beneficial
Ross, Rollings and Cantrell, 2021	Mouse	**P2** – P14 naïve $CD8^+$ T cells activated via TCR stimulation for 48 hours and expanded for 4 days in normoxia (18% O_2). Cells were then exposed to normoxia or hypoxia (1% O_2) for 24 hours.	Hypoxic CTLs upregulated co-inhibitory receptors PD-1, CTLA-4, Tim-3 and Lag-3, and upregulated co-stimulatory receptors ICOS, GITR, 4-1BB and OX40 compared to CTLs in normoxia. Hypoxic CTLs also increased protein abundance of CD3ε and CD3ζ in the TCR. Hypoxia also modulated the ratios of expression of co-stimulatory and co-inhibitory receptors.	May reflect the gain of an exhausted phenotype or heightened activation in hypoxia

Saragovi *et al.*, 2020	Mouse and human	**P1** – Splenocytes, or human PBMC, activated via CD3 and CD28 in atmospheric or 1% O_2 for 72 hours.	Mouse and human $CD8^+$ T cells reduced surface expression of CD25 when activated in 1% O_2 vs. 21% O_2.	Hypoxia inhibitory
Scharping *et al.*, 2022	Mouse	**P2/3** – OT-1 TCR transgenic T cells activated overnight with cognate peptide in normoxia (21% O_2), and then either cultured alone, + B16 cells, or + B16-expressing ovalbumin in normoxia or hypoxia (1.5% O_2) for 5 days + IL-2. Also performed experiments when isolated polyclonal T cells and activated with anti-CD3 and anti-CD28 overnight in normoxia (+ IL-2 + IL-12). Then cultured with IL-2 (acute activation), or with anti-CD3/CD28 + IL-2 (continuous activation) for 5 days in normoxia or hypoxia.	The presence of persistent antigen (continued stimulation) in hypoxia increased expression of PD-1 and Tim-3 and reduced T cell expansion compared to the other conditions (left). When T cells experience hypoxia or continuous stimulation alone, functionality is maintained. However when T cells experience hypoxia + continuous activation they increased expression of co-inhibitory receptors, CD39, and Tox (exhausted phenotype).	May reflect the gain of an exhausted phenotype in hypoxia

Vuillefroy de Silly *et al.*, 2015	Mouse	**P2/3** – Leucocytes isolated from spleen or lymph nodes of Pmel-1, OT-I or C57BL/6 mice and primed with relevant stimuli. Cells cultured at 21% or 5% O_2 for CTL expansion. Some cells moved to 1% O_2 for a killing assay or re-activation.	Increased CD25 on CTLs reactivated in hypoxia (1% O_2) vs. 21% or 5% O_2.	Hypoxia beneficial
Zhang *et al.*, 2017	Mouse	**P2, P3** – Isolated $CD8^+$ T cells from splenocytes prior to stimulation with anti-CD3/CD28 in 21% O_2 for 4 days, +/- with the last 16 hours in 1% O_2.	$CD8^+$ T cells exposed to hypoxia for the final 16 hours of culture demonstrate reduced blast formation than those kept in normoxia for the entire culture period. $CD8^+$ T cells exposed to hypoxia had reduced expression of PD-1 and T-bet and increased expression of Lag-3.	May suggest a reduction in activation due to hypoxia
Impacts of hypoxia on $CD8^+$ T cell cytotoxicity				
Caldwell *et al.*, 2001	Mouse	**P1** – Isolated splenocytes and differentiated into CTLs over 5-6 days. Cultured in 20% vs 2.5% vs 1% O_2. The reducing agent 2-ME	^{51}Cr release assays demonstrated that whilst fewer CD8 CTLs differentiated in hypoxic (2.5% O_2) vs normoxic condition	Hypoxia beneficial

		was included in media for 20% O_2 cultures, but not 2.5% or 1% O_2. NB: both $CD4^+$ and $CD8^+$ T cells included.	(20% O_2), on a per cell basis, they had greater cytolytic capacity. No difference in the expression of perforin, FasL and CTLA4 was observed between CTLs differentiated in normoxia and hypoxia.	
Doedens *et al.*, 2013	Mouse	**P2** – Isolated $CD8^+$ T cells from splenocytes via negative selection and activated with anti-CD3/CD28 for 48 hours. Then cultured with fresh media + IL-2 +/- IL-4 for 24-48 hours to differentiate into CTLs. Cultured in 21% or 1% O_2 for 6 hours.	In hypoxia, $CD8^+$ T cells had increased granzyme B expression than those in normoxia.	Hypoxia beneficial
Finlay *et al.*, 2012	Mouse	**P2** – Isolated lymphocytes from P14-LCMV or OT-I transgenic or non-transgenic mice, activated with LCMV or OT-I specific peptide, or anti-CD3, for 48 hours. Then, cells cultured for 6 days + IL-2 to generate CTLs. CTLs	CTLs switched to culture in hypoxia upregulated protein expression of perforin compared to those kept in normoxia for the entire culture period. This shown to be an	Hypoxia beneficial

		switched from 21% to 1% O_2 for 24 hours of culture.	indirect effect on gene expression (e.g., from a reduction in glucose levels).	
Gropper *et al.*, 2017	Mouse	**P3** – Naïve $CD8^+$ T cells isolated from OT-I spleens, activated in normoxia, and expanded into CTLs in 20% vs 1% O_2 for 5 days. At 3 days, cells were activated with SINFEKL peptide + IL-2. ***In vivo* –** implanted B16-OVA-td tomato tumour cells into mice. 7 days later, hypoxic vs normoxic CTLs (expanded as above) *i.v.* administered to mice.	$CD8^+$ T cells expanded into CTLs in hypoxia packaged more granzyme B into each cytolytic granule than those expanded to CTLs in normoxia. Perforin was similar in normoxic and hypoxic CTLs. *In vivo,* mice treated with CTLs expanded in hypoxia had improved survival and greater regression of tumours compared to mice treated with normoxia expanded CTLs.	Hypoxia beneficial
Liu *et al.*, 2020	Human	**P2** *(cells activated just prior to hypoxic exposure)* – Isolated T cells from peripheral blood samples of healthy donors, activated with OKT3 (anti-CD3), and then exposed to normoxia (21% O_2, normal cell culture) or hypoxia (1% O_2) for 48 hours.	Activated T cells exposed to hypoxia for 48 hours decreased secretion of granzyme B compared to those kept in normoxia.	Hypoxia inhibitory

		NB: both $CD4^+$ and $CD8^+$ T cells included.		
Palazon *et al.*, 2017	Mouse	**P2** – $CD8^+$ activated with anti-CD3/CD28 for 48 hours, expanded for 5 days + IL-2 (form CTLs). Then, cultured for 24 hrs in 21% vs 1% O_2.	Exposure of CTLs to hypoxia increased the expression of granzyme B.	Hypoxia beneficial
Ross, Rollings and Cantrell, 2021	Mouse	**P2 –** P14 naïve $CD8^+$ T cells activated via TCR stimulation for 48 hours and expanded for 4 days in normoxia (18% O_2). Cells were then exposed to normoxia or hypoxia (1% O_2) for 24 hours.	Increase in perforin and granzyme A protein in hypoxic CTLs compared to normoxic – shown to be due to the increased loading of granules with cytotoxic molecules, not due to increased activity of secretory mechanisms.	Hypoxia beneficial
Vuillefroy de Silly *et al.*, 2015	Mouse	**P2/3** – Leucocytes isolated from spleen or lymph nodes of Pmel-1, OT-I or C57BL/6 mice and primed with relevant stimuli. Cells cultured at 21% or 5% O_2 for CTL expansion. Some cells moved to 1% O_2 for a killing assay.	CTLs generated in 5% vs 21% O_2 had higher effector profile (increased granzyme B) and killing capacity. CTLs generated in 21% O_2 and exposed to 1% O_2 for 3 days before a killing assay had improved cytotoxicity, whilst CTLs generated in 5%	Hypoxia beneficial

			O_2 and exposed to 1% O_2 for 3 days did not.	
Zhang *et al.*, 2017	Mouse	**P2, P3** – To study resting $CD8^+$ T cells, isolated $CD8^+$ T cells from splenocytes and stimulated with anti-CD3/CD28 for 48 hours in normoxia. Then switched to media containing IL-2 without any additional stimulation for 96 hours in normoxia. Finally cultured in either 21% or 1% O_2 for 36 hours.	Resting $CD8^+$ T cells exposed to hypoxia had increased production of granzyme B, whilst polyfunctionality and effector molecule production were impaired compared to resting $CD8^+$ T cells kept in normoxia.	Hypoxia inhibitory for most functions, except granzyme B production
Impacts of hypoxia on $CD8^+$ T cell cytokine release and production				
Caldwell *et al.*, 2001	Mouse	**P1** – Isolated splenocytes and differentiated into CTLs over 5-6 days. Cultured in 20% vs 2.5% vs 1% O_2. The reducing agent 2-ME was included in media for 20% O_2 cultures, but not 2.5% or 1% O_2. NB: both $CD4^+$ and $CD8^+$ T cells included.	IL-2 accumulation was greater in CTLs differentiated in normoxia compared to hypoxia. Similarly, the amount, and rate of increase, of IFN-γ was greater in the supernatants of CTLs differentiated in normoxia than hypoxia.	Hypoxia may be inhibitory for IFN-γ and IL-2 accumulation. Hypoxia beneficial for VEGF expression.

			CTLs differentiated in 2.5% O_2 had quicker expression of VEGF than those differentiated in 20% O_2.	
Gropper *et al.*, 2017	Mouse	**P3** – Naïve $CD8^+$ T cells isolated from OT-I spleens, activated in normoxia, and expanded into CTLs in 20% vs 1% O_2 for 5 days. At 3 days, cells were activated with SINFEKL peptide + IL-2.	$CD8^+$ T cells expanded into CTLs in hypoxia had a higher secretion of IFN-γ compared to those expanded into CTLs in normoxia.	Hypoxia beneficial
Krieger, Landsiedel and Lawrence, 1996	Human	**P1** – Whole PBMC isolated from peripheral blood samples of healthy donors at atmospheric or 5% O_2. Cultured and stimulated with ConA in the two O_2 conditions.	CD69 raised in PBMC cultured in low O_2 conditions. Production of IFN-γ, IL-2 and IL-4 from PBMC was improved at 5% vs atmospheric O_2 when stimulated with ConA.	Hypoxia beneficial
Liu *et al.*, 2020	Human	**P2** *(cells activated just prior to hypoxic exposure)* – Isolated T cells from peripheral blood samples of healthy donors, activated with OKT3 (anti-CD3), and then exposed to normoxia (21% O_2, normal cell culture) or hypoxia (1% O_2) for 48 hours.	Activated T cells exposed to hypoxia for 48 hours decreased secretion of IFN-γ compared to those kept in normoxia.	Hypoxia inhibitory

		NB: both $CD4^+$ and $CD8^+$ T cells included.		
Naldini *et al.*, 1997	Human	**P1** – PBMC isolated from healthy human donors and cultured for 16 hours or 40 hours in 20% or 2% O_2 in the presence or absence of PHA. NB: both $CD4^+$ and $CD8^+$ T cells included.	No differences in viability between PBMC activated with PHA in normoxia and hypoxia. Hypoxia increased the production of IL-2, IL-4, IL-6, and IFN-γ 16 hours after PHA activation of PBMC vs. normoxia. TNF-α not affected by hypoxia. Production of IL-10 inhibited by hypoxia.	Hypoxia beneficial
Palazon *et al.*, 2017	Mouse	**P2** – $CD8^+$ activated with anti-CD3/CD28 for 48 hours, expanded for 5 days + IL-2 (form CTLs). Then, cultured for 24 hrs in 21% vs 1% O_2.	Exposure of CTLs to hypoxia increased production of IFN-γ and TNF-α.	Hypoxia beneficial
Ross, Rollings and Cantrell, 2021	Mouse	**P2 –** P14 naïve $CD8^+$ T cells activated via TCR stimulation for 48 hours and expanded for 4 days in normoxia (18% O_2). Cells were	Hypoxic CTLs had decreased protein expression of TNF and LTA, and increased IL-10 and IL-24 than normoxic CTLs. In resting CTLs, hypoxia did not impair IFN-γ	Hypoxia inhibitory

		then exposed to normoxia or hypoxia (1% O_2) for 24 hours.	release, but in antigen-stimulated CTLs, 24 hours of hypoxia led to decreased IFN-γ release. No difference was observed in TNF-α release.	
Scharping *et al.*, 2022	Mouse	**P2/3** – OT-1 TCR transgenic T cells activated overnight with cognate peptide in normoxia (21% O_2), and then either cultured alone, + B16 cells, or + B16-expressing ovalbumin in normoxia or hypoxia (1.5% O_2) for 5 days + IL-2. Also performed experiments when isolated polyclonal T cells and activated with anti-CD3 and anti-CD28 overnight in normoxia (+ IL-2 + IL-12). Then cultured with IL-2 (acute activation), or with anti-CD3/CD28 + IL-2 (continuous activation) for 5 days in normoxia or hypoxia.	The presence of persistent antigen (continued stimulation) in hypoxia reduced cytokine production polyfunctionality compared to the other conditions (left). When T cells experience hypoxia or continuous stimulation alone, functionality is maintained. However, hypoxic culture with continuous activation reduced polyfunctionality of cytokine production.	Hypoxia (+ continued activation) inhibitory

Vuillefroy de Silly *et al.*, 2015	Mouse	**P2/3** – Leucocytes isolated from spleen or lymph nodes of Pmel-1, OT-I or C57BL/6 mice and primed with relevant stimuli. Cells cultured at 21% or 5% O_2 for CTL expansion. Some cells moved to 1% O_2 for a killing assay or reactivation. Purified $CD8^+$ TILs for cytokine analysis.	CTLs in hypoxia secreted less IFN-γ, TNF-α, and IL-2. Re-activation of TILs in hypoxia decreased secretion of IFN-γ.	Hypoxia inhibitory on cytokine production
Zhang *et al.*, 2017	Mouse	**P2, P3** – Isolated $CD8^+$ T cells from splenocytes prior to stimulation with anti-CD3/CD28 in 21% O_2 for 4 days, +/- with the last 16 hours in 1% O_2. To study resting $CD8^+$ T cells, isolated $CD8^+$ T cells from splenocytes and stimulated with anti-CD3/CD28 for 48 hours in normoxia. Then switched to media containing IL-2 without any additional stimulation for 96 hours	$CD8^+$ T cells exposed to hypoxia for the final 16 hours of culture demonstrate reduced production of IFN-γ, granzyme B, and perforin than those kept in normoxia for the entire culture period – hypoxic exposure results in an overall reduction in polyfunctionality. Resting $CD8^+$ T cells exposed to hypoxia had increased production of granzyme B, whilst polyfunctionality and effector	Hypoxia inhibitory (beneficial for granzyme production in resting $CD8^+$ T cells)

		in normoxia. Finally cultured in either 21% or 1% O_2 for 36 hours.	molecule production were impaired compared to resting $CD8^+$ T cells kept in normoxia.	
Other impacts of hypoxia on $CD8^+$ T cell function				
Atkuri, Herzenberg and Herzenberg, 2005	Human	**P1** – Isolated PBMC in media at 10% O_2, then cultured for 5 days at 20%, 10% or 5% O_2 with stimulation with soluble PHA or ConA, or anti-CD3/CD28 coated plates.	Proliferation of PBMC ($CD4^+$ and $CD8^+$ T cells) was greatest in 20% O_2 compared to 10% and 5% O_2 with anti-CD3/CD28 and ConA stimulation. Proliferation of PBMC stimulated with PHA showed no differences between any of the O_2 levels. $CD8^+$ T cells survive or proliferate better with any stimulation than $CD4^+$ T cells at all O_2 levels.	Hypoxia inhibitory
Caldwell *et al.*, 2001	Mouse	**P1** – Isolated splenocytes and differentiated into CTLs over 5-6 days. Cultured in 20% vs 2.5% vs 1% O_2. The reducing agent 2-ME	CTLs expanded quicker after activation with SINFEKL peptide in 20% compared to 2.5% O_2 culture conditions.	Hypoxia inhibitory

		was included in media for 20% O_2 cultures, but not 2.5% or 1% O_2. NB: both $CD4^+$ and $CD8^+$ T cells included.	Higher expression of TCR and LFA-1 observed on CTLs differentiated in 2.5% compared to 20% O_2.	
Gropper *et al.*, 2017	Mouse	**P3** – Naïve $CD8^+$ T cells isolated from OT-I spleens, activated in normoxia, and expanded into CTLs in 20% vs 1% O_2 for 5 days. At 3 days, cells were activated with SINFEKL peptide + IL-2.	CTLs expanded in normoxia and hypoxia survived, and no excess cell death was observed. However, CTLs expanded in hypoxia had reduced proliferation and final cell counts.	Hypoxia inhibitory
Hasan *et al.*, 2021	Human	**P1** – Sorted naïve ($CD45RA^+$ $CCR7^+$) $CD8^+$ T cells from PBMC, equilibrated overnight in 20% or 2% O_2, activated the following morning via anti-CD3/CD28 beads for 4 days. TGF-β1 then added to culture for 2 days.	Naïve $CD8^+$ T cells differentiated in 2% O_2 with TGF-β1 vs. 20% O_2 with TGF-β1 upregulated various genes relevant to tissue-resident memory T cells (incl. CD69, CD103, PD1, CXCR6). Genes for T cell recirculation were downregulated in hypoxia with TGF-β1. Hypoxia induces $CD69^+$ cells, TGF-β1 induces $CD103^+$ cells, together synergistically promote tissue resident memory cells.	Hypoxia with TGF-β1 promotes the acquisition of a tissue-resident memory T cell phenotype.

Krieger, Landsiedel and Lawrence, 1996	Human	**P1** – Whole PBMC isolated from peripheral blood samples of healthy donors at atmospheric or 5% O_2. Cultured and stimulated with ConA in the two O_2 conditions. NB: both $CD4^+$ and $CD8^+$ T cells included.	CD69 raised in PBMC cultured in low O_2 conditions. Proliferation PBMC was improved at 5% vs atmospheric O_2 when stimulated with ConA.	Hypoxia beneficial
Larbi *et al.*, 2010	Human	**P1** – Human PBMC isolated from healthy donor peripheral blood, rested in 20% or 2% O_2 for 24 hours, and activated with anti-CD3/CD28 beads in the same O_2 conditions. NB: both $CD4^+$ and $CD8^+$ T cells included.	PBMC activated and cultured in 2% O_2 had impaired proliferation and had greater susceptibility to apoptosis compared to those activated and cultured in 20% O_2. Increased consumption of glucose observed in PBMC activated and cultured in 2% O_2 vs. 20% O_2, even in resting cells.	Hypoxia inhibitory
Liu *et al.*, 2020	Human	**P2** *(cells activated just prior to hypoxic exposure)* – Isolated T cells from peripheral blood samples of healthy donors, activated with OKT3 (anti-CD3), and then exposed to normoxia (21% O_2, normal cell culture) or hypoxia (1% O_2) for 48 hours.	Activated T cells (both $CD4^+$ and $CD8^+$ T cells) exposed to hypoxia for 48 hours had reduced proliferation than those kept in normoxia.	Hypoxia inhibitory

		NB: both $CD4^+$ and $CD8^+$ T cells included.		
Makino *et al.*, 2003	Human	**P2** *(re-activation in hypoxia vs normoxia)* – Isolated PBMC from peripheral blood, and then separated on nylon-wool columns to obtain the T cell rich fraction. T cells activated with PHA-M for 48 hours to generate T cell blasts, and then resuspended in fresh medium + IL-2. Cells were then cultured on anti-CD3 coated plates either in normoxia (21% O_2) or hypoxia (1% O_2). NB: both $CD4^+$ and $CD8^+$ T cells included.	Method of culture induced activation-induced cell death (AICD) in T cells in normoxia, which was reduced when cells were re-activated in hypoxia. Culturing T cells at a range of O_2 tensions (between 21% and 1% O_2) demonstrated that with anti-CD3 re-activation survival increased as O_2 levels decreased, whilst with no re-activation survival decreased with reducing O_2 levels. This is dependent on HIF-1α.	Hypoxia beneficial for AICD
Naldini *et al.*, 1997	Human	**P1** – PBMC isolated from healthy human donors and cultured for 16 hours or 40 hours in 20% or 2% O_2 in the presence or absence of PHA. NB: both $CD4^+$ and $CD8^+$ T cells included.	No differences in viability between PBMC activated with PHA in normoxia and hypoxia. Proliferation of PHA activated PBMC impaired in hypoxia vs. normoxia.	Hypoxia inhibitory
Palazon *et al.*, 2017	Mouse	**P2** – $CD8^+$ activated with anti-CD3/CD28 for 48 hours, expanded for 5 days + IL-2 (form	Exposure of CTLs to hypoxia reduced their survival.	Hypoxia inhibitory

		CTLs). Then, cultured for 24 hrs in 21% vs 1% O_2.		
Ross, Rollings and Cantrell, 2021	Mouse	**P2 –** P14 naïve $CD8^+$ T cells activated via TCR stimulation for 48 hours and expanded for 4 days in normoxia (18% O_2). Cells were then exposed to normoxia or hypoxia (1% O_2) for 24 hours.	CTLs in hypoxia had reduced proliferation than those in normoxia. CTLs in hypoxia had a slight reduction in the activity of protein translation, but not abundance of translation machinery than those in normoxia.	Hypoxia inhibitory
Saragovi *et al.*, 2020	Mouse and human	**P1** – Splenocytes, or human PBMC, activated via CD3 and CD28 in atmospheric or 1% O_2 for 72 hours.	Mouse and human $CD8^+$ T cells reduced proliferation when activated in 1% O_2 vs. 21% O_2.	Hypoxia inhibitory
Scharping *et al.*, 2022	Mouse	**P2/3** – OT-1 TCR transgenic T cells activated overnight with cognate peptide in normoxia (21% O_2), and then either cultured alone, + B16 cells, or + B16-expressing ovalbumin in normoxia or hypoxia (1.5% O_2) for 5 days + IL-2.	Both exposure to hypoxia and continuous activation alone slightly impaired T cell activation, however the combination of the two conditions decreased cell number accumulation. This was not due to a lack of proliferation but a susceptibility to increased cell death.	Hypoxia inhibitory

		Also performed experiments when isolated polyclonal T cells and activated with anti-CD3 and anti-CD28 overnight in normoxia (+ IL-2 + IL-12). Then cultured with IL-2 (acute activation), or with anti-CD3/CD28 + IL-2 (continuous activation) for 5 days in normoxia or hypoxia.	Cells experiencing both hypoxia and continuous stimulation develop a transcriptional phenotype indicative of an exhausted-like state. Effects appear to be independent of HIF (see **Table 5.1.**)	
Other methods to induce hypoxia and impacts on $CD8^+$ T cell function				
Colombani *et al.*, 2023	Mouse	Isolated OT-I T cells and co-cultured with B16-OVA tumour cells in a hypoxia-inducing cyrogel. B16-OVA cells cultured for 3 hours in either a blank, or hypoxia-inducing, cryogel in normoxia, then co-cultured with OT-I T cells for 24 hours in normoxia (standard incubator, 18.6% O_2) or hypoxia (1% O_2).	Both hypoxia and co-culture in the hypoxia-inducing cyrogels diminished the cytotoxic activity of OT-I T cells and their ability to kill B16-OVA tumour cells. Hypoxia and hypoxia-inducing cryogels both increased expression of CD69, CTLA4, and H2Kb on the OT-I T cells, but decreased expression of CD25, MHC-I, CD44, LAG3, CD137, and PD1 on the	Hypoxia inhibitory to cytotoxic function

			surface of OT-I T cells. The ability of OT-I T cells to produce perforin, granzyme B, IFN-γ and TNF-α were also impaired in hypoxia and hypoxia-inducing cryogels.	
de Almedia *et al.*, 2020	Mouse	Anti-VEGF treatment increased HIF-1α protein in *in vitro* experiments. Treatment of mice with CT26 or Cloudman tumours with anti-VEGF increased pimonidazole staining in tumours via disruption of angiogenesis. $CD8^+$ T cells analysed *ex vivo* or stimulated with PMA and ionomycin for 5 hours.	Anti-VEGF treatment reduced the expression of inhibitory molecules PD-1 and TIM3 but increased the expression of co-stimulatory molecule OX40 on $CD8^+$ T cells analysed *ex vivo*, compared to no treatment. Treatment with anti-VEGF resulted in a higher $CD8^+$ T cell frequency producing IFN-γ, TNF-α, or both, after PMA/ionomycin stimulation, than no treatment. $CD8^+$ T cells from tumours of anti-VEGF treated mice had a greater production of	Hypoxia induced by anti-VEGF treatment beneficial for $CD8^+$ T cell function

			granzyme B and an upregulation of PRF1 than from tumours of non-treated mice. Effects also seen in an antigen-specific manner.	
de Ponte Conti *et al.*, 2021	Mouse	Mice injected with pimonidazole and puromycin, 1 hour later $CD8^+$ TILs purified and stained for analysis.	There is an inverse relationship between pimonidazole and puromycin staining – as O_2 tension drops (pimonidazole staining increases), puromycin staining decreases and translation efficiency drops.	Hypoxia inhibitory to translation efficiency
Saragovi *et al.*, 2020	Mouse	C57BL/6 mice primed with a viral challenge (Lv-OVA) for 24 hours before transfer to chambers at 21% or 8% O_2 (chronic hypoxia) for 6 days. Cells extracted from lymph nodes and analysed by flow cytometry.	Mice treated under chronic hypoxia had decreased ratios of numbers of $CD62L^-CD25^+$ and $CD62L^-CD44^+CD25^+$ Ova-associated $CD8^+$ T cells compared to control. Decrease in percentage of Ki67 positive Ova-associated $CD8^+$ T cells in chronic hypoxia compared to control.	Hypoxia inhibitory

Zhang *et al.*, 2021	Mouse	Overexpression of DLL1 in tumour cell lines which induced normalisation of tumour vasculature. This reduced tissue hypoxia.	Overexpression of DLL1 (and reduction of hypoxia) improved the production of IFN-γ in $CD8^+$ T cells, alongside upregulating the expression of genes for anti-tumour function (*Ifng*, *Tnfa*, *Prf1* and *Gzmb*).	Hypoxia may be inhibitory to $CD8^+$ T cell function

* *Time of exposure to hypoxia, level of oxygen during activation, method of activation, etc.*

1.3.1. Studies using P1 to explore CD8$^+$ T cells in hypoxia

1.3.1.1. Impact of using P1 on CD8$^+$ T cell activation in hypoxia

In murine experiments, a fewer number of splenocytes differentiated to CTLs in hypoxia vs. normoxia expressed CD25, a key activation marker, however, activated CTLs in hypoxia had a greater surface density of CD25 (Caldwell *et al.*, 2001). Thus, while hypoxia may appear to inhibit CD25 expression at the population level, individual CTLs in hypoxia were more activated. In another study, mouse and human CD8$^+$ T cells activated via CD3/CD28 in hypoxia demonstrated reduced expression of CD25 compared to those activated at atmospheric conditions (Saragovi *et al.*, 2020). Therefore, it is not clear the impact of hypoxia specifically on T cell activation status.

1.3.1.2. Impact of using P1 on CD8$^+$ T cell cytotoxicity in hypoxia

Mouse splenocytes differentiated to CTLs in hypoxia had improved cytolytic capacity over those differentiated in normoxia, however no difference in the expression of perforin or Fas ligand was observed (Caldwell *et al.*, 2001). Thus, it is unclear from the study precisely how the activation of human T cells in hypoxia impacts their cytotoxicity.

1.3.1.3. Impact of using P1 on CD8$^+$ T cell cytokine release and production in hypoxia

CTLs differentiated from mouse splenocytes in hypoxia had impaired IFN-γ and IL-2 production compared to those differentiated in normoxia (Caldwell *et al.*, 2001), suggesting activation of freshly isolated T cells in hypoxia inhibits cytokine release and production. In contrast, activation of peripheral blood mononuclear cells (PBMC) with

concanavalin A improved the production of IFN-γ, IL-2 and IL-4 in 5% O_2 (physioxia) compared to atmospheric O_2 (Krieger, Landsiedel and Lawrence, 1996), and healthy human PBMC activated with phytohaemagglutinin P (PHA) in hypoxia had greater production of IFN-γ, IL-2, IL-4, and IL-6, and reduced production of IL-10, than those activated in normoxia (Naldini *et al.*, 1997). Therefore, the method of T cell stimulation impacts the functional outcomes of hypoxia, but generally, the differentiation of CTLs in hypoxia impairs their cytokine production.

1.3.1.4. Impact of using P1 on other $CD8^+$ T cell functions in hypoxia

Proliferation of mouse splenocytes differentiated to CTLs in hypoxia was impaired compared to those differentiated in normoxia (Caldwell *et al.*, 2001), which was similarly shown in human T cells activated in hypoxia (Larbi *et al.*, 2010). Mouse and human $CD8^+$ T cells activated via CD3/CD28 in hypoxia had impaired proliferation compared to those activated in atmospheric O_2 conditions (Saragovi *et al.*, 2020). In human PBMC stimulated via CD3/CD28, it has been reported that increasing O_2 level correlates with improved proliferation, therefore hypoxia is inhibitory to T cell proliferation (Atkuri, Herzenberg and Herzenberg, 2005). However, this is not the case with PHA stimulation of human PBMC (Naldini *et al.*, 1997; Atkuri, Herzenberg and Herzenberg, 2005). Proliferation of PBMC was improved in 5% (physioxia) vs atmospheric O_2 when stimulated with concanavalin A (Krieger, Landsiedel and Lawrence, 1996). Hence, it appears hypoxia inhibits T cell proliferation after recent activation via CD3/CD28, but not with other methods of T cell stimulation.

1.3.2. Studies using P2 or P3 to explore $CD8^+$ T cells in hypoxia

1.3.2.1. Impact of using P2 or P3 on $CD8^+$ T cell activation in hypoxia

Isolated T cells from human peripheral blood cultured in hypoxia after activation increased expression of CD39, programmed cell death protein-1 (PD-1), and T cell immunoglobulin and mucin-domain containing-3 (Tim-3) compared to those in normoxia (Liu *et al.*, 2020). This may reflect a greater activation status of T cells in hypoxia or be reflective of an exhausted phenotype. Importantly these cells were activated prior to hypoxic exposure so no conclusions can be drawn about the impact of hypoxia on activation. When $CD8^+$ T cells are isolated from mouse splenocytes, expanded into CTLs in normoxia and then cultured briefly in hypoxia they express greater levels of co-stimulatory and co-inhibitory receptors than those cultured constantly in normoxia (Doedens *et al.*, 2013; Palazon *et al.*, 2017; Ross, Rollings and Cantrell, 2021), suggesting an improvement of activation status with hypoxia. CTLs differentiated in hypoxia compared to normoxia expressed greater levels of TIM3 and lymphocyte-activation gene 3 (LAG3), but not cytotoxic T-lymphocyte associated protein 4 (CTLA4) or PD-1 (Gropper *et al.*, 2017), which may reflect increased activation status or inhibitory receptor expression. However, another study showed that moving $CD8^+$ T cells to hypoxia for the final 16 hours of a 4-day normoxic stimulation reduced blast formation, PD-1 and T-box transcription factor (TBX21, T-bet) expression, but increased Lag-3 expression (Zhang *et al.*, 2017), potentially reflective of a reduced activation status when moved to normoxia. Importantly, T cells experiencing continuous stimulation and hypoxia simultaneously developed an exhausted phenotype (Scharping *et al.*, 2021). CTLs reactivated in 1% O_2 upregulated CD25 expression compared to CTLs reactivated in 21% or 5% O_2 (Vuilleyfroy de Silly

et al., 2015). Overall, T cells previously differentiated to CTLs in normoxia may develop an improved activation status when moved to hypoxia, however this also may reflect an exhausted phenotype.

1.3.2.2. Impact of using P2 or P3 on CD8$^+$ T cell cytotoxicity in hypoxia

When human T cells are activated in normoxia prior to exposure to hypoxia they reduced their secretion of granzyme B, suggesting an inhibitory effect of hypoxia (Liu *et al.*, 2020). However, when T cells are expanded into CTLs from mouse splenocytes in normoxia prior to hypoxic exposure, they develop a more cytolytic phenotype in hypoxia. For example, an increased granzyme B expression (Doedens *et al.*, 2013; Palazon *et al.*, 2017) and perforin expression (Finlay *et al.*, 2012; Ross, Rollings and Cantrell, 2021) was observed in CTLs cultured briefly in hypoxia. For CTLs expanded and re-activated in hypoxia, they increased the production of, and the amount of granzyme B packaged into each cytolytic granule than CTLs expanded in normoxia (Vuilleyfroy de Silly *et al.*, 2015; Gropper *et al.*, 2017). A similar effect with increased granzyme B expression was observed in resting T cells cultured for 36 hours in hypoxia (Zhang *et al.*, 2017). Therefore, unlike when T cells are activated in hypoxia (P1) or immediately exposed to hypoxia following activation (Liu *et al.*, 2020), CTL culture in hypoxia after expansion appears to be beneficial to cytotoxic function.

1.3.2.3. Impact of using P2 or P3 on CD8$^+$ T cell cytokine release and production in hypoxia

Unlike P1, hypoxic culture of CTLs previously expanded in normoxia, or further expansion of CTLs in hypoxia, appears to promote IFN-γ and TNF-α secretion

(Gropper *et al.*, 2017; Palazon *et al.*, 2017). In contrast, hypoxia and continuous activation resulted in a reduction of overall polyfunctionality of cytokine production (Scharping *et al.*, 2021), which was similar to culture of resting $CD8^+$ T cells in hypoxia for the final 16 hours of their culture (Zhang *et al.*, 2017). Activated human T cells exposed to hypoxia, compared to normoxia, had a reduction in IFN-γ secretion (Liu *et al.*, 2020). CTLs activated and expanded in normoxia before 24 hours in hypoxia reduced release of IFN-γ, but not of TNF-α (Ross, Rollings and Cantrell, 2021). In another study, CTLs reactivated in hypoxia reduced secretion of IFN-γ, TNF-α, and IL-2 compared to those in 5% or 21% O_2 (Vuilleyfroy de Silly *et al.*, 2015). It is apparent that the conditions of T cell culture impact the overall outcomes on cytokine release and production.

1.3.2.4. Impact of using P2 or P3 on other $CD8^+$ T cell functions in hypoxia

Whilst each different protocol appears to impact T cell functions such as cytokine release and cytotoxicity, proliferation of T cells is generally reported to be impaired in hypoxia (Ross, Rollings and Cantrell, 2021), even in CTLs that have previously been expanded and re-activated in hypoxia (Gropper *et al.*, 2017). Exposure of already differentiated CTLs to hypoxia also impairs their survival (Palazon *et al.*, 2017), whilst continuous activation and hypoxic exposure increased susceptibility to cell death (Scharping *et al.*, 2021). In contrast, PBMC activated with PHA to generate T cell blasts in normoxia and then re-activated in hypoxia had a reduction in susceptibility to activation-induced cell death (Makino *et al.*, 2003).

1.3.3. Impact of using other methods to induce hypoxia on $CD8^+$ T cell function

In one study, researchers induced hypoxia by using an anti-VEGF treatment to disrupt angiogenesis in tumours (de Almeida *et al.*, 2020). As generally observed with P2 and P3, hypoxia induced in this method appears to improve cytotoxic molecule and cytokine production in $CD8^+$ T cells (de Almeida *et al.*, 2020). On the other hand, OT-I T cells co-cultured with B16-OVA tumour cells in a hypoxia-inducing cryogel had impaired cytokine and cytotoxic molecule production compared to those co-cultured in a blank cryogel (Colombani *et al.*, 2023). Similarly, reduction of hypoxia via overexpression of delta-like 1 (DLL1) and tumour vessel normalisation improved $CD8^+$ T cell production of IFN-γ and upregulated the expression of anti-tumour genes (Zhang *et al.*, 2021). Mice administered a viral challenge prior to housing in a chamber set at 8% O_2 for 6 days had a reduction in $CD8^+$ T cells positive for the proliferation marker, antigen kiel 67 (Ki67), and CD25 compared to those housed at 21% O_2 (Zhang *et al.*, 2021). Thus, the method used to induce hypoxia has an impact on overall T cell function.

The different impacts on $CD8^+$ T cell function from the timing of hypoxic exposure has been explored by Saragovi *et al.* (2020). The researchers showed that $CD8^+$ T cells activated in normoxia and transferred to hypoxia for 5 hours had impaired CD25 surface expression and proliferation compared to those kept in normoxia, whilst $CD8^+$ T cells transferred to hypoxia for 18 hours did not experience effects to the same extent (Saragovi *et al.*, 2020). Therefore, it is important to analyse findings depending on the protocol used. The overall impacts of each protocol on T cell activation and function are summarised in **Figure 1.6.** below.

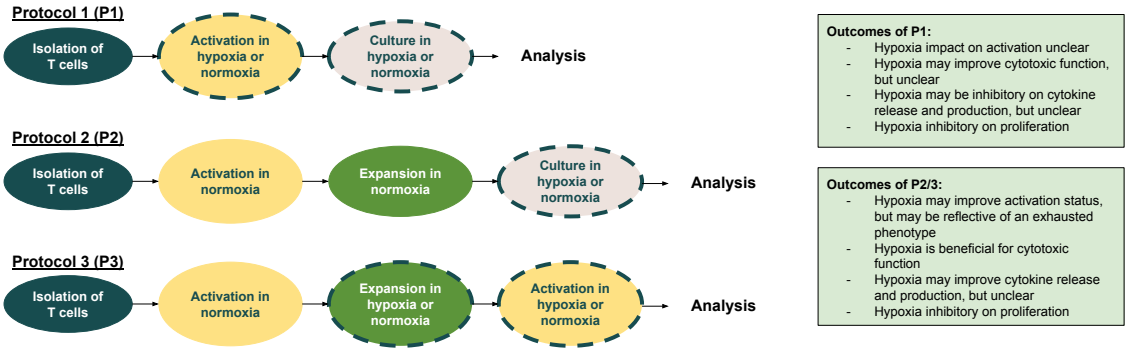

Figure 1.6. Diagram demonstrating three broad protocols typically implemented in the literature for *in vitro* experiments of T cells in hypoxia, with overall impacts of each protocol on T cell activation and function shown. Top = Protocol 1; Middle = Protocol 2; Bottom = Protocol 3. Blue = isolation of $CD8^+$ T cells/splenocytes. Yellow = activation of cells. Green = expansion into cytotoxic lymphocytes (CTLs) or differentiated $CD8^+$ T cells. Grey = culture of $CD8^+$ T cells/splenocytes. Dotted line = comparison of hypoxia and normoxia. Right: overall impacts of each protocol on T cell activation and function.

1.4. Introduction to multiple myeloma (MM)

Multiple myeloma (MM), a haematological cancer, arises from the abnormal clonal proliferation of plasma cells in the bone marrow (BM) (Cowan *et al.*, 2022). Roughly 6,000 individuals are diagnosed with MM every year and the disease accounts for 2% of all new UK cancer diagnoses (2016-2018 data) (Cancer Research UK, 2015). MM is a disease of the older adult, with incidence rates highest in individuals aged 85 to 89 years (2016-2018 data) (Cancer Research UK, 2015). Whilst significant improvements have been made in the treatment and management of MM, it remains an incurable disease (Ravi *et al.*, 2018). This section will introduce MM and current therapeutic options, before exploring the importance of $CD8^+$ T cells and hypoxia in the disease.

1.4.1. MM pathophysiology

Plasma cells originate from the lymphoid B-cell lineage and represent a terminally differentiated phenotype, typically characterised by expression of CD38, CD138 and B cell maturation antigen (BCMA) (Bataille *et al.*, 2006). MM belongs to a spectrum of disease known as plasma cell dyscrasias, since it arises from the clonal proliferation of plasma cells (Kazandjian, 2016). Importantly, plasma cell dyscrasias encompass benign and malignant disease states, including monoclonal gammopathy of undetermined significance (MGUS), smouldering multiple myeloma (SMM), and MM (Kazandjian, 2016). MGUS is an asymptomatic precursor to MM (Landgren *et al.*, 2004). Whilst all MM cases originate from MGUS (Landgren *et al.*, 2004; Weiss *et al.*, 2009), not all individuals with MGUS will develop MM (Kyle *et al.*, 2004). SMM reflects individuals who meet the diagnostic criteria for MM but are asymptomatic and do not develop end-organ damage (Kazandjian *et al.*, 2014). Similar to MGUS, all MM cases

develop from SMM, but not all individuals with SMM will progress to MM (Kazandjian, 2016).

The diagnostic criteria for MM and other plasma cell dyscrasias have been developed by the International Myeloma Working Group (Rajkumar, 2022). The MM diagnostic criteria includes, but is not limited to, the presence of ≥ 10% BM clonal plasma cells and end-organ damage (Rajkumar, 2022). End-organ damage in MM arises from the production and accumulation of monoclonal immunoglobulins, or paraprotein, from clonal plasma cells which result in the presentation of 'CRAB' complications: hypercalcaemia ('C'), renal insufficiency ('R'), anaemia ('A'), and bone lesions ('B') (Albagoush, Shumway and Azevedo, 2023). Patients may present with a diverse and complicated set of symptoms which often makes diagnosis difficult or late (Albagoush, Shumway and Azevedo, 2023). In the United Kingdom, the most common route to MM diagnosis is via emergency presentation (Howell *et al.*, 2017).

1.4.1.1. $CD8^+$ T cell dysfunction in MM

It is well reported that the immune system, including T cell populations, is dysfunctional in MM, which importantly correlates with patient outcomes (Pratt, Goodyear and Moss, 2007). For example, decreased $CD4^+$ and $CD8^+$ T cell frequency is associated with a worse survival (Kay *et al.*, 2001). MM patients have been shown to have abnormal CD4:CD8 ratios (Mills and Cawley, 1983), downregulated T cell surface CD28 expression (Brown *et al.*, 1998), and disrupted cytokine networks (Frassanito, Cusmai and Dammacco, 2001). We have recently reported that $CD8^+$ T cells present in the BM in MM are dysfunctional when compared to their peripheral blood (PB) counterparts,

and when compared to healthy control BM cells (Gudgeon *et al.*, 2023). Specifically, BM $CD8^+$ T cells produce less IFN-γ, TNF-α, IL-2 and granzyme-B, than $CD8^+$ T cells in the PB of MM patients, which was not the case of $CD4^+$ T cells (Gudgeon *et al.*, 2023). Since cytotoxic $CD8^+$ T cells are key effectors in the destruction of malignant myeloma cells, their dysfunction may be detrimental to patient outcomes.

1.4.2. Immuno-therapeutic strategies in MM

1.4.2.1. Autologous stem cell transplantation

The treatment strategy for newly diagnosed MM firstly determines if the individual is symptomatic or asymptomatic (Bird and Boyd, 2019). Asymptomatic patients are regularly monitored, but generally do not undergo active treatment, with key exceptions (Bird and Boyd, 2019). On the other hand, symptomatic patients are classified according to their suitability to undergo autologous stem cell transplantation. Patients deemed suitable for stem cell transplantation undergo intensive induction treatment to reduce disease burden before transplantation (Gertz and Dingli, 2014). Usually this includes drugs from three classes, for example, immunomodulatory drugs (IMiDs) (e.g., thalidomide), a proteosome inhibitor (e.g., bortezomib), and a corticosteroid (e.g., dexamethasone) (Gertz and Dingli, 2014). After induction, patients undergo autologous stem cell transplantation (Gertz and Dingli, 2014). This includes collection of haemopoietic stem cells from the patient, high dose chemotherapy to remove malignant cells, and stem cell transplantation to encourage early reconstitution of the BM (Gertz and Dingli, 2014). Since MM is a disease of the older individual, many patients have co-morbidities which deem them unsuitable for stem cell transplantation (Bird and Boyd, 2019). Instead, they are managed with a combination of therapies in

two or three different drug classes, at lower doses, but for longer periods (Bird and Boyd, 2019). These include IMiDs, chemotherapy, and corticosteroids (National Institute for Health and Care Excellence, 2018; Bird and Boyd, 2019).

1.4.2.2. Immunomodulatory drugs (IMiDs) and engagement of $CD8^+$ T cells

IMiDs, including thalidomide and second-generation lenalidomide and pomalidomide, are widely used in MM. IMiDs conduct both direct effects against the myeloma cells, and indirect effects by engaging the function of other cells in the BM microenvironment, including immune cells. Importantly, IMiDs harness the function of $CD8^+$ T cells (Zhu, Kortuem and Stewart, 2013). *In vitro* experiments have demonstrated that administration of thalidomide to CD3-activated T cells can increase production of IFN-γ and IL-2, especially in $CD8^+$ T cells (Haslett *et al.*, 1998). Second-generation IMiDs are increasingly potent at engaging T cells in MM therapy (Corral *et al.*, 1999; Marriott *et al.*, 2002). The protein cereblon (CRBN) has been characterised as responsible for the anti-myeloma activity of IMiDs (Zhu *et al.*, 2011). CRBN signals downstream and inhibits interferon regulatory factor 4 (IRF4), a critical protein for myeloma cell survival (Zhu, Kortuem and Stewart, 2013). Inhibition of CRBN expression in human T cells treated with IMiDs reduced IL-2 and TNF-α production compared to cytokine production by human T cells with intact CRBN treated with IMiDs (Lopez-Girona, 2012). IMiDs are also reported to enhance T cell co-stimulation (Zhu, Kortuem and Stewart, 2013). Therefore, IMiDs partially rely on the effective functioning of $CD8^+$ T cells for their therapeutic outcomes.

1.4.2.3. Monoclonal antibodies

A number of monoclonal antibodies have been approved for use in MM, including anti-CD38 (e.g., daratumumab) (Shah and Mailankody, 2020). MM cells have much greater expression of CD38 than normal immune cells, so targeting CD38 with daratumumab induces direct anti-tumour activity (Sanchez *et al.*, 2016). Daratumumab also has immunomodulatory activity, engaging immune mechanisms. For example, depletion of CD38-expressing Tregs with daratumumab stimulates the expansion of effector T cell populations and function (Krejcik *et al.*, 2016).

1.4.2.4. Chimeric-antigen receptor (CAR)-T cells

Chimeric-antigen receptor, or CAR-, T cells are genetically modified autologous or allogenic human T cells that are encoded to express a receptor for a specific tumour antigen (Shah and Mailankody, 2020). In MM, CAR-T cells are being trialled targeting BCMA present on the MM cell surface (Shah and Smith, 2019), which follows the success of CD19 targeting CAR-T cells in refractory large B cell lymphoma and acute lymphoblastic leukaemia (Neelapu *et al.*, 2017; Maude *et al.*, 2018). Of course, for a CAR-T cell to be effective in engaging and killing tumour cells the modified T cells need to be functional within the TME.

1.4.2.5. Bispecific antibodies

Bispecific monoclonal antibodies engage cytotoxic T cells and tumour cells and bring them into direct contact to encourage anti-tumour killing (Shah and Mailankody, 2020). One type of bispecific antibody are bispecific T cell engagers (BiTE) (Cohen, 2019). Compared to IgG-like bispecific antibodies, BiTE's have a short half-life and thus, their

efficacy relies upon continuous infusion (Cohen, 2019; Ma, J. *et al.*, 2021). In MM, BiTEs are being developed which engage CD3 on T cells and BCMA on the MM cells (e.g., AMG 420) (Shah and Mailankody, 2020). AMG 420 has shown efficacy in preclinical and early phase human MM studies (Hipp *et al.*, 2017; Topp *et al.*, 2020). Since BiTEs rely on cytotoxic activity from patient T cells, the effective functioning of T cells within the TME is crucial for their optimal efficacy.

Overall, it is clear that that despite T cells being shown to be dysfunctional in the MM TME, many therapeutic strategies to kill MM cells rely on the effective functioning of T cells.

1.4.3. Hypoxia in MM

Since the BM has low physiological O_2 tensions (Chow *et al.*, 2001; Harrison *et al.*, 2002; Spencer *et al.*, 2014), and it is well known that many solid TME are hypoxic (Muz *et al.*, 2015), it can be expected that the TME of MM is also hypoxic. Many technical challenges arise when assessing the O_2 level of the BM, given the difficulty with sample access and exposure to the surrounding atmosphere. However, Colla et al. (2010) showed vast HIF-1α protein expression by immunohistochemistry in the BM of MM patients in $CD38^+$ MM cells, indicating a hypoxic environment, although no difference in HIF-1α target gene mRNA was observed between MM and MGUS samples (Colla *et al.*, 2010). Use of the 5T2MM murine model and staining with the 2-nitroimidazole hypoxia marker, pimonidazole, revealed a hypoxic environment in both healthy and MM BM, albeit the MM BM was more hypoxic (Asosingh *et al.*, 2005). Pimonidazole works by becoming reductively activated and forming stable adducts with thiol groups

in amino acids and proteins specifically within hypoxic cells (Raleigh and Koch, 1990; Aguilera and Brekken, 2014). HIF-1α staining was also increased in MM BM compared to control mice (Asosingh *et al.*, 2005). A more recent study collected data from the Gene Expression Omnibus database and used a collection of 198 hypoxia-related genes to group MM patients into hypoxia 'high' or 'low' groups (Li *et al.*, 2022). They classified patients also by immune status and found that MM patients with higher immune scores had improved survival (Li *et al.*, 2022). MM patients with a 'low' hypoxia, but 'high' immune status had the best survival, whilst patients with a 'high' hypoxia, but 'low' immune status had the worst survival, suggesting that the immune microenvironment and hypoxic nature of the MM BM are functionally interlinked (Li *et al.*, 2022). However, whether the hypoxic nature of the TME is directly related to the immune dysfunction in MM is not well understood.

1.5. Aims and objectives

I hypothesise that the hypoxic nature of the TME may contribute to $CD8^+$ T cell immunosuppression in MM. Understanding if and how hypoxia impairs $CD8^+$ T cell function, in the context of MM, will help to explore this hypothesis. Therefore, this study will assess the functional and metabolic consequences of human $CD8^+$ T cell activation in hypoxia (1% O_2) compared to physiological (5% O_2) and atmospheric levels (21% O_2). *In vitro* work will help to understand any dysfunction at a mechanistic level and access to MM patient samples will help contextualise this in the MM tumour setting. The aims for this thesis are:

1. To interrogate $CD8^+$ T cell activation and function in hypoxia
2. To understand $CD8^+$ T cell signalling and metabolism in hypoxia
3. To explore a mechanistic basis for $CD8^+$ T cell dysfunction in hypoxia
4. To assess relevance in MM by testing effects of hypoxia on $CD8^+$ T cell responses to bispecific antibodies and by assessment of BM and PB cells from patients with MM.

2. Methods

2. Methods

2.1. Cell culture

2.1.1. Healthy volunteer peripheral blood donors

Healthy human peripheral blood mononuclear cells (PBMCs) were isolated from fully anonymised leucocyte cones provided by the National Health Service (NHS) Blood and Transplant (NHSBT) Centre, Birmingham, UK, or from healthy human volunteer donors. All volunteers were required to sign a consent form, and all studies were approved by the University of Birmingham STEM Ethics Committee (Ref. ERN 17_1743).

2.1.2. Multiple myeloma (MM): bone marrow aspirate and peripheral blood donors

Patients with multiple myeloma (MM) were recruited from haematology clinics at University Hospitals Birmingham **(Table 2.1)**. Individual MM patient data are shown in **Supplementary 1**. Each patient provided informed written consent and bone marrow (BM) aspirates and peripheral blood (PB) samples were taken. The study received ethical approval (Ref: 10/H1206/58). Mononuclear cells from BM aspirates, and PBMCs from PB samples, were isolated by density-gradient centrifugation using Ficoll-Paque (Cytiva, Cat# 17144003) in small sterile Leucosep tubes (Greiner Bio-One, Cat# 163290) Cells were washed with phosphate-buffered saline (PBS, Sigma, Cat# D8537), counted and frozen in freezing medium (10% DMSO: Sigma-Aldrich, Cat# 472301; 90% foetal calf serum (FCS): Sigma, Cat# F9665) or stained for flow cytometry immediately (as in **'2.2.9. Flow cytometry analysis of multiple myeloma (MM) patient samples'**).

Table 2.1. General and clinical characteristics of MM patients and controls.

n	8
Age – Median (Range)	74 (67-86)
Sex - % male	63
Trephine % MMPC – Median (Range)	60 (45-80)
PP level (g/L) – Median (Range)	41.7 (16.8-74.2)
IgG (%)	37.5
IgA (%)	50
Light Chain (%)	12.5

2.1.3. $CD8^+$ T cell isolation and culture in 21%, 5% or 1% O_2

Human PBMCs were isolated from fresh leucocyte cones by density gradient centrifugation using Ficoll-Paque (Cytiva, Cat# 17144003) in sterile Leucosep tubes (Greiner Bio-one, Cat# 227290). PBMCs were positively selected using CD8 Microbead Kit (Miltenyi Biotech, Cat# 135-045-201) and LS columns (Miltenyi Biotech, Cat# 130-042-401). Purity was generally >95%. Purified $CD8^+$ T cells were cultured at a density of 1 x 10^6/ml in RPMI-1640 (Sigma-Aldrich, Cat# R8758) containing 100 IU/ml penicillin and streptomycin (Sigma-Aldrich, Cat# P4333), 10% foetal calf serum (FCS, Sigma, Cat# F9665), and 50 IU/ml recombinant IL-2 (PeproTech, Cat# 200-02) overnight at atmospheric (21% O_2) or reduced (5% or 1% O_2, Don Whitley Hypoxystation) oxygen (O_2) levels, to ensure pre-equilibration of the media, plate and cells to the required O_2 levels prior to the start of the experiment. Unless otherwise stated, cells were then activated with 12 μg/ml ImmunoCult Human CD3/CD28 T Cell Activator (STEMCell Technologies, Cat# 10971) and cultured in the respective O_2 tension for the time period indicated. For some experiments, as indicated, deferoxamine mesylate salt (DFO, Sigma-Aldrich, Cat# D9533), 2-Deoxy-D-glucose

(2-DG, Sigma-Aldrich, Cat# D6134), Rapamycin (Sigma-Aldrich, Cat# 553210) and an AMPK inhibitor (Compound C, Sigma-Aldrich, Cat# 171261) were added to cell culture.

2.1.4. Mouse splenocyte isolation and culture in 21% or 1% O_2

Mouse spleens were obtained from wild-type (WT), Nuclear receptor subfamily 4 group A member 3 (Nr4a3)-Timer of cell kinetics and activity (Tocky) or Nuclear receptor subfamily 4 group A member 1 (Nr4a1, Nu77)-Timer rapidly expressed in lymphocytes (TEMPO) mice (Bending *et al.*, 2018; Elliott *et al.*, 2022). Spleens were crushed and resuspended in eBioscience™ 1 X Red Blood Cell Lysis Buffer (Invitrogen, Cat #2450711) for incubation on ice for 8 minutes. Red blood cell lysis was blocked by RPMI-1640 + 10% FCS. Splenocytes were cultured overnight at a density of 1 x 10^6/ml in RPMI-1640 with penicillin and streptomycin, 10% FCS, 50 IU/ml IL-2, and 2-Mercaptoethanol (Gibco™, Cat #21985023) at either 21% or 1% O_2 (as in **'2.1.3. $CD8^+$ T cell isolation and culture in 21%, 5% or 1% O_2'**). The following morning, splenocytes were stimulated with 1 μg/ml soluble Ultra-LEAF™ Purified anti-mouse CD3ε Antibody (Biolegend, Cat #100340) and 5 μg/ml soluble Purified NA/LE Hamster Anti-Mouse CD28 (BD Pharmingen™, clone 37.51, Cat #553294) and cultured for the indicated time period in 21% or 1% O_2.

2.2. Flow cytometry

2.2.1. Flow cytometry cell sorting

$CD8^+$ T cells were isolated from healthy human PBMC (as in '1.3. $CD8^+$ T cell isolation and culture in 21%, 5% or 1% O_2') prior to surface staining with anti-human CD45RA, CD62L and CD8 antibodies **(Table 2.2)** in sterile FACS buffer (1% FCS in 1X PBS: Sigma, Cat# D8537) for 20 minutes on ice. Cells were washed in FACS buffer before resuspension in SILAC™-RPMI 1640 Flex Media (Gibco, Cat #A24942-01) containing 1% FCS, 100 IU/ml penicillin and streptomycin, 50 IU/ml recombinant IL-2 (PeproTech, Cat# 200-02) at a density of 30 x 10^6/ml. Cells were filtered in a 75 μm mesh FACS tube prior to sorting. Naïve ($CD45RA^+$ $CD62L^+$), central memory (CM, $CD45RA^-$ $CD62L^+$), effector memory (EM, $CD45RA^-$ $CD62L^-$), and terminally differentiated effector memory cells re-expressing CD45RA (EMRA, $CD45RA^+$ $CD62L^-$) $CD8^+$ T cells were collected into separate sterile FACS tubes containing RPMI-1640 media with 20% FCS, 100 IU/ml penicillin and streptomycin, and 50 IU/ml recombinant IL-2 and resuspended (as in **'2.1.3. $CD8^+$ T cell isolation and culture in 21%, 5% or 1% O_2'**) for subsequent experiments.

2.2.2. Flow cytometry analysis of cell surface protein expression

To analyse cell surface protein expression, $CD8^+$ T cells were stained in FACS buffer (1% FCS in 1X PBS) with specific monoclonal antibodies and live/dead probe for 30 minutes at 4°C. Surface antibodies and live/dead probes used are detailed in **Table 2.2**. Cells were washed and resuspended in FACS buffer for analysis on a flow cytometer (BD LSRFortessa™ Cell Analyser).

2.2.3. Flow cytometry analysis of proliferation

To analyse $CD8^+$ T cell proliferation, immediately following isolation, cells were incubated with cell trace violet (CTV, 5 μM, Invitrogen, Cat# C34557) for 20 minutes at 21% O_2, 37°C and 5% CO_2. Cells were washed and cultured (as in **'2.1.3. $CD8^+$ T cell isolation and culture in 21%, 5% or 1% O_2'**) for a total of 6 days following activation. At the end of the experiment, cells were analysed for CTV dilution.

2.2.4. Flow cytometry analysis of intracellular cytotoxic granule and cytokine abundance

For intracellular cytokine staining, following 48 hours of culture +/- activation in the indicated O_2 condition, $CD8^+$ T cells were re-stimulated with Cell Activation Cocktail with Brefeldin A (PMA/Ionomycin, Biologend, Cat# 423303) or with 12 μg/ml ImmunoCult Human CD3/CD28 T Cell Activator in combination with Brefeldin A (10 μg/ml, Acros Organics, Cat# 297140050) for 4 hours, or left unstimulated.

For analysis of intracellular cytotoxic granule abundance, following pre-equilibration in the indicated O_2 condition, $CD8^+$ T cells were stimulated with ImmunoCult Human CD3/CD28 T Cell Activator in combination with Brefeldin A and monensin (Biolegend, Cat# 420701) for 5 hours, or left unstimulated. Anti-CD107a **(Table 2.2)** was included during the culture period for measurement of degranulation.

For both intracellular cytokine staining and cytotoxic granule abundance, cells were stained for viability (as in **'2.2.2. Flow cytometry analysis of cell surface protein expression'**), before resuspension in FoxP3 fixation/permeabilisation solution

(eBioscience, Cat# 00-5523-00) for 20 minutes at room temperature in the dark for fixation. Cells were washed with FoxP3 permeabilisation buffer (eBioscience, Cat# 00-5523-00) and incubated with antibodies for 20 minutes at room temperature in the dark. Antibodies used are detailed in **Table 2.2**. Cells were washed with FoxP3 permeabilisation buffer and resuspended in FACS buffer prior to analysis by flow cytometry.

2.2.5. Flow cytometry analysis of intracellular protein expression and phosphorylation

For analysis of phosphorylated proteins in the TCR signalling pathway, $CD8^+$ T cells were activated for the indicated time, prior to resuspension in fixation buffer (Biolegend, Cat# 420801, containing 4% paraformaldehyde) for 15 minutes at 37°C and 5% CO_2. Cells were washed and permeabilised in True-Phos™ Perm Buffer (Biolegend, Cat# 42540) via dropwise addition of permeabilisation buffer and continuous vortexing and incubated for -20°C for 60 minutes. Cells were washed and stained in FACS buffer for phospho-proteins (phospho-Lck (p-Lck) and phospho-ERK (p-ERK)) for 30 minutes at room temperature in the dark, prior to washing and resuspension in FACS buffer for analysis. Protocol for phospho-flow for p-Lck and p-ERK was adapted with advice from Dr Alastair Copland (Copland *et al.*, 2023).

For analysis of intracellular proteins (mTOR, p70S6K, DNA-damage-inducible transcript 4 (DDIT4), c-Myc, BCL2 Interacting Protein 3 (BNIP3), and Rheb) cells were first stained for viability (as in **'2.2.2. Flow cytometry analysis of cell surface protein expression'**), before fixation with FoxP3 fixation solution for 20 minutes at room

temperature in the dark. For analysis of the phosphorylation of intracellular proteins (p-mTOR, p-p70S6K, p-AKT) cells were immediately fixed with pre-warmed FoxP3 fixation solution for 20 minutes at 37°C. Cells were then washed with FoxP3 permeabilisation buffer and incubated with primary antibodies **(Table 2.2)** for 30 minutes at room temperature in the dark. Cells were washed well with FoxP3 permeabilisation buffer prior to incubation with secondary antibodies **(Table 2.2)** for 20 minutes at room temperature in the dark if the primary antibody was not conjugated to a fluorophore. Protocol for analysis of p-mTOR, p-p70S6K, p-AKT developed following advice from Dr Emma Bishop (Bishop, 2023). Cells were washed and resuspended in FACS buffer for analysis.

2.2.6. Flow cytometry analysis of NFAT translocation to the nucleus

2.2.6.1. Nuclei isolation

'Sucrose buffer A' was prepared with 10 mM HEPES (Sigma-Aldrich, Cat# H3375), 8 mM $MgCl_2$ (Sigma-Aldrich, Cat# M1028), 320 mM sucrose (Sigma-Aldrich, Cat# S0389), 0.1% Triton-X 100 (Sigma-Aldrich, Cat# X100), Protease and Phosphatase Inhibitor Cocktail (Sigma-Aldrich, Cat# PPC1010), and diluted with distilled H_2O. 'Sucrose buffer B' was prepared as for 'sucrose buffer A' but without 0.1% Triton-X 100. After pre-equilibration, $CD8^+$ T cells were stimulated for 1 hour with ImmunoCult Human CD3/CD28 T Cell Activator in the indicated O_2 conditions prior to washing and incubation on ice for 15 minutes with 'sucrose buffer A'. Cells were centrifuged at 2000g for 5 minutes at 4°C and washed twice with 'sucrose buffer B' at the same centrifuge settings. Paraformaldehyde 16% w/v aqn. Soln., methanol free (Thermo Scientific Chemicals, Cat# 043368-9M) was diluted with 'sucrose buffer B' to yield a

4% paraformaldehyde solution and used to fix the cells for 30 minutes on ice in the dark. Following centrifugation and supernatant removal, nuclei pellets were washed with FACS buffer containing $MgCl_2$ (1X PBS, 2% FCS, 8 mM $MgCl_2$) at 1000g for 5 minutes at 4°C, and once with permeabilisation buffer (FACS buffer containing $MgCl_2$ and 0.3% Triton-X 100 v/v) at the same centrifuge settings.

2.2.6.2. Nuclei staining

Nuclei were stained with fluorescent-labelled antibodies **(Table 2.2)** in permeabilisation buffer containing $MgCl_2$ for 1 hour at 4°C. Nuclei pellets were washed twice and resuspended in FACS buffer containing $MgCl_2$ prior to analysis on the flow cytometer. Protocol for nuclei isolation and staining adapted from Gallagher, Conley and Berg (2018).

2.2.7. Flow cytometry analysis of mitochondrial mass, membrane potential and reactive oxygen species (ROS)

For analysis of mitochondrial mass and membrane potential, $CD8^+$ T cells were pre-equilibrated overnight and stimulated for 48 hours with 12 μg/ml ImmunoCult Human CD3/CD28 T Cell Activator in the respective O_2 condition. MitoView Green (50 nM; Biotium, Cat# 70054) and MitoSpy Orange (MSO, 25 nM; Biolegend, Cat# 424804) +/- the mitochondrial uncoupler, Bam-15 (3 μM; Sigma-Aldrich, Cat# 5737) were added for 20 minutes at 37°C, 5% CO_2, and the respective O_2 condition for assessment of mitochondrial mass and membrane potential ($\Delta\Psi m$), respectively. Cells were washed and analysed by flow cytometry. Data are presented as a ratio of MSO MFI in absence of Bam-15 / MSO MFI in presence of Bam-15.

For analysis of mitochondrial reactive oxygen species (ROS), $CD8^+$ T cells were pre-equilibrated overnight and stimulated for 48 hours with 12 μg/ml ImmunoCult Human CD3/CD28 T Cell Activator in the respective O_2 condition. Cells were stained with mitoSOX (5 μM, Invitrogen, Cat# M36008) in HBSS (Gibco™, Cat# 24020117) for 20 minutes at 21% O_2, 37°C and 5% CO_2 prior to staining for viability **(Table 2.2)**, washing and analysis. Positive controls of antimycin A and rotenone (5 μM for both, antimycin A: Sigma-Aldrich, Cat# A8674, rotenone: Sigma-Aldrich, Cat# R8875) were added at the point of staining with mitoSOX.

For analysis of total ROS, $CD8^+$ T cells were pre-equilibrated overnight and stimulated for 48 hours with 12 μg/ml ImmunoCult Human CD3/CD28 T Cell Activator in the respective O_2 condition. 2,3-Dimethoxy-1,4-naphthoquinone (DMNQ, 1:1000, Cayman Chemical, Cat# 19571) was used as a positive control and added during cell culture. Cells were stained with 2',7'-Dichlorofluorescin Diacetate (20 μM DCFDA, Sigma, Cat# D6883) in RPMI-1640 containing 10% FCS for 20 minutes 37°C and 5% CO_2 at the respective O_2 condition, prior to staining for viability **(Table 2.2)**, washing and analysis.

2.2.8. Flow cytometry analysis of bispecific antibody-mediated cytotoxicity and T cell activation

B cell maturation antigen (BCMA)-expressing multiple myeloma cell lines (JJN3, AMO and L363) were kindly provided by Professor Chris Bunce (University of Birmingham) and labelled with CTV prior to experiments (as in **'2.2.3. Flow cytometry analysis of proliferation'**). Isolated $CD8^+$ T cells were co-cultured with the BCMA-expressing

multiple myeloma cell lines at indicated T cell : target cell ratios with or without the presence of a BCMAxCD3 bispecific antibody **(Table 2.2)** at 21% or 1% O_2 for 24 hours. Flow cytometry analysis of live/dead probe exclusion within the CTV-labelled target cells was used to quantify target cell death. Simultaneously, in another well, $CD8^+$ T cells and target cells were co-cultured with or without the presence of a BCMAxCD3 bispecific antibody **(Table 2.2)** at 21% or 1% O_2 for 24 hours, and the following morning brefeldin A, monensin and anti-CD107a added for 4 hours (as in **'2.2.4. Flow cytometry analysis of intracellular cytotoxic granule and cytokine abundance'**). Cells were surface stained for CD8, CD25 and CD69 (as in **'2.2.2. Flow cytometry analysis of cell surface protein expression'**) before fixation and permeabilisation (as in **'2.2.4. Flow cytometry analysis of intracellular cytotoxic granule and cytokine abundance'**). CTV-negative $CD8^+$ T cells were quantified for the abundance of intracellular molecules detailed in **Table 2.2**.

2.2.9. Flow cytometry analysis of multiple myeloma (MM) patient samples

Mononuclear cells and PBMCs were thawed or freshly isolated from MM patient BM aspirates or PB samples, respectively (as in **'2.1.2. Multiple myeloma (MM) bone marrow (BM) aspirate and peripheral blood (PB) donors'**), washed twice in cold RPMI-1640 containing 10% FCS and cells counted. Cells were either stained immediately (panels 1 and 1a) or rested overnight in 21% or 1% O_2 in RPMI-1640 containing 10% FCS at a density of 1 x 10^6/ml (panels 2 and 3).

Cells for panels 1 and 1a were stained for viability with efluor780 (Invitrogen, Cat#13539140) and fluorophore-conjugated antibodies for cell surface markers **(Table**

2.2 and Figure 2.1). Cells were fixed with FoxP3 fixation/permeabilisation solution, washed with FoxP3 permeabilisation solution, and stained for intracellular antibodies in permeabilisation solution for 20 minutes at room temperature in the dark. Where antibodies were not fluorophore-conjugated, cells were stained in permeabilisation buffer with a secondary antibody for 20 minutes at room temperature in the dark. **(Table 2.2 and Figure 2.1)**.

Cells for panel 2 were rested overnight in 21% or 1% O_2 in RPMI-1640 containing 10% FCS at a density of 1 x 10^6/ml and re-stimulated the following morning with 12 μg/ml ImmunoCult Human CD3/CD28 T Cell Activator in combination with Brefeldin A for 4 hours in the respective O_2 condition. Cells were stained for viability and surface markers prior to fixation, permeabilisation and staining for anti-cytokine fluorophore-conjugated antibodies and intracellular antibodies for 20 minutes at room temperature in the dark **(Table 2.2 and Figure 2.1)**. Cells were stained with a secondary antibody where indicated for 20 minutes at room temperature in the dark **(Table 2.2 and Figure 2.1)**.

Cells for panel 3 were rested overnight in 21% or 1% O_2 in RPMI-1640 containing 10% FCS at a density of 1 x 10^6/ml prior to addition of MitoView Green and MitoSpy Orange +/- the mitochondrial uncoupler Bam-15 for 20 minutes at 37°C, 5% CO_2 and the respective O_2 condition. Cells were washed in FACS buffer and analysed by flow cytometry. Data presented as in '**2.2.7. Flow cytometry analysis of mitochondrial mass, membrane potential and reactive oxygen species**'.

Panel 1	
CD8	AF700
CD56	BV510
CD4	BV785
CD45RA	BV421
CCR7	BUV737
PD1	BV605
TIGIT	BUV395
BNIP3	AF555 (PE)
Rheb	PE-Cy7
Ki67	FITC
L/D	APC-Cy7

Panel 1a	
CD8	AF700
CD56	BV510
CD4	BV785
CD45RA	BV421
CCR7	BUV737
PD1	BV605
TIGIT	BUV395
c-Myc	AF555 (PE)
L/D	APC-Cy7

Panel 2	
CD8	AF700
CD56	BV510
CD4	BV785
CD45RA	BV421
CCR7	BUV737
PD1	BV605
TIGIT	BUV395
BNIP3	AF555 (PE)
Rheb	PE-Cy7
IFNy	FITC
TNFa	APC
L/D	APC-Cy7

Panel 3	
CD8	AF700
CD56	BV510
CD4	BV785
CD45RA	BV421
CCR7	BUV737
PD1	BV605
TIGIT	BUV395
MSO	PE
MVG	AF488 (FITC)
L/D	APC-Cy7

Key:

	Cell subsets
	Naïve/memory

	Activation
	Hypoxia

	Proliferation
	Metabolic

	Cytokines
	Live/dead

Figure 2.1. Multiple myeloma patient staining panels for BM aspirates and PB samples.

2.2.10. Flow cytometry analysis of amino-acid induced mTOR activity

Isolated $CD8^+$ T cells were pre-equilibrated and stimulated for 24 hours in 21% or 1% O_2 (as in '**2.1.3. $CD8^+$ T cell isolation and culture in 21%, 5% or 1% O_2**'). Cells were serum starved for 4 hours by washing and transfer to PBS. Where indicated, cells were provided 10 mM leucine (Sigma-Aldrich, Cat# L8000) for 30 minutes prior to staining for phospho- and total- p70S6K (as in **'2.2.5. Flow cytometry analysis of intracellular protein expression and phosphorylation'**).

2.2.11. Flow cytometry analysis of Nr4a1-Tempo and Nr4a3-Tocky Murine Reporter Systems

After **'2.1.4. Mouse splenocyte isolation and culture in 21% or 1% O_2**', splenocytes were washed in FACS buffer and stained for viability and surface markers (**'2.2.2. Flow cytometry analysis of cell surface protein expression'**). Antibodies used are indicated in **Table 2.2**. Samples were analysed immediately.

2.2.12. Flow cytometry analysis of puromycin assay

Splenocytes (as in **'2.1.4. Mouse splenocyte isolation and culture in 21% or 1% O_2**') were incubated in 21% or 1% O_2 after activation for 24 hours. Puromycin (Sigma-Aldrich, Cat# P8833) and a live/dead stain **(Table 2.2)** were then added to the cell culture, in the respective O_2 condition, for 15 minutes. Cells were washed in ice-cold FACS buffer and stained for surface antibodies in for 30 minutes at 4°C. Cells were washed in FACS buffer and fixed with FoxP3 fixation/permeabilisation solution and washed and stained for anti-puromycin **(Table 2.2)** in permeabilisation solution for 20

minutes at 4°C. Cells were washed and resuspended in FACS buffer for analysis by flow cytometry.

2.3. Calcium (Ca^{2+}) flux assay

$CD8^+$ T cells were isolated as in **'2.1.3. $CD8^+$ T cell isolation and culture in 21%, 5% or 1% O_2'** and pre-equilibrated overnight in 21% or 1% O_2 in RPMI-1640 containing 100 IU/ml penicillin and streptomycin, 10% FCS, and 50 IU/ml recombinant IL-2. The following day, cells were resuspended in Fluo-4 Direct™ calcium assay buffer (Component C, from Fluo-4 Direct™ Calcium Assay Kit, Starter Pack, Invitrogen, Cat #F10471) and transferred to a pre-coated poly-D-lysine (Gibco™, Cat #A3890401) 96-U bottom well plate. After 60 minutes, an equal volume of 2X Fluo-4 Direct™ calcium assay reagent with a 5 mM final concentration of probenecid (Component A, from Fluo-4 Direct™ Calcium Assay Kit – diluted with assay buffer and water-soluble probenecid; Component B, from Fluo-4 Direct™ Calcium Assay Kit) was added to the cells and incubated for another 60 minutes. Cells were then transferred to an atmospheric controlled fluorescent plate reader (CLARIOstar® Plus Plate Reader) set at 5% CO_2, 37°C and either 21% or 1% O_2, respectively. Whilst in the plate reader, injections were used to stimulate the cells with a high concentration (10 μl) of ImmunoCult™ Human CD3/CD28 T cell Activator, Cell Activation Cocktail with Brefeldin A, or left unstimulated and distilled H_2O added at the same volume. Fluorescence was subsequently read over roughly 4 minutes at an excitation of 494 nm and an emission of 516 nm.

2.4. Measurement of glucose and lactate in supernatants

$CD8^+$ T cells isolated from human PBMC were pre-equilibrated overnight in 21% or 1% O_2, activated the following morning with 12 μg/ml ImmunoCult Human CD3/CD28 T Cell Activator, or left unstimulated, and cultured up to 72 hours in 21% or 1% O_2, in RPMI-1640 containing 100 IU/ml penicillin and streptomycin, 10% FCS, and 50 IU/ml recombinant IL-2 at a density of 1 x 10^6/ml. Supernatants were collected from culture at 8, 24, 48 and 72 hours. Glucose and lactate concentrations were measured using Glucose-Glo (Promega, Cat# J6021) and Lactate-Glo (Promega, Cat# J5021), respectively, according to the manufacturer's instructions.

2.5. Stable isotope based metabolic tracing

2.5.1. $^{13}C_5$-glutamine and $^{13}C_6$-glucose tracing

$CD8^+$ T cells isolated from human PBMC (4 x 10^6 per condition) were pre-equilibrated overnight in 21% or 1% O_2, activated the following morning with 12 μg/ml ImmunoCult Human CD3/CD28 T Cell Activator and cultured for 24 hours in 21% or 1% O_2, in SILAC RPMI-1640 (Gibco, Cat# A2494201) supplemented with 10% FCS, recombinant human IL-2, 20 mg/ml L-arginine (Sigma-Aldrich, Cat# A8094), 4 mg/ml L-lysine (Sigma-Aldrich, Cat# L8662), and either 2 mM U-$^{13}C_5$ glutamine (CK Isotopes, Cat# CNLM-1275) and 10 mM glucose (Sigma-Aldrich, Cat# G8270), or 2 mM L-glutamine (Sigma-Aldrich, Cat# G8540) and 10 mM U-$^{13}C_6$ glucose (CK Isotopes, Cat# CLM-1396-1). Following culture, cells were washed with ice-cold 0.9% saline solution and cell pellets snap frozen for storage at -80°C.

In another experiment, $CD8^+$ T cells isolated from human PBMC were pre-equilibrated overnight in 21% or 1% O_2, activated the following morning with 12 μg/ml ImmunoCult Human CD3/CD28 T Cell Activator and cultured for 24 hours in 21% or 1% O_2, in RPMI-1640 containing 100 IU/ml penicillin and streptomycin, 10% FCS, and 50 IU/ml recombinant IL-2 at a density of 1 x 10^6/ml (4 x 10^6 per condition). Cells in 1% O_2 were then moved back to 21% O_2, and all cells washed and resuspended in SILAC RPMI-1640 supplemented with 10% FCS, recombinant human IL-2, 20 mg/ml L-arginine, 4 mg/ml L-lysine, and 2 mM U-$^{13}C_5$ glutamine and 10 mM glucose for 6 hours of tracing at 21% O_2 only. Cells were washed with ice-cold 0.9% saline solution and cell pellets snap frozen for storage at -80°C.

2.5.2. Metabolic extraction

Cell pellets were resuspended in 1:1:1 pre-chilled methanol (Thermo Fisher Scientific, Cat #10093880), HPLC-grade water containing 1.75 μg/ml D6-glutaric acid (Pentanedioic-d6 acid, CDN Isotopes, Cat #D-5227), and chloroform (Sigma-Aldrich, Cat #650498) for extraction. The extracts were shaken at 1400 rpm for 15 minutes at 4°C and then centrifuged at 12,000 g for 15 minutes at 4°C. The upper aqueous layer was collected and evaporated under vacuum for collection of dried polar metabolites.

2.5.3. Metabolite derivatisation

Metabolite derivatisation was performed using an Agilent autosampler. The dried polar metabolites were dissolved in 15 μL 2% methoxyamine hydrochloride in pyridine (Thermo Fisher Scientific, Cat #25104) at 55°C, followed by an equal volume of N-tert-

Butyldimethylsilyl-N-methyltrifluoroacetamide with 1% tertbutyldimethylchlorosilane after 60 minutes, and incubation for a further 90 minutes at 55°C.

2.5.4. Gas chromatography-mass spectrometry (GC-MS) analysis

Gas chromatography-mass spectrometry (GC-MS) analysis was performed using an Agilent 6890GC equipped with a 30m D8-35 MS capillary column. The GC was connected to an Agilent 5975C MS operating under electron impact ionisation at 70 eV. The MS source was held at 230°C and the quadrupole at 150°C. The detector was operated in scan mode and 1 μL of derivatised sample was injected in splitless mode. Helium was used as the carrier gas at a flow rate of 1 mL/min. The GC oven temperature was kept at 80°C for 6 minutes and increased to 325°C at a rate of 10°C/minute for 4 minutes. The run time for each sample was 59 minutes. For determination of the mass isotopomer distributions (MIDs), spectra were corrected for natural isotope abundance. MATLAB was used for data processing.

2.6. Enzyme-linked immunosorbent assay (ELISA)

$CD8^+$ T cell culture supernatants were collected between 8-72 hours, as indicated, following activation in the respective O_2 condition, and stored at -20°C before analysis by enzyme-linked immunosorbent assay (ELISA). IFN-γ concentration was measured using anti-IFN-γ capture (Bio-Rad, Clone AbD00676, Cat# HCA043) and biotinylated detection (Bio-Rad, Clone 2503, Cat# HCA044P) antibodies, recombinant IFN-γ standard (Bio-Rad, Cat# PHP050), streptavidin-HRP (Sigma-Aldrich, Cat# E2866) and TMB substrate (BD Biosciences, Cat# 555214). TNF-α concentration was measured using TNF alpha matched antibody pair and ELISA buffer kit (Invitrogen, Cat#

CHC1753 and Cat# CNB0011). A standard curve was generated to retrieve the relative concentration of cytokine in the supernatants.

2.7. Western blot

2.7.1. Cell lysis

$CD8^+$ T cells were isolated and cultured (as in **'2.1.3. $CD8^+$ T cell isolation and culture in 21%, 5% or 1% O_2'**) and stimulated for the indicated time period. Cell lysates were prepared in Pierce™ RIPA buffer (Thermo Fisher Scientific, Cat# 89900) or directly lysed in Sample Buffer, Laemelli 2x concentration (Sigma-Aldrich, Cat# S3401) diluted 1:1 with PBS, following washing with PBS. Lysates were frozen at -20°C until use. Protein concentrations were determined with a BCA protein assay kit (for samples in RIPA only, Thermo Fisher Scientific, Cat# 23225).

2.7.2. SDS-PAGE

Whole-cell lysates were combined with Sample Buffer, Laemelli 2x concentration and heated at 95°C for 5 minutes. Samples were loaded onto an 8-12% gel and run at 100-150V for around 40 minutes, or until samples had reached the bottom of the gel. The iBlot® 2 gel transfer system (Invitrogen™) was used for semi-dry transfer onto a nitrocellulose membrane (iBlot® 2 NC Regular Stacks, Invitrogen, Cat# IB23001).

2.7.3. Antibody incubation and protein visualisation

Membranes were blocked with non-fat, skimmed, dried milk powder (5%, Marvel) or 5% Bovine Serum Albumin (BSA, Sigma-Aldrich, Cat# A8022) in PBS and 0.02% Polysorbate-20 (Tween-20, Thermo Fisher Scientific, Cat# L15029.AP) for 1 hour at

room temperature with gentle shaking. Primary antibodies **(Table 2.2)** were diluted in 5% milk or 5% BSA in PBS and 0.02% Polysorbate-20 and added to membranes for incubation overnight at 4°C with gentle shaking. Membranes were then washed with PBS and 0.02% Polysorbate-20 and secondary antibodies conjugated to HRP **(Table 2.2)** diluted as above, were added to membranes for 1 hour at room temperature with gentle shaking. Membranes were washed with PBS and 0.02% Polysorbate-20 and developed with the HRP-ECL (BioRad Clarity Western ECL Substrate Cat# 170-5061) for band visualisation.

2.8. Clustered Regularly Interspaced Short Palindromic Repeats (CRISPR)-CRISPR associated protein 9 (Cas9) knockout of BNIP3 in primary human $CD8^+$ T cells

2.8.1. Preparation of $CD8^+$ T cells

Isolated $CD8^+$ T cells were rested in 21% O_2 for 48 hours in RPMI-1640 containing 100 IU/ml penicillin and streptomycin, 10% FCS, and 50 IU/ml recombinant IL-2, additionally supplemented with 50 ng/mL IL-7 (Biolegend, Cat #581904) and 50 ng/mL IL-15 (Biolegend, Cat# 570302).

2.8.2. Preparation of reagents

BNIP3 knockout (KO) and negative control crRNA (Integrated DNA Technologies, KO: Hs.Cas9.BNIP3.1.AA, Alt-R® Clustered Regularly Interspaced Short Palindromic Repeats (CRISPR)-CRISPR associated protein 9 (Cas9) crRNA; Negative control: Alt-R® Cas9 Negative Control crRNA, Cat# 1072544) and tracRNA were resuspended in nuclease-free duplex buffer (Integrated DNA Technologies, Cat# 11-01-03-01) to a

concentration of 200 μM. Duplex RNA was generated by mixing 1:1 KO or negative control crRNA with tracRNA in a sterile Eppendorf and boiling at 95°C for 5 minutes. Duplex RNA was cooled at room temperature until use. RNP complexes were generated by mixing duplex RNA with Alt-R™ S.p. HiFi Cas9-green fluorescent protein (GFP) V3 (Integrated DNA Technologies, Cat# 10008100) in a 3:1 ratio for both KO and negative control duplex RNA. For RNP complex formation, these were incubated for 15 minutes at room temperature and then kept on ice until use.

2.8.3. Electroporation for transfection

$CD8^+$ T cells were counted, and 2 x 10^6 cells resuspended in roughly 40-100 ul P3 buffer with supplement added (P3 Primary Cell Solution box, Lonza, Cat# PBP3-00675). 5.86 μL of RNP complex was added to each sample, with negative controls and KO being added to the respective sample. Cells were transfected in a NucleofectorTM Transfection II/2b device (Lonza) with the 'Unstimulated T cells, High Efficiency' program code. Transfected cells were resuspended in pre-warmed RPMI-1640 containing 100 IU/ml penicillin and streptomycin, 20% FCS, and 50 IU/ml recombinant IL-2 and transferred to a 24 well plate for resting in 21% O_2, 37°C and 5% CO_2 overnight.

2.8.4. Stimulation of transfected $CD8^+$ T cells and staining

The following morning, $CD8^+$ T cells were resuspended in RPMI-1640 containing 100 IU/ml penicillin and streptomycin, 10% FCS, and 50 IU/ml IL-2 at a density of 1 x 10^6/ml. Cells were moved to 21% or 1% O_2 and stimulated with 12 μg/ml ImmunoCult Human CD3/CD28 T Cell Activator 2 hours later. Cells were cultured for 72 hours in

21% or 1% O_2 and stained for viability, surface markers and intracellular antibodies and cytokines detailed in **Table 2.2** as in **'2.2.2', '2.2.4'** and **'2.2.5'**. In these experiments, paraformaldehyde 16% (Thermo Scientific Chemicals, Cat# 043368-9M) was diluted with PBS to yield a 2% paraformaldehyde solution and used to fix the cells for 20 minutes at 37°C in order to retain the GFP signal. Antibodies used are indicated in **Table 2.2**.

2.9. Bulk RNA-sequencing and analysis

2.9.1. Bulk RNA-sequencing

$CD8^+$ T cells were pre-equilibrated and stimulated for 24 hours in 21% and 1% O_2 (as in **'2.1.3. $CD8^+$ T cell isolation and culture in 21%, 5% or 1% O_2'**), prior to washing in PBS and snap freezing of cell pellets for storage at -80°C. mRNA was isolated from cell pellets using NucleoSpin® RNA Mini Kit (Machery-Nagel, Cat# 740955.5) according to the manufacturer's instructions. RNase Zap™ (Sigma-Aldrich, Cat# R2020) was used to clean all surfaces during the mRNA extraction. RNA samples were submitted to Genomics Birmingham for RNA sequencing. Sequencing libraries were prepared using the QuantSeq 3' mRNA-Seq Library Preparation Kit (Lexogen). Libraries were sequenced using the NextSeq 500 with a Mid 150v2.5 flow cell.

2.9.2. RNA-sequencing analysis

FASTQ files were downloaded from Illumina base space and uploaded to BlueBEAR (University of Birmingham). All 4 lanes were merged to create FASTQ files for each sample which were quality checked by FastQC v0.11.9 (Andrews, 2010). For trimming of low-quality read, poly(A) tails, rRNA and adapter contamination Bbduk v37.99 from

the bbmap suite was used (Bushnell, 2014). To align reads to the human genome STAR v2.7.2b aligner was used (Dobin *et al.*, 2013). To generate counts for mRNA species HTSeq-count v0.13.5 was used (Anders, Pyl and Huber, 2015) and raw read counts used for analysis by DESeq2 v1.30.1 in R v4.0.5 (Love *et al.*, 2014). Data were filtered to remove genes where 6 or fewer samples had a read count of 10 or above. Differentially expressed genes (DEGs) were determined as those with an adjusted p value < 0.05. org.Hs.eg.db v3.12.0 (Carlson, 2019) and clusterProfiler v3.18.1 for volcano plots (Wickham *et al.*, 2016). Protocol for analysis from Bishop, 2023.

2.10. Statistical analysis

Data are presented as the mean and individual replicate values. Paired data were analysed by paired Students *t* test or Wilcoxon matched-pairs signed rank test for two conditions, by repeated measures ANOVA with or without the Geisser-Greenhouse correction with Holm-Sidak's post-hoc test for more than two conditions, with a single pooled variance or individual variances computed for each comparison, or an ordinary two-way ANOVA with Sidak's, or Tukey's, multiple comparisons post-hoc test for more than one parameter, with a single pooled variance. Unpaired data were analysed by multiple unpaired t-tests with two-stage linear step-up procedure of Benjamin, Krieger and Yekutieli post-hoc test for more than two conditions. Normalised data were analysed by Multiple Mann-Whitney tests for more than two conditions with two-stage linear step-up procedure of Benjamin, Krieger and Yekutieli post-hoc test to help control the false discovery rate at the desired level *q* (Benjamini, Krieger and Yekutieli, 2006). Data were analysed using Prism version 10.2.1 and flow cytometry data with Flow Jo version 10.10.0.

2.11. Antibodies

Table 2.2. Table of antibody details, including clone, fluorophore, supplier, catalogue number (Cat#), concentration (conc.), protocol used, and any additional notes

Antibody	Clone	Fluorophore	Supplier	Cat#	Conc.	Protocol(s)	Notes
Fixable viability dye eFluor™ 780	N/A	APC-Cy7	Invitrogen	65-0865-14	1:1000	Various	
Zombie violet fixable viability kit	N/A	BV421	Biolegend	423114	1:500	Various	Stain in PBS
Anti-human CD8	SK1	AF700	Biolegend	344724	1:50	2.2.1., 2.2.2., 2.2.9.	
Anti-human CD4	OKT4	BV785	Biolegend	317442	1:50	2.2.2., 2.2.9.	
Anti-human CD45RA	HI100	BV421	Biolegend	304130	1:50	2.2.1., 2.2.2., 2.2.9.	
Anti-human CD62L	DREG-56	AF647	Biolegend	304818	1:50	2.2.1., 2.2.2.	
Anti-human CCR7 (CD197)	2-L1-A	BUV737	BD OptiBuild	749676	1:50	2.2.2., 2.2.9.	
Anti-human CD56 (NCAM)	HCD56	BV510	Biolegend	318340	1:50	2.2.2., 2.2.9.	
Anti-human CD25	BC96	BV605	Biolegend	302632	1:50	2.2.1., 2.2.2., 2.2.8., 2.8.4.	
Anti-human CD69	FN50	APC	Biolegend	310910	1:50	2.2.1., 2.2.2., 2.2.8., 2.8.4.	
Anti-human CD279 (PD-1)	EH12.2H7	PE-Cyanine 7	Biolegend	329918	1:100	2.2.2.	
Anti-human CD279 (PD-1)	EH12.2H7	BV605	Biolegend	329924	1:50	2.2.2., 2.2.9.	
Anti-human CD223 (LAG-3)	11C3C65	FITC	Biolegend	369308	1:100	2.2.2.	
Anti-human CD366 (Tim-3)	F38-2E2	PE	Biolegend	345006	1:100	2.2.2.	
Anti-human TIGIT	741182	BUV395	BD OptiBuild	747845	1:50	2.2.2., 2.2.9.	
Anti-human CD269 (BCMA)	19F2	PE	Biolegend	357504	1:50	2.2.2., 2.2.8.	
Anti-human IFN-gamma	B27	FITC	Biolegend	506504	1:50	2.2.1., 2.2.4., 2.2.9.	
Anti-human IFN-gamma	4S.B3	BUV737	BD Horizon™	612845	1:50	2.2.4., 2.2.8., 2.8.4.	
Anti-human TNF-alpha	MAb11	PE	Biolegend	502909	1:150	2.2.1., 2.2.4., 2.2.8.	
Anti-human TNF-alpha	MAb11	AF647	Biolegend	502916	1:50	2.2.4., 2.2.9., 2.8.4.	

Anti-human Granzyme B	GB11	AF700	BD Pharmingen™	561016	1:50	2.2.4.	
Anti-human/mouse Granzyme B	QA16A02	PE-Cy5.5	Biolegend	372212	1:30	2.2.4., 2.2.8.	
Anti-human CD107a	H4A3	FITC	BD Biosciences	555800	1:50	2.2.4., 2.2.8.	
Anti-human Perforin	δG9	PE-Cyanine 7	Invitrogen	25-9994-42	1:50	2.2.4., 2.2.8.	
Anti-mouse/human Ki67	11F6	FITC	Biolegend	151212	1:50	2.2.4., 2.2.9.	
Anti-Lck Phospho (Tyr505)	A17013A	PE	Biolegend	699704	1:50	2.2.5.	
Anti-ERK1/2 Phospho (Thr202/Tyr204)	4B11B69	AF647	Biolegend	675504	1:50	2.2.5.	
NFAT1 (D43B1) XP(R) Rabbit mAb	Unknown	AF647	Cell Signalling Technology	14201S	1:50	2.2.6.2.	
Anti-Hu/Mo Phospho-mTOR (Ser2448)	MRRBY	PE	Invitrogen	12-9718-42	1:100	2.2.5., 2.8.4.,	
mTOR (7C10) Rabbit mAb	Unknown	AF647	Cell Signalling Technology	5048S	1:50	2.2.5.	
P-Akt (T308) (C31E5E) Rabbit mAb	Unknown	Unconjugated	Cell Signalling Technology	2965L	1:100	2.2.5.	
P-p70 S6 Kinase (T421/S424) Rabbit Ab	Unknown	Unconjugated	Cell Signalling Technology	9204S	1:100	2.2.5., 2.2.10.	
p70S6 kinase	Unknown	Unconjugated	Cell Signalling Technology	9202S	1:50	2.2.5.	
c-Myc (E5Q6W) Rabbit mAb	Unknown	Unconjugated	Cell Signalling Technology	18583S	1:200	2.2.5., 2.2.9., 2.8.4.	
DDIT4 Polyclonal Antibody	Unknown	Unconjugated	Invitrogen	PA5-109213	1:100	2.2.5.	
BNIP3 (D7U1T) Rabbit mAb	Unknown	Unconjugated	Cell Signalling Technology	44060S	1:100	2.2.5., 2.2.9., 2.7.3., 2.8.4.	
Rheb monoclonal antibody	GT39819	Unconjugated	Invitrogen	MA5-27777	1:100	2.2.5., 2.2.9., 2.8.4.	PE-Cy7 (ab102903)
Donkey anti-rabbit IgG (H+L)	Unknown	AF555	Invitrogen	A31572	1:500	Various	Secondary
Donkey anti-rabbit IgG (min. x-reactivity)	Poly4064	BV421	Biolegend	406410	1:100	Various	Secondary
Goat anti-mouse IgG (minimal x-reactivity)	Poly4053	PE-Cyanine 7	Biolegend	405315	1:100	Various	Secondary
Anti-mouse CD8a	53-6.7	AF700	Biolegend	100730	1:100	2.2.2., 2.2.11.	
Anti-mouse CD8a	53-6.7	PE-Cyanine 7	Biolegend	100721	1:200	2.2.2., 2.2.11., 2.2.12.	

Anti-mouse CD4	GK1.5	APC	Biolegend	100412	1:100	2.2.2., 2.2.11.	
Rat Anti-mouse CD4	GK1.5	BUV395	BD Horizon™	563790	1:200	2.2.2., 2.2.11., 2.2.12.	
Anti-mouse TCR beta	H57-597	PerCP-Cyanine5.5	TONBO Biosciences	65-5961-U100	1:200	2.2.2., 2.2.11., 2.2.12.	
Anti-puromycin	12D10	AF647	Merck	MABE343-AF647	1:300	2.2.12.,	
CD3 theta (CD3-12) Rat mAb	N/A	Unconjugated	Cell Signalling Technology	Component of 14541 (4443)	1:1000	2.7.3.	
Phospho-Lck (Tyr505)	N/A	Unconjugated	Cell Signalling Technology	Component of 14541 (2751)	1:1000	2.7.3.	
Phospho-Src Family (Tyr416) (D49G4) Rabbit mAb	N/A	Unconjugated	Cell Signalling Technology	Component of 14541 (6943)	1:1000	2.7.3.	
Phospho-Zap-70 (Tyr493)/Syk (Tyr526) Antibody	N/A	Unconjugated	Cell Signalling Technology	Component of 14541 (2704)	1:1000	2.7.3.	
Phospho-Zap-70 (Tyr319)/Syk (Tyr352) (65E4) Rabbit mAb	N/A	Unconjugated	Cell Signalling Technology	Component of 14541 (2717)	1:1000	2.7.3.	
Phospho-SLP-76 (Ser376) (D9D6E) Rabbit mAb	N/A	Unconjugated	Cell Signalling Technology	Component of 14541 (14745)	1:1000	2.7.3.	
Anti-rat IgG, HRP-linked Antibody	Unknown	HRP-linked	Cell Signalling Technology	Component of 14541 (7077)	1:2000	2.7.3.	
Anti-rabbit IgG, HRP-linked Antibody	Unknown	HRP-linked	Cell Signalling Technology	7074S	1:2000	2.7.3.	
BCMAxCD3 bispecific Ab	N/A	N/A	Invivogen	bimab-hbcmacd3-05	10ng/ml	2.2.8.	

3. Results Chapter 1

Interrogation of $CD8^+$ T cell activation and function in hypoxia

3. Results Chapter 1: Interrogation of CD8$^+$ T cell activation and function in hypoxia

3.1. Introduction

For a CD8$^+$ T cell to be efficient at targeting a cancer cell, it must be activated to produce effector molecules and direct a cytotoxic response. If the CD8$^+$ T cell is unable to activate appropriately, then its resultant effector functions are likely to be diminished and the response against the target cell attenuated. Whilst intrinsic features of the CD8$^+$ T cell may impact its activation, such as differentiation and exhaustion status, other features of the surrounding environment also have a role.

It is well documented that the TME is hypoxic, including in MM (Asosingh *et al.*, 2005; Colla *et al.*, 2010; Ikeda and Tagawa, 2021; Li *et al.*, 2022). Previous studies have explored the relationship between T cell function and hypoxia but have produced diverse and contradictory findings. If you break down the literature according to T cell species of origin, method of activation and protocol used for hypoxic exposure, it becomes clear that the time period a cell experiences hypoxia for, and when this occurs relative to T cell activation, are crucial for the resultant effects on the T cell. For the purpose of this thesis, I have divided protocols into 3 categories based on the time of hypoxic exposure, T cell expansion, and point of activation **(Figures 1.5 and 1.6)**. **Table 1.1** gives an overview of the literature concerning CD8$^+$ T cells exposed to hypoxia, broken down by species, protocol and key results. P1 describes a method in which T cells are isolated from the host, and immediately transferred to hypoxia for activation and culture. P2 includes methods where T cells are isolated, activated and expanded or differentiated in standard, normoxic, culture conditions, and then later

transferred to hypoxia prior to analysis; and P3 includes studies where T cells are isolated, activated in normoxia, and then expanded or differentiated in hypoxia where they may receive a re-stimulation (P3). **Figure 1.6** demonstrates the overall effects observed with each of these protocol systems.

Recent work has shown that T cells must be re-activated within the tumour site to acquire effector functions (Prokhnevska *et al.*, 2023), so it is important that $CD8^+$ T cells are able to respond to stimulation in hypoxia, which is relevant to P1. Previous work using P1 has shown that $CD8^+$ T cells activated and cultured within hypoxia may have impaired cytokine release and proliferation (Caldwell *et al.*, 2001; Liu *et al.*, 2020), however this work is limited. The impact of hypoxia on $CD8^+$ T cell activation and cytotoxicity is also unclear (Caldwell *et al.*, 2001; Liu *et al.*, 2020). To understand how human $CD8^+$ T cells activate and function in hypoxia I have utilised P1 in this thesis. $CD8^+$ T cells are pre-conditioned in normoxia or hypoxia immediately after isolation, activated within these O_2 conditions and cultured over various time points.

3.2. Aims

I hypothesise that the hypoxic nature of TME may inhibit $CD8^+$ T cell activation and function. I have conducted *in vitro* experiments with primary human $CD8^+$ T cells exposed to hypoxia or normoxia during TCR and CD28 stimulation and analysed for activation status and functional capacity. The aims for this chapter include:

1. To determine $CD8^+$ T cell activation status in hypoxia
2. To understand the downstream functional impacts of $CD8^+$ T cell activation in hypoxia
3. To explore these effects in sorted populations of naïve and memory $CD8^+$ T cells activated in hypoxia

3.3. Results

3.3.1. $CD8^+$ T cells survive, but do not efficiently activate in hypoxia

To assess $CD8^+$ T cell survival and activation in hypoxia, purified human $CD8^+$ T cells were cultured overnight in 21% (atmospheric), 5% (physiological) or 1% (hypoxic) O_2 tensions, to allow pre-equilibration of the O_2 levels into the media, plate and cells. The following morning, cells were activated by anti-CD3 and anti-CD28 and later assessed for viability with a fluorescent live/dead probe. Activation status was measured with the expression of cell-surface activation markers, CD25 and CD69. There was no difference in the percentage of live or dead activated (A), or non-activated (NA), $CD8^+$ T cells after culture for 48 hours in 21%, 5% or 1% O_2 **(Figure 3.1A)**. **Figure 3.1B** shows the gating strategy used throughout to gate on lymphocytes and then live (APC-$Cy7^-$) cells. Live cells were next stained for CD25 and CD69 expression as a measure of activation **(Figure 3.1C)**. A significant decrease in the percentage of $CD25^+$ $CD8^+$ T cells was present after 48 hours of stimulation and culture in 1% O_2 compared to 21% and 5% O_2 **(Figure 3.1C and 3.1D)**. However, no difference was observed in the percentage of $CD69^+$ $CD8^+$ T cells in 21%, 5% or 1% O_2, and in fact, an increasing trend of CD69 expression was observed with decreasing O_2 tension **(Figure 3.1C and 3.1D)**. There were significantly fewer $CD25^+$ $CD69^+$ $CD8^+$ T cells in 1% compared to 21% and 5% O_2 **(Figure 3.1C and 3.1D)**. The mean fluorescence intensity (MFI) of CD25 was significantly reduced in $CD8^+$ T cells in 1% compared to 21% and 5% O_2 **(Figure 3.1E)**. The MFI of CD25 was slightly but significantly increased in $CD8^+$ T cells in 5% compared to 21% O_2 **(Figure 3.1E)**, whilst the MFI of CD69 significantly increased with reduced O_2 tensions **(Figure 3.1E)**. In $CD25^+$ $CD8^+$ T cells, the MFI of CD25 was significantly reduced in 1% vs. 5% O_2 and tended to reduce in 1% vs 21%

O_2 **(Figure 3.1F)**, demonstrating that $CD8^+$ T cells that activated in hypoxia had a reduced activation status compared to those that activated in normoxia. Therefore, whilst there was no observed impact on survival, hypoxia decreased CD25 expression of $CD8^+$ T cells compared to atmospheric and physiological O_2 levels.

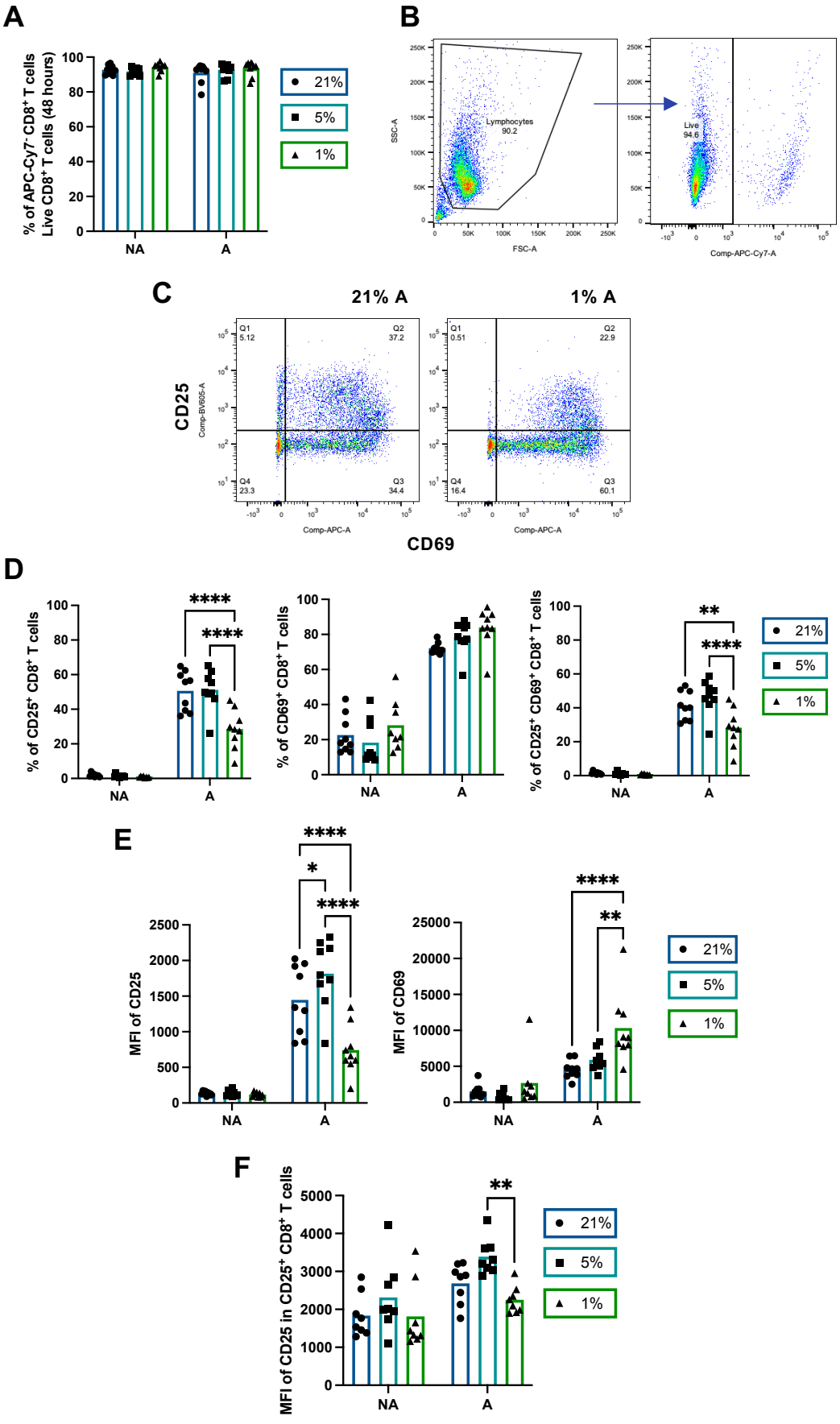
A
% of APC-Cy7⁻ CD8⁺ T cells
Live CD8⁺ T cells (48 hours)
NA
A
21%
5%
1%
B
Lymphocytes
90.2
SSC-A
FSC-A
Live
94.6
Comp-APC-Cy7-A
C
21% A
1% A
CD25
Comp-BV605-A
Q1
5.12
Q2
37.2
Q4
23.3
Q3
34.4
Q1
0.51
Q2
22.9
Q4
16.4
Q3
60.1
Comp-APC-A
CD69
D
% of CD25⁺ CD8⁺ T cells
% of CD69⁺ CD8⁺ T cells
% of CD25⁺ CD69⁺ CD8⁺ T cells
****
**
E
MFI of CD25
MFI of CD69
*
F
MFI of CD25 in CD25⁺ CD8⁺ T cells

Figure 3.1. $CD8^+$ T cell viability and activation status in hypoxia vs. normoxia. Isolated $CD8^+$ T cells were pre-conditioned overnight in 21%, 5%, or 1% O_2 conditions as indicated, activated the following morning with anti-CD3/CD28, and cultured in the same O_2 conditions for 48 hours. A) $CD8^+$ T cells were activated in 21%, 5%, or 1% O_2 and stained for viability, n = 9; B) Example gating strategy for viability. $CD8^+$ T cells were activated in 21%, 5%, or 1% O_2 and stained for CD25 (BV605) and CD69 (APC), C) Example histograms for 21% A and 1% A CD25 and CD69 staining; D) Percentage of $CD25^+$, $CD69^+$, and $CD25^+$ $CD69^+$ Live $CD8^+$ T cells shown in 21%, 5%, or 1% O_2, n = 9; E) Mean fluorescence intensity (MFI) of CD25 (BV605) and CD69 (APC) in live $CD8^+$ T cells in 21%, 5%, or 1% O_2, n = 9; F) MFI of CD25 (BV605) in live $CD25^+$ $CD8^+$ T cells in 21%, 5%, or 1% O_2, n = 9. NA = non-activated; A = activated. Blue bars = 21% O_2; Teal bars = 5% O_2; Green bars = 1% O_2. Data were analysed by (A, D, E, F) two-way ANOVA and Tukey's multiple comparisons post-hoc test, with a single pooled variance. * $p < 0.05$, ** $p < 0.005$, *** $p < 0.005$, ns = non-significant or 'blank', $p > 0.05$.

To understand if $CD8^+$ T cells activated in 1% O_2 alter expression of co-inhibitory receptors, PD-1, Lag-3, and Tim-3 were assessed at 48 hours post-activation in $CD8^+$ T cells stimulated and cultured in 21% and 1% O_2. Importantly, these co-inhibitory markers are upregulated upon T cell activation (Schnell *et al.*, 2020). A decrease in the expression of PD-1, Lag-3, and Tim-3 was observed in $CD8^+$ T cells activated and cultured for 48 hours in 1% compared to 21% O_2 **(Figure 3.2A)**. **Figure 3.2B** are representative flow plots of PD-1, Lag-3, and Tim-3 staining in $CD8^+$ T cells activated for 48 hours in 21% and 1% O_2.

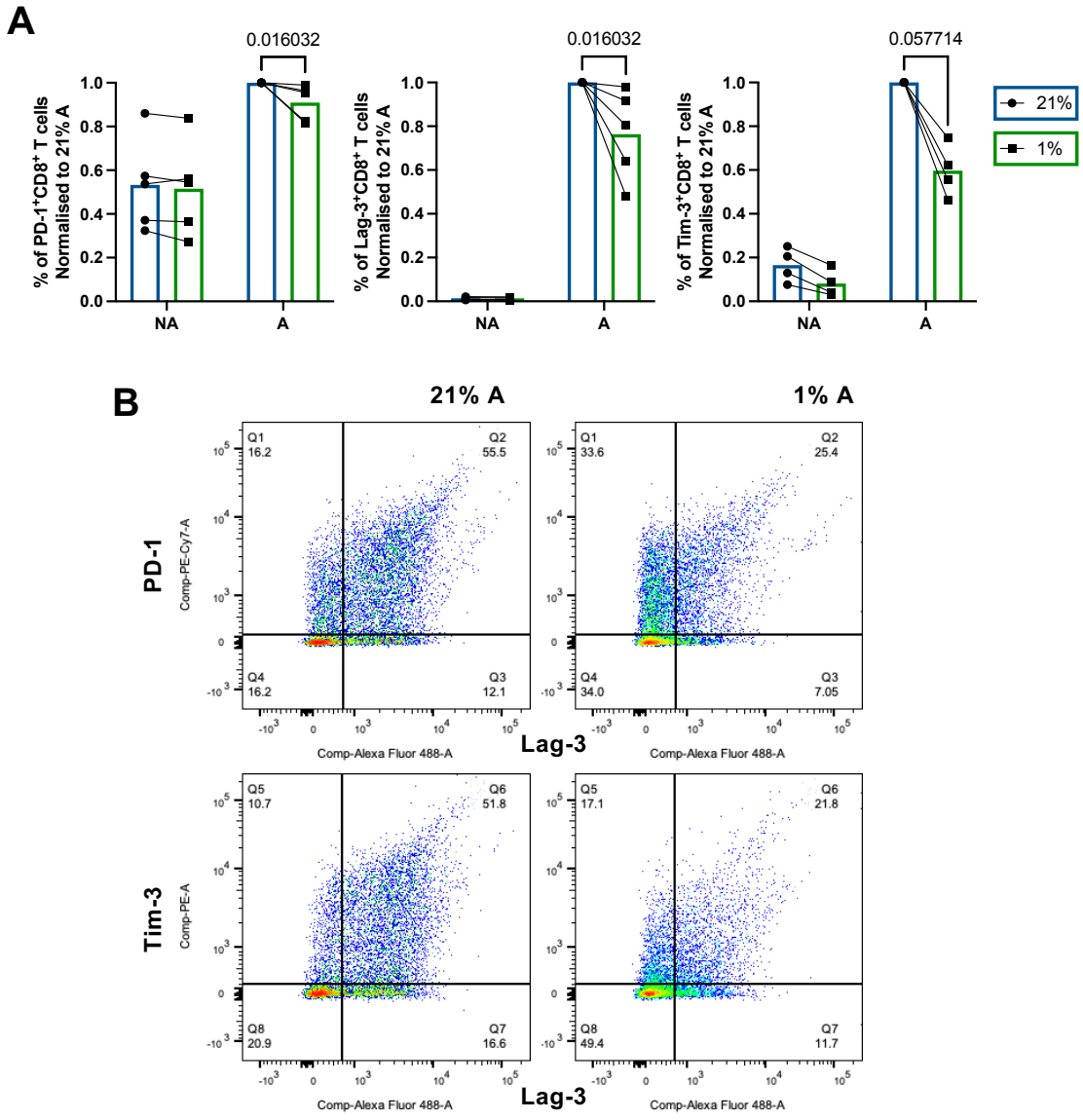

Figure 3.2. Expression of PD-1, Lag-3 and Tim-3 on CD8$^+$ T cells activated in hypoxia vs. normoxia. Isolated CD8$^+$ T cells were pre-conditioned overnight in 21% or 1% O_2 conditions, activated the following morning with anti-CD3/CD28, and cultured in the same O_2 conditions for 48 hours. A) CD8$^+$ T cells were activated in 21% or 1% O_2 for 48 hours and stained for PD-1 (PE-Cy7), Lag-3 (AF488), and Tim-3 (PE). Percentage of PD-1$^+$, Lag-3$^+$, and Tim-3$^+$ Live CD8$^+$ T cells shown, n = 5, normalised to 21% A as 1.0, Multiple Mann-Whitney tests; B) Example histograms of 21% A and 1% A sample staining, n = 1 out of 5. Blue bars = 21% O_2; Green bars = 1% O_2. 'n' refers to individual donors. Data were analysed by (A) Multiple Mann-Whitney tests with two-stage linear step-up procedure of Benjamin, Krieger and Yekutieli post-hoc test. P values shown, 'blank', $p > 0.05$.

3.3.2. IFN-gamma (IFN-γ), but not TNF-alpha (TNF-α), production and release are impaired in CD8⁺ T cells activated and cultured in hypoxia

To assess how $CD8^+$ T cell cytokine secretion is impacted by activation under hypoxia, isolated $CD8^+$ T cells were pre-conditioned overnight in either 21%, 5%, or 1% O_2, activated via anti-CD3/CD28 the following day, and supernatants harvested at 48 hours. Supernatants were analysed by ELISA for IFN-γ and TNF-α. There was a decrease in the secretion of IFN-γ from activated $CD8^+$ T cells in 1% O_2 compared to 21% and 5% O_2, and a non-significant trend for TNF-α secretion to decrease in 1% O_2 vs. 21% and 5% O_2 however this effect was not as great as for IFN-γ **(Figure 3.3A)**.

Previous studies have reported that TNF-α is rapidly secreted upon T cell activation (Brehm, Daniels and Welsh, 2005). Therefore, to understand if the lesser effect of hypoxia was related to a shorter duration of hypoxic exposure prior to cytokine secretion, or the availability of pre-formed cytokine within the cell, isolated $CD8^+$ T cells were pre-conditioned overnight in 21% or 1% O_2, activated via anti-CD3/CD28 the following day, and supernatants harvested over a time course of 8 to 72 hours. Relatively little IFN-γ was secreted within the first 8 hours of culture in 21% and 1% O_2, whilst approximately 50% of TNF-α was secreted by this time point **(Figure 3.3B)**. Thus, differential secretion kinetics exist for each cytokine. At 24 and 48 hours, IFN-γ secretion had reached 50% and 100%, respectively, and was significantly decreased at all time points in 1% O_2 **(Figures 3.3B and 3.3C)**. TNF-α secretion continued at 24 and 48 hours of culture, at a similar rate in 21% and 1% O_2 **(Figures 3.3B and 3.3C)**.

To understand how activation of $CD8^+$ T cells in hypoxia may impact cytokine production, intracellular cytokine flow cytometric staining was performed. $CD8^+$ T cells were pre-conditioned overnight in 21% or 1% O_2 prior to stimulation with anti-CD3/CD28 the following morning, 48 hours later $CD8^+$ T cells were re-stimulated with anti-CD3/CD28 or with PMA and ionomycin for 4 hours. At re-stimulation, brefeldin-A was added to prevent secretion of cytokines out of the cell. When $CD8^+$ T cells were initially stimulated and re-activated with anti-CD3/CD28, intracellular cytokine staining demonstrated significantly fewer IFN-γ^+ $CD8^+$ T cells in 1% O_2 compared to 21% O_2 **(Figure 3.3D)**, consistent with cytokine release data assessed by ELISA above **(Figures 3.3A-3.3C)**. No effect was observed in TNF-α production with anti-CD3/CD28 activation in the two O_2 conditions, whilst the percentage of IFN-γ^+ TNF-α^+ $CD8^+$ T cells trended towards a reduction in 1% compared to 21% O_2 **(Figure 3.3D)**. Importantly, when $CD8^+$ T cells were re-activated after the initial 48 hours with PMA and ionomycin the effect on IFN-γ^+ $CD8^+$ and IFN-γ^+ TNF-α^+ $CD8^+$ T cells was lost **(Figure 3.3D)**. Since PMA and ionomycin stimulation bypasses the T cell signalling pathway (Ai *et al.*, 2013), this suggests a potential defect specific to CD3/CD28 T cell signalling. **Figure 3.3E** are representative plots showing the staining of IFN-γ and TNF-α in $CD8^+$ T cells activated and re-stimulated with anti-CD3/CD28 or with PMA/ionomycin as a positive control in 21% and 1% O_2. In sum, bulk $CD8^+$ T cells activated and cultured in hypoxia demonstrate a defect in IFN-γ production and release that is not observed in TNF-α.

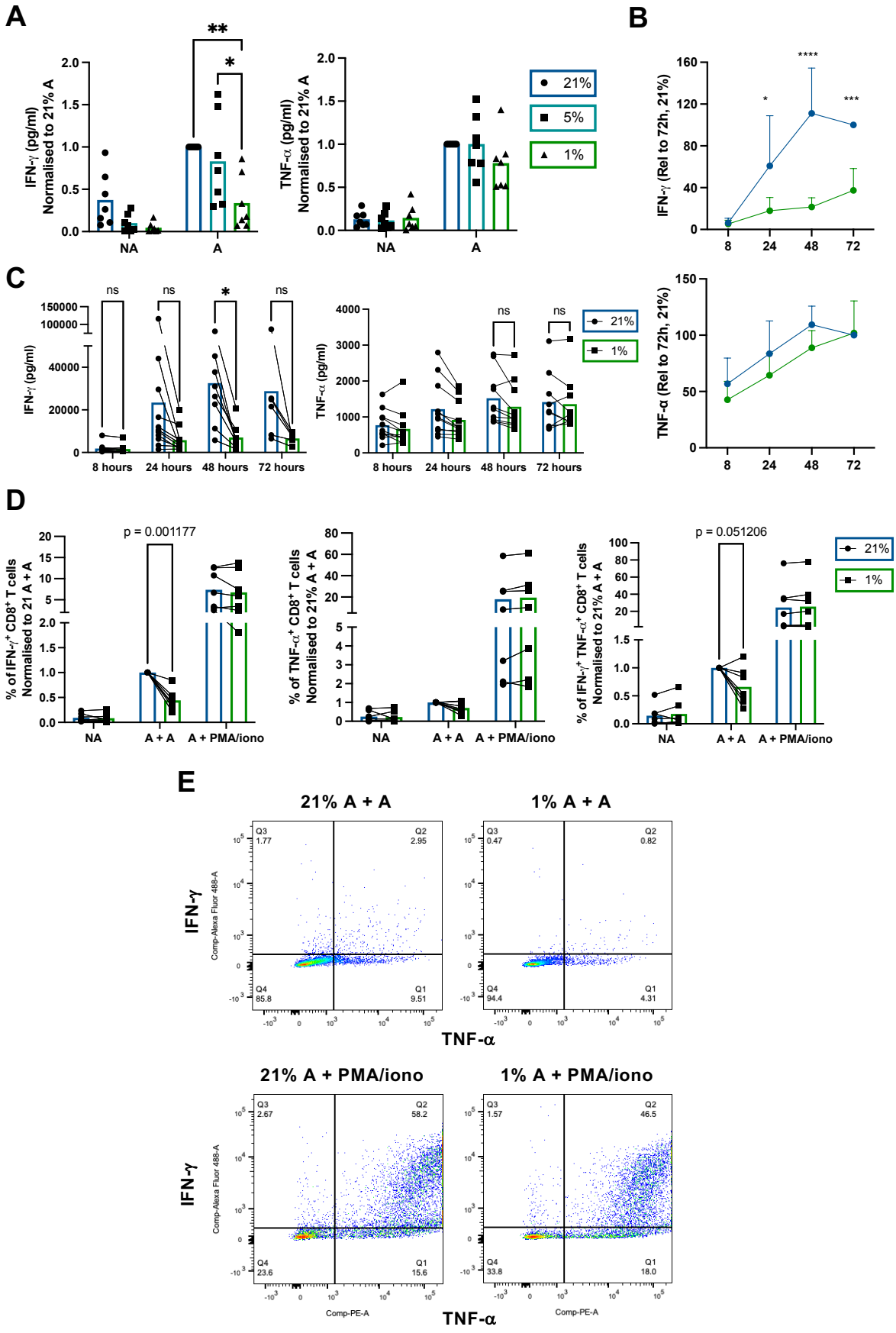
A
IFN-γ (pg/ml) Normalised to 21% A
TNF-α (pg/ml) Normalised to 21% A
NA
A
21%
5%
1%
B
IFN-γ (Rel to 72h, 21%)
TNF-α (Rel to 72h, 21%)
C
IFN-γ (pg/ml)
TNF-α (pg/ml)
8 hours
24 hours
48 hours
72 hours
ns
D
% of IFN-γ+ CD8+ T cells Normalised to 21 A + A
% of TNF-α+ CD8+ T cells Normalised to 21% A + A
% of IFN-γ+ TNF-α+ CD8+ T cells Normalised to 21% A + A
p = 0.001177
p = 0.051206
A + A
A + PMA/iono
E
21% A + A
1% A + A
21% A + PMA/iono
1% A + PMA/iono
IFN-γ
TNF-α
Comp-Alexa Fluor 488-A
Comp-PE-A

Figure 3.3. Production and release of IFN-γ and TNF-α in $CD8^+$ T cells activated and cultured in hypoxia vs. normoxia. Isolated $CD8^+$ T cells were pre-conditioned overnight in 21%, 5%, or 1% O_2 conditions, activated the following morning with anti-CD3/CD28, and cultured in the same O_2 conditions for the time point indicated. A) $CD8^+$ T cells were activated in 21%, 5%, or 1% O_2 for 48 hours and ELISAs performed on the supernatants of cultured cells, IFN-γ and TNF-α concentrations shown, n = 7, normalised to 21% A; B) $CD8^+$ T cells were activated in 21% or 1% O_2 for 8-72 hours and ELISAs performed on the supernatants of cultured cells, IFN-γ and TNF-α concentrations shown, normalised to 72 hours 21%, n = 5; C) $CD8^+$ T cells were activated in 21% or 1% O_2 for 8-72 hours and ELISAs performed on the supernatants of cultured cells, IFN-γ and TNF-α concentrations shown, n = 11. $CD8^+$ T cells were activated in 21% or 1% O_2 for 48 hours, and then re-activated for 4 hours with anti-CD3/CD28 or PMA/ionomycin (iono) with brefeldin A for intracellular cytokine staining. D) Percentage of IFN-γ^+, TNF-α^+, or IFN-γ^+ TNF-α^+ Live $CD8^+$ T cells shown, n = 8, normalised to 21% A + A; E) Example histograms of IFN-γ (AF488) and TNF-α (PE) intracellular staining in 21% or 1% O2 with A+A or A+PMA/ionomycin (iono) stimulation. Blue bars = 21% O_2; Teal bars = 5% O_2; Green bars = 1% O_2. Data were analysed by (A) repeated measures two-way ANOVA with the Geisser-Greenhouse correction with the Holm-Sidak's multiple comparisons post-hoc test, with individual variances computed for each comparison, (B) repeated measures two-way ANOVA with Holm-Sidak's multiple comparisons post-hoc test, with a single pooled variance, (C) ordinary two-way ANOVA with Sidak's multiple comparisons post-hoc test, with a single pooled variance, (D) Multiple Mann-Whitney tests with two-stage linear step-up procedure of Benjamin, Krieger and Yekutieli post-hoc test. * $p < 0.05$, ** $p < 0.005$, *** $p < 0.005$, or p values shown; ns = non-significant or 'blank', $p > 0.05$.

3.3.3 The hypoxia-induced defect in CD25 expression and IFN-γ release can be partially rescued by return of $CD8^+$ T cells to normoxia

Since **Figure 3.3E** suggested that the defect on IFN-γ production in $CD8^+$ T cells activated in 1% O_2 was specific to CD3/CD28 T cell signalling, I wanted to understand if the decreased CD25 expression and IFN-γ release observed in 1% O_2 compared to 21% O_2 could be rescued with the return to normoxia after activation and initial signalling events had taken place. $CD8^+$ T cells were stimulated via anti-CD3/CD28 in 21% or 1% O_2 for 48 hours or activated in 21% or 1% O_2 and moved to the alternative O_2 condition after 30 minutes for the remainder of culture. **Figure 3.4A** demonstrates the set-up for these experiments. The decrease in the percentage of $CD25^+$ $CD69^+$ $CD8^+$ and $CD25^+$ $CD8^+$ T cells observed in 1% O_2 compared to 21% O_2 could be rescued by the return to normoxia after 30 minutes of activation **(Figure 3.4B)**.

However, the decrease of CD25 expression in 1% O_2 compared to 21% O_2 was not statistically significant in these experiments, as previously observed **(Figure 3.4B)**. No differences were observed in the percentage of $CD69^+$ $CD8^+$ T cells across the various O_2 conditions. A partial rescue of IFN-γ release was observed in $CD8^+$ T cells activated in 1% O_2 and moved to 21% O_2 30 minutes later, however this did not reach the concentration of IFN-γ when cultured at 21% O_2 for the entire time period **(Figure 3.4C)**. When $CD8^+$ T cells were activated in 21% O_2 and transferred to 1% O_2 30 minutes later, a significant decrease in IFN-γ release was observed, almost to the level of those cells activated and cultured in 1% O_2 for the entire duration of the experiment **(Figure 3.4C)**. In contrast, the same experiment performed for TNF-α release demonstrated no differences across the various O_2 culture conditions **(Figure 3.4C)**. Therefore, the defect of hypoxia on activation status and IFN-γ release can be partially rescued by return of $CD8^+$ T cells to normoxia after activation.

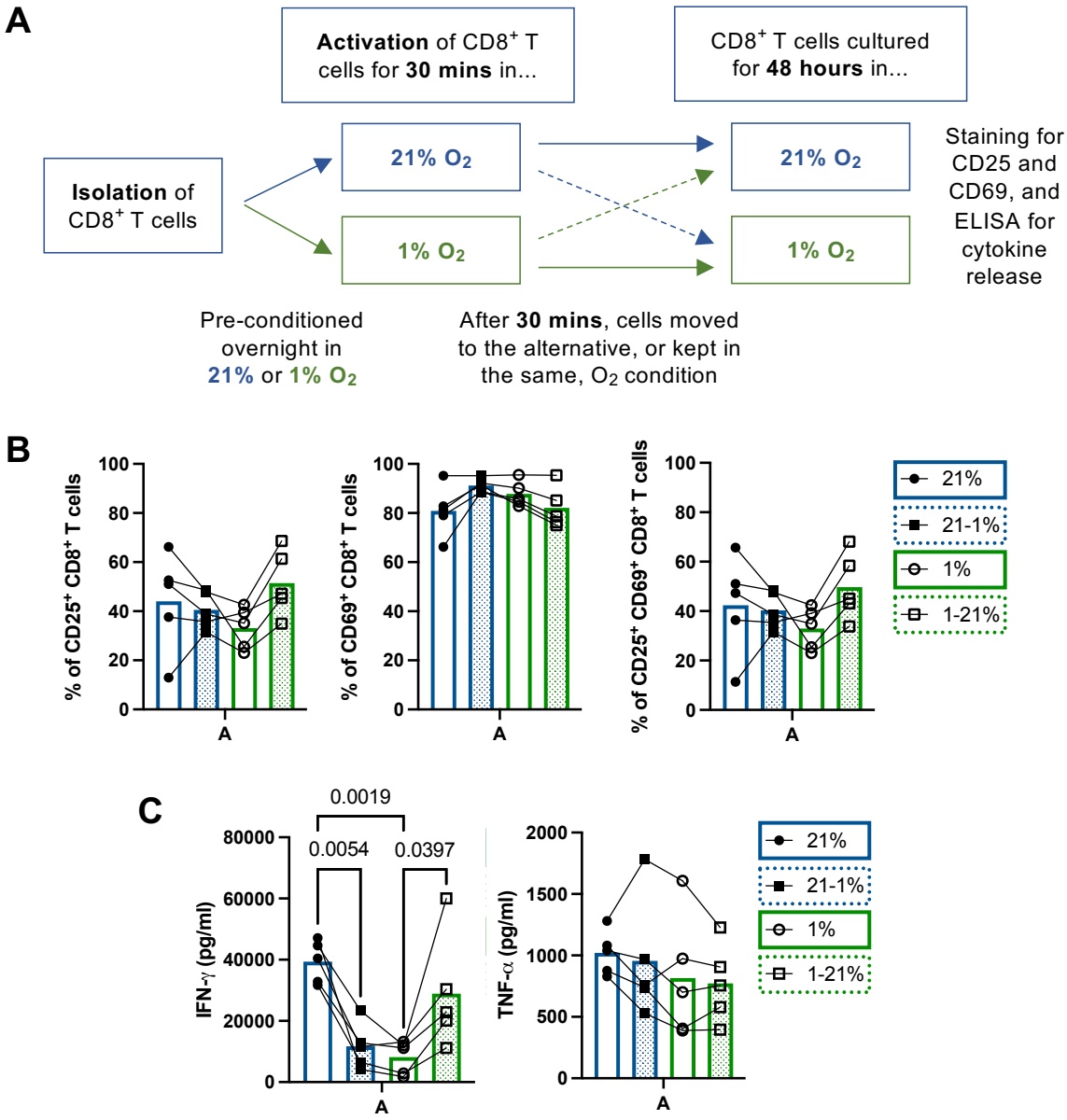

Figure 3.4. Production and release of IFN-γ and TNF-α in CD8$^+$ T cells activated and cultured in hypoxia vs. normoxia with reversal to the alternative O_2 condition. Isolated CD8$^+$ T cells were pre-conditioned overnight in 21% or 1% O_2 conditions, activated the following morning with anti-CD3/CD28, and cultured in the same O_2 conditions for 48 hours. A) Diagram of experiment set-up; B) CD8$^+$ T cells were activated in 21% or 1% O_2 for 48 hours or activated in 21% or 1% O_2 for 30 minutes and then moved to the alternative O_2 condition for the remainder of the 48 hours. Percentage of CD25$^+$, CD69$^+$, and CD25$^+$ CD69$^+$ Live CD8$^+$ T cells shown, n = 5; C) CD8$^+$ T cells were activated in 21% or 1% O_2 for 48 hours or activated in 21% or 1% O_2 for 30 minutes and then moved to the alternative O_2 condition for the remainder of the 48 hours, ELISAs performed on the supernatants of cultured cells, IFN-γ and TNF-α concentrations shown, n = 5. Blue bars = 21% O_2; Green bars = 1% O_2, filled bars = moved to alternative O_2 condition. Data were analysed by (A, B) ordinary one-way ANOVA with Tukey's multiple comparisons post-hoc test, with a single pooled variance. * $p < 0.05$, ** $p < 0.005$, *** $p < 0.005$, ns = non-significant or 'blank', $p > 0.05$.

3.3.4. Cytotoxic capacity of $CD8^+$ T cells does not appear to be impaired by activation and culture in hypoxia

To begin to assess the cytotoxic capacity of $CD8^+$ T cells activated in hypoxia, isolated $CD8^+$ T cells were pre-conditioned overnight to the relevant O_2 level and activated the following day via anti-CD3/CD28 for 5 hours in 21% or 1% O_2. For the activation period, brefeldin A and monensin were added to prevent cytotoxic molecule release from the cell, alongside a CD107a (lysosomal-associated membrane protein-1, LAMP-1) antibody to measure degranulation occurring across the whole time period of activation. The addition of brefeldin A and monensin results in granzyme B and perforin becoming trapped inside and not released from the cell, which can then be measured by intracellular staining. CD107a is well recognised membrane protein for the transport of cytolytic granules, thus having the anti-CD107a present during the entire experiment measures the cytotoxic activity of the cell (Aktas *et al.*, 2009). No differences in the expression of cytolytic granzyme-B (GzmB) and perforin-A (PrfA) **(Figure 3.5A)** were observed in $CD8^+$ T cells in activated 1% compared to 21% O_2. Similarly, CD107a trafficking to the membrane as an indicator of degranulation activity did not differ between $CD8^+$ T cells activated in 21% or 1% O_2 **(Figure 3.5A)**. **Figure 3.5B** are representative plots of GzmB, PrfA, and CD107a staining in $CD8^+$ T cells activated for 5 hours in 21% or 1% O_2 conditions. Overall, the cytotoxic capacity of $CD8^+$ T cells pre-conditioned and activated in hypoxia does not appear to be impaired compared to those pre-conditioned and activated in normoxia.

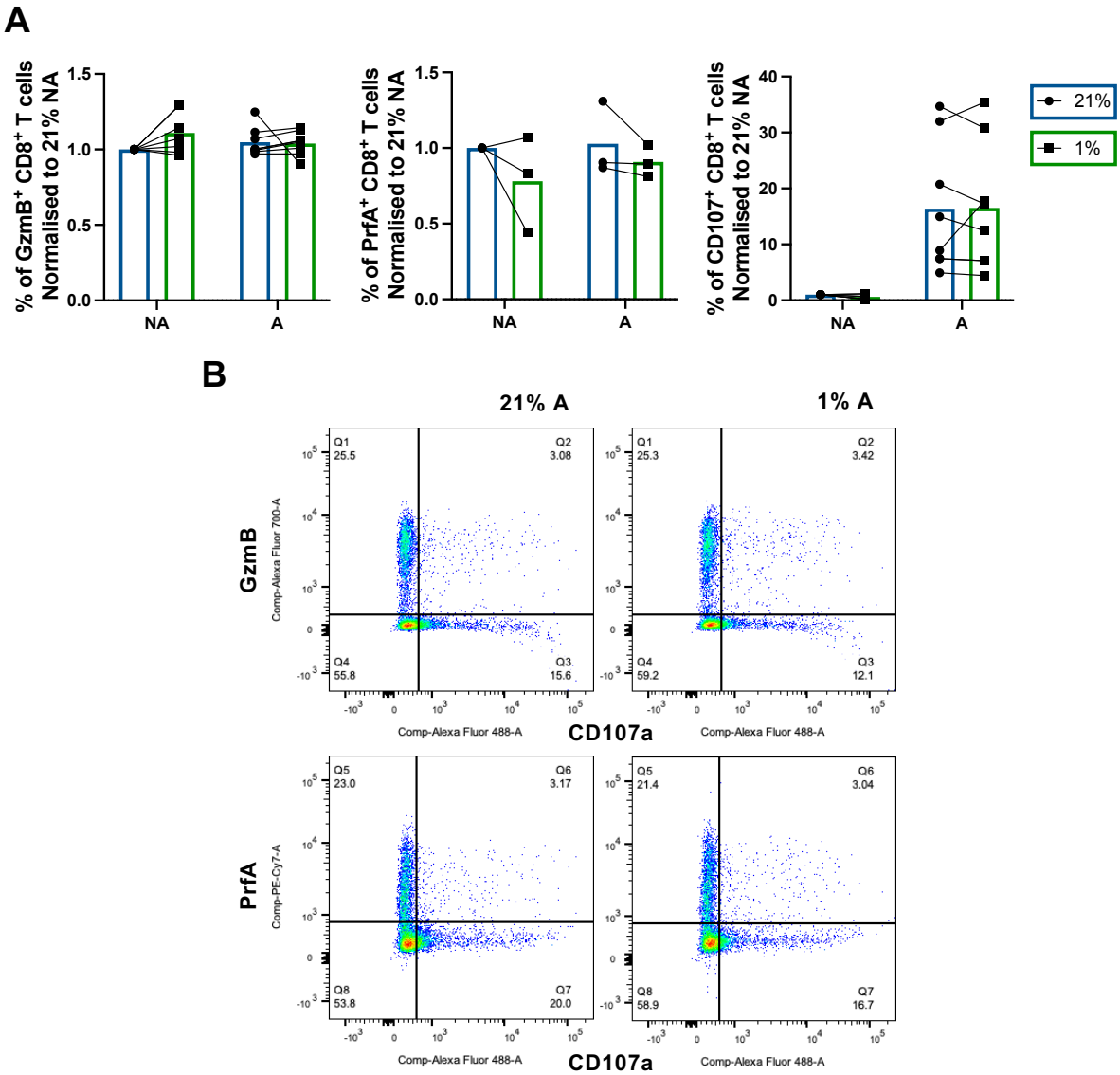

Figure 3.5. Cytotoxic capacity of CD8$^+$ T cells activated and cultured in hypoxia vs. normoxia. Isolated CD8$^+$ T cells were pre-conditioned overnight in 21% or 1% O_2 conditions, activated the following morning with anti-CD3/CD28, and cultured in the same O_2 conditions for 5 hours with brefeldin A, monensin and anti-CD107a. A) Percentage of GzmB$^+$, PrfA$^+$, and CD107a$^+$ Live CD8$^+$ T cells shown, n = 9, or 3 for PrfA, normalised to 21% NA; B) Example histograms of 21% A and 1% A sample staining, n = 1. Blue bars = 21% O_2; Green bars = 1% O_2. Data were analysed by (A) Multiple Mann-Whitney tests with two-stage linear step-up procedure of Benjamin, Krieger and Yekutieli post-hoc test. P values shown, 'blank', $p > 0.05$.

3.3.5. Proliferation of $CD8^+$ T cells is impaired when activated and cultured in hypoxia

To analyse proliferation of $CD8^+$ T cells activated and cultured in hypoxia, purified $CD8^+$ T cells were labelled with cell-trace violet (CTV), pre-equilibrated to the relevant O_2 condition overnight, and activated the following day via anti-CD3/CD28. Cells were then cultured for 5 days in either normoxia or hypoxia and analysed by flow cytometry. Interestingly, and unlike after 48 hours **(Figure 3.1A)**, after a total of 6 days culture in 21% or 1% O_2, non-activated (NA) $CD8^+$ T cells in 1% O_2 had increased survival compared to those in 21% O_2 **(Figure 3.6A)**. There was a non-significant trend of decreased survival in activated (A) $CD8^+$ T cells for 6 days in 1% vs. 21% O_2 **(Figure 3.6A)**. $CD8^+$ T cells cultured and activated in 1% O_2 demonstrated significantly reduced proliferation compared to cells cultured and activated in 21% O_2, as shown in the two representative histograms in **Figure 3.6B**. $CD8^+$ T cells activated in 1% O_2 had a reduced division index compared to those activated in 21% O_2 **(Figures 3.6C)**, which was consistent with an increased proportion of undivided cells (generation 0) in 1% O_2 and a reduction in the number of cells in generations 5 and 6 in 1% compared to 21% O_2 **(Figure 3.6D)**. The division index describes the average number of cell divisions undergone by a cell in the original population, including the undivided peak. Overall, $CD8^+$ T cells pre-conditioned, activated, and cultured for a total of 6 days in hypoxia had significantly reduced proliferation compared to those in normoxia.

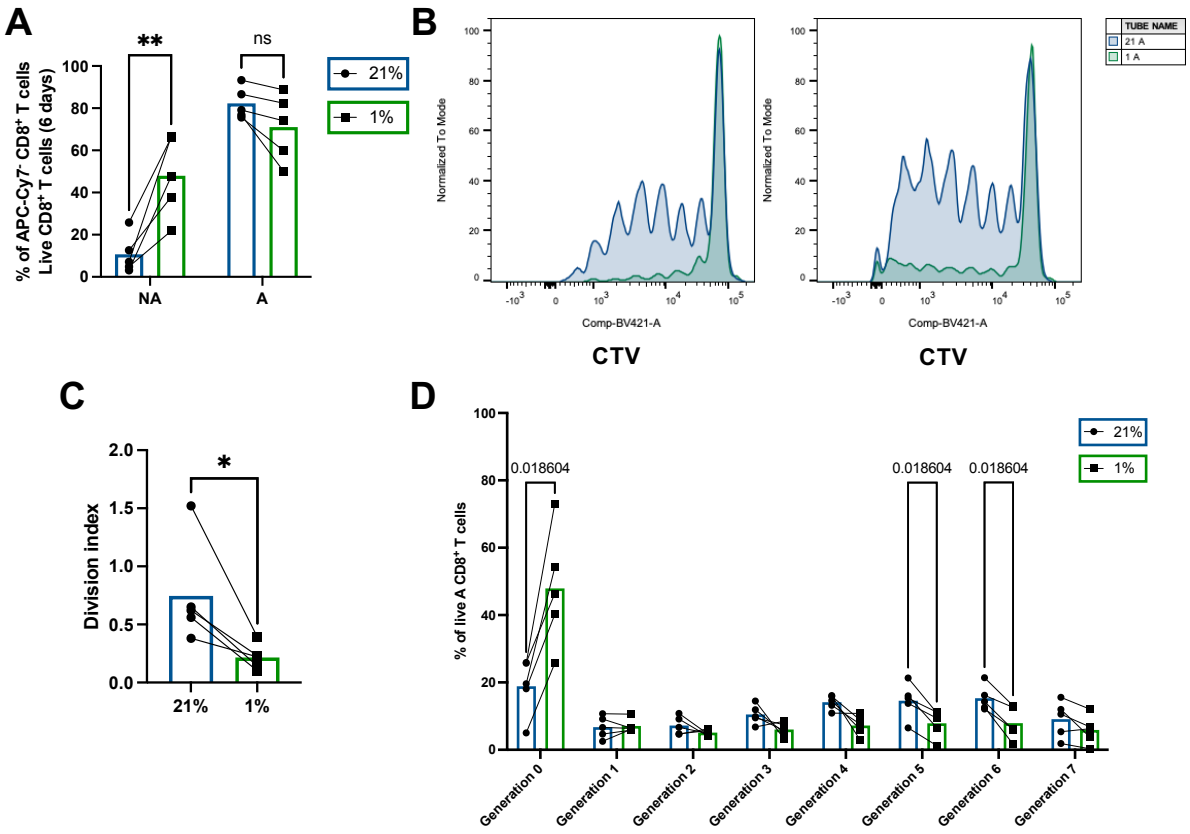

Figure 3.6. Proliferation of CD8$^+$ T cells activated and cultured in hypoxia vs. normoxia. Isolated CD8$^+$ T cells were labelled with Cell Trace Violet (CTV), pre-conditioned overnight in 21% or 1% O_2 conditions, activated the following morning with anti-CD3/CD28, and cultured in the same O_2 conditions for 6 days. A) CD8$^+$ T cells were left unstimulated (NA) or activated (A) in 21% or 1% O_2 for 6 days and measured for viability, shown is percentage of APC-Cy7 negative (live) CD8$^+$ T cells, n = 5; B) Example histograms of CTV staining in 21% and 1% A samples, n = 2; C) Division index of CD8$^+$ T cells activated in 21% or 1% O_2 for 6 days, n = 5. Division index calculated by taking the average number of divisions undergone by a cell in the original population, includes the undivided peak; D) Frequency of activated live CD8$^+$ T cells present in each peak, or generation, in 21% A or 1% A samples, n = 5. Blue bars = 21% O_2; Green bars = 1% O_2. Data were analysed by (A) ordinary two-way ANOVA with Sidak's multiple comparisons post-hoc test, with a single pooled variance, (C) paired t-test, (D) multiple paired t-tests with two-stage linear step-up procedure of Benjamini, Krieger and Yekutieli post-hoc test. * $p < 0.05$, ** $p < 0.005$, *** $p < 0.005$, or p values shown; ns = non-significant or 'blank', $p > 0.05$.

3.3.6. Naïve and memory $CD8^+$ T cell populations are impacted similarly by culture and activation in hypoxia

Naïve and memory $CD8^+$ T cells have different roles and functions in immune surveillance and anti-tumour responses. There is also a wide variety of $CD8^+$ T cell differentiation states present within the tumour site (Van der Leun, Thommen and Schumacher, 2020). Therefore, to understand if different naïve and memory $CD8^+$ T cell populations would be similarly impacted by hypoxia, purified $CD8^+$ T cells were sorted by fluorescence-activated cell sorting (FACS) by the expression of two surface markers: CD45RA and CD62L. Sorting in this manner separates bulk $CD8^+$ T cells into four individual populations: Naïve ($CD45RA^+$ $CD62L^+$), central memory (CM, $CD45RA^-$ $CD62L^+$), effector memory (EM, $CD45RA^-$ $CD62L^-$), and terminally differentiated effector memory cells (EMRA, $CD45RA^+$ $CD62L^-$). **Figure 3.7A** demonstrates the gating strategy used for the FACS sorting and **Figure 3.7B** is a diagram showing how CD45RA and CD62L expression is used to separate the four different populations. The number of replicates for each experiment depended on the number of cells gained from the FACS sorting of bulk $CD8^+$ T cells. After FACS sorting, cells of each population were pre-conditioned, activated via anti-CD3/CD38 and cultured at 21% or 1% O_2 for 48 hours. Naïve $CD8^+$ T cells had the greatest survival after FACS sorting and culture than the other three populations, which was similar between 1% and 21% O_2 **(Figure 3.7C)**. CM had the next best survival, then EM, and EMRA $CD8^+$ T cells had the worst survival in culture after FACS sorting, and no differences were observed between O_2 conditions **(Figure 3.7C)**. The percentage of $CD25^+$ $CD8^+$ T cells was decreased in each population in 1% compared to 21% O_2, significant in all but EM $CD8^+$ T cells **(Figure 3.7D)**. Similarly, the percentage of $CD25^+$ $CD69^+$ double positive

$CD8^+$ T cells tended to decrease in 1% vs. 21% O_2 for EM and EMRA, and significantly decreased in 1% O_2 for naïve and CM $CD8^+$ T cells **(Figure 3.7D)**. **Figure 3.7E** gives representative flow plots for the staining of CD25 and CD69 in activated cells across all the $CD8^+$ populations. Therefore, all naïve and memory $CD8^+$ T cell populations appear to have similar defects in CD25 expression, or activation, in hypoxia compared to normoxia, whilst the same is not observed in CD69 expression.

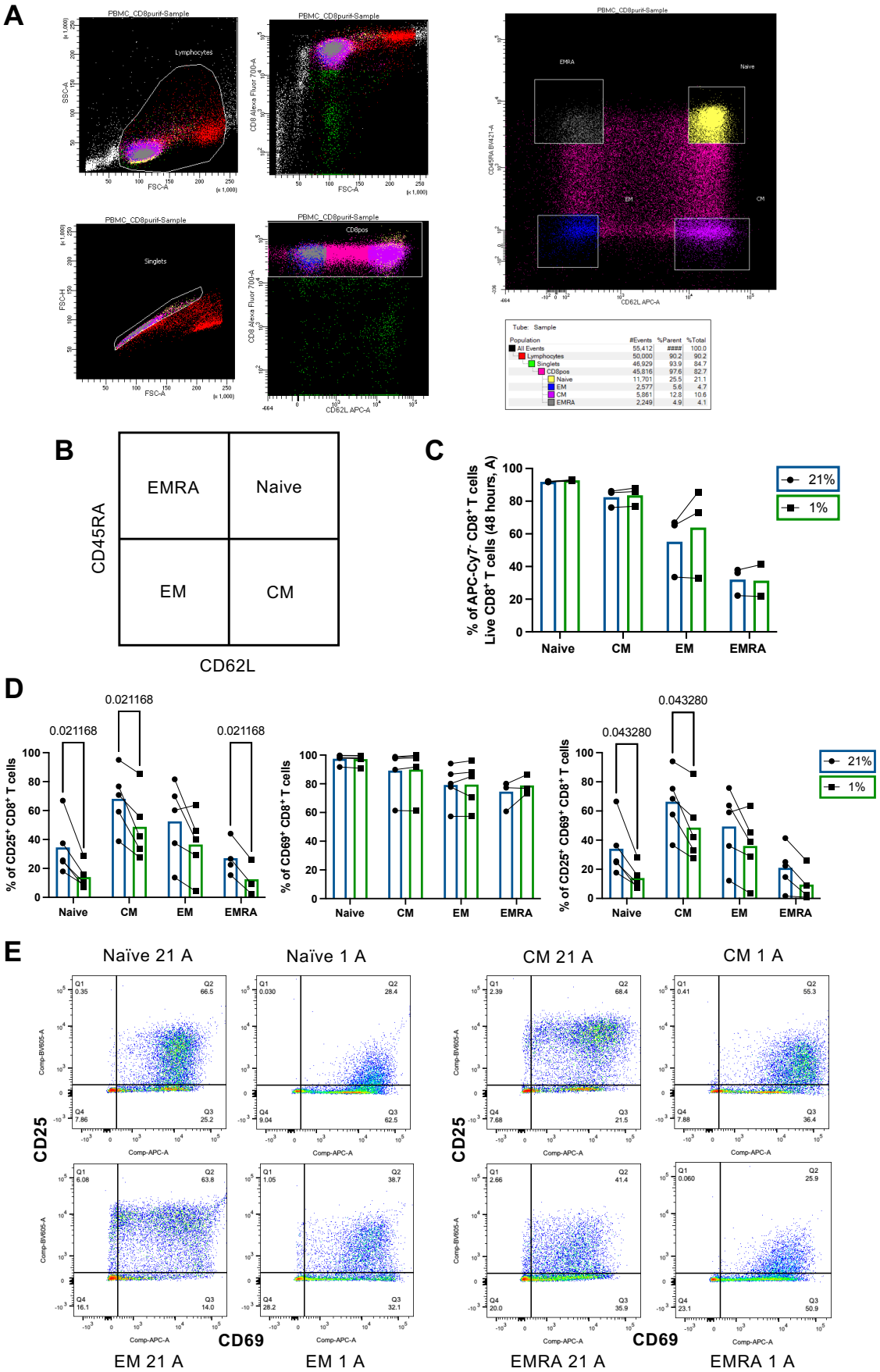
A
PBMC_CD8purif-Sample
Lymphocytes
SSC-A
FSC-A
CD8 Alexa Fluor 700-A
Singlets
FSC-H
CD8pos
CD62L APC-A
EMRA
Naive
EM
CM
CD45RA BV421-A
Tube: Sample
Population #Events %Parent %Total
All Events 55,412 #### 100.0
Lymphocytes 50,000 90.2 90.2
Singlets 46,929 93.9 84.7
CD8pos 45,816 97.6 82.7
Naive 11,701 25.5 21.1
EM 2,577 5.6 4.7
CM 5,861 12.8 10.6
EMRA 2,249 4.9 4.1
B
EMRA
Naive
EM
CM
CD45RA
CD62L
C
% of APC-Cy7- CD8+ T cells
Live CD8+ T cells (48 hours, A)
21%
1%
Naive
CM
EM
EMRA
D
0.021168
0.021168
0.021168
% of CD25+ CD8+ T cells
% of CD69+ CD8+ T cells
0.043280
0.043280
% of CD25+ CD69+ CD8+ T cells
21%
1%
Naive
CM
EM
EMRA
E
Naïve 21 A
Naïve 1 A
CM 21 A
CM 1 A
CD25
CD69
Comp-BV605-A
Comp-APC-A
Q1 0.35
Q2 66.5
Q4 7.86
Q3 25.2
Q1 0.030
Q2 28.4
Q4 9.04
Q3 62.5
Q1 2.39
Q2 68.4
Q4 7.68
Q3 21.5
Q1 0.41
Q2 55.3
Q4 7.88
Q3 36.4
Q1 6.08
Q2 63.8
Q4 16.1
Q3 14.0
Q1 1.05
Q2 38.7
Q4 28.2
Q3 32.1
Q1 2.66
Q2 41.4
Q4 20.0
Q3 35.9
Q1 0.060
Q2 25.9
Q4 23.1
Q3 50.9
EM 21 A
EM 1 A
EMRA 21 A
EMRA 1 A

Figure 3.7. FACS sorting of $CD8^+$ T cells into naïve, CM, EM and EMRA populations and viability and activation status in hypoxia vs. normoxia. Isolated $CD8^+$ T cells were FACS sorted by CD45RA and CD62L to obtain 4 populations – $CD45RA^+$ $CD62L^+$ (Naïve), $CD45RA^-$ $CD62L^+$ (CM), $CD45RA^-$ $CD62L^-$ (EM), and $CD45RA^+$ $CD62L^-$ (EMRA) and experiments performed as in Figures 3.1 and 3.3. A) Example of FACS gating strategy; B) Diagram to demonstrate the various $CD8^+$ T cell populations; C) $CD8^+$ T cells of the various populations were activated in 21% or 1% O_2 for 48 hours and stained for viability, n = 3; D) $CD8^+$ T cells of the various populations were activated in 21% or 1% O_2 for 48 hours and stained for CD25 and CD69. Percentage of $CD25^+$, $CD69^+$, and $CD25^+$ $CD69^+$ Live $CD8^+$ T cells, of the various populations, shown, n = 5; E) Example histograms of CD25 and CD69 staining in the various populations as indicated, n = 1. Blue bars = 21% O_2; Green bars = 1% O_2. Data were analysed by (D) multiple paired t-tests with two-stage linear step-up procedure of Benjamini, Krieger and Yekutieli post-hoc test. p values shown; ns = non-significant or 'blank', $p > 0.05$.

Each naïve and memory $CD8^+$ T cell population pre-conditioned, activated, and cultured for 48 hours in 21% or 1% O_2, appeared to reduce secretion of IFN-γ in 1% compared to 21% O_2, however this did not reach significance for any population **(Figure 3.8A)**. EM secreted the greatest concentration of IFN-γ and EMRA the least, although there was variability between donors, and the low cell viability of EM and EMRA should also be taken into account **(Figures 3.7C and 3.8A)**. Similarly, all populations tended towards a reduction of TNF-α secretion in 1% compared to 21% O_2 **(Figure 3.8A)**, however this was not significant and the effect on IFN-γ was greater than on TNF-α **(Figure 3.8B)**. The secretion of TNF-α was greatest in CM and lowest in EMRA $CD8^+$ T cells **(Figure 3.8A)**. Therefore, naïve, CM, EM and EMRA $CD8^+$ T cells act similarly to bulk $CD8^+$ T cells in terms of cytokine release into the supernatants.

As with bulk $CD8^+$ T cells, intracellular cytokine staining was performed on each individual naïve and memory population. For these experiments, each population was activated via anti-CD3/CD28 for 48 hours in 21% or 1% O_2, as above, but then re-

activated with anti-CD3/CD28 for 4 hours in the respective O_2 condition with the addition of brefeldin A. PMA/ionomycin stimulation was not conducted here because of constraints of cell number, and since CD3/CD28 stimulation was more informative in bulk $CD8^+$ T cell cultures. The percentage of IFN-γ^+ $CD8^+$ T cells trended towards a reduction in CM and EM populations in 1% compared to 21% O_2, whilst naïve and EMRA populations did not differ between the O_2 conditions **(Figure 3.8C)**. As with cytokine secretion, EM $CD8^+$ T cells expressed the most IFN-γ (highest frequency of cytokine positive cells), whilst EMRA and naïve $CD8^+$ T cells had the fewest cytokine positive cells **(Figure 3.8C)**. Variable effects were observed on TNF-α production across the different populations, however as with bulk cells, little impact of 1% O_2 was seen on TNF-α production **(Figure 3.8C)**. EM and CM produced roughly equal amounts of TNF-α **(Figure 3.8C)**. The percentage of IFN-γ^+ TNF-α^+ $CD8^+$ T cells may reduce in 1% O_2 in CM and EM $CD8^+$ T cells, but not naïve and EMRA, however this did not reach statistical significance **(Figure 3.8C)**. Importantly, the decreased viability observed in EM and EMRA $CD8^+$ T cells **(Figure 3.7C)** may impact the production and secretion of IFN-γ and TNF-α of these populations and should be taken into account during interpretation of results. Overall, IFN-γ production may be impaired in hypoxia in specific memory populations, however further work is required to support this. As with bulk $CD8^+$ T cells, TNF-α production does not appear to be impaired by activation in hypoxia.

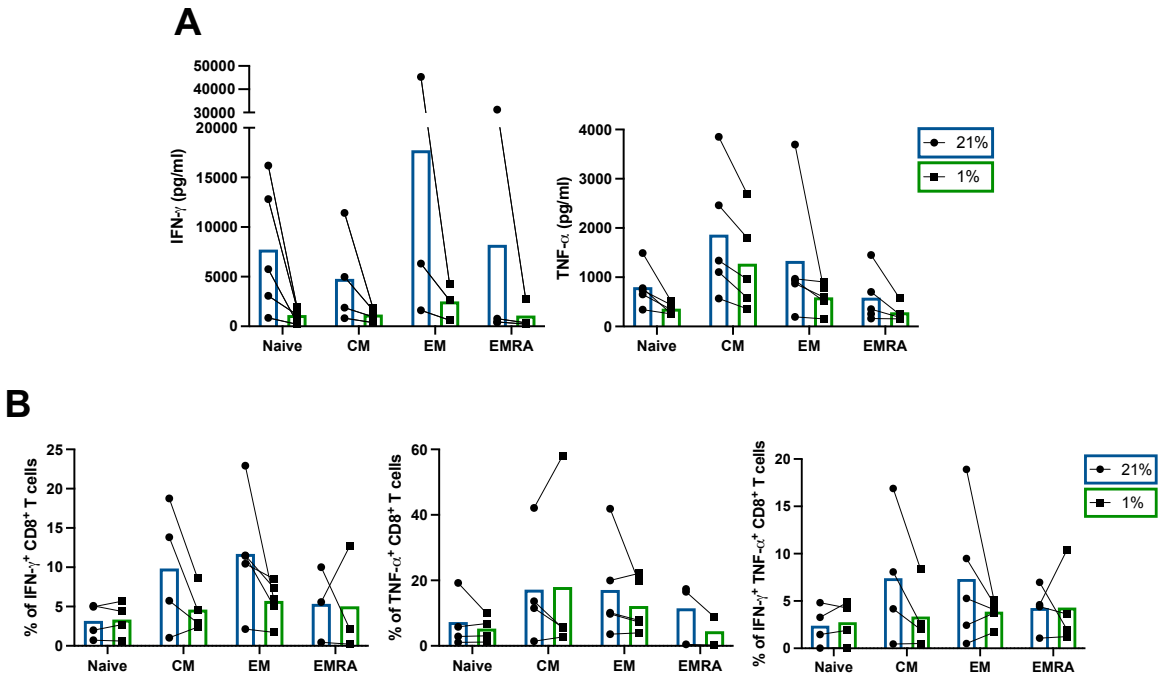

Figure 3.8. Production of IFN-γ and TNF-α in naïve, CM, EM and EMRA $CD8^+$ T cells activated and cultured in hypoxia vs. normoxia. Isolated $CD8^+$ T cells were FACS sorted by CD45RA and CD62L to obtain 4 populations – $CD45RA^+$ $CD62L^+$ (Naïve), $CD45RA^-$ $CD62L^+$ (CM), $CD45RA^-$ $CD62L^-$ (EM), and $CD45RA^+$ $CD62L^-$ (EMRA) and experiments performed as in Figures 3.1 and 3.3. A) $CD8^+$ T cells, of the various populations, were activated in 21% or 1% O_2 for 48 hours and ELISAs performed on the supernatants of cultured cells, IFN-γ and TNF-α concentrations shown, n = 5; B) Percentage of IFN-γ^+, TNF-α^+, or IFN-γ^+ TNF-α^+ Live $CD8^+$ T cells, of each population, shown, n = 5. Blue bars = 21% O_2; Green bars = 1% O_2. Data were analysed by (A, B) multiple paired t-tests with two-stage linear step-up procedure of Benjamini, Krieger and Yekutieli post-hoc test. p values shown; ns = non-significant or 'blank', $p > 0.05$.

3.4. Discussion

The TME is hypoxic, including in MM (Asosingh *et al.*, 2005; Colla *et al.*, 2010; Ikeda and Tagawa, 2021; Li *et al.*, 2022), however how this impacts the immune cell environment remains incompletely understood. Importantly, cytotoxic T cells, a key eliminator of cancerous cells, are known to be immunosuppressed within the TME of MM (Mills and Cawley, 1983; Brown *et al.*, 1998; Frassanito, Cusmai and Dammacco, 2001; Kay *et al.*, 2001; Pratt, Goodyear and Moss, 2007; Gudgeon *et al.*, 2023). It is crucial to understand if hypoxia in the TME contributes to T cell suppression, as this may impact cancer outcomes and therapeutics. This chapter has begun to elucidate the impact of hypoxia on $CD8^+$ T cell activation and function by utilising *in vitro* assays.

For optimum immune system function, $CD8^+$ T cells need to survive in the TME, be sufficiently activated, and appropriately produce effector cytokines and cytotoxic molecules. To explore these read-outs under hypoxia, I isolated healthy human $CD8^+$ T cells and activated them in various O_2 tensions: 21%, 5% and 1% O_2. 21% O_2 reflects atmospheric O_2, the level present in the atmosphere and what the majority of researchers use as 'normal' in culture (McKeown, 2014), whilst 1% O_2 is reflective of what is often seen in tumours as pathological (Muz *et al.*, 2015). However, it is well known that physiological O_2 levels within the human body are much lower than atmospheric, with the bloodstream at roughly 5% O_2 (McKeown, 2014; Ortiz-Prado *et al.*, 2019). Therefore, it was important I included this as a condition to explore whether this was different to atmospheric or pathological sites. Indeed, for two key functional read-outs, activation and cytokine secretion, results were similar between 21% and 5% O_2, indicating cells behave similarly under these oxygen tensions and that atmospheric

O_2 can be used to model physiological oxygen in the body **(Figures 3.1 and 3.3)**. I therefore continued experiments comparing continued comparing 21% and 1% O_2 only, since it was not practically feasible to continue to employ two oxygen-controlled environments (i.e., 5% and 1% O_2) in parallel. However, these findings are important for other researchers working in the immunology field, as it suggests that 21% O_2 used in the majority of laboratory methods is a good surrogate for physiological levels.

There was no change in survival of $CD8^+$ T cells across the three O_2 tensions, however expression of CD25 was significantly reduced in $CD8^+$ T cells activated in 1% O_2 **(Figure 3.1)**. Since CD25, the alpha-chain of the IL-2 receptor, is a well-recognised late marker of T cell activation (Reddy *et al.*, 2004; Peng *et al.*, 2023), this suggests an impairment of activation in hypoxia. A murine study published in 2001 isolated splenocytes and differentiated these into CTLs in three O_2 tensions: 20%, 2.5% and 1% O_2 (Caldwell *et al.*, 2001). They demonstrated that in hypoxia fewer CTLs upregulated CD25 (Caldwell *et al.*, 2001), similar to my experiments in activated human $CD8^+$ T cells. However, they showed that activated cells in hypoxia expressed a greater CD25 surface density than in normoxia (Caldwell *et al.*, 2001). They suggested that whilst fewer CTLs overall express CD25, those that do develop in hypoxia do so more slowly and with greater activation levels (Caldwell *et al.*, 2001). In my data, the MFI of CD25 was significantly reduced in all $CD8^+$ T cells activated in 1% vs 21% O_2 and tended to reduce in $CD25^+$ $CD8^+$ T cells activated in 1% vs. 21% O_2 suggesting that this was not the case in my culture setting **(Figure 3.1)**. On the other hand, an earlier marker of T cell activation, CD69 (Reddy *et al.*, 2004), did not differ between O_2 tensions upon $CD8^+$ T cell activation **(Figure 3.1)**. In 2017, a study

demonstrated that a direct relationship exists between CD69 and HIF-1α, where HIF-1α drives CD69 expression (Labiano *et al.*, 2017). Since HIF-1α is readily stabilised in hypoxia (Ivanova, Park and Kenneth, 2019), it likely increases the expression of CD69, which may mask any effect of hypoxia on T cell activation. For this reason, CD69 is an unreliable marker for T cell activation in hypoxia. Alongside activation markers, various co-inhibitory receptors are upregulated on the $CD8^+$ T cell surface upon activation, for example, PD-1, Lag-3 and Tim-3 (Schnell *et al.*, 2020). $CD8^+$ T cells activated in hypoxia also demonstrated reduced expression of these co-inhibitory receptors compared to normoxic cells **(Figure 3.2)**, which may reflect a decreased activation state rather than a reduction in an exhausted phenotype as they are often used to measure (Marraco *et al.*, 2015; Wherry and Kurachi, 2015), particularly since my experiments are relatively short-term and not designed to induce T cell exhaustion, for example by repeated antigen stimulation. In 2020, a study isolated peripheral T cells from human donors, activated these with anti-CD3 under normoxic conditions, and then cultured cells in 20% vs 1% O_2 for 48 hours (Liu *et al.*, 2020). In contrast to my experiments, they showed that activated T cells subsequently cultured in hypoxia increased PD-1 and TIM-3 expression compared to those in normoxia (Liu *et al.*, 2020). Of note, the T cells in this study were activated prior to hypoxic exposure (Liu *et al.*, 2020), whilst in my methods, T cells were activated whilst present in hypoxia. Therefore, it is likely the activation of T cells within hypoxia that downregulates co-inhibitory receptors and may reflect a reduced activation state. Overall, these human *in vitro* experiments suggest that $CD8^+$ T cells have impaired activation when stimulated within hypoxia.

A recent study by Prokhnevska et al. (2023) proposed a two-step model of T cell activation in the tumour context (Prokhnevska *et al.*, 2023). They reported that T cells responding to a range of human cancers, and similarly in mouse models, are initially primed by activation in tumour-draining lymph nodes (Prokhnevska *et al.*, 2023). Here, they are capable of proliferation but are retained in a stem-like state (Prokhnevska *et al.*, 2023). On moving to the tumour site, these stem-like cells must be re-activated with co-stimulation to acquire effector functions (Prokhnevska *et al.*, 2023). This is important when considering the model of our hypoxic exposure compared to others in the literature. Since it is important that T cells are re-activated in the hypoxic tumour site, my method to activate T cells within hypoxia, and not prior to exposure, is relevant.

When human $CD8^+$ T cells were pre-conditioned and activated in hypoxia, they released and produced less IFN-γ than their normoxic counterparts **(Figure 3.3)**, which was similarly observed by Caldwell et al. (2001) in their differentiation of splenocytes to CTLs in hypoxia (Caldwell *et al.*, 2001), and Liu et al. (2020) when exposing already activated human T cells to hypoxia (Liu *et al.*, 2020). Interestingly, I did not observe the same effect on the release and production of TNF-α, suggesting a specific mechanism of hypoxia on IFN-γ **(Figure 3.3)**. This indicates that a defect in IFN-γ, but not TNF-α, release and production may exist as within a resting T cell there is a greater amount of pre-formed TNF-α messenger ribonucleic acid (mRNA) than IFN-γ (Salerno *et al.*, 2017). This means upon T cell activation, TNF-α is more rapidly translated and secreted than IFN-γ and requires less energy for translation, a feature limiting in hypoxia (Wheaton and Chandel, 2011). In addition, hypoxia impairs global translation rates via mTOR (Chee, Lohse and Brothers, 2019), which has been previously

demonstrated in $CD8^+$ T cells in hypoxia (De Ponte Conti, 2021). Thus, the translation of cytokines is likely to be impaired in hypoxia and will further potentiate the defect of IFN-γ production compared to TNF-α. Of note, another study has reported that CTLs differentiated in normoxia and then conditioned in hypoxia for 24 hours prior to antigen-stimulation demonstrated both impaired IFN-γ and TNF-α release, highlighting again that hypoxia can have varied effects on $CD8^+$ T cell function depending on timing of exposure relative to cellular differentiation status (Ross, Rollings and Cantrell, 2021).

Interestingly, $CD8^+$ T cells activated in hypoxia and transferred to normoxia 30 minutes later experience a partial rescue in their IFN-γ release, suggesting the effects of hypoxia on T cell function may be reversed **(Figure 3.4)**. Alternatively, $CD8^+$ T cells activated in normoxia but transferred to hypoxia 30 minutes later will experience a defect in IFN-γ release by 48 hours **(Figure 3.4)**, similar to that observed by Liu *et al.* (2020). This indicates that there are several mechanisms at play resulting in the impairment of T cell function in hypoxia, some related to T cell activation and others more global effects. Importantly however, return of $CD8^+$ T cells to normoxia after activation in hypoxia does appear to rescue the functional defects observed.

Naïve and memory $CD8^+$ T cell subsets demonstrate different roles and functions in immune surveillance and in anti-tumour responses. Research has reported a wide range of $CD8^+$ T cell phenotypes present in tumour types, from naïve to effector to terminally differentiated cells, and there is not one classification for the cells likely to be functioning against the tumour (Van der Leun, Thommen and Schumacher, 2020). Memory $CD8^+$ T cells are likely to be the responders to the tumour antigen in the TME,

thus encountering hypoxia, whilst naïve $CD8^+$ T cells instead encounter antigen presentation in secondary lymphoid organs (Han *et al.*, 2020). However, a recent study has shown that all $CD8^+$ T cells in the TME require a secondary stimulation to direct their anti-tumour response (Prokhnevska *et al.*, 2023). Since total $CD8^+$ T cells contain a large proportion of naïve cells **(Figure 3.7)**, it is important to consider the impact of hypoxia on memory $CD8^+$ T cells individually. Each naïve and memory $CD8^+$ T cell subset has a different differentiation and metabolic state. In general, naïve $CD8^+$ T cells rely on oxidative metabolism to generate small amounts of ATP to maintain their quiescent state (Fox, Hammerman and Thompson, 2005; Gerriets and Rathmell, 2012), terminally differentiated effector cells (EMRA) have high production of IFN-γ but low proliferation and dysfunctional mitochondria (Larbi and Fulop, 2014; Di Benedetto *et al.*, 2015; Dimeloe *et al.*, 2017), and memory $CD8^+$ T cells reorganise their mitochondria to adopt FAO and lipid oxidation with CM $CD8^+$ T cells being highly proliferative and EM $CD8^+$ T cells producing high quantities of effector cytokines (Sallusto, Geginat and Lanzavecchia, 2004; Willinger *et al.*, 2005; Rivera *et al.*, 2021). EM subsets are less dependent on OXPHOS than CM, and CM have a preference for FAO (Sullivan, 2019). Crucially, each $CD8^+$ T cell subset is likely to have a different tolerance to hypoxia depending on their differentiation and metabolic state. It is therefore important to look at various subtypes of T cells as they may be entering the tumour as a different phenotypes and functional capacities. By FACS sorting bulk $CD8^+$ T cells by CD45RA and CD62L I investigated the impact of hypoxia on naïve, CM, EM, and EMRA $CD8^+$ T cells **(Figures 3.7 and 3.8)**. I showed that hypoxia impacted the activation of the naïve and memory populations similarly in terms of CD25 expression and IFN-γ release **(Figures 3.7 and 3.8)**. Hypoxia had the greatest effect of IFN-γ

production in the memory populations, which is consistent with these cells being the primary cytokine producers **(Figures 3.7 and 3.8)**. EMRA $CD8^+$ T cells may have had lower cytokine production across the O_2 tensions than expected due to their reduced viability after sorting and culture **(Figures 3.7 and 3.8)** (Larbi and Fulop, 2014; Di Benedetto *et al.*, 2015; Dimeloe *et al.*, 2017). Importantly, viability should be taken into account when interpretating findings from these experiments. Overall, my experiments suggest that whichever population of $CD8^+$ T cell present in the TME, it is likely to be impacted by hypoxia similarly relative to its intrinsic functional capacity.

Whilst certain functional read-outs of $CD8^+$ T cells are impaired when activated in hypoxia, others, such as cytotoxic capacity, do not appear to be impacted **(Figure 3.5)**. Of note, cells that were granzyme-B or perforin-A positive appeared to be CD107a negative, and vice versa **(Figure 3.5)**. It may be that cells which are expressing CD107a and have degranulated have lost their granzyme-B and perforin-A, whilst those which do not express CD107a have not degranulated and still contain intracellular granzyme-B and perforin-A. To clarify this, it may be useful to conduct an ELISA for granzyme-B or perforin-A in the future in conjunction with CD107a staining. Overall, these experiments confirm that hypoxia is creating specific, and not global, effects on the cell. In contrast, in studies when $CD8^+$ T cells are differentiated into CTLs prior to hypoxia, experiments demonstrated improved cytotoxic ability under hypoxia, e.g., increased granzyme-B production (Doedens *et al.*, 2013; Gropper *et al.*, 2017; Palazon *et al.*, 2017; Zhang *et al.*, 2017), perforin expression (Finlay *et al.*, 2012), and packaging of granzyme-B into each cytolytic granule (Gropper *et al.*, 2017). Similarly, Caldwell *et al.* (2001) used ^{51}Cr-release assays to show that individual CTLs had a

greater cytolytic capacity when differentiated in hypoxia (Caldwell *et al.*, 2001), but Liu *et al.* (2020) showed that activated T cells exposed to hypoxia decreased granzyme-B secretion (Liu *et al.*, 2020). The engagement of HIF-1α and STAT3 has been suggested to contribute to the impairment of CTL killing in hypoxia by driving target cell resistance to killing, but not through intrinsic changes to CTLs, in a cell line lysis model (Noman *et al.*, 2009). It is clear that the differentiation and culture method of $CD8^+$ T cells in hypoxia significantly impacts their ability to produce cytotoxic molecules, degranulate, and efficiently kill. Therefore, future work should concentrate on dissecting these results further.

Re-stimulation with PMA and ionomycin completely rescued the defect of IFN-γ production in $CD8^+$ T cells activated by anti-CD3/CD28 in hypoxia **(Figure 3.3)**. Since activation with PMA and ionomycin bypasses the T cell signalling pathway (Ai *et al.*, 2013), I hypothesised that the defects in T cell function were originating from impaired T cell signalling. Therefore, I investigate T cell signalling in hypoxia in '**4. Results Chapter 2**'.

3.5. Conclusion

My experiments here have shown that $CD8^+$ T cells stimulated under hypoxia have a reduced activation state and proliferative capacity, reduced production and release of IFN-γ, but not TNF-α, and are just as cytotoxic as their normoxic counterparts. These impacts of hypoxia are consistent across naïve and memory $CD8^+$ T cell populations. Experiments indicate that functional defects, particularly for cytokine expression may relate to T cell signalling, which will be followed up in the next chapter.

4. Results Chapter 2

Exploring $CD8^+$ T cell signalling and metabolism in hypoxia

4. Results Chapter 2: Exploring CD8$^+$ T cell signalling and metabolism in hypoxia

4.1. Introduction

Upon CD8$^+$ T cell activation, TCR and CD28 co-stimulatory signalling pathways converge on key transcription factors and mediators to direct effector responses. In brief, upon initial TCR contact the CD8 co-receptor recruits Lck to the membrane (Palacios and Weiss, 2004). Lck creates binding sites for Zap70, which phosphorylates LAT (Iwashima *et al.*, 1994; Isakov *et al.*, 1995; Wange, 2000). A complex containing LAT activates PLCγ1, which hydrolyses PIP_2 into DAG and IP_3 (Beach *et al.*, 2007; Zhong *et al.*, 2008; Berridge, 2009). DAG signals downstream to the PKCθ-NF-kβ pathway, and IP_3 signals downstream to the Ca^{2+}-calcineurin-NFAT pathway (Beach *et al.*, 2007; Zhong *et al.*, 2008; Berridge, 2009). The NF-kβ pathway and Ca^{2+}-calcineurin-NFAT pathways result in the translocation of the transcription factors NF-kβ and NFAT, respectively, to the nucleus where they initiate transcription of key effector genes (Macian, 2005; Liu *et al.*, 2017). The DAG secondary messenger further signals to the Ras/MAPK-Erk1-AP-1 pathway, which promotes activity of transcription factor AP-1, and the mTOR pathway (Zhong *et al.*, 2008; Chapman and Chi, 2015). mTOR activity is also regulated by other pathways including PI3K-AKT signalling downstream of CD28 co-stimulation and the AMPK stress pathway (Chi, 2012; Chapman and Chi, 2015). To direct its effects, mTOR, specifically mTORC1, signals through p-S6K, and suppresses 4E-BP1 (Chapman and Chi, 2015). mTORC1 stimulates various transcription factors, including HIF-1α and c-Myc (Chapman and Chi, 2015). T cell signalling is a complex network of pathways, but each component is crucial to allow efficient activation and effector function. The impact of hypoxia on CD8$^+$ T cell signalling is not well described, and literature primarily investigates read-outs of

T cells function. Additionally, in '**3. Results Chapter 1**', I demonstrated that re-stimulation of $CD8^+$ T cells in hypoxia with PMA and ionomycin completely rescued the defect of IFN-γ production in $CD8^+$ T cells activated by anti-CD3/CD28 **(Figure 3.3)**. Since activation with PMA and ionomycin bypasses the T cell signalling pathway (Ai *et al.*, 2013), this suggests that the defects in T cell function may originate from impaired T cell signalling.

Another component of effective T cell function is the substantial metabolic reprogramming that occurs upon activation. In their resting state, naïve $CD8^+$ T cells are primarily oxidative, however upon activation, they switch to a more glycolytic metabolism to support increased energy and biomass requirements (Fox, Hammerman and Thompson, 2005; Gerriets and Rathmell, 2012). This is aerobic glycolysis, similar to that observed in cancer cells as the Warburg effect (Liberti and Locasale, 2016). $CD8^+$ T cells also increasingly rely upon glutaminolysis upon activation (Rivera *et al.*, 2021). In contrast, memory $CD8^+$ T cells revert back to a more oxidative metabolism and reorganise mitochondria for lipid metabolism and FAO, but on activation will become glycolytic once again (Rivera *et al.*, 2021). If a $CD8^+$ T cell has a failure in its metabolic reprogramming machinery, or there is limitation of required metabolites, it will experience dysfunction in its effector function. Importantly in hypoxia it is also well known that cells supress OXPHOS and switch to a primarily glycolytic metabolism (Kierans and Taylor, 2021). Cells are also reported to direct glutamine derived α-KG towards reductive carboxylation to generate citrate (Eales, Hollinshead and Tennant, 2016). Therefore, both activation and hypoxic exposure can alter metabolic status of T cells.

HIF-1α is a key transcription factor stabilised in hypoxia (Semenza, 2010). It is well known that amongst its gene targets are glycolytic enzymes and glucose transporters which drive increased glycolysis in hypoxia (Kierans and Taylor, 2021). Doedens *et al.* (2013) deleted the Vhl gene in $CD8^+$ T cells of P14 mice and transferred WT or KO $CD8^+$ T cells into B6 hosts infected with LCMV clone 13 (Doedens *et al.*, 2013). Vhl usually targets HIF-1α for degradation in normoxia (Maxwell *et al.*, 1999), thus its deletion leads to the stabilisation of HIF-1α independent of O_2 status. Vhl deficient cells demonstrated upregulation of glycolytic gene expression and enhanced glycolytic activity (Doedens *et al.*, 2013). Similarly, a study deleting PHD enzymes, partners of Vhl for HIF-1α degradation, in T cells by a CD4-driven Cre recombinase increased expression of glycolytic genes (Clever *et al.*, 2016). It is known that hypoxia drives HIF-1α expression in murine $CD8^+$ T cells, alongside its target Glut1 (Zhang *et al.*, 2017). The increase in glycolytic genes and glucose and lactate transporters has been confirmed by a more recent proteomic analyses of CTLs exposed to hypoxia (Ross, Rollings and Cantrell, 2021).

Consistently, extracellular acidification rate (ECAR), as a measure of glycolysis, increases in $CD8^+$ T cells cultured in hypoxia after activation, whilst oxygen consumption rate (OCR), reflective of oxidative metabolism, decreases (Zhang *et al.*, 2017). Proteomic analyses have also observed a reduction in the expression of specific components of OXPHOS machinery in CTLs exposed to hypoxia (Ross, Rollings and Cantrell, 2021). Alongside a reduction of OXPHOS, mitochondrial membrane potential decreases in murine $CD8^+$ T cells in hypoxia and mitochondrial ROS have been shown to increase (Zhang *et al.*, 2017). Interestingly, this study also showed $CD8^+$ T cells

activated for 4 days under 21% O_2, or for the last 16 hours in 1% O_2, to rely upon fatty acid (FA) metabolism to generate energy and biomass, both with uptake and FAO (Zhang *et al.*, 2017). Another study found that human PBMC activated with OKT3 (anti-CD3) in 1% O_2 vs. normal cell culture had fewer mitochondria, reduced total ATP production, and blunted both OCR and ECAR rates, suggesting a difference of activating cells within hypoxia rather than before (Liu *et al.*, 2020). Therefore, whilst it is expected for glycolysis to increase in activated $CD8^+$ T cells in hypoxia, contradictory evidence exists, and further exploration will be useful to determine their metabolic state.

4.2. Aims

For a $CD8^+$ T cell to efficiently activate and harness its effector function it requires correct signalling and metabolic reprogramming. If either of these aspects is aberrant, the $CD8^+$ T cell may experience functional defects. This chapter will interrogate $CD8^+$ T cell signalling and metabolism after activation in hypoxia. The aims for this chapter include:

- To explore $CD8^+$ T cell signalling following activation in hypoxia by assessing signalling protein abundance and phosphorylation status in human cells
- To further probe the impact of hypoxia on $CD8^+$ T cell signalling using murine signalling reporter models
- To interrogate $CD8^+$ T cell metabolic reprogramming upon activation in hypoxia

4.3. Results

4.3.1. A defect exists in NFAT and calcium signalling in $CD8^+$ T cells activated in hypoxia, but initial TCR signalling is not impaired

To begin to interrogate $CD8^+$ T cell signalling in hypoxia, I first assessed activity of the TCR signalling pathway upon activation. Initially this was investigated by western blot of phosphorylated proteins in the TCR signalling pathway. $CD8^+$ T cells were pre-conditioned in their respective O_2 condition, activated for the time point indicated, and lysed for protein extraction **(Figure 4.1A)**. Western blots were run for CD3, phospho (p)-Lck, p-Src, p-Zap70 (at two tyrosine residues), and p-SLP. β-actin was used as a loading control. However, bands representing phosphorylated proteins were consistently observed even within non-activated samples where there should be no phosphorylated protein **(Figure 4.1A)**, so no reliable information could be extracted from these experiments. To understand if contact with magnetic beads during positive selection was partially activating the $CD8^+$ T cells, similar blots were run with Jurkats and fresh PBMCs that had not come into contact with magnetic beads. However, similar bands were observed in non-activated samples, suggesting this was not the reason for the abnormal bands **(Figure 4.1B)**. Since these experiments proved inconclusive, analysis of signalling continued with an alternative approach.

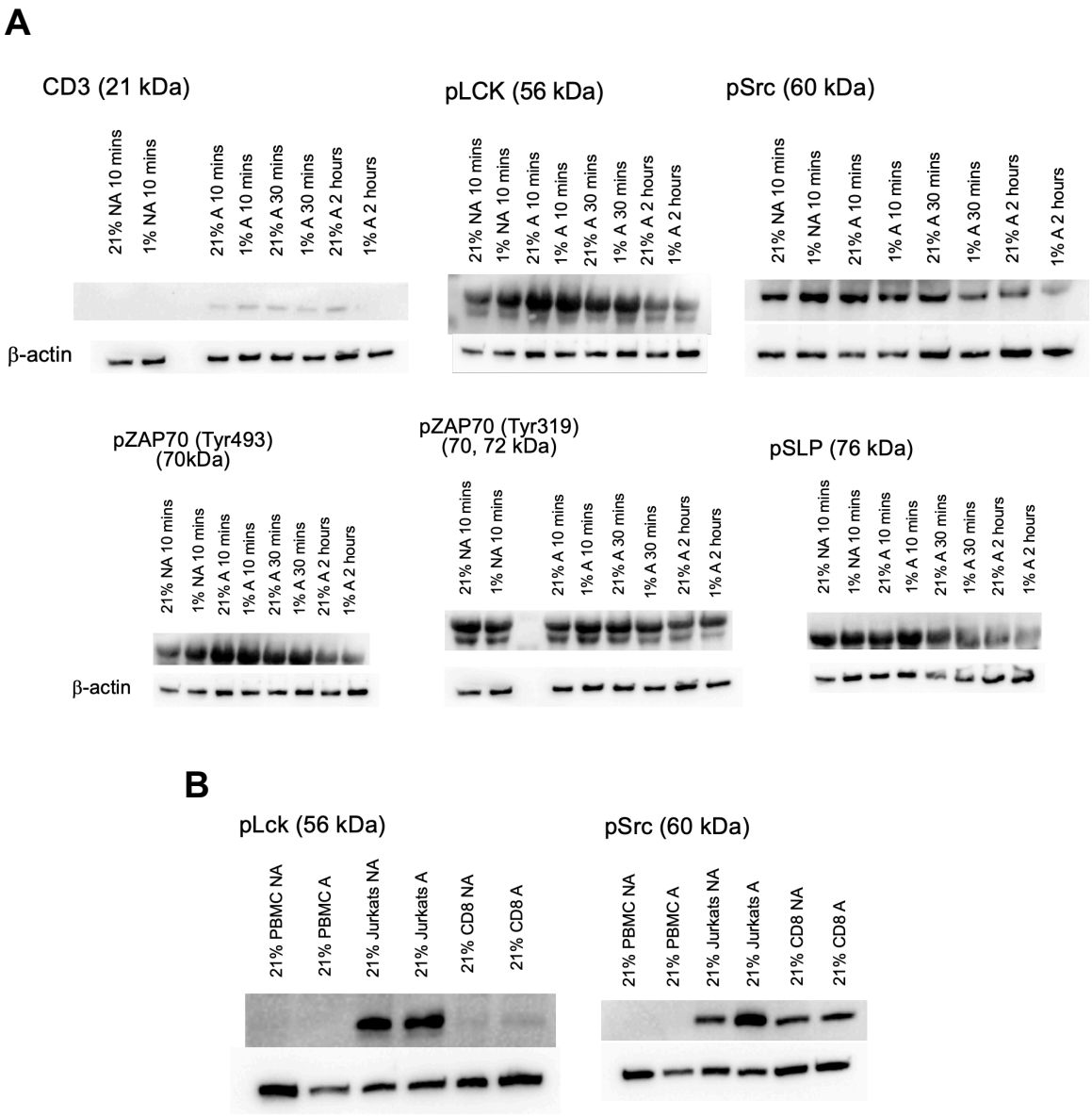

Figure 4.1. Western blot of phosphorylated proteins in the TCR signalling pathway in $CD8^+$ T cells activated in hypoxia vs. normoxia. $CD8^+$ T cells were pre-conditioned in 21% or 1% O_2, activated the following morning with anti-CD3/CD28 for the time point indicated and lysed immediately for protein extraction. A) Representative western blot for CD3, phospho (p)-Lck, p-Src, p-Zap70 (Tyr493), p-Zap70 (Tyr319), and pSLP. β-actin used as a loading control. Samples are non-activated (NA) or activated (A) $CD8^+$ T cells cultured and activated in 21% or 1% O_2 for the time point indicated, n = 1; B) Representative western blot for p-Lck and p-Src in PBMC, Jurkats, or bulk $CD8^+$ activated and cultured in 21% O_2 only, n = 1.

Initial signalling events following stimulation of the TCR include phosphorylation of Lck and ERK (Shah *et al.*, 2021). To analyse the efficiency of this process after activation I conducted flow cytometric analysis of phosphorylated proteins. Here, after pre-conditioning, isolated $CD8^+$ T cells were activated by anti-CD3/CD28 for 15 minutes or 1 hour and stained for phospho (p)-Lck and p-ERK, respectively **(Figures 4.2A and 4.2B)**. Despite the staining not being very bright, an increase in the MFI of p-Lck and the geometric mean fluorescence intensity of p-ERK could be observed with T cell activation **(Figures 4.2A and 4.2B)**. There was little or no difference in the MFI of p-Lck staining in $CD8^+$ T cells activated in 21% compared to 1% O_2, which is also the case for the geometric mean fluorescence intensity of p-ERK **(Figures 4.2A and 4.2B)**. Thus, early TCR signalling appears to be unaffected by activation in hypoxia.

To probe a further downstream aspect of $CD8^+$ T cell signalling, I assessed the abundance of NFAT within nuclei. To isolate nuclei, cells were resuspended in one of two buffers which created a sucrose gradient and centrifuged at high speeds. The isolated nuclei were then stained for NFAT expression for flow cytometric analysis. The MFI of nuclei isolated NFAT was significantly reduced in activated $CD8^+$ T cells in 1% O_2 compared to those in 21% O_2 **(Figure 4.2C)**. Since the MFI of total NFAT protein did not change between O_2 tensions **(Figure 4.2D)**, this suggests that this defect is due to impaired NFAT translocation to the nucleus. **Figure 4.2E** demonstrates the successful isolation of nuclei via the sucrose gradient protocol, as indicated by lack of staining of the cytoplasmic protein β-tubulin. Therefore, whilst upstream TCR signalling appears to be intact in hypoxia, the translocation of downstream target NFAT to the nucleus is impaired.

Another immediate event following TCR stimulation is increased cytosolic calcium (Ca^{2+}) concentrations (Samakai, Go and Soboloff, 2018). The flux of Ca^{2+} following TCR engagement is crucial to harmonise signalling pathways for T cell activation (Samakai, Go and Soboloff, 2018). Importantly, NFAT and Ca^{2+} signalling pathways are closely related (Fracchia, Pai and Walsh, 2013; Park *et al.*, 2020). To assess the efficiency of Ca^{2+} flux in $CD8^+$ T cells activated in hypoxia, isolated $CD8^+$ T cells were pre-conditioned overnight in 21% or 1% O_2, activated via anti-CD3/CD28 or PMA and ionomycin, and Ca^{2+} flux measured by an atmosphere-controlled fluorescent plate reader, set at 1% or 21% O_2 as needed **(Figure 4.2F)**. Optimisation of the method was required, as initially addition of any solution into the plate altered the fluorescent read-out. Therefore, even in non-activated wells a solution of equal volume was added to mitigate for this effect. Once controlled for, activated cells did increase Ca^{2+} flux compared to non-activated cells as expected **(Figure 4.2F)**. $CD8^+$ T cells activated in 1% O_2 via anti-CD3/CD28 had reduced Ca^{2+} flux compared to those activated in 21% O_2 **(Figure 4.2F)**. However, $CD8^+$ T cells activated with PMA/ionomycin in 1% O_2 also demonstrated reduced Ca^{2+} flux compared to 21% O_2. Since PMA/ionomycin stimulation directly promotes Ca^{2+} flux independent of TCR signalling, this contrasts the specificity to the TCR observed in other functional read-outs **(3. Results Chapter 1, Figure 3.3).** The defect of Ca^{2+} flux upon stimulation seen in hypoxia may impact other T cell signalling pathways.

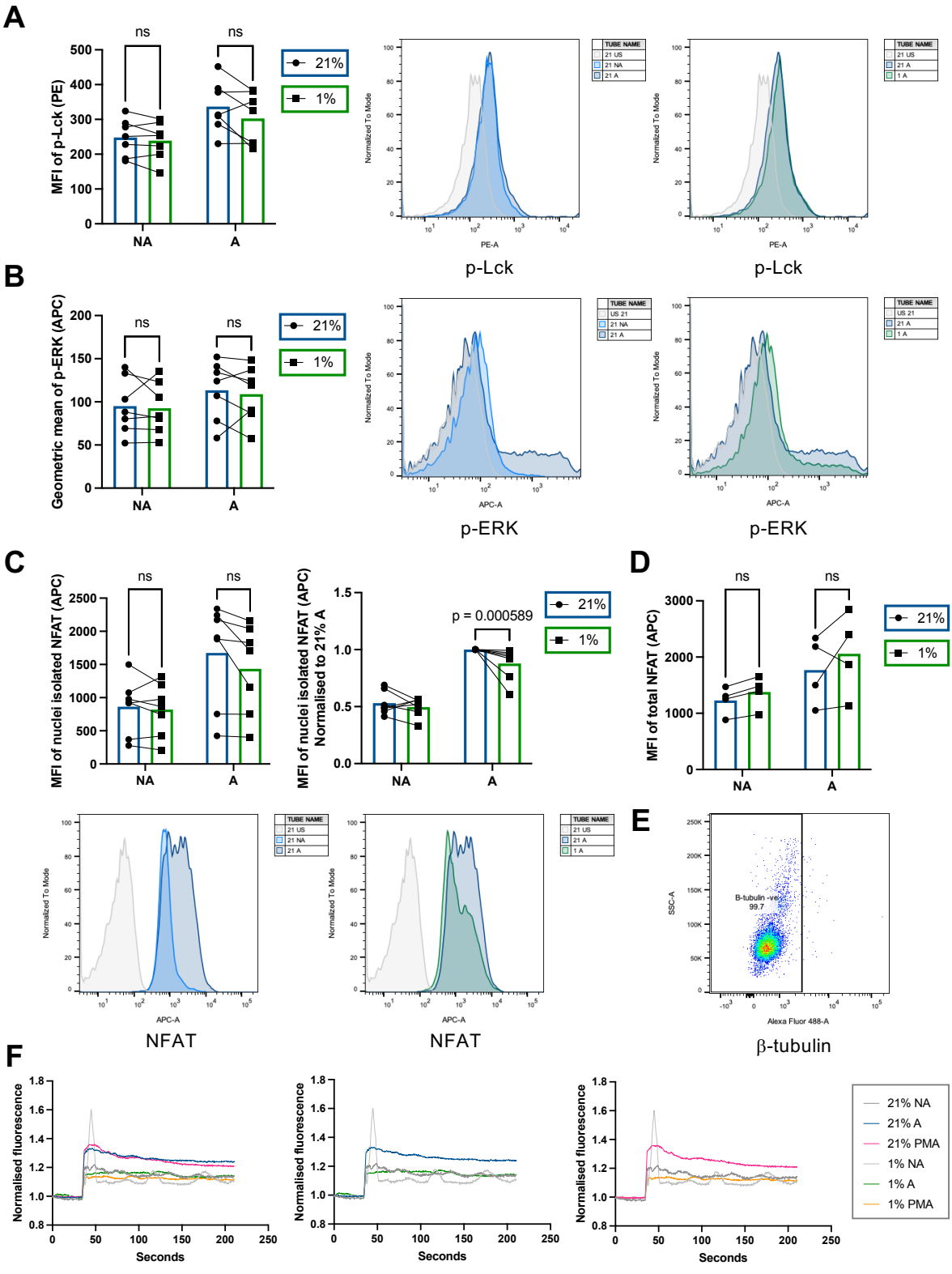

Figure 4.2. Expression of phospho- (p-) Lck and ERK, nuclei isolated NFAT and calcium flux in $CD8^+$ T cells activated in hypoxia vs. normoxia. Isolated $CD8^+$ T cells were pre-conditioned overnight in 21% or 1% O_2 conditions, activated the following morning with anti-CD3/CD28, and cultured in the same O_2 conditions for the time point indicated. A) Left: $CD8^+$ T cells were activated in

21% or 1% O_2 for 15 mins and stained for phospho (p)-Lck, n = 7, Right: Example histogram of p-Lck staining in 21 NA vs 21 A and 21 A vs 1 A, n = 1; B) Left: $CD8^+$ T cells were activated in 21% or 1% O_2 for 1 hour and stained for p-ERK, n = 7, Right: Example histogram of p-ERK staining in 21 NA vs 21 A and 21 A vs 1 A, n = 1; C) Top left: $CD8^+$ T cells were activated in 21% or 1% O_2 for 1 hour, nuclei were isolated via a sucrose gradient and stained for NFAT, n = 7, Top right: normalised to 21% A, n = 7, Bottom: Example histogram of nuclei NFAT staining in 21 NA vs 21 A and 21 A vs 1 A, n = 1; D) $CD8^+$ T cells were activated in 21% or 1% O_2 for 1 hour and stained for NFAT (total), n = 4; E) Example dot-plot of β-tubulin (AF488) staining in 21 A after nuclei isolation via a sucrose gradient, n = 1; F) $CD8^+$ T cells were activated in 21% or 1% O_2 to measure calcium (Ca^{2+}) flux upon activation, n = 7, average of all data shown as one line. Blue bars = 21% O_2; Green bars = 1% O_2. Data analysed by (A, B, C Left, D) ordinary two-way ANOVA with Sidak's multiple comparison post-hoc test, with a single pooled variance, (C Right) Multiple Mann-Whitney tests with two-stage linear step-up procedure of Benjamin, Krieger and Yekutieli post-hoc test. * $p < 0.05$, ** $p < 0.005$, *** $p < 0.005$, ns = non-significant or 'blank', $p > 0.05$.

4.3.2. Activation of $CD8^+$ T cells in hypoxia leads to a signalling defect at the level of mTOR

Alongside TCR signalling, localisation of NFAT to the nucleus is also prompted by signalling via the CD28 co-stimulatory pathway (Riha and Rudd, 2010). Since NFAT nuclear translocation was impaired in hypoxia, I next investigated the phosphorylation of proteins in the CD28 pathway in $CD8^+$ T cells activated in hypoxia. $CD8^+$ T cells were pre-conditioned, activated in 21% or 1% O_2 for 24 hours, and stained for p-AKT, p-mTOR and p-p70S6K. An increase in the MFI of p-AKT was observed in $CD8^+$ T cells upon activation, however no difference existed between cells activated in 21% and 1% O_2 **(Figure 4.3A)**. In contrast, mTOR phosphorylation was reduced in $CD8^+$ T cells activated in 1% vs. 21% O_2 **(Figure 4.3B)**, as was that of its downstream target, p70S6K **(Figure 4.3C)**. Total levels of mTOR and p70S6K protein were not impacted by hypoxia **(Figures 4.3D and 4.3E)**, suggesting this is a signalling defect and not a more widespread effect on protein translation and abundance.

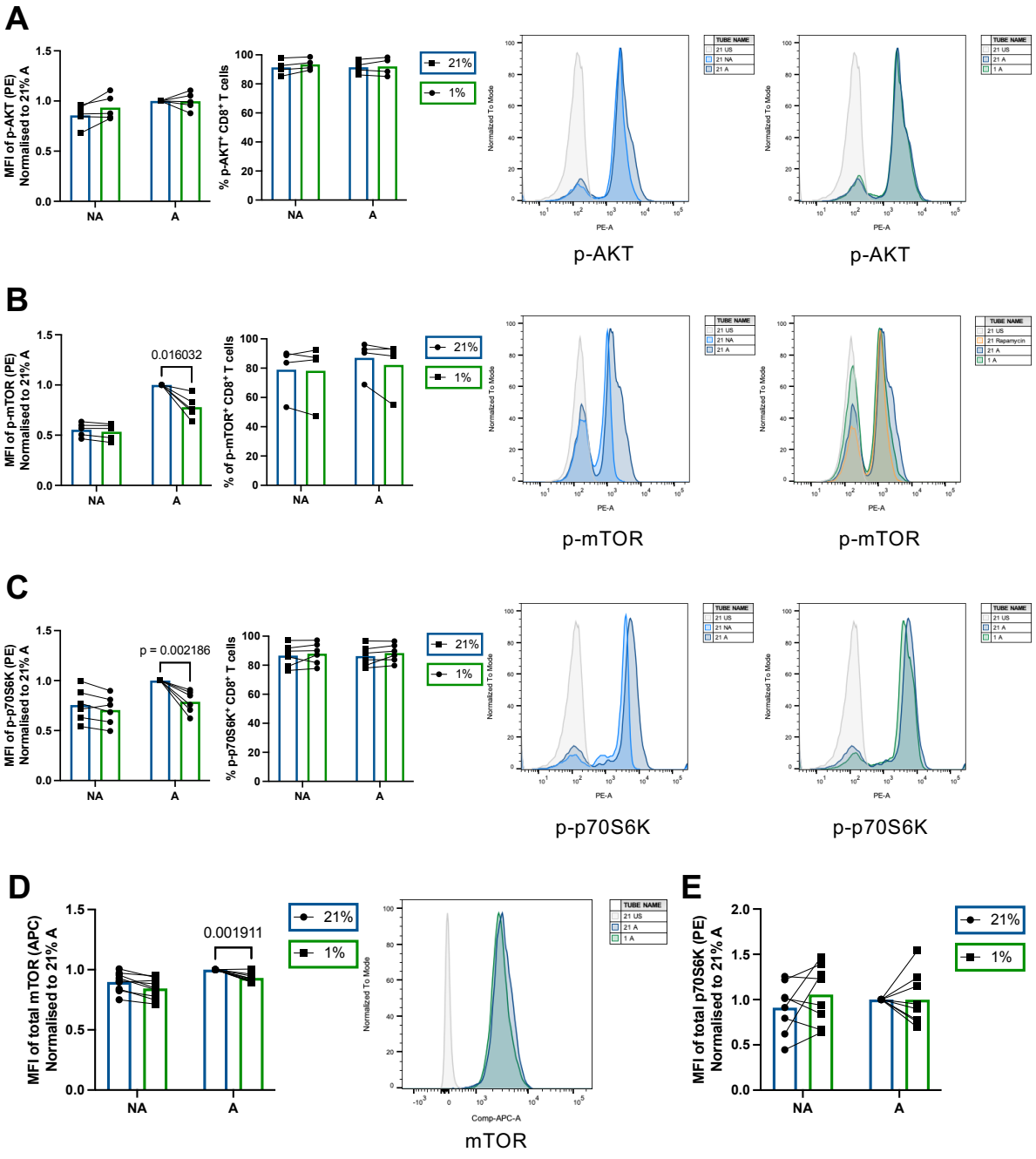

Figure 4.3. Expression of phospho- (p-) AKT, p70S6K and mTOR, and total mTOR and p70S6K in $CD8^+$ T cells activated in hypoxia vs. normoxia. Isolated $CD8^+$ T cells were pre-conditioned overnight in 21% or 1% O_2 conditions, activated the following morning with anti-CD3/CD28, and cultured in the same O_2 conditions for the time point indicated. A) Left: $CD8^+$ T cells were activated in 21% or 1% O_2 for 24 hours and stained for phospho (p)-AKT, MFI shown n = 7, normalised to 21% A, Middle: Percentage of $p\text{-}AKT^+$ $CD8^+$ T cells, n = 7, Right: Example histogram of p-AKT staining in 21 NA vs 21 A and 21 A vs 1 A, n = 1; B) Left: $CD8^+$ T cells were activated in 21% or 1% O_2 for 24 hours and stained for p-mTOR, n = 5, normalised to 21% A, Middle: Percentage of $p\text{-}mTOR^+$ $CD8^+$ T cells, n = 5, Right: Example histogram of p-mTOR staining in 21 NA vs 21 A and 21 A vs 1 A, n = 1; C) Left: $CD8^+$ T cells were activated in 21% or 1% O_2 for 24 hours and stained for p-p70S6K, n = 8, normalised to 21% A,

Middle: Percentage of p-p70S6K$^+$ CD8$^+$ T cells, n = 8, Right: Example histogram of p-p70S6K staining in 21 NA vs 21 A and 21 A vs 1 A, n = 1; D) Left: CD8$^+$ T cells were activated in 21% or 1% O_2 for 24 hours and stained for total mTOR, n = 9, normalised to 21% A, Right: Example histogram of total mTOR staining shown, n = 1; E) CD8$^+$ T cells were activated in 21% or 1% O_2 for 24 hours and stained for total p70S6K, n = 9, normalised to 21% A. Blue bars = 21% O_2; Green bars = 1% O_2. Data were analysed by (A, B, C, D, E) Multiple Mann-Whitney tests with two-stage linear step-up procedure of Benjamin, Krieger and Yekutieli post-hoc test for normalised data, and (A, B, C) ordinary two-way ANOVA with Sidak's multiple comparison post-hoc test, with a single pooled variance for middle graphs. * $p < 0.05$, ** $p < 0.005$, *** $p < 0.005$, ns = non-significant or 'blank', $p > 0.05$.

4.3.3. A defect in CD8$^+$ T cell signalling is confirmed by murine TCR-reporter systems in hypoxia

To further probe the defect in CD8$^+$ T cell signalling in hypoxia, two murine TCR-reporter mice were used: the Nr4a1(Nur77)-TEMPO and Nr4a3-Tocky murine reporter systems (Bending *et al.*, 2018; Elliott *et al.*, 2022). Upon TCR activation and signalling via Nr4a1 and Nr4a3, respectively, a blue fluorescent reporter protein (Timer-blue) is translated (Bending *et al.*, 2018; Elliott *et al.*, 2022). Over time, this protein matures into a red fluorescent reporter protein (Timer-red), with a maturation half-life of 4 hours (Bending *et al.*, 2018; Elliott *et al.*, 2022). A new, or recent, signal is therefore indicated by Timer-blue expression, whilst cells which have previously received a TCR signal, but not within the last 4 hours (arrested signal) is indicated by Timer-red without Timer-blue expression (Bending *et al.*, 2018; Elliott *et al.*, 2022) **(Figure 4.4A)**. Cells expressing both Timer-red and Timer-blue are described as having a persistent TCR signal (Bending *et al.*, 2018; Elliott *et al.*, 2022) **(Figure 4.4A)**.

First, the applicability of these reporter systems to my experimental set-up was assessed. Since the capacity to generate the Timer-blue protein relies on efficient protein translation (Bending *et al.*, 2018; Elliott *et al.*, 2022), and protein translation has been reported to be impaired in hypoxia (Hochachka *et al.*, 1996; Koumenis *et al.*,

2002; Liu and Simon, 2004), it was important to first understand if murine $CD8^+$ T cell protein translation was impacted by hypoxia in my experimental settings. To do this, a puromycin assay was conducted in $CD8^+$ T cells from wild-type (WT) mice in hypoxia. This assay involves adding puromycin to cell culture, which induces peptide puromycylation proportional to the protein translation rate (Aviner, 2020). Puromycylated proteins can then be detected with an anti-puromycin antibody (Aviner, 2020). The protein translation rate of murine $CD8^+$ T cells trended towards a non-significant, and slight, reduction in 1% compared to 21% O_2 conditions at 24 hours, which was not observed at 48 hours **(Figure 4.4B)**. Therefore, I assumed the readout from the Timer-blue reporter to be a useful indicator of T cell signalling for this experimental set-up.

In the Nr4a3-Tocky model, after 24 hours of CD3 and CD28 activation of $CD8^+$ T cells in normoxia, a clear upregulation of Timer-blue expression is observed **(Figure 4.4C)**. This also spreads into Timer-$blue^+$ Timer-red^+ demonstrating a recent and persistent signal after TCR activation **(Figure 4.4C)**. The initial induction of Timer-blue expression was impaired in $CD8^+$ T cells activated in 1% compared to 21% O_2 at 4 and 24 hours **(Figure 4.4D and 4.4G)**. At 24 hours, it appears as though the signal is halted in 1% O_2 from transforming into a Timer-$blue^+$ Timer-red^+ signal and suggests a time lag **(Figure 4.4E)**. This apparent time lag is consistent to 48 hours **(Figure 4.4F)** and shows an increased Timer-blue expression in 1% vs. 21% O_2 activated $CD8^+$ T cells **(Figure 4.4G)**. Timer-red expression is decreased upon $CD8^+$ T cell activation in 1% compared to 21% O_2 at 24 hours **(Figure 4.4H)**.

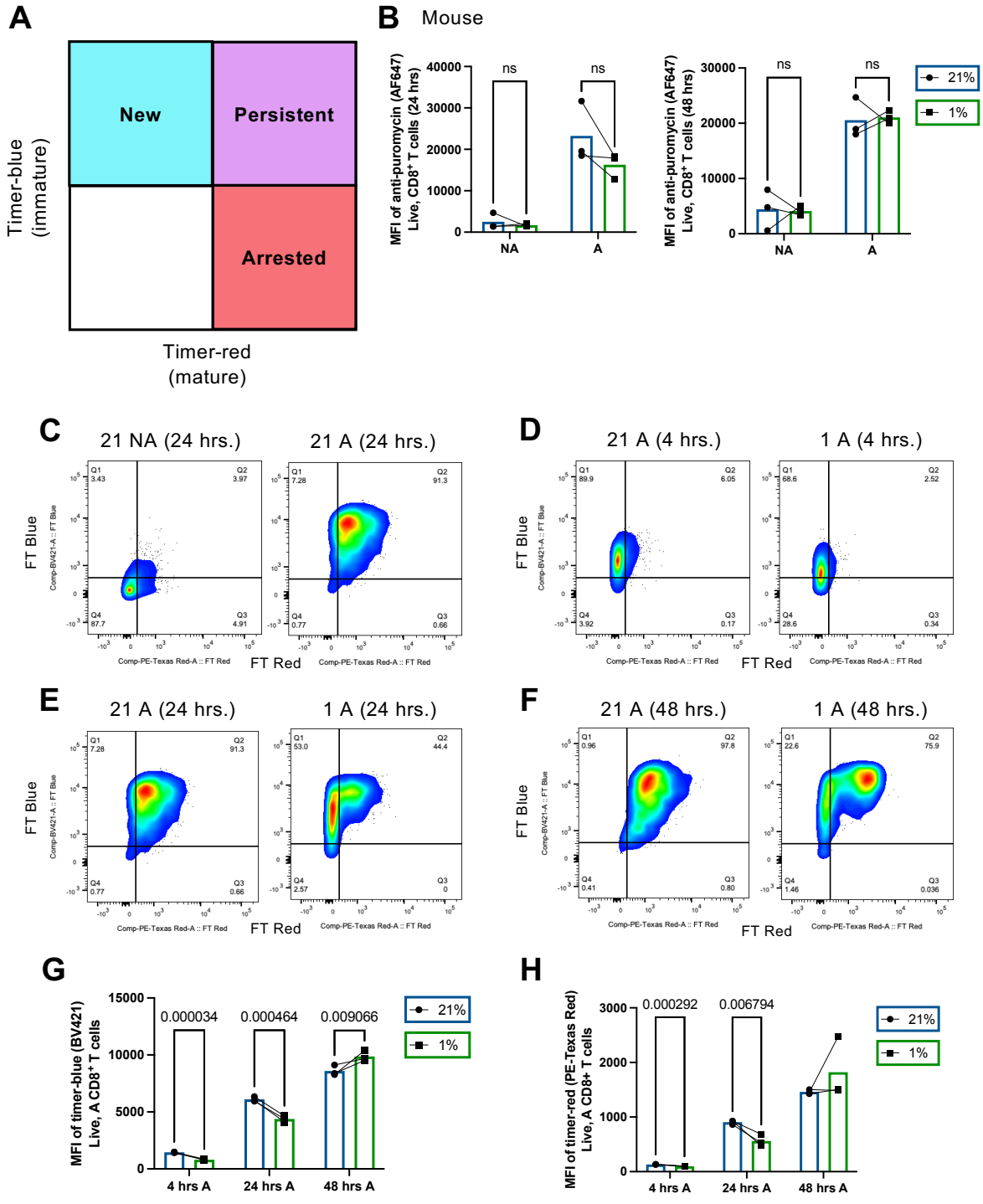

Figure 4.4. Analysis of the Nr4a3 (Tocky) murine TCR reporter system in hypoxia vs. normoxia. Splenocytes were isolated from Nr4a3 (Tocky), or WT, mouse spleens, pre-conditioned overnight in 21% or 1% O_2 conditions, activated the following morning with anti-CD3/CD28, and cultured in the same O_2 conditions for the time point indicated. A) Schematic to demonstrate Timer-red and Time-blue intensity and its relation to signal type; B) Splenocytes isolated from WT mouse spleens and activated for 24 hours with anti-CD3/CD28, after pre-conditioning. Puromycin added for 15 minutes and stained with anti-puromycin (AF647) to measure translation rate, n = 3; C-F) Example plots of Nr4a3-splenocytes after activation with anti-CD23/CD28, n = 1, for C) for 24 hours,

21 NA vs 21 A; D) for 4 hours, 21 A vs 1 A; E) for 24 hours, 21 A vs 1 A; and F) for 48 hours, 21 A vs 1 A; G-H) Nr4a3-splenocytes activated with anti-CD3/CD38 for 4-48 hours, G) MFI of timer-blue (BV421), n = 3; H) MFI of timer-red (PE-Texas Red), n = 3. Blue bars = 21% O_2; Green bars = 1% O_2. Data analysed by (B) ordinary two-way ANOVA with Sidak's multiple comparison post-hoc test, with a single pooled variance, (G, H) multiple unpaired t-tests with two-stage linear step-up procedure of Benjamin, Krieger and Yekutieli post-hoc test. * $p < 0.05$, ** $p < 0.005$, *** $p < 0.005$, or p-value shown, ns = non-significant or 'blank', $p > 0.05$.

The Nur77-Tempo model also showed a clear increase in expression of Timer-blue and Timer-red with $CD8^+$ T cell activation after 24 hours **(Figure 4.5A)**. However, experiments in hypoxia interestingly yielded different results. At 4 hours there was no impact of hypoxia on Timer-blue, unlike for the Nr4a3 reporter, and a small decrease in Timer-red expression in 1% compared to 21% O_2 **(Figure 4.5B, 4.5E and 4.5F).** At 24 hours after activation $CD8^+$ T cells from Nur77-Tempo increased Timer-blue expression in 1% vs. 21% O_2, compared to the decrease observed in Nr4a3-Tocky, and decreased Timer-red expression **(Figure 4.5C, 4.5E and 4.5F)**. At 48 hours after activation $CD8^+$ T cells from Nur77-Tempo increased Timer-blue, but increased Timer-red expression in 1% vs. 21% O_2 **(Figure 4.5D, 4.5E and 4.5F)**.

To directly compare the initial activation difference between the Nr4a3-Tocky and Nu77-Tempo murine models, I plotted the 4-hour Timer-blue expression on the same graph **(Figure 4.5G)**. Here it is clear that $CD8^+$ T cells from the Nr4a3-Tocky model demonstrate impaired activation-induced reporter expression in 1% vs. 21% O_2, whilst $CD8^+$ T cells from the Nu77-Tempo model do not **(Figure 4.5G)**. The major difference between these reporter systems is that *Nr4a3*, but not *Nr4a1* expression requires NFAT signalling (Bending *et al.*, 2018; Elliott *et al.*, 2022). These findings are therefore

in agreement with my previous data indicating impaired NFAT translocation in human $CD8^+$ T cells in hypoxia.

$CD8^+$ T cells initially activated in 21% O_2 for 4 hours and then moved to 1% O_2 for the remainder of 24 hours had a Timer-red expression between those kept in 21% and 1% O_2 for the entire time point **(Figure 4.5H)**. This demonstrates that the transition of Timer-blue to the Timer-red protein is impaired by hypoxia and we should avoid making any conclusions from this readout. Overall, these experiments show that initial $CD8^+$ T cell activation-induced signalling is impaired in hypoxia but is related to a defect in NFAT signalling.

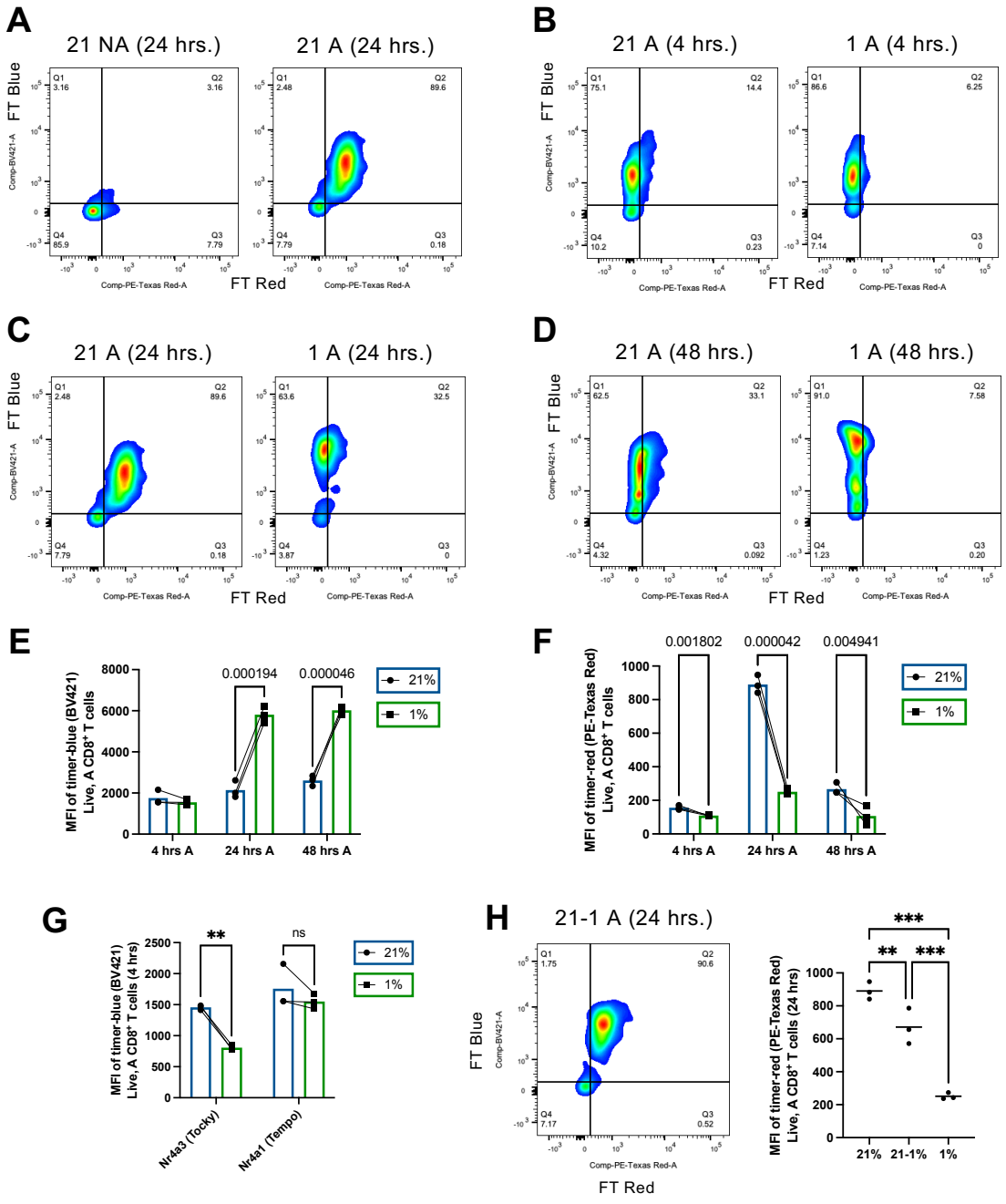

Figure 4.5. Analysis of the Nr4a1 (Tempo) murine TCR reporter system in hypoxia vs. normoxia. Splenocytes were isolated from Nr4a1 (Tempo) mouse spleens, pre-conditioned overnight in 21% or 1% O_2 conditions, activated the following morning with anti-CD3/CD28, and cultured in the same O_2 conditions for the time point indicated. A-D) Example plots of Nr4a3-splenocytes after activation with anti-CD23/CD28, n = 1, for A) for 24 hours, 21 NA vs 21 A; B) for 4 hours, 21 A vs 1 A; C) for 24 hours, 21 A vs 1 A; and D) for 48 hours, 21 A vs 1 A; E-F) Nr4a1-splenocytes activated with anti-CD3/CD38 for 4-48 hours, E) MFI of timer-blue (BV421), n = 3; F) MFI of timer-red (PE-Texas Red), n = 3; G) Nr4a3 (Tocky) vs Nr4a1 (Tempo) MFI of timer-blue (BV421) at 4 hrs of anti-CD3/CD28 activation in 21% or 1% O_2, n = 3; H) Nr4a1-splenocytes activated with anti-CD3/CD38 for 4 hours in 21% O_2 and then moved to 1% O_2, example plot n = 1, shown is MFI of timer-red of 21 A, 21-1 A and 1 A at 24 hours, n = 3. Blue bars = 21% O_2; Green bars = 1% O_2. Data analysed by (E, F) multiple unpaired t-tests with two-stage linear step-up procedure of

Benjamin, Krieger and Yekutieli post-hoc test, (G) ordinary two-way ANOVA with Sidak's multiple comparison post-hoc test, with a single pooled variance, (H) ordinary two-way ANOVA with main effects only with Tukey's multiple comparisons post-hoc test, with a single pooled variance. * $p < 0.05$, ** $p < 0.005$, *** $p < 0.005$, or p-value shown, ns = non-significant or 'blank', $p > 0.05$.

4.3.4. $CD8^+$ T cells in hypoxia have impaired activation-induced increases in glycolysis, glucose oxidation, and glutaminolysis

Upon activation, $CD8^+$ T cells undergo metabolic reprogramming, increasing activity, particularly of glycolysis, and to a lesser extent OXPHOS (Gerriets and Rathmell, 2012). This provides the energy and biomass production required for their effector response (Gerriets and Rathmell, 2012). Defects in, or limitations in substrate availability for, this activation-induced metabolic switch results in impaired T cell effector function (Cham and Gajewski, 2005; Cham *et al.*, 2008; Carr *et al.*, 2010; Rivera *et al.*, 2021). One key transcription factor responsible for directing $CD8^+$ T cell activation-induced metabolic reprogramming is c-Myc (Wang *et al.*, 2011), which is known to be stimulated by mTOR for upregulation of glycolysis, glutaminolysis and the transcription of various glutamine receptors (Chapman and Chi, 2015; Gupta, Wang and Chen, 2020). Since we observed a defect in mTOR signal in activated $CD8^+$ T cells in hypoxia **(Figure 4.3)**, I next analysed c-Myc expression. For this, I isolated $CD8^+$ T cells from human PBMC, pre-conditioned the cells overnight in 21%, 5% or 1% O_2, activated the following morning via CD3 and CD28 for 48 hours and flow cytometrically stained for c-Myc. Expression of c-Myc was significantly lower in $CD8^+$ T cells activated in 1% O_2 compared to both 21% and 5% O_2, indicating a potential defect in the capacity to metabolically reprogram **(Figure 4.6A)**. Interestingly, $CD8^+$ T cells activated in 5% O_2 trended towards a slightly higher expression of c-Myc than cells activated in 21% O_2 **(Figure 4.6A)**.

When $CD8^+$ T cells are switching to a glycolytic metabolism upon activation they begin to uptake higher amounts of glucose and produce more lactate (Gerriets and Rathmell, 2012). Similarly, in hypoxia, you would expect cells to switch to a more glycolytic metabolism (Kierans and Taylor, 2021). Thus, I measured the concentration of glucose and lactate in $CD8^+$ T cells pre-conditioned, activated via CD3 and CD28 and cultured in 21% and 1% O_2 for 8-72 hours. Whilst activated $CD8^+$ T cells increased their glucose uptake and lactate production over the time course, this was not significantly different between 1% and 21% O_2 **(Figure 4.6B)**.

To track fate of glucose uptake in $CD8^+$ T cells activated in 21% or 1% O_2 conditions, I performed stable isotope-based tracing experiments. Here, I added fully labelled $^{13}C_6$-glucose to my cell cultures, pre-conditioned to 21% or 1% O_2, activated via CD3/CD28, and analysed metabolites after 24 hours for ^{13}C incorporation by mass spectrometry. Incorporation of ^{13}C-glucose into pyruvate and lactate increased with $CD8^+$ T cell activation, demonstrating increased glycolysis, but this wasn't significantly different between 21% and 1% O_2 **(Figure 4.6C)**. Relatively little labelling from ^{13}C-glucose into metabolites of the TCA cycle was observed in my activated $CD8^+$ T cells, which was similar between normoxic and hypoxic cells **(Figure 4.6D)**.

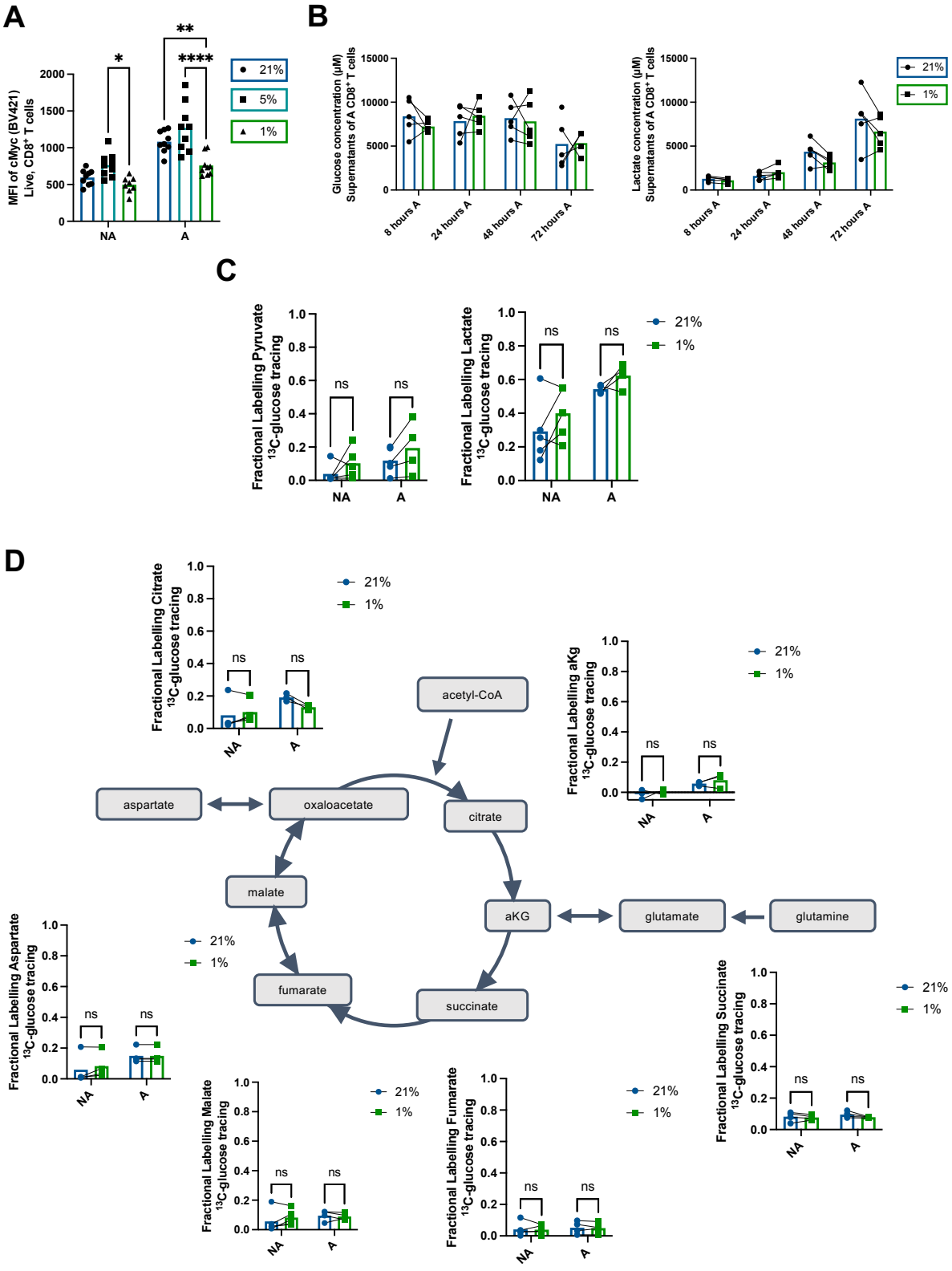

Figure 4.6. Expression of c-Myc, concentrations of glucose and lactate, and stable isotope-based tracing for $^{13}C_6$-glucose in CD8$^+$ T cells activated in hypoxia vs. normoxia. Isolated CD8$^+$ T cells were pre-conditioned overnight in 21%, 5%, or 1% O_2 conditions, activated the following morning with anti-CD3/CD28, and cultured in the same O_2 conditions for the time point indicated. A) Left:

$CD8^+$ T cells were activated in 21% or 1% O_2 for 48 hours and stained for c-Myc, n = 9, Right: Example histogram of c-Myc staining 21 A vs 5 A vs 1 A, n = 1; B) $CD8^+$ T cells were activated in 21% or 1% O_2 for 8-72 hours and supernatants collected for measurement of glucose and lactate concentrations (μM), n = 5; C) $CD8^+$ T cells were labelled with ^{13}C-glucose and activated in 21% or 1% O_2 for 48 hours to measure glucose incorporation, shown is fractional labelling into pyruvate and lactate, n = 5; D) $CD8^+$ T cells were labelled with ^{13}C-glucose and activated in 21% or 1% O_2 for 48 hours to measure glucose incorporation, shown is fractional labelling into various metabolites of the TCA cycle, n = 5. Blue bars = 21% O_2; Green bars = 1% O_2. Data analysed by (A) ordinary two-way ANOVA with Tukey's multiple comparison post-hoc test, with a single pooled variance, (B) multiple paired t-tests with two-stage linear step-up procedure of Benjamin, Krieger and Yekutieli post-hoc test, (C, D) ordinary two-way ANOVA with Sidak's multiple comparison post-hoc test, with a single pooled variance. * $p < 0.05$, ** $p < 0.005$, *** $p < 0.005$, ns = non-significant or 'blank', $p > 0.05$.

It is well documented that $CD8^+$ T cells increase oxidation of glutamine in the TCA cycle upon activation (Rivera *et al.*, 2021). Thus, I also labelled $CD8^+$ T cells with $^{13}C_5$-glutamine and traced for 24 hours after activation, to better understand TCA cycle activity. A large increase in incorporation of ^{13}C-glutamine into TCA cycle metabolites was observed with $CD8^+$ T cell CD3 and CD28 activation **(Figure 4.7A)**. Importantly, reduced ^{13}C-glutamine incorporation into TCA cycle metabolites was also observed in $CD8^+$ T cells activated in 1% O_2 compared to 21% O_2, which could be consistent with a limitation of metabolic reprogramming **(Figure 4.7A)**. **Figure 4.7B** provides the mass isotopologue distributions (MIDs) for various TCA cycle metabolites. In general, a greater amount of unlabelled (M+0) TCA cycle metabolites are observed in activated $CD8^+$ T cells in 1% vs 21% O_2 **(Figure 4.7B)**, as with **Figure 4.7A**. Increased abundance of M+5 citrate and M+3 malate isotopomers in activated $CD8^+$ T cells in 1% vs. 21% O_2 are reflective of reductive carboxylation of glutamine-derived α-KG, a metabolic process well documented to occur with impaired mitochondrial ETC function and hypoxia (Metallo *et al.*, 2011; Eales, Hollinshead and Tennant, 2016; Yoo *et al.*, 2020). The reduced ^{13}C-glutamine incorporation into TCA cycle metabolites in 1% O_2

was not due to impaired glutamine uptake, as fractional labelling of glutamine itself does not change between 21% and 1% O_2 and is fully labelled (M+5) **(Figure 4.7C)**.

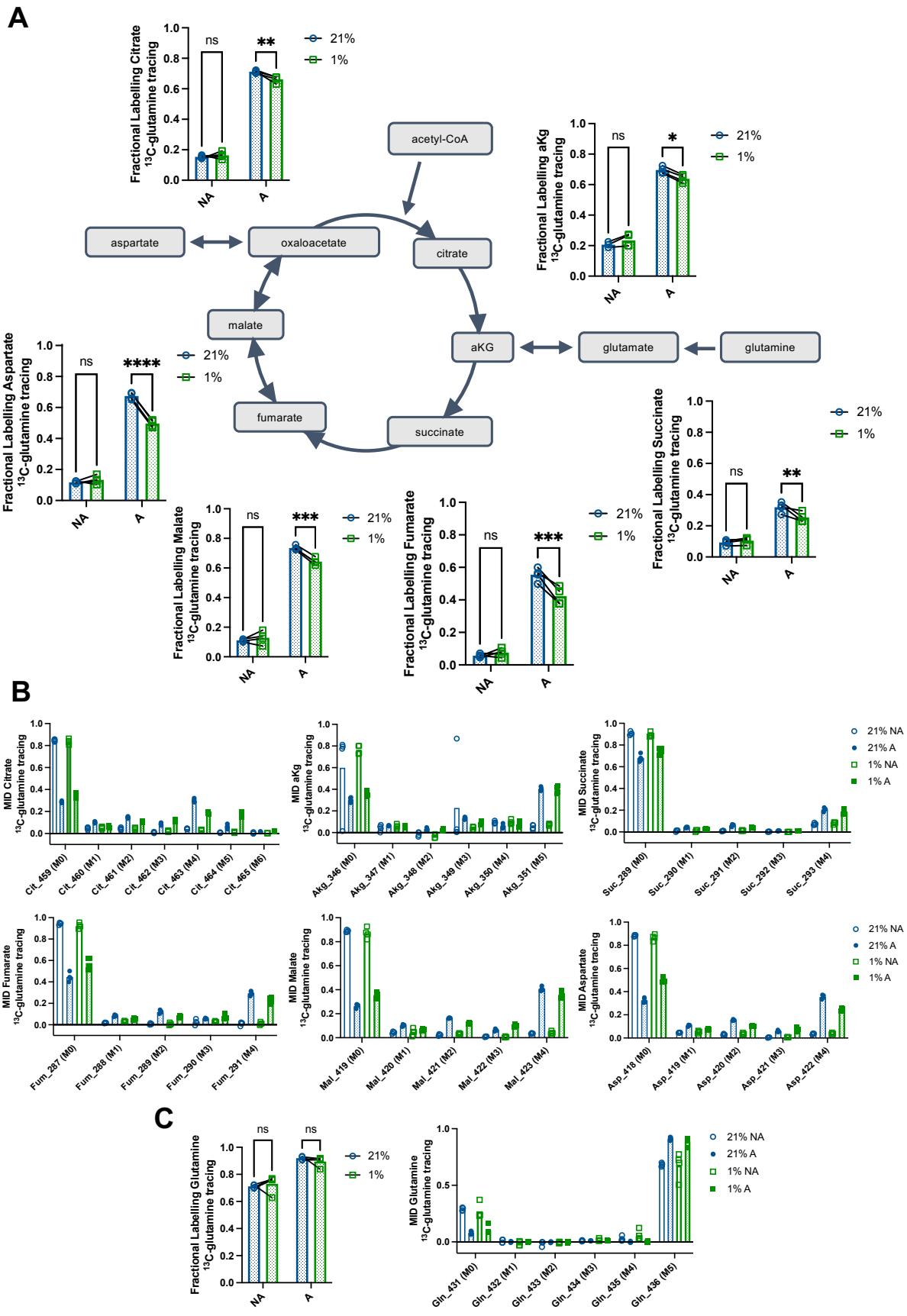
A
Fractional Labelling Citrate
13C-glutamine tracing
ns
**
21%
1%
NA
A
acetyl-CoA
aspartate
oxaloacetate
citrate
malate
aKG
glutamate
glutamine
fumarate
succinate
Fractional Labelling aKg
13C-glutamine tracing
ns
*
Fractional Labelling Aspartate
13C-glutamine tracing
ns
****
Fractional Labelling Malate
13C-glutamine tracing
ns
***
Fractional Labelling Fumarate
13C-glutamine tracing
ns
***
Fractional Labelling Succinate
13C-glutamine tracing
ns
**
B
MID Citrate
13C-glutamine tracing
Cit_459 (M0)
Cit_460 (M1)
Cit_461 (M2)
Cit_462 (M3)
Cit_463 (M4)
Cit_464 (M5)
Cit_465 (M6)
MID aKg
13C-glutamine tracing
Akg_346 (M0)
Akg_347 (M1)
Akg_348 (M2)
Akg_349 (M3)
Akg_350 (M4)
Akg_351 (M5)
MID Succinate
13C-glutamine tracing
Suc_289 (M0)
Suc_290 (M1)
Suc_291 (M2)
Suc_292 (M3)
Suc_293 (M4)
21% NA
21% A
1% NA
1% A
MID Fumarate
13C-glutamine tracing
Fum_287 (M0)
Fum_288 (M1)
Fum_289 (M2)
Fum_290 (M3)
Fum_291 (M4)
MID Malate
13C-glutamine tracing
Mal_419 (M0)
Mal_420 (M1)
Mal_421 (M2)
Mal_422 (M3)
Mal_423 (M4)
MID Asparate
13C-glutamine tracing
Asp_418 (M0)
Asp_419 (M1)
Asp_420 (M2)
Asp_421 (M3)
Asp_422 (M4)
C
Fractional Labelling Glutamine
13C-glutamine tracing
ns
ns
MID Glutamine
13C-glutamine tracing
Gln_431 (M0)
Gln_432 (M1)
Gln_433 (M2)
Gln_434 (M3)
Gln_435 (M4)
Gln_436 (M5)

Figure 4.7. Stable isotope-based tracing for $^{13}C_5$-glutamine in $CD8^+$ T cells activated in hypoxia vs. normoxia. Isolated $CD8^+$ T cells were pre-conditioned overnight in 21% or 1% O_2 conditions, activated the following morning with anti-CD3/CD28, and cultured in the various O_2 conditions for the time point indicated. A) $CD8^+$ T cells were labelled with ^{13}C-glutamine and activated in 21% or 1% O_2 for 48 hours to measure glutamine incorporation, shown is fractional labelling into various metabolites of the TCA cycle, n = 4; B) $CD8^+$ T cells were labelled with ^{13}C-glutamine and activated in 21% or 1% O_2 for 48 hours to measure glutamine incorporation, shown is MID of various metabolites of the TCA cycle, n = 4; C) $CD8^+$ T cells were labelled with ^{13}C-glutamine and activated in 21% or 1% O_2 for 48 hours to measure glutamine incorporation, shown is glutamine fractional labelling and MID of glutamine, n = 4. Blue bars = 21% O_2; Green bars = 1% O_2. Data analysed by (A, C) ordinary two-way ANOVA with Sidak's multiple comparison post-hoc test, with a single pooled variance. * $p < 0.05$, ** $p < 0.005$, *** $p < 0.005$, ns = non-significant or 'blank', $p > 0.05$.

4.3.5. Return of $CD8^+$ T cells previously activated in hypoxia to normoxia may rescue incorporation of ^{13}C-glutamine into TCA cycle metabolites

To understand if return of $CD8^+$ T cells activated in hypoxia to normoxia would rescue metabolic flux, as with function **(3. Results Chapter 1, Figure 3.4),** I cultured human $CD8^+$ T cells in 21% or 1% O_2 overnight, activated the following morning via CD3 and CD28 for 24 hours, moved cells in 1% O_2 back to 21% O_2, and added $^{13}C_5$-labelled glutamine for the final 6 hours. Similarly, an increased incorporation of ^{13}C-glutamine was observed into TCA cycle metabolites with T cell activation **(Figure 4.8A)**. These experiments demonstrated a return of ^{13}C-glutamine incorporation into TCA cycle metabolites of $CD8^+$ T cells activated in 1% O_2 that had been moved back to 21% O_2 for tracing to similar levels as $CD8^+$ T cells activated and cultured in 21% O_2 for the entire time period **(Figure 4.8A)**. **Figure 4.8B** demonstrates the MIDs of TCA cycle metabolites and shows a blunting of the reductive carboxylation of α-KG (increased M+5 citrate and M+3 malate) compared to when cells were traced in 1% O_2 for the entire time period **(Figure 4.8B)**. Similarly, glutamine influx into the cell was similar in both O_2 conditions. Therefore, this experiment demonstrates that, as with function **(3.**

Chapter 1, Figure 3.4), $CD8^+$ T cell glutaminolysis and reductive carboxylation can be rescued with return of cells to normoxia after activation in hypoxia.

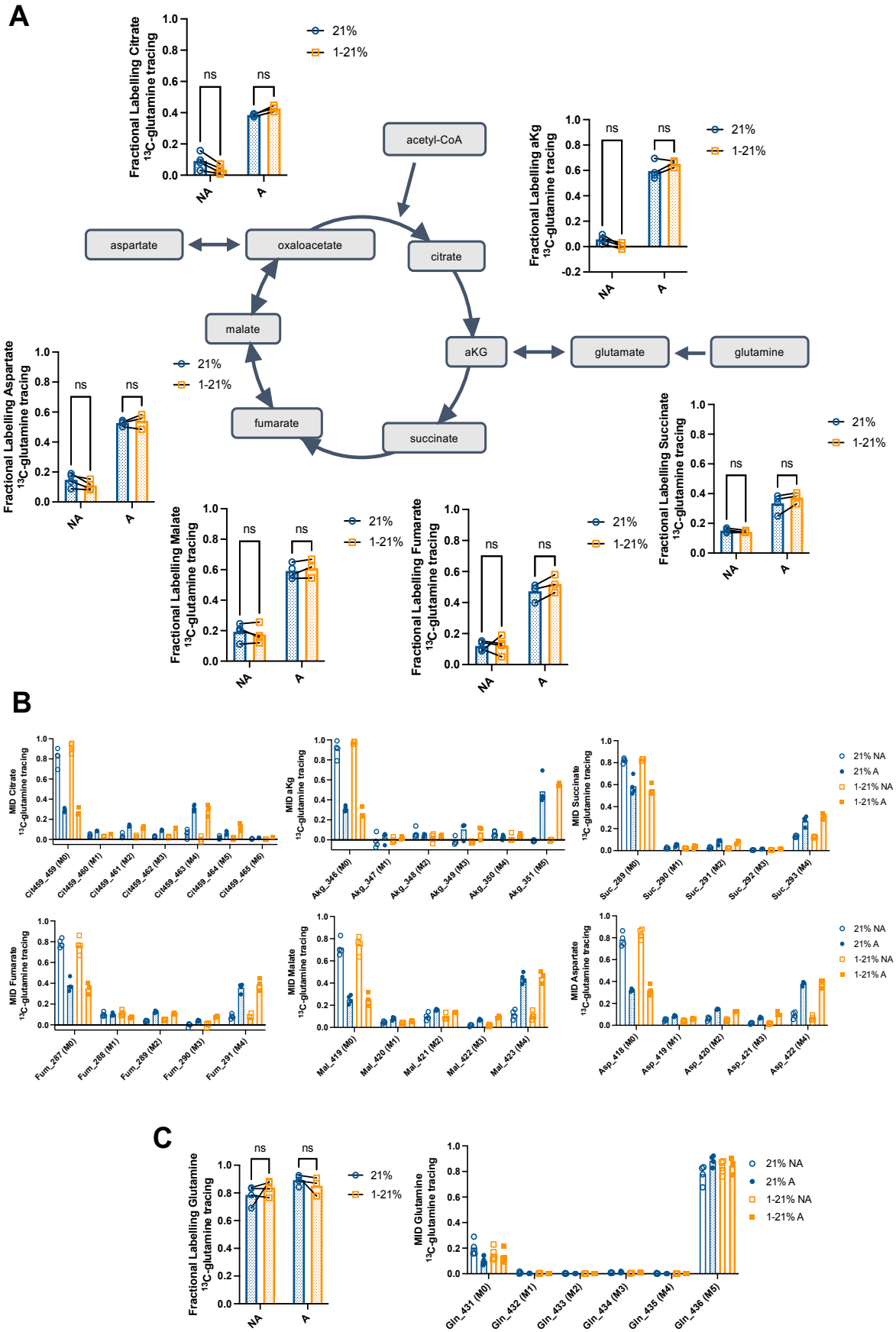
A
Fractional Labelling Citrate
13C-glutamine tracing
21%
1-21%
ns
NA
A
acetyl-CoA
aspartate
oxaloacetate
citrate
malate
aKG
glutamate
glutamine
fumarate
succinate
Fractional Labelling aKg
Fractional Labelling Aspartate
Fractional Labelling Malate
Fractional Labelling Fumarate
Fractional Labelling Succinate
B
MID Citrate
MID aKg
MID Succinate
MID Fumarate
MID Malate
MID Aspartate
21% NA
21% A
1-21% NA
1-21% A
C
Fractional Labelling Glutamine
MID Glutamine

Figure 4.8. Stable isotope-based tracing for $^{13}C_5$-glutamine in $CD8^+$ T cells initially activated in hypoxia and returned to normoxia for metabolic tracing. Isolated $CD8^+$ T cells were pre-conditioned overnight in 21% or 1% O_2 conditions, activated the following morning with anti-CD3/CD28, and cultured in 21% or 1% O_2 for 24 hours. Cells in 1% O_2 were moved back to 21% O_2 for 6 hours of 13C-glutamine tracing of both conditions. A) $CD8^+$ T cells were labelled with ^{13}C-glutamine and activated in 21% or 1% O_2 for 24 hours, and then both traced in 21% O_2 for 6 hours, to measure glutamine incorporation, shown is fractional labelling into various metabolites of the TCA cycle, n = 4; B) $CD8^+$ T cells were labelled with ^{13}C-glutamine and activated in 21% or 1% O_2 for 24 hours and both conditions traced in 21% O_2 for 6 hours to measure glutamine incorporation, shown is MID of various metabolites of the TCA cycle, n = 4; C) $CD8^+$ T cells were labelled with ^{13}C-glutamine and activated in 21% or 1% O_2 for 24 hours and both conditions traced in 21% O_2 for 6 hours to measure glutamine incorporation, shown is glutamine fractional labelling and MID of glutamine, n = 4. Blue bars = 21% O_2; Orange bars = 1-21% O_2 (activated in hypoxia, traced in normoxia). Data analysed by (A, C) ordinary two-way ANOVA with Sidak's multiple comparison post-hoc test, with a single pooled variance * $p < 0.05$, ** $p < 0.005$, *** $p < 0.005$, ns = non-significant or 'blank', $p > 0.05$.

4.3.6. $CD8^+$ T cells activated in hypoxia reduce their mitochondrial membrane potential and produce less reactive oxygen species (ROS)

To further interrogate mitochondrial activity in $CD8^+$ T cells activated and cultured in hypoxia I pre-conditioned $CD8^+$ T cells overnight in 21% and 1% O_2, activated the following morning via CD3 and CD28, cultured in 21% and 1% O_2 for 48 hours and stained with fluorescent mitochondrial probes. $CD8^+$ T cells activated and cultured in 1% O_2 for 48 hours did not alter their mitochondrial mass (MVG staining) compared to those in 21% O_2 **(Figure 4.9A)**, however mitochondrial membrane potential (expressed as a ratio of MSO fluorescence in untreated cells/mitochondrial uncoupler-treated cells (Bam-15)) of those in 1% O_2 did decrease vs. 21% O_2 **(Figure 4.9B)**. In addition, both mitochondrial ROS and total cellular ROS were reduced in $CD8^+$ T cells activated and cultured in hypoxia **(Figures 4.9C and 4.9D)**, consistent with decreased mitochondrial activity. A combination of antimycin and rotenone was used as a positive control for mitochondrial ROS measurements and demonstrates an increase in mitochondrial ROS production in both 21% and 1% O_2 (**Figure 4.9C)**. However, the

positive control for total cellular ROS (1:1000, 2,3-Dimethoxy-1,4-naphthoquinone, DMNQ) did not work consistently **(Figure 4.9D)**. The decrease observed in mitochondrial membrane potential and ROS production in $CD8^+$ T cells activated in hypoxia are consistent with a reduction in TCA cycle activity **(Figure 4.7)**.

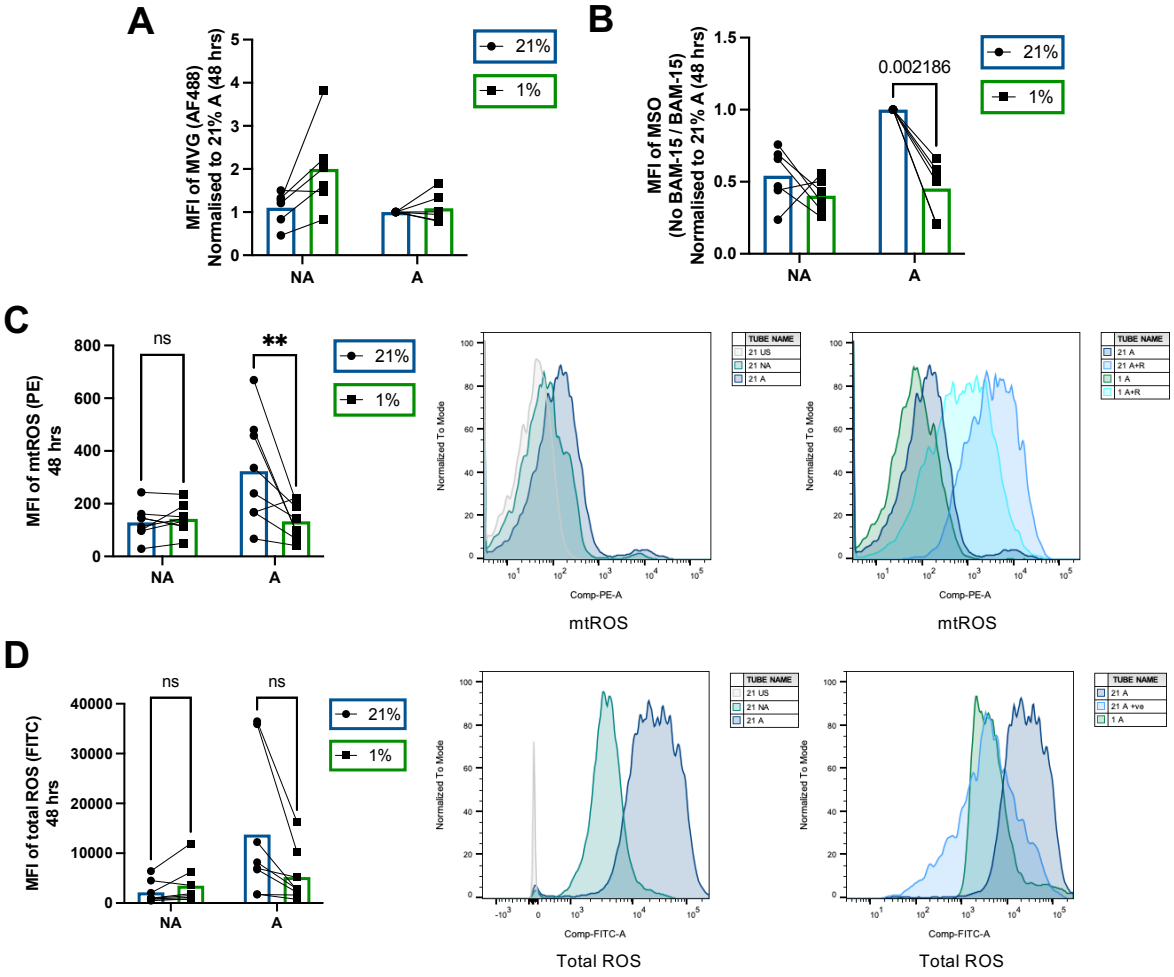

Figure 4.9. Mitochondrial membrane potential and mass, and reactive oxygen species (ROS) production in $CD8^+$ T cells activated in hypoxia vs. normoxia. Isolated $CD8^+$ T cells were pre-conditioned overnight in 21% or 1% O_2 conditions, activated the following morning with anti-CD3/CD28, and cultured in the same O_2 conditions for 48 hours. A) $CD8^+$ T cells were activated in 21% or 1% O_2 for 48 hours and stained with MVG to measure mitochondrial mass, n = 6; B) $CD8^+$ T cells were activated in 21% or 1% O_2 for 48 hours and stained with MSO +/- BAM-15 to measure mitochondrial mass, shown is MFI without BAM-15 / MFI with BAM-15, n = 6; C) $CD8^+$ T cells were activated in 21% or 1% O_2 for 48 hours and stained with mitoSOX to measure mitochondrial (mt)-ROS, n = 8, Example histograms shown for 21 NA vs 21 A and 21 A vs 1 A +/- positive control antimycin + rotenone (A+R); D) $CD8^+$ T cells were activated in 21% or 1% O_2 for 48 hours and stained with DCFDA, n = 8. Blue bars = 21% O_2; Green bars = 1% O_2. Data analysed by (A, B) Multiple Mann-Whitney tests with two-stage linear step-up procedure of Benjamin, Krieger and Yekutieli post-hoc test, (C, D) ordinary two-way ANOVA with Sidak's multiple comparisons post-hoc test, with a single pooled variance.* $p < 0.05$, ** $p < 0.005$, *** $p < 0.005$, or p-value shown, ns = non-significant or 'blank', $p > 0.05$.

4.3.7. Addition of a glycolysis inhibitor to $CD8^+$ T cell culture inhibits their activation and cytokine production

To understand the importance of glycolysis for $CD8^+$ T cells cultured and activated in hypoxia and normoxia I added a glycolysis inhibitor, 2-deoxyglucose (2-DG), to my cell cultures. 2-DG is a glucose mimetic where the 2-hydroxyl group is replaced with a hydrogen molecule (Pajak *et al.*, 2020). 2-DG is taken up by the cell and phosphorylated to 2-deoxy-D-glucose-6-phosphate (2-DG-6-P) which is unable to be converted to fructose-6-phosphate and becomes trapped in the cell, preventing glycolysis (Pajak *et al.*, 2020). Addition of 2-DG to cell cultures did not alter the viability of $CD8^+$ T cells cultured in 21% O_2 but did significantly reduce the survival of $CD8^+$ T cells activated and cultured in 1% O_2 **(Figure 4.10A)**. 2-DG did reduce the percentage of $CD25^+$, and $CD25^+$ $CD69^+$, $CD8^+$ T cells in both 21% and 1% O_2 **(Figure 4.10B)**, demonstrating a reduction of activation when glycolysis is inhibited regardless of O_2 tension. However, the scale of reduction with 2-DG addition was greater in 21% than 1% O_2 for the percentage of $CD25^+$, and $CD25^+$ $CD69^+$, $CD8^+$ T cells **(Figure 4.10B)**. Similarly, the release of IFN-γ detected in the supernatants of cultured cells by ELISA was significantly reduced by 2-DG addition in both 21% and 1% O_2, and to a greater extent in 21% O_2 **(Figure 4.10C)**. TNF-α release was significantly inhibited by 2-DG addition in 1% O_2, and whilst not significant, did trend towards a reduction in 21% O_2 also **(Figure 4.10C)**. This chapter has demonstrated a defect in activation-induced signalling in $CD8^+$ T cells in hypoxia at the level of NFAT and mTOR. $CD8^+$ T cells in hypoxia have impaired activation-induced upregulation of glutaminolysis and glycolysis, which is consistent with reduced c-Myc expression, mitochondrial membrane potential, and production of ROS.

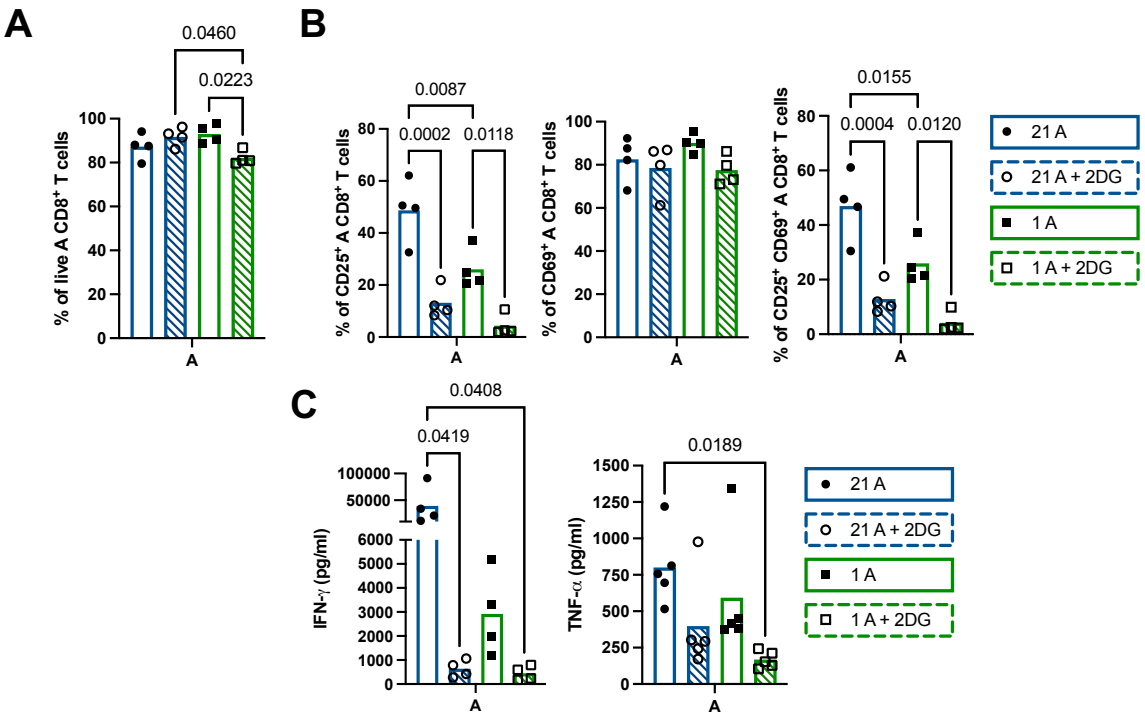

Figure 4.10. Addition of a glycolysis inhibitor and analysis of viability, activation status, and cytokine production in $CD8^+$ T cells activated in hypoxia vs. normoxia. Isolated $CD8^+$ T cells were pre-conditioned overnight in 21% or 1% O_2 conditions, activated the following morning with anti-CD3/CD28, and cultured in the same O_2 conditions for 48 hours. A) $CD8^+$ T cells were activated in 21% or 1% O_2 for 48 hours +/- 10 mM 2DG. Shown is percentage of live, $CD25^+$, $CD69^+$, and $CD25^+$ $CD69^+$, live, activated $CD8^+$ T cells, n = 4; B) $CD8^+$ T cells were activated in 21% or 1% O_2 for 48 hours +/- 10 mM 2DG, and ELISAs performed on the supernatants of cultured cells, IFN-γ and TNF-α concentrations shown, n = 4. Blue bars = 21% O_2; Green bars = 1% O_2. Data analysed by (A, B, C) ordinary one-way ANOVA with Tukey's multiple comparisons post-hoc test, with a single pooled variance. * $p < 0.05$, ** $p < 0.005$, *** $p < 0.005$, or p-value shown, ns = non-significant or 'blank', $p > 0.05$.

4.4. Discussion

In vitro experiments conducted in '**3. Results Chapter 1**' suggested the functional defects of hypoxia on T cell function may originate from a defect in T cell signalling. Therefore, I explored the impact of hypoxia on $CD8^+$ T cell signalling pathways. I began by probing for key phosphorylated signalling proteins in the TCR pathway by western blot, however this proved inconclusive due to the persistent presence of bands for phosphorylated proteins in non-activated $CD8^+$ T cells **(Figure 4.1)**. I hypothesised that the presence of this band may be due to a partial activation of T cells received from the isolation method, for example, positive selection with magnetic beads. Thus, to troubleshoot, I conducted similar western blots in Jurkats and whole PBMC that had not been magnetically sorted **(Figure 4.1)**. Unfortunately, a band was still observed in non-activated samples and this method was deemed unsuitable. Instead, I conducted flow cytometry analysis of phosphorylation of signalling proteins in human $CD8^+$ T cells activated and cultured in hypoxia **(Figures 4.2 and 4.3)**. Despite relatively low signal, phospho-Lck and -ERK, upstream TCR signalling, appeared to be intact in hypoxia **(Figure 4.2)**. However, immediate calcium flux upon activation was impaired in low O_2 conditions **(Figure 4.2)**. These findings are consistent with previous reports that show hypoxia to inhibit calcium influx via L-type and store-operated calcium (SOC) channels (Kanatous *et al.*, 2009). Similarly, previous reports have demonstrated that hypoxia reduces the CD3/CD38 activation-induced increase in cytoplasmic Ca^{2+} in human T cells (Robbins *et al.*, 2005). This study suggested the modulation of Ca^{2+} flux was due to inhibition of the voltage-dependent potassium ion (K^+) channel 3 (Kv1.3) and membrane depolarisation which reduces the flux of Ca^{2+} into cells (Robbins *et al.*, 2005). The inhibition of Kv1.3 has been suggested to contribute to the hypoxia-induced

deficits on T cell activation (Szigligeti *et al.*, 2006). Furthermore, NFAT signalling and calcium flux are closely related (Fracchia, Pai and Walsh, 2013), thus it was not surprising to find a defect in NFAT translocation to the nucleus in $CD8^+$ T cells activated in hypoxia **(Figure 4.2)**.

I next utilised Nur77-Tempo and Nr4a3-Tocky murine models to further probe T cell signalling in hypoxia **(Figures 4.4 and 4.5)** (Bending *et al.*, 2018; Elliott *et al.*, 2022). Since the blue-reporter protein is required to be translated after activation, and protein translation can be impaired in hypoxia (Chee, Lohse and Brothers, 2019; De Ponte Conti *et al.*, 2021), I first used a puromycin assay to assess the impact of hypoxia on protein translation in my experimental setting **(Figure 4.4)**. The small effect size reassured that conclusions may be made using the Timer-blue signal. Interestingly, in cells from the Nur77-TEMPO mice, no effect of hypoxia on the blue-signal was observed, whilst this was observed for cells from Nr4a3-Tocky mice **(Figures 4.4 and 4.5)**. I hypothesise that because the Tempo reporter expression is independent of NFAT signalling, whilst Tocky reporter expression is NFAT dependent (Bending *et al.*, 2018; Elliott *et al.*, 2022), this would be consistent with observations of reduced nuclear NFAT in human $CD8^+$ T cells activated in hypoxia **(Figure 4.2)**. Further experiments revealed the Timer-red signal to not be reliable as a read-out of an arrested TCR signal, as hypoxia prevented the transition from the blue- to red- reporter protein **(Figures 4.4 and 4.5)**.

Upon T cell activation, CD28 co-stimulation initiates signalling via the PI3K-AKT pathway which feeds into various pathways, including NFAT and mTOR (Riha and

Rudd, 2010). Phosphorylation of Akt in $CD8^+$ T cells activated in hypoxia was similar to those activated in normoxia **(Figure 4.3)**. However, further downstream, a defect in the phosphorylation of mTOR existed in hypoxia and fed to its downstream target p70S6K **(Figure 4.3)**. mTOR has several roles directing T cell effector functions, activation, proliferation and differentiation (Chapman and Chi, 2015).

It has previously been reported that mTOR signalling is crucial for cytokine production in T cells via a PKC interaction with the PI3K pathway and mTOR dependent translation of cytokines (Salerno *et al.*, 2017). Interestingly, IFN-γ has been shown to have greater dependence on calcium signalling than TNF-α (Salerno *et al.*, 2017), which is consistent with the observed defects in cytokine production and activation-dependent calcium deficit in $CD8^+$ T cells in hypoxia **(Figures 3.3 and 4.2)**. Therefore, the defects observed in mTOR and calcium/NFAT signalling pathways observed in $CD8^+$ T cells activated in hypoxia may play a role in the functional defects described in '**3. Results Chapter 1**'.

Importantly, mTOR has close associations with HIF-1α and roles within $CD8^+$ T cell metabolic reprogramming upon activation (Chapman and Chi, 2015). mTOR works alongside c-Myc to drive the increase in glycolytic activity observed upon T cell activation (Chi, 2012), as T cells deficient in the mTOR suppressor TSC2 are highly glycolytic following activation (Michalek *et al.*, 2011). Importantly, whilst mTOR and c-Myc are required for T cell metabolic reprogramming upon activation, deletion of HIF-1α did not impact activation-induced glutaminolysis and glycolysis in $CD8^+$ T cells (Yoo *et al.*, 2020), suggesting it is not so important in this context. Alongside the defect in

mTOR signalling, $CD8^+$ T cells activated in hypoxia had a reduction in expression of c-Myc **(Figure 4.6)**. Since mTOR and c-Myc are both crucial regulators of activation-induced T cell metabolic reprogramming, this suggests that $CD8^+$ T cells activated in hypoxia may have impaired metabolic reprogramming.

Upon activation, $CD8^+$ T cells upregulate glycolytic metabolism, take up greater quantities of glucose and, from this, produce lactate (Gerriets and Rathmell, 2012). Similarly, in hypoxia, glycolysis is also upregulated and OXPHOS suppressed (Kierans and Taylor, 2021). Therefore, I wondered if over the time course of *in vitro* experiments $CD8^+$ T cells activated in hypoxia were taking up so much glucose to lead to a deficit in the environment, which might explain their functional impairment. Indeed, understanding this was important as glucose deprivation is known to limit $CD8^+$ T cell IFN-γ production and suppress expression of genes for effector function and cell cycle (Cham and Gajewski, 2005; Cham *et al.*, 2008). With increased glycolysis, an excess of lactate will also arise. Importantly, lactate accumulation is also suppressive for $CD8^+$ T cell function through inhibition of proliferation, cytokine production and signalling (Rostamian *et al.*, 2022). It was important I ruled out the limitation of glucose or accumulation of lactate as these may be confounding drivers on the functional impacts I observe in hypoxia. When I measured glucose and lactate in the supernatants of $CD8^+$ T cells cultured in hypoxia up to 72 hours I observed the expected increased glucose uptake and lactate production with activation, however this was not significantly different between hypoxia and normoxia **(Figure 4.6)**. These findings have previously been observed in human PBMC activated in hypoxia with PHA, whereby glucose uptake and lactate production were not significantly different to PBMC

activated by PHA in normoxia (Naldini *et al.*, 1997). Overall, glucose deprivation and lactate accumulation do not account for the functional effects observed when activating $CD8^+$ T cells in hypoxia.

To understand how $CD8^+$ T cells utilise glucose and glutamine when activated in hypoxia I performed ^{13}C-stable isotope tracing **(Figures 4.6 and 4.7)**. Whilst I observed expected increases of ^{13}C-glucose labelling into pyruvate and lactate with $CD8^+$ T cell activation, labelling into TCA cycle intermediates was limited **(Figure 4.6)**. Consistent with other studies (Blagih *et al.*, 2015; Matheson *et al.*, 2022), ^{13}C-glutamine labelling into TCA cycle intermediates with activation was much greater than with ^{13}C-glucose in $CD8^+$ T cells **(Figures 4.6 and 4.7)**. In hypoxia, increased ^{13}C-glucose labelling into lactate in non-activated $CD8^+$ T cells indicates expected adoption of hypoxia-induced glycolysis, but this was less clear in activated cells **(Figure 4.6)**. Labelling of TCA cycle intermediates with ^{13}C-glutamine was reduced in $CD8^+$ T cells activated in hypoxia, compared to those in normoxia, suggesting a defect in activation-induced glutaminolysis **(Figure 4.7)**. However, it should be taken into consideration that this effect is likely compounded by reduced mitochondrial function under limited O_2 availability.

Consistent with this, activated $CD8^+$ T cells in hypoxia had increased abundance of M+5 citrate and M+3 malate **(Figure 4.7)**, a feature indicative of the reductive carboxylation of glutamine-derived α-KG that is often observed in hypoxia and situations of impaired mitochondrial ETC activity (Eales, Hollinshead and Tennant, 2016). Previous studies have shown that citrate generated from reductive

carboxylation of α-KG is important for lipid synthesis in hypoxia (Metallo *et al.*, 2011; Yoo *et al.*, 2020). Further work should explore how reductive carboxylation of α-KG and lipid synthesis is used in $CD8^+$ T cells that are activated within hypoxia. Interestingly, it is reported that $CD8^+$ T cells that have been activated for 4 days under normoxia and moved for the final 16 hours to hypoxia increasingly rely upon the uptake of FA and FAO (Zhang *et al.*, 2017). The role of FAO and FA metabolism in $CD8^+$ T cells activated in hypoxia should be explored further, for example with liquid chromatography-mass spectrometry (LC-MS).

Consistent with the reduction of carbon incorporation originating from glutamine into TCA cycle metabolites in hypoxia, I also observed a decrease in mitochondrial membrane potential **(Figure 4.9)**, similar to previous studies (Zhang *et al.*, 2017). However, whilst this previous study observed an increase in mitochondrial ROS with hypoxia (Zhang *et al.*, 2017), I observed a reduction in this **(Figure 4.9)**. This appears to be a relatively unique finding as the majority of cell types experience an increase in ROS on hypoxic exposure (Hamanaka and Chandel, 2009), and this finding may be related to the impaired activation of these cells in hypoxia. Indeed, my data indicate that activation under normoxia significantly increase mitochondrial ROS production **(Figure 4.9)**. Mitochondrial ROS are a major component of total cellular ROS in activated T cells, and I consistently observed a reduction in total cellular ROS in hypoxia **(Figure 4.9)**. Interestingly, previous work has shown that mitochondrial ROS stabilise and promote translocation of NFAT during T cell activation (Sena *et al.*, 2013). Thus, the decreased mitochondrial ROS observed in activated $CD8^+$ T cells in hypoxia aligns with the defect of NFAT signalling discussed above **(Figure 4.2)**.

Finally, I explored the dependency of $CD8^+$ T cells in hypoxia on glycolysis as a metabolic pathway by addition of the glycolytic inhibitor, 2-DG **(Figure 4.10)**. Viability of activated $CD8^+$ T cells was not impaired with 2-DG addition in normoxia, but 2-DG addition in hypoxia slightly reduced survival suggesting a greater dependence on glycolysis **(Figure 4.10)**. However, whilst inhibition of glycolysis impaired activation and cytokine release of $CD8^+$ T cells activated in hypoxia and normoxia, the effect was greater in normoxia **(Figure 4.10)**. This may be because the levels of activation and cytokine release are already lower in $CD8^+$ T cells in hypoxia or may suggest different dependencies on glycolysis by function. It would be interesting to follow the dependencies on different metabolic pathways further, for example, via Single Cell ENergetIc metabolism by profilIng Translation inhibition (SCENITH) (Argüello *et al.*, 2020).

4.5. Conclusion

This chapter has confirmed a defect in $CD8^+$ T cell signalling upon activation lies at the level of mTOR, alongside the calcium-NFAT pathway. $CD8^+$ T cells in hypoxia fail to completely metabolically reprogram upon activation and have impaired activation-induced increases in glycolysis, glucose oxidation and glutaminolysis. These signalling and metabolic defects may play a role in the functional impairments in IFN-γ release and production, proliferation, and activation observed in Chapter 1, but further work is required to prove this.

5. Results Chapter 3

Interrogating potential mechanisms of defective $CD8^+$ T cell function in hypoxia

5. Results Chapter 3: Interrogating potential mechanisms of defective CD8$^+$ T cell function in hypoxia

5.1. Introduction

Whilst several pathways converge to coordinate the cellular response to hypoxia, the primary player is the transcription factor, HIF-1α. In normal O_2 conditions, HIF-1α is targeted for degradation by PHDs and its transcriptional activities inhibited by FIH (Ebert and Bunn, 1998; Maxwell *et al.*, 1999; Epstein *et al.*, 2001; Jaakkola *et al*, 2001; McNeill *et al.*, 2002). In hypoxia, HIF-1α protein is stabilised, complexes with HIF-1β, and translocates to the nucleus to bind HREs and initiate transcription of target genes (Semenza, 2010). HIF-target genes are broad but include those which enable cellular survival and efficient metabolism in hypoxia (Dengler, Galbraith and Espinosa, 2014). Therefore, it is expected that HIF-1α has significant roles in the regulation of CD8$^+$ T cell function and metabolism in hypoxia. Previous literature has explored the regulation of CD8$^+$ T cell function by HIF-1α through various murine models. **Table 5.1** summarises the key literature in this context. In general, the stabilisation of HIF-1α appears to be beneficial for T cell function, specifically for the expression of activation markers, cytokine production, and cytotoxic molecule production (Finlay *et al.*, 2012; Doedens *et al.*, 2013; Clever *et al.*, 2016; Palazon *et al.*, 2017; Zhang *et al.*, 2017; Liikanen *et al.*, 2021). Another study showed HIF-2α, but not HIF-1α, to be beneficial for T cell function (Veliça *et al.*, 2021). However, other experiments do contradict these findings (Thiel *et al.*, 2007; Zhang *et al.*, 2017; Wei *et al.*, 2023). HIF-1α knockdown of T cells exposed to hypoxia improved granzyme B and IFN-γ production, suggesting that in hypoxia HIF-1α expression may be inhibitory (Zhang *et al.*, 2017). Alternatively, when HIF-deficient T cells are exposed to hypoxia, the functional defects caused by

hypoxia are not restored (Scharping *et al.*, 2021). Therefore, the regulation of T cell function by HIF-1α is controversial, however it appears that the hypoxia-induced functional defects on T cells may be independent of HIF-1α stabilisation.

Given these findings, it is important to acknowledge other pathways that may play a role in regulating T cell function in hypoxia. The AMPK pathway is activated following energetic stress and regulates T cell function (Corton, Gillespie and Hardie, 1994; Hawley *et al.*, 2010; Mungai *et al.*, 2011; Blagih *et al.*, 2015). Thus, it is plausible that the energetic stress derived from hypoxia engages the AMPK pathway on T cells. Hypoxia is also described to activate the NF-κB and AP-1 pathways, which are known to impact T cell function and initiate transcription of cytokine genes, respectively (Bandyopadhyay, Phelan and Faller, 1995; Macián, López-Rodríguez and Rao, 2001; Barnes *et al.*, 2015; D'Ignazio and Rocha, 2016). Hence, these pathways should also be considered when interrogating the mechanism driving a suppression of specific $CD8^+$ T cell functions in hypoxia.

In '**4. Results Chapter 2**' I reported a defect in activation-induced mTOR signalling in $CD8^+$ T cells stimulated in hypoxia **(Figure 4.3)**. mTOR deficiency, and rapamycin treatment, is reported to suppress T cell proliferation (Delgoffe *et al.*, 2009; Yang *et al.*, 2013; Chapman and Chi, 2015). One study showed that mTOR is required for continuous proliferation and for the long-term production of IFN-γ by human naïve and effector memory $CD8^+$ T cells (Setoguchi, Matsui and Mouri, 2015). EMRA $CD8^+$ T cells, which produce less IFN-γ, also had impaired mTOR signalling compared to other $CD8^+$ T cell subsets (Setoguchi, Matsui and Mouri, 2015). Therefore, the defect

observed in mTOR signalling in $CD8^+$ T cells activated in hypoxia may contribute to the functional defects in IFN-γ production and proliferation.

Importantly, mTOR is documented to drive the accumulation of HIF-1α protein (Dodd *et al.*, 2015), and several mechanisms have been proposed to explain the suppression of mTOR in hypoxia (Brugarolas *et al.*, 2004; Li *et al.*, 2007). These include the HIF-dependent upregulation of regulated in development and DNA damage response 1(REDD1)/DNA-damage-inducible transcript 4 (DDIT4) which directly inhibits mTOR in hypoxia, and the HIF-dependent upregulation of BCL2 Interacting Protein 3 (BNIP3) expression which interacts with and degrades an activator of mTOR, Rheb, in hypoxia (Brugarolas *et al.*, 2004; Li *et al.*, 2007; Vadysirisack and Ellisen, 2012). However, a specific mechanism driving mTOR suppression in activated $CD8^+$ T cells hypoxia is yet to be described.

Table 5.1. Table to summarise previous literature exploring the regulation of $CD8^+$ T cell function by HIF-1α.

Study ID	Species	Protocol (Method*)	Key findings	HIF beneficial or inhibitory?
Impacts of HIF modulation on T cell function				
Clever *et al.*, 2016	Mouse	Isolated T cells and analysed ex vivo. Mice analysed at 3 months of age. **Mice with a deletion of all 3 PHD (Egln1, Egln2, Egln3 transcripts) proteins in T cells ($CD4^+$, $CD8^+$, NKT) via a Cd4-Cre.** NB: both $CD4^+$ and $CD8^+$ T cells analysed.	T cells in the lung of PHD-KO mice had a greater expression of the activation markers CD44, CD25, GITR, and CTLA-4, increased IFN-γ expression, and greater expression of cytotoxic molecules than WT mice. A greater IFN-γ^+ effector T cell to Treg ratio was observed in the lung of PHD-KO mice.	PHD deletion = enhanced HIF expression. HIF beneficial for enhanced T cell function
Doedens *et al.*, 2013	Mouse	Isolated $CD8^+$ T cells from splenocytes via negative selection and activated with anti-CD3/CD28 for 48 hours. Then cultured with fresh media + IL-2 +/- IL-4 for 24-48 hours to differentiate into CTLs.	1) Mice with Vhl-deficiency in their $CD8^+$ T cells were vulnerable to a chronic LCMV infection, unlike Vhl-sufficient mice, whilst both groups survived acute LCMV infection. 2) Vhl-deficiency led to upregulated mRNA expression of granzymes, perforin and	Deletion of Vhl = enhanced HIF expression. HIF beneficial for cytotoxic molecule expression, activation and cytokines.

		Deletion of Vhl gene in mature CD8$^+$ T cells with a Cre recombinase against a dLck, deletion of Hif1-a via a CD4 Cre, or deletion of Epas1 via a Tie2 Cre. 1) Challenged mice with either acute or chronic LCMV infection. 2) Transferred Vhl-sufficient or -deficient CTLs into WT mice and challenged with chronic LCMV infection.	TNF, alongside upregulated expression of mRNA encoding activation genes (OX40, 4-1BB, GITR, and SLAMF7) and co-inhibitory transcripts (Ctla4, Lag3, Havcr2, Cd244). On the protein level, greater expression of granzyme B and perforin observed in VHL-deficient cells compared to VHL-sufficient. Expression of PD-1 lower in VHL-deficient cells than VHL-sufficient. VHL-deficient cells had greater production of IFN-γ and TNF-α than VHL-sufficient cells, more cytotoxic in an *in vivo* assay and refractory to exhaustion. Also relevant in the cancer setting.	
Finlay *et al.*, 2012	Mouse	Isolated lymphocytes from P14-LCMV or OT-I transgenic or non-transgenic mice, activated with LCMV or OT-I specific peptide, or anti-	HIF-1β null CD8$^+$ T cells blasted and upregulated CD25, CD71, and CD44 similarly to WT CD8$^+$ T cells.	HIF expression beneficial for perforin expression, but not other functional aspects of CD8$^+$ T cells.

		CD3, for 48 hours. Then, cells cultured for 6 days + IL-2 to generate CTLs. **Deletion of HIF1-β in $CD8^+$ T cells, CTLs, with a CD4 Cre recombinase.**	HIF-1β null $CD8^+$ T cells displayed no alterations in proliferation compared to WT $CD8^+$ T cells and did not alter expression of transcription factors for T cell differentiation. HIF-1β null $CD8^+$ T cells had reduced expression of perforin 1 and various granzymes (G, D, E, and F) compared to WT $CD8^+$ T cells, whilst expression of IFN-γ did not change. Expression of Fas ligand and lymphotoxin B increased in HIF-1β null $CD8^+$ T cells comparatively to WT. HIF-1β null $CD8^+$ T cells increased gene expression of chemokines and their receptors, as well as adhesion molecules compared to WT (e.g., CCR7 and CD62L).	

Liikanen *et al.*, 2021	Mouse	*In vivo:* Introduced B16.gp33 melanoma or MC38.gp33 colorectal adenocarcinoma to WT mice. Then adoptive transfer of *ex vivo* activated WT or Vhl-deficient P14 $CD8^+$ T cells. Some experiments cells were restimulated *ex vivo* with gp33 peptide. **Deletion of Vhl in mature $CD8^+$ T cells, with a Cre recombinase against dLck. Crossed with TCR transgenic P14 mice (recognise peptide gp33) to assess ability of Vhl-deficient, antigen specific, $CD8^+$ T cells in tumour control.**	*In vivo:* $CD8^+$ T cells deficient in Vhl were able to maintain improved tumour control and mice survival in both models. Shown to be dependent on HIF-1α expression as HIF-1α and HIF-2α knockout removed this effect. Vhl-deficient $CD8^+$ T cells shown to have a survival advantage compared to their WT counterparts in tumours (higher expression of STAT5 and higher CD25 in Vhl-deficient $CD8^+$ T cells removed from tumours). Vhl-deficient $CD8^+$ T cells produced more IFN-γ and TNF-α upon *ex vivo* restimulation vs WT $CD8^+$ T cells, and expressed higher levels of PD-1, TIM-3 and LAG-3 overtime than WT cells. Granzyme B production also higher in Vhl-deficient $CD8^+$ T cells than	Deletion of Vhl = enhanced HIF-1α and HIF-2α protein expression. HIF-1α and HIF-2α expression beneficial for tumour control and $CD8^+$ T cell survival, cytokine production, activation status and cytotoxic potential.

			WT, which co-existed with greater lysis of target cells by Vhl-deficient $CD8^+$ T cells than WT.	
Lukashev *et al.*, 2006	Mouse	Genetic deletion of HIF-1α isoform I.1 in mice, or T cell specific deletion of HIF-1α via a Lck-Cre. T cells isolated from splenocytes and activated via CD3/CD28 for 24 hours at 20% or 2% O_2. **Deletion of HIF-1α isoform I.1 or T cell specific deletion of HIF-1α via a Lck-Cre.**	At either O_2 tension, T cells deficient in HIF-1α had improved secretion and production ($CD8^+$ T cells) of IFN-γ than WT T cells. Deficiency of HIF-1α isoform I.1 (activation-inducible isoform) in mice resulted in improved production of proinflammatory cytokines. Work expanded by Georgiev *et al.* (2013) in a murine bacterial peritonitis model (Georgiev *et al.*, 2013).	HIF-1α (and specific expression of the activation-inducible isoform) expression inhibitory for cytokine production.
Palazon *et al.*, 2017	Mouse	Genetically deleted *HIF-1α* (exon 2) or Epas (*Hif-2α*) alleles by a Cre recombinase under the control of dLck = deletion in $CD8^+$ T cells.	Loss of HIF-1α, but not HIF-2α, impaired upregulation of glycolysis in CTLs in hypoxia and slightly reduced survival.	HIF-1α expression beneficial for tumour control and $CD8^+$ T cell

		Cultured control and mutant CTLs under 21% or 1% O_2. Also, LLC and B16-F10 melanoma given to mice lacking HIF-1α or HIF-2α, or to WT mice. Antigen specific model – OT-I mice with HIF-1α or HIF-2α mutations, activated with SINFEKL peptide. **Deletion of HIF-1α or HIF-2α in $CD8^+$ T cells via a Cre recombinase under the control of the distal promotor of Lck (dLck).**	Loss of HIF-1α, but not HIF-2α, significantly reduced production of IFN-γ, TNF-α and granzyme-B. Tumours in mice without HIF-1α grew more rapidly than mice without HIF-2α or WT mice. Antigen specific model – T cells with loss of HIF-1α have reduced production of IFN-γ, TNF-α and granzyme-B. HIF-1α mutant mice with MC38 colon tumours had impaired response to immune checkpoint inhibition compared to WT mice.	cytokine production and cytolytic granule production.
Scharping *et al.*, 2022	Mouse	OT-1 TCR transgenic T cells activated overnight with cognate peptide in normoxia (21% O_2), and then either cultured alone, +	When exposed to hypoxia and continuous stimulation, T cells deficient in HIF did not change their upregulation of co-inhibitory	HIF did not rescue the inhibitory effects of hypoxia

		B16 cells, or + B16-expressing ovalbumin in normoxia or hypoxia (1.5% O_2) for 5 days + IL-2. Also performed experiments when isolated polyclonal T cells and activated with anti-CD3 and anti-CD28 overnight in normoxia (+ IL-2 + IL-12). Then cultured with IL-2 (acute activation), or with anti-CD3/CD28 + IL-2 (continuous activation) for 5 days in normoxia or hypoxia. **HIF-1α deficiency induced in T cells via a CD4 Cre recombinase.**	receptors and did not rescue their loss of polyfunctionality of cytokine production (see hypoxia table). This suggests these functional effects are independent of HIF.	
Thiel *et al.*, 2007	Mouse	T cell targeted deletion of HIF-1α with a Cre-lox-P system, analysed in an *in vivo* model of bacterial sepsis. **HIF-1α deficiency induced in T cells via a Lck Cre-lox-P system.**	HIF-1α deletion in T cells resulted in increased TCR-induced proliferation and IFN-γ secretion. Better survival of mice with bacterial sepsis when HIF-1α deleted in T cells. Mechanism related to increased NF-	HIF-1α inhibitory to T cell function

			κB activation in HIF-1α deleted T cells in mice.	
Velica *et al.*, 2021	Mouse	Isolated mouse $CD8^+$ T cells activated with anti-CD3/CD28, or SIINFEKL (for OT-I mice) for 24 hours, then transduced and expanded for 3-5 days + IL-2 prior to analysis. **Retroviral vectors designed to express HIF-1α and/or HIF-2α, +/- regulation by oxygen-dependent mechanisms (VHL or FIH).**	Ectopic HIF-2α increased expression of Prf1 and Gzmb, and co-stimulatory receptors (OX40, 4-1BB, CD30) and co-inhibitory receptors (CTLA4, LAG3). A reduction in the expression of IFNγ gene and increased expression of gene for CD25 observed with ectopic HIF-2α. Similar results were observed in protein expression. TCR complex expression was lost when HIF-2α ectopically transduced. IFN-γ production of OT-I cells activated with OVA was reduced when HIF-2α ectopically transduced (VHL-insensitive), whilst	HIF-2α, and not HIF-1α, expression augments the cytotoxic potential of $CD8^+$ T cells.

			PMA/ionomycin activation did not create this effect.	
Wei *et al.*, 2023	Mouse	HIF-1α knockout and WT mice challenged with B16F10 (melanoma cell line). Also used a HIF-1α inhibitor, Acriflavin. C57BL/6 mice crossed with HIF-1α loxP/loxP mice, then crossed with Tg(Cd4-Cre)1Cwi and LSL-EYFP lines to obtain HIF-1α loxP/loxP; LSL-EYFP; CD4-Cre mice. **T-cell specific HIF-1α knockout mice generated via a CD4 Cre system.**	Tumours grew slower in mice with T cells that had a KO of HIF-1α compared to their WT counterparts. Effects compared in a metastatic tumour murine model. Mice with T cell specific HIF-1α KO had greater production of IFN-γ than WT by $CD8^+$ TILs, and greater killing of p15Epeptide-pulsed splenocytes. Similar results observed when using a HIF-1α inhibitor.	HIF-1α expression inhibitory for tumour control and $CD8^+$ T cell function.
Zhang *et al.*, 2017	Mouse	Isolated $CD8^+$ T cells from splenocytes prior to stimulation with anti-CD3/CD28 in 21% O_2 for 4 days, +/- with the last 16 hours in 1% O_2.	Knockdown of HIF-1α in $CD8^+$ T cells activated with anti-CD3/CD28 reduced LAG-3 expression, increased granzyme-B	HIF-1α expression beneficial for LAG-3 expression and perforin

		HIF-1α knockdown with 3 lentiviruses expressing different HIF-1α shRNA or scrambled shRNA.	production, and decreased perforin production. In hypoxia, knockdown of HIF-1α reduces LAG-3 expression, but not PD-1 expression. HIF-1α knockdown also improved production of granzyme B and IFN-γ in hypoxia. Similar results observed when introducing HIF-1α knockdown $CD8^+$ T cells into tumour-bearing, treated mice.	production, inhibitory on granzyme-B production. In hypoxia, HIF-1α expression inhibitory on granzyme B and IFN-γ production.

* *Method of HIF modulation, T cell differentiation process, method and timings of T cell activation.*

5.2. Aims

This chapter will begin to explore potential mechanisms driving the suppression of mTOR in $CD8^+$ T cells activated in hypoxia and to understand the link between mTOR signalling and defective $CD8^+$ T cell functions in hypoxia. The aims of this chapter are as follows:

1. To conduct bulk RNA sequencing to identify pathways of interest in $CD8^+$ T cells activated in hypoxia
2. To begin to understand the role of the AMPK pathway in $CD8^+$ T cells activated in hypoxia
3. To explore a potential mechanism of mTOR suppression via a BNIP3/Rheb/mTOR interaction in hypoxia using CRISPR-Cas9 knockout models in primary human $CD8^+$ T cells

5.3. Results

5.3.1. Characteristic differentially expressed genes (DEGs) are upregulated and downregulated in CD8$^+$ T cells activated in normoxia and hypoxia

Bulk RNA-sequencing was performed on CD8$^+$ T cells pre-conditioned overnight, then activated the following morning with anti-CD3/CD28 or left unstimulated, at 21% or 1% O_2 for 24 hours (4 groups total, 5 replicate donors). Initially, non-activated (NA) and activated (A) samples in 21% and 1% O_2 were compared. Principal component analysis (PCA) demonstrated that samples clustered according to activation status **(Figure 5.1A and 5.1B)**. There were 4779 differentially expressed genes (DEGs) between NA and A CD8$^+$ T cells at 21% O_2 which are demonstrated in a volcano plot in **Figure 5.1C**. 2532 DEGs were upregulated in 21% O_2 A CD8$^+$ T cells compared to NA cells and included those in the oxidative phosphorylation, cell cycle, proteasome, and DNA replication pathways, among others, as would be expected **(Figure 5.1D)**. 2247 DEGs were downregulated in 21% O_2 A CD8$^+$ T cells compared to NA cells and included those in endocytosis, FoxO signalling, autophagy, lysosome, and longevity regulating pathways **(Figure 5.1D)**. Between NA and A CD8$^+$ T cells in 1% O_2 there were 4740 DEGs, and samples similarly clustered by activation status **(Figure 5.1E)**. **Figure 5.1F** is a volcano plot of upregulated and downregulated DEGs between NA and A CD8$^+$ T cells in 1% O_2. 2530 DEGs were upregulated in 1% O_2 A CD8$^+$ T cells, which were in similar pathways to those in 21% O_2 but also included biosynthesis of amino acids and carbon metabolism **(Figure 5.1G)**. Interestingly, upregulated DEGs in 1% O_2 A vs. NA CD8$^+$ T cells did not include genes in the cell cycle pathway, as observed at 21% O_2 **(Figure 5.1G)**. 2210 DEGs were downregulated in 1% O_2 A CD8$^+$

T cells and included the phospholipase D and phosphatidylinositol signalling pathways in addition to pathways similarly seen in 21% O_2 **(Figure 5.1G)**.

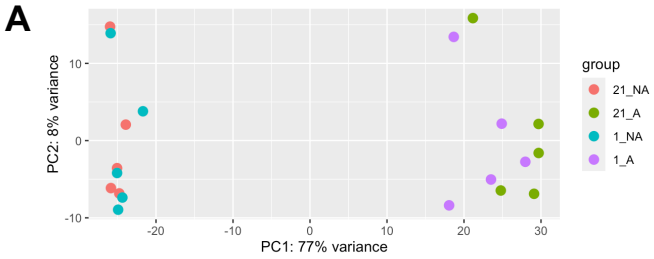
A
PC2: 8% variance
PC1: 77% variance
group
21_NA
21_A
1_NA
1_A

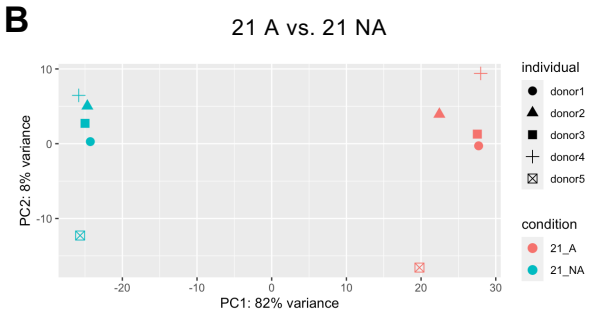
B
21 A vs. 21 NA
PC2: 8% variance
PC1: 82% variance
individual
donor1
donor2
donor3
donor4
donor5
condition
21_A
21_NA

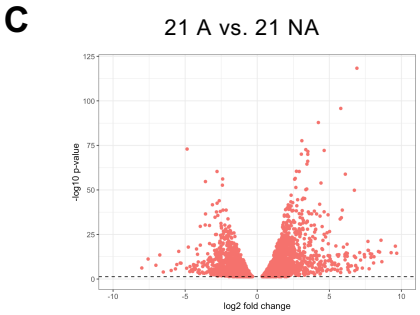
C
21 A vs. 21 NA
-log10 p-value
log2 fold change

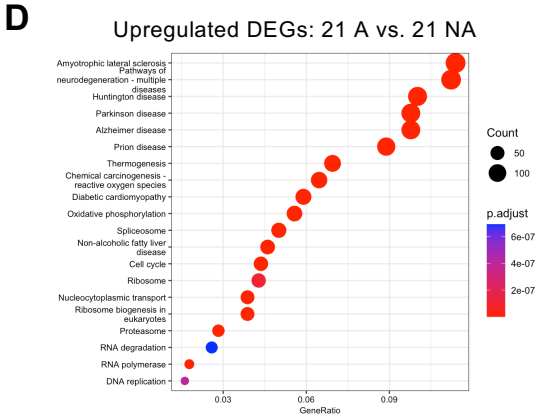
D
Upregulated DEGs: 21 A vs. 21 NA
Amyotrophic lateral sclerosis
Pathways of neurodegeneration - multiple diseases
Huntington disease
Parkinson disease
Alzheimer disease
Prion disease
Thermogenesis
Chemical carcinogenesis - reactive oxygen species
Diabetic cardiomyopathy
Oxidative phosphorylation
Spliceosome
Non-alcoholic fatty liver disease
Cell cycle
Ribosome
Nucleocytoplasmic transport
Ribosome biogenesis in eukaryotes
Proteasome
RNA degradation
RNA polymerase
DNA replication
GeneRatio
Count
p.adjust

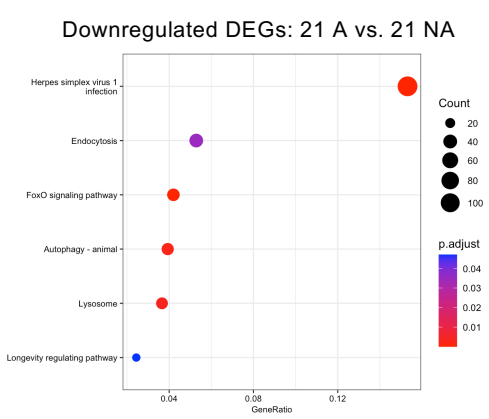
Downregulated DEGs: 21 A vs. 21 NA
Herpes simplex virus 1 infection
Endocytosis
FoxO signaling pathway
Autophagy - animal
Lysosome
Longevity regulating pathway
GeneRatio
Count
p.adjust

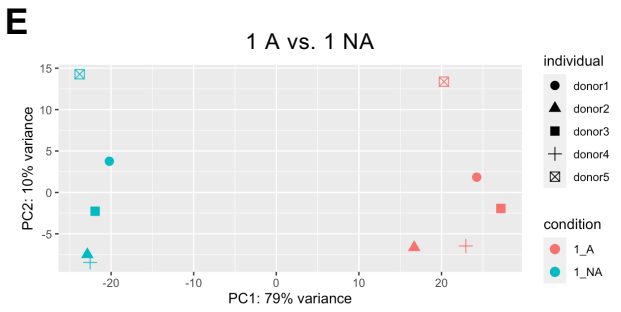
E
1 A vs. 1 NA
PC2: 10% variance
PC1: 79% variance
individual
donor1
donor2
donor3
donor4
donor5
condition
1_A
1_NA

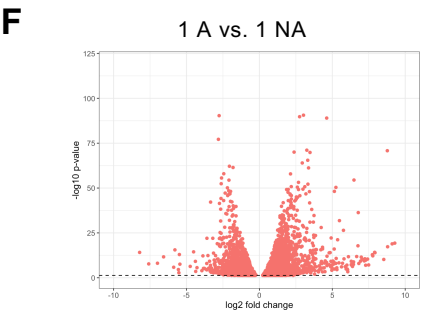
F
1 A vs. 1 NA
-log10 p-value
log2 fold change

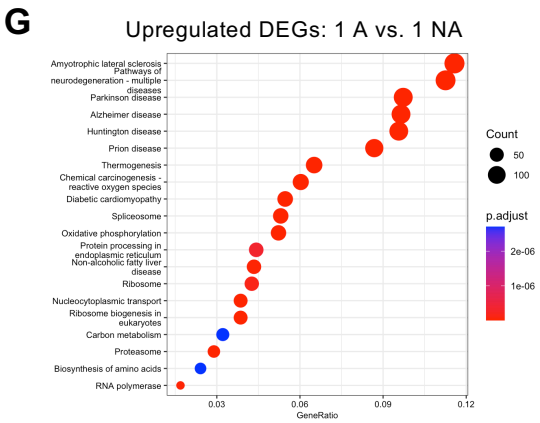
G
Upregulated DEGs: 1 A vs. 1 NA
Amyotrophic lateral sclerosis
Pathways of neurodegeneration - multiple diseases
Parkinson disease
Alzheimer disease
Huntington disease
Prion disease
Thermogenesis
Chemical carcinogenesis - reactive oxygen species
Diabetic cardiomyopathy
Spliceosome
Oxidative phosphorylation
Protein processing in endoplasmic reticulum
Non-alcoholic fatty liver disease
Ribosome
Nucleocytoplasmic transport
Ribosome biogenesis in eukaryotes
Carbon metabolism
Proteasome
Biosynthesis of amino acids
RNA polymerase
GeneRatio
Count
p.adjust

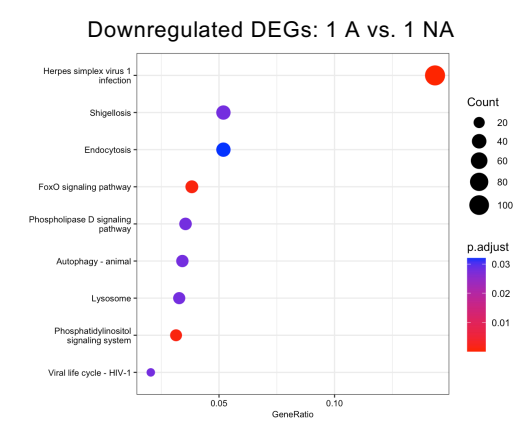
Downregulated DEGs: 1 A vs. 1 NA
Herpes simplex virus 1 infection
Shigellosis
Endocytosis
FoxO signaling pathway
Phospholipase D signaling pathway
Autophagy - animal
Lysosome
Phosphatidylinositol signaling system
Viral life cycle - HIV-1
GeneRatio
Count
p.adjust

Figure 5.1. Bulk RNA sequencing and DEGs of $CD8^+$ T cells activated and cultured in hypoxia vs. normoxia. Isolated $CD8^+$ T cells were pre-conditioned overnight in 21% or 1% O_2 conditions, left unstimulated or activated the following morning with anti-CD3/CD28, and cultured in the same O_2 conditions for 24 hours. RNA was extracted and bulk RNA sequencing performed. Analysis of the resultant data is shown. A) PCA plot of $CD8^+$ T cells unstimulated (NA) or activated (A) for 24 hours in 21% or 1% O_2 (21 NA, 21 A, 1NA, 1A), n = 5; B) PCA plot of $CD8^+$ T cells unstimulated (NA) or activated (A) for 24 hours in 21% O_2 (21 NA or 21 A), n = 5; C) Volcano plot of $CD8^+$ T cells NA or A for 24 hours in 21% O_2 (21 NA or 21 A), n = 5; D) Upregulated (left) and downregulated (right) differentially expressed genes (DEGs) in $CD8^+$ T NA or A for 24 hours in 21% O_2 (21 NA or 21 A), n = 5; E) PCA plot of $CD8^+$ T cells NA or A for 24 hours in 1% O_2 (1 NA or 1 A), n = 5; F) Volcano plot of $CD8^+$ T cells NA or A for 24 hours in 1% O_2 (1 NA or 1 A), n = 5; G) Upregulated (left) and downregulated (right) differentially expressed genes (DEGs) in $CD8^+$ T cells NA or A for 24 hours in 1% O_2 (1 NA or 1 A), n = 5.

5.3.2. $CD8^+$ T cells activated in hypoxia demonstrate upregulated and downregulated DEGs compared to those activated in normoxia

I next compared DEGs that were present when comparing NA vs. A $CD8^+$ T cells, at both 21% and 1% O_2, finding 3780 shared DEGs between NA and A $CD8^+$ T cells under both conditions **(Figure 5.2A)**. Conversely, 999 DEGs were unique to the 21% O_2 A vs. NA $CD8^+$ T cell comparison and 961 DEGs were unique to the 1% O_2 A vs. NA $CD8^+$ T cell comparison **(Figure 5.2A)**. Examples of genes that were unique to the 21% O_2 A vs. NA $CD8^+$ T cell comparison included those in the cell cycle pathway **(Figure 5.2B)**, as well as genes involved in fatty acid metabolism and degradation, amino acid metabolism, nucleotide excision repair, and cellular senescence. Examples of genes unique to the 1% O_2 A vs. NA $CD8^+$ T cell comparison included those in mitophagy pathways, and included BNIP3 **(Figure 5.2C)**, protein processing in ER genes, and the phosphatidylinositol signalling system **(Figure 5.1D and 5.1G)**.

Next, I compared DEGs between A $CD8^+$ T cells in 1% vs. 21% O_2 conditions which clustered well by O_2 tension **(Figure 5.2D)**. 232 DEGs were present between A $CD8^+$ T cells in 1% and A $CD8^+$ T cells in 21% O_2, which are shown in the volcano plot in

Figure 5.2E. 133 of these DEGs were upregulated in A $CD8^+$ T cells in 1% vs. 21% O_2, which included those in the HIF-1 signalling pathway, glycolysis and gluconeogenesis, carbon metabolism, biosynthesis of amino acids, and other metabolic pathways **(Figure 5.2F)**. Within these 133 upregulated genes in 1% O_2 several were HIF-1α targets, including BNIP3, DDIT4 and VEGFA. 99 of these DEGs were downregulated in A $CD8^+$ T cells in 1% vs. 21% O_2, and included those in the cell cycle, cellular senescence, and the p53 signalling pathway **(Figure 5.2F)**, consistent with the suppression of proliferation in $CD8^+$ T cells activated in 1% vs. 21% O_2 **(3. Chapter 1, Figure 3.6)**, and the lack of cell cycle genes in in the 1% O_2 A vs. NA comparison. Interestingly, IFNG was not a DEG between A $CD8^+$ T cells in 1% and 21% O_2, suggesting that it is not the transcription of the gene impaired in $CD8^+$ T cells in hypoxia and instead perhaps some translational or post-translational modification effect that causes the defect in IFN-γ production and release in hypoxia **(3. Chapter 1, Figure 3.3)**.

Finally, I compared NA $CD8^+$ T cells in 1% vs. 21% O_2 conditions which did not cluster well by O_2 tension but could be grouped into donors **(Figure 5.2G)**. There were only 46 DEGs between NA $CD8^+$ T cells in 1% vs. 21% O_2, of which all were up regulated in 1% O_2 **(Figure 5.2H)**. Pathways included the HIF-1 signalling pathway, glycolysis and gluconeogenesis, carbon metabolism, and biosynthesis of amino acids **(Figure 5.2H)**, as expected with hypoxic exposure. However, the lack of substantial differences between these two groups of samples indicates that hypoxia plays a more important role in determining $CD8^+$ T cell transcriptional profiles upon activation than at rest.

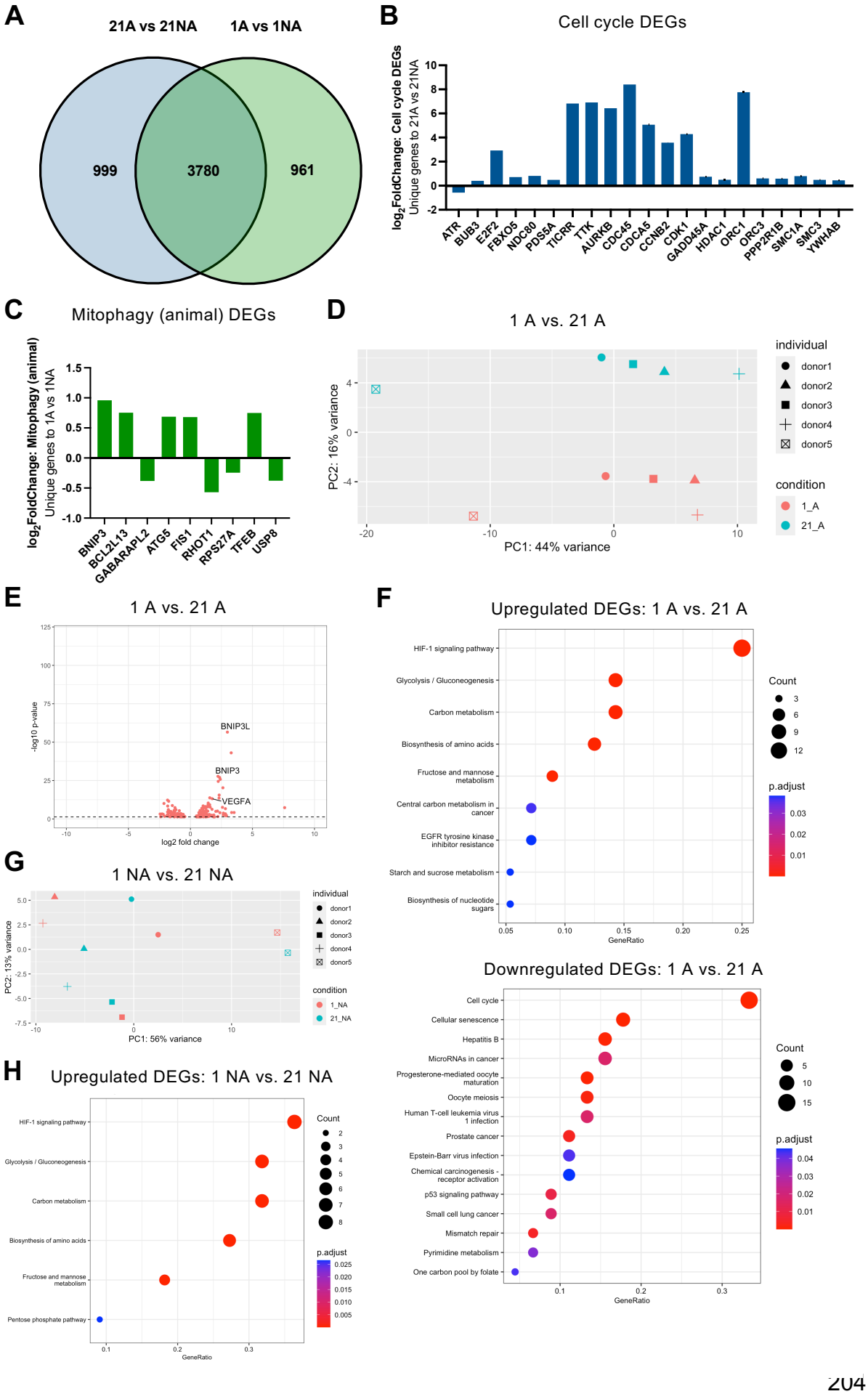
A
21A vs 21NA
1A vs 1NA
999
3780
961
B
Cell cycle DEGs
log2FoldChange: Cell cycle DEGs
Unique genes to 21A vs 21NA
ATR
BUB3
E2F2
FBXO5
NDC80
PDS5A
TICRR
TTK
AURKB
CDC45
CDCA5
CCNB2
CDK1
GADD45A
HDAC1
ORC1
ORC3
PPP2R1B
SMC1A
SMC3
YWHAB
C
Mitophagy (animal) DEGs
log2FoldChange: Mitophagy (animal)
Unique genes to 1A vs 1NA
BNIP3
BCL2L13
GABARAPL2
ATG5
FIS1
RHOT1
RPS27A
TFEB
USP8
D
1 A vs. 21 A
PC2: 16% variance
PC1: 44% variance
individual
donor1
donor2
donor3
donor4
donor5
condition
1_A
21_A
E
1 A vs. 21 A
-log10 p-value
log2 fold change
BNIP3L
BNIP3
VEGFA
F
Upregulated DEGs: 1 A vs. 21 A
HIF-1 signaling pathway
Glycolysis / Gluconeogenesis
Carbon metabolism
Biosynthesis of amino acids
Fructose and mannose metabolism
Central carbon metabolism in cancer
EGFR tyrosine kinase inhibitor resistance
Starch and sucrose metabolism
Biosynthesis of nucleotide sugars
GeneRatio
Count
p.adjust
Downregulated DEGs: 1 A vs. 21 A
Cell cycle
Cellular senescence
Hepatitis B
MicroRNAs in cancer
Progesterone-mediated oocyte maturation
Oocyte meiosis
Human T-cell leukemia virus 1 infection
Prostate cancer
Epstein-Barr virus infection
Chemical carcinogenesis - receptor activation
p53 signaling pathway
Small cell lung cancer
Mismatch repair
Pyrimidine metabolism
One carbon pool by folate
GeneRatio
Count
p.adjust
G
1 NA vs. 21 NA
PC2: 13% variance
PC1: 56% variance
individual
donor1
donor2
donor3
donor4
donor5
condition
1_NA
21_NA
H
Upregulated DEGs: 1 NA vs. 21 NA
HIF-1 signaling pathway
Glycolysis / Gluconeogenesis
Carbon metabolism
Biosynthesis of amino acids
Fructose and mannose metabolism
Pentose phosphate pathway
GeneRatio
Count
p.adjust

Figure 5.2. Bulk RNA sequencing and DEGs of $CD8^+$ T cells activated in hypoxia compared to those activated in normoxia. Isolated $CD8^+$ T cells were pre-conditioned overnight in 21% or 1% O_2 conditions, activated the following morning with anti-CD3/CD28, and cultured in the same O_2 conditions for 24 hours. RNA was extracted and bulk RNA sequencing performed. Analysis of the resultant data is shown. A) Diagram to illustrate the number of differentially expressed genes (DEGs) unique or overlapping between 21 A vs. 21 NA and 1 A vs. 1 NA conditions; B) Unique genes to 21 A vs. 21 NA in the cell cycle pathway, n = 5; C) Unique genes to 1 A vs. 1 NA in the mitophagy (animal) pathway, n = 5; D) PCA plot of $CD8^+$ T cells activated for 24 hours in 21% or 1% O_2 (21 A or 1 A), n = 5; E) Volcano plot of $CD8^+$ T cells activated for 24 hours in 21% or 1% O_2 (21 A or 1 A), n = 5; F) Upregulated (top) and downregulated (bottom) DEGs in $CD8^+$ T cells activated for 24 hours in 21% or 1% O_2 (21 A or 1 A), n = 5; G) PCA plot of $CD8^+$ T cells left unstimulated for 24 hours in 21% or 1% O_2 (21 NA or 1 NA), n = 5; H) Upregulated DEGs in $CD8^+$ T cells left unstimulated for 24 hours in 21% or 1% O_2 (21 NA or 1 NA), n = 5.

5.3.3. The AMPK pathway does not appear to be responsible for the $CD8^+$ T cell functional defects in hypoxia

The AMPK pathway is activated in response to a reduction in available energy or altered AMP/ATP rations, and cellular stress (Corton, Gillespie and Hardie, 1994; Hawley *et al.*, 2010; Mungai *et al.*, 2011). Since hypoxia inhibits mitochondrial OXPHOS and alters cellular AMP/ATP rations (induces energetic stress) (Corton, Gillespie and Hardie, 1994; Hawley *et al.*, 2010; Mungai *et al.*, 2011), I investigated the role of the AMPK pathway in $CD8^+$ T cells activated and cultured in hypoxia. Importantly, previous studies have shown an increase in the AMP/ATP ratio in mouse $CD8^+$ T cells exposed to hypoxia and treated with oligomycin to induce respiratory restriction (Saragovi *et al.*, 2020). $CD8^+$ T cells were isolated from human PBMC and cultured overnight in 21% or 1% O_2. The following morning cells were activated with anti-CD3/CD28 and cultured in 21% or 1% O2 for 48 hours with or without the AMPK inhibitor, Compound C (5 or 10 μM). Supernatants were collected for analysis by ELISA for IFN-γ and TNF-α concentration and rapamycin, a mTOR inhibitor, used as a positive control. Addition of 10 μM compound C tended to increase IFN-γ release in

$CD8^+$ T cells activated in 21% O_2 for 48 hours and reduce IFN-γ release in $CD8^+$ T cells activated in 1% O_2, albeit neither to a significant level **(Figure 5.3A)**. 5 μM did not produce the same effect on IFN-γ release in $CD8^+$ T cells activated in 21% O_2, but still reduced IFN-γ release in $CD8^+$ T cells activated in 1% O_2 **(Figure 5.3A)**. In contrast, 5 and 10 μM compound C did not impact TNF-α release in $CD8^+$ T cells activated in 21% O_2 for 48 hours compared to control but did appear to non-significantly reduce TNF-α release in $CD8^+$ T cells activated in 1% O_2 **(Figure 5.3A)**. Rapamycin reduced release of IFN-γ and TNF-α $CD8^+$ T cells activated in 21% and 1% O_2 as expected **(Figure 5.3A)**. Overall, AMPK inhibition may impact the release of cytokines in normoxia but does not rescue the functional defect on IFN-γ release observed in hypoxia. Therefore, the AMPK energetic stress pathway does not appear to play a key role in the defect of IFN-γ release in $CD8^+$ T cells activated in hypoxia. Importantly, compound C has been shown to have several off-target effects aside from AMPK inhibition (Saito *et al.*, 2012), thus conclusions from these data should be made cautiously.

5.3.4. A potential mechanism may exist to inhibit mTOR via a BNIP3/Rheb interaction in $CD8^+$ T cells activated in hypoxia

To further explain the defect of mTOR signalling in hypoxia I interrogated potential drivers of mTOR suppression in hypoxia. The HIF-1α target gene, REDD1 or DDIT4 has previously been shown to be responsible for the suppression of mTOR in hypoxia (Vadysirisack and Ellisen, 2012) and was a significantly upregulated DEG in activated $CD8^+$ T cells in 1% vs. 21% O_2 **(Figure 5.2)**. Therefore, I measured REDD1/DDIT4 protein abundance in NA or A $CD8^+$ T cells in 21% or 1% O_2 by flow cytometry. Despite the differences in gene expression, this analysis indicated that REDD1/DDIT4 protein

levels were not substantially or consistently increased in $CD8^+$ T cells activated in 1% compared to 21% O_2 **(Figure 5.3B)**, suggesting it unlikely to be responsible for the suppression of mTOR observed.

BNIP3 was also highlighted as a gene of interest and a significantly upregulated DEG in activated $CD8^+$ T cells in 1% vs. 21% O_2 **(Figure 5.2)**. HIF-1α dependent upregulation of BNIP3 in hypoxia has been reported to mediate mTOR suppression by interacting with and degrading Rheb (Li *et al.*, 2007). Rheb, a GTP binding protein, localises to the lysosomal membrane to stimulate the kinase activity of mTOR via indirect and direct mechanisms (Li *et al.*, 2007). Of note, one direct mechanism described requires the presence of extracellular amino acids, particularly leucine, to contribute to amino acid-dependent mTOR activation (Long *et al.*, 2005; Groenewoud and Zwartkruis, 2013). Exposure to 1% O_2 of NA $CD8^+$ T cells resulted in a trend for BNIP3 expression to increase, whilst exposure to 1% O_2 of A $CD8^+$ T cells significantly increased BNIP3 protein expression compared to 21% O_2 **(Figure 5.3C)**. On western blot, BNIP3 protein expression increased in 1% vs. 21% O_2 with the addition of a HIF-1α-inducer (Desferrioxamine, DFO) **(Figure 5.3D)**. This finding may suggest BNIP3 upregulation is HIF-1α dependent, however, the inhibition of HIF-1α and subsequent downregulation of BNIP3 would be required to confirm this. In agreement with the reported BNIP3-dependent Rheb degradation, expression of Rheb in A $CD8^+$ T cells in 1% O_2 was reciprocally decreased compared to 21% O_2 **(Figure 5.3E)**. Optimisation was required for this staining, since the anti-mouse secondary antibody produced a large background signal, even when used alone without primary antibody, potentially due to interaction with murine elements on positive selection magnetic beads or

CD3/CD28 activation solution. Blocking with mouse serum was attempted but was not successful, thus a ratio of the secondary antibody signal alone to the sample MFI is presented to minimise variations in background secondary signal **(Figure 5.3E)**. In future experiments **('6. Results Chapter 4')**, the Rheb primary antibody was conjugated to a PE-Cy7 fluorophore to remove the need to stain with an anti-mouse secondary antibody.

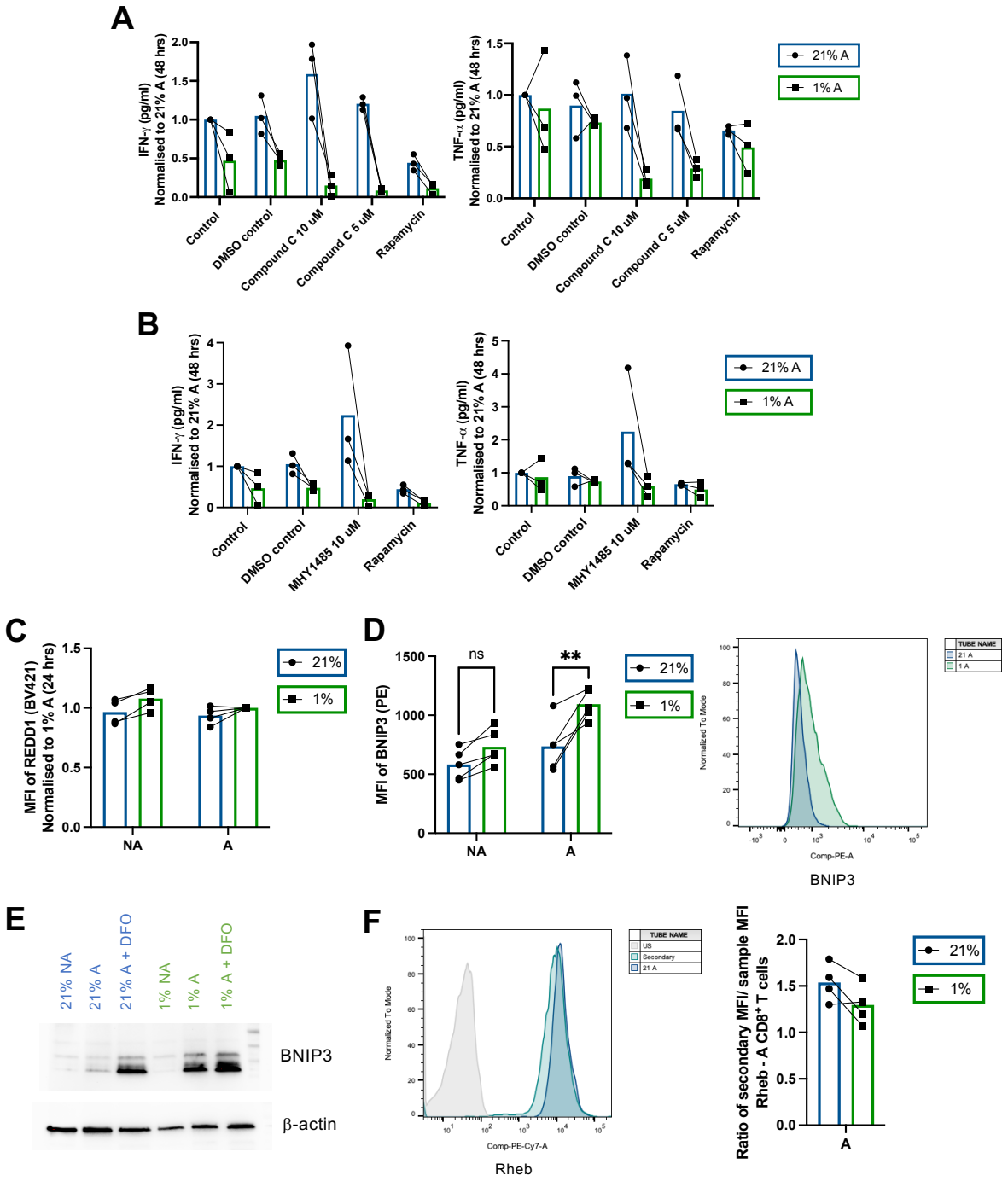

Figure 5.3. Exploration of potential mechanisms driving the suppression of mTOR in $CD8^+$ T cells activated in hypoxia. Isolated $CD8^+$ T cells were pre-conditioned overnight in 21% or 1% O_2 conditions, activated the following morning with anti-CD3/CD28, and cultured in the same O_2 conditions for the time point indicated. A) $CD8^+$ T cells were activated in 21% or 1% O_2 for 48 hours +/- metabolic modulators (Compound C (AMPK inhibition), and rapamycin as positive control) and ELISAs performed on the supernatants of cultured cells, IFN-γ and TNF-α concentrations shown, n = 3, normalised to 21% A; B) $CD8^+$ T cells were activated in 21% or 1% O_2 for 24 hours and stained for REDD1 (DDIT4, BV421), n = 4, normalised to 1% A; C) $CD8^+$ T cells were activated in 21% or 1% O_2 for 24 hours and stained for BNIP3 (PE), shown is MFI, n = 5, and a representative histogram of 21 A and 1 A

BNIP3 expression; D) Western blot of BNIP3 protein expression in $CD8^+$ T cells activated in 21% or 1% O_2 for 24 hours +/- DFO (HIF inducer), blot representative n = 1; E) $CD8^+$ T cells were activated in 21% or 1% O_2 for 24 hours and stained for Rheb, shown is example histogram of 21 A sample, secondary alone and US control, and ratio of secondary alone MFI / sample MFI in activated (A) samples, n = 4. Blue bars = 21% O_2; Green bars = 1% O_2. Data analysed by (A, B, C) Multiple Mann-Whitney tests with two-stage linear step-up procedure of Benjamin, Krieger and Yekutieli post-hoc test, (D) Ordinary two-way ANOVA with Sidak's multiple comparisons post-hoc test, with a single pooled variance, (F) Wilcoxon matched-pairs signed rank test. * $p < 0.05$, ** $p < 0.005$, *** $p < 0.005$, or p values shown; ns = non-significant or 'blank', $p > 0.05$.

Since abundance of Rheb was consistently decreased in $CD8^+$ T cells activated under hypoxia, I next investigated capacity for amino acid-dependent mTOR activation, which can be Rheb dependent (Long *et al.*, 2005; Groenewoud and Zwartkruis, 2013). Removal of leucine from culture inhibits mTOR activation and the binding of Rheb to mTOR (Long *et al.*, 2005), therefore, leucine was used as the amino acid for the following assay. To do so, $CD8^+$ T cells were activated in 21% or 1% O_2 for 24 hours following pre-conditioning then serum-starved for 4 hours prior to exposure to 10 mM leucine for 30 minutes where indicated. Phospho- and total-p70S6K were stained for to measure the activity of mTOR. **Figure 5.4A** represents a flow cytometry histogram example of phospho-p70S6K staining in A $CD8^+$ T cells with or without the addition of leucine in 21% or 1% O_2. The abundance of phospho- vs. total- p70S6K increased with leucine addition in 21% O_2 **(Figure 5.4B)**, but this did not increase in 1% O_2 **(Figure 5.4B and 5.4C)**. These experiments confirm impaired amino-acid dependent mTOR activation of $CD8^+$ T cells activated in hypoxia.

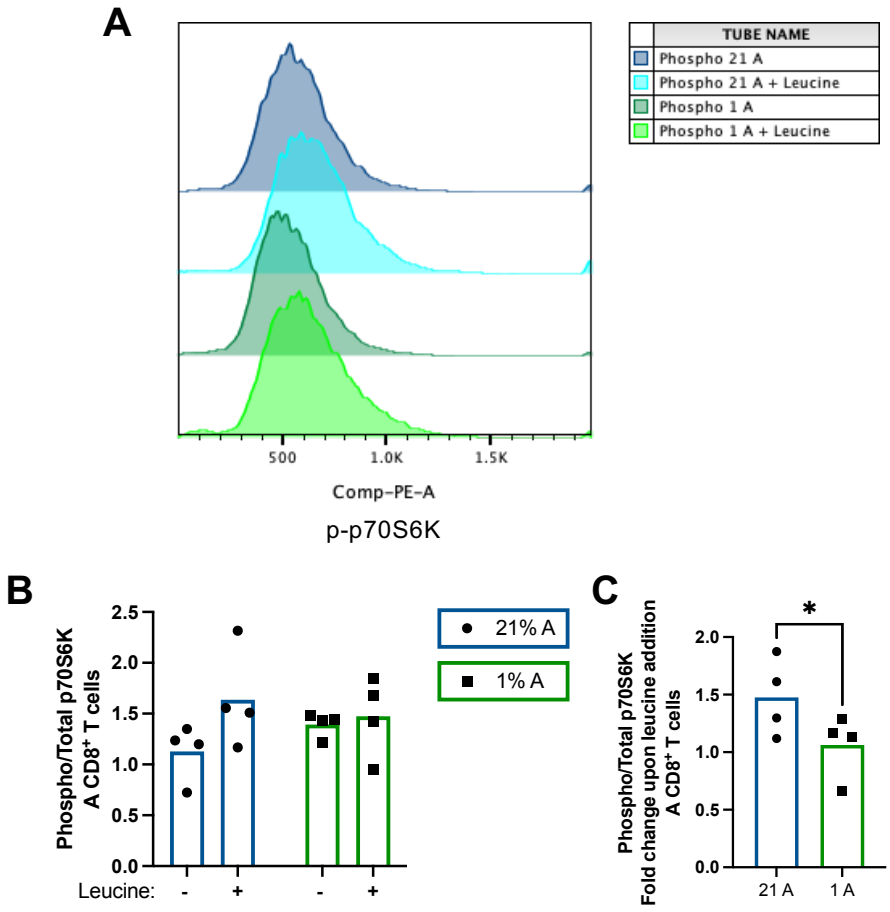

Figure 5.4. Capacity of amino acid-dependent mTOR activation in $CD8^+$ T cells activated in hypoxia vs. normoxia. Isolated $CD8^+$ T cells were pre-conditioned overnight in 21% or 1% O_2 conditions, activated the following morning with anti-CD3/CD28 for 24 hours, serum starved for 4 hours then provided 10 mM leucine where indicated for 30 minutes, prior to measurement of phospho- and total- p70S6K. A) Representative flow cytometry histograms of phospho-p70S6K in A $CD8^+$ T cells +/- leucine 10 mM in 21% or 1% O_2, n = 1; B) Ratio of phospho- to total p70S6K in A $CD8^+$ T cells +/- leucine 10 mM in 21% or 1% O_2, n = 4; C) Change of the ratio of phospho- to total p70S6K in A $CD8^+$ T cells upon leucine addition in in 21% or 1% O_2, n = 4. Blue bars = 21% O_2; Green bars = 1% O_2. Data analysed by (B) repeated measures two-way ANOVA with Holm-Sidak's multiple comparisons post-hoc test, with a single pooled variance, (C) paired t-test. * $p < 0.05$, ** $p < 0.005$, *** $p < 0.005$, or p values shown; ns = non-significant or 'blank', $p > 0.05$.

5.3.5. CRISPR knock out of BNIP3 in primary human $CD8^+$ T cells did not appear to successfully rescue mTOR suppression in hypoxia

My data so far indicate that BNIP3 is upregulated in activated $CD8^+$ T cells under hypoxia, alongside a reciprocal decrease in abundance in its interaction partner Rheb. This may have implications for mTOR activity and associated $CD8^+$ T cell metabolism and function, since Rheb is required for amino acid-dependent mTOR activation which does not occur in hypoxic $CD8^+$ T cells. To further explore whether this mechanism could explain the observed decreases in $CD8^+$ T cell function in hypoxia, a CRISPR-Cas9 system was employed to knock-out BNIP3 expression in primary human $CD8^+$ T cells. $CD8^+$ T cells were isolated from human PBMC and rested for 48 hours in IL-7 and IL-15 in 21% O_2 before transfection with either a negative control (-ve C) or BNIP3 knockout (KO) duplex RNA and a GFP-tagged Cas9 nuclease by electroporation. After transfection, cells were rested overnight in 21% O_2 prior to activation with anti-CD3/CD28 and culture in 21% or 1% O_2 for 72 hours. **Figure 5.5** provides a schematic of the method used for CRISPR Cas9-knockout of BNIP3 in primary human $CD8^+$ T cells and investigation in hypoxia and normoxia.

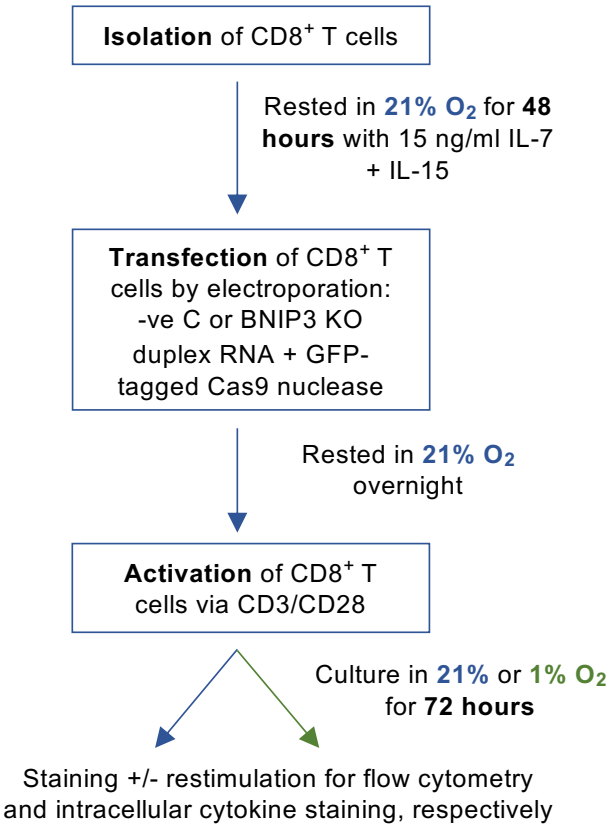

Figure 5.5. Schematic of CRISPR-Cas9 knockout (KO) of BNIP3 in human $CD8^+$ T cells. Isolated $CD8^+$ T cells were rested in 21% O_2 for 48 hours in 50 ng/ml IL-7 and IL-15 before transfection with a negative control (-ve C) or KO duplex RNA and a GFP Cas9 nuclease. Cells were rested overnight before a media change and activation with anti-CD3/CD28 the following morning. Transfected activated $CD8^+$ T cells were cultured in 21% or 1% O_2 for 72 hours prior to staining or restimulation as indicated.

Following the culture period, transfected activated $CD8^+$ T cells were stained for viability. By fixing with 2% paraformaldehyde (**Methods**), instead of FoxP3 fixation/permeabilisation solution, the GFP signal was retained in cells. As expected, a greater frequency of transfected (either with the -ve C or KO duplex RNA) $CD8^+$ T cells were dead compared to cells which had not been electroporated for transfection **(Figure 5.6A)**. Since the Cas9 nuclease was tagged with GFP, I could use the GFP signal to determine which $CD8^+$ T cells had been transfected during electroporation. **Figure 5.6B** provides an example of GFP staining in a KO $CD8^+$ T cell sample compared to one which had not been electroporated for transfection. Next, I gated on GFP^+ cells and compared these to GFP^- cells to investigate the difference between cells that had been transfected or not. Interestingly, $CD8^+$ T cells transfected with the -ve C duplex RNA had a reduction in BNIP3 MFI in 21% O_2 conditions in the GFP^+ vs. the GFP^- population **(Figure 5.6C)**. Therefore, the transfection process itself appears to be impacting the cells, making it challenging to draw conclusions from this data. However, comparison of GFP^+ vs. GFP^- populations of cells only provided with the BNIP3 KO duplex RNA (i.e., without also comparing to -ve C treated cells) does indicate consistent decrease in BNIP3 MFI in GFP^+ cells in both 21% and 1% O_2 **(Figure 5.6C and 5.6D)**, suggesting some successful KO of BNIP3.

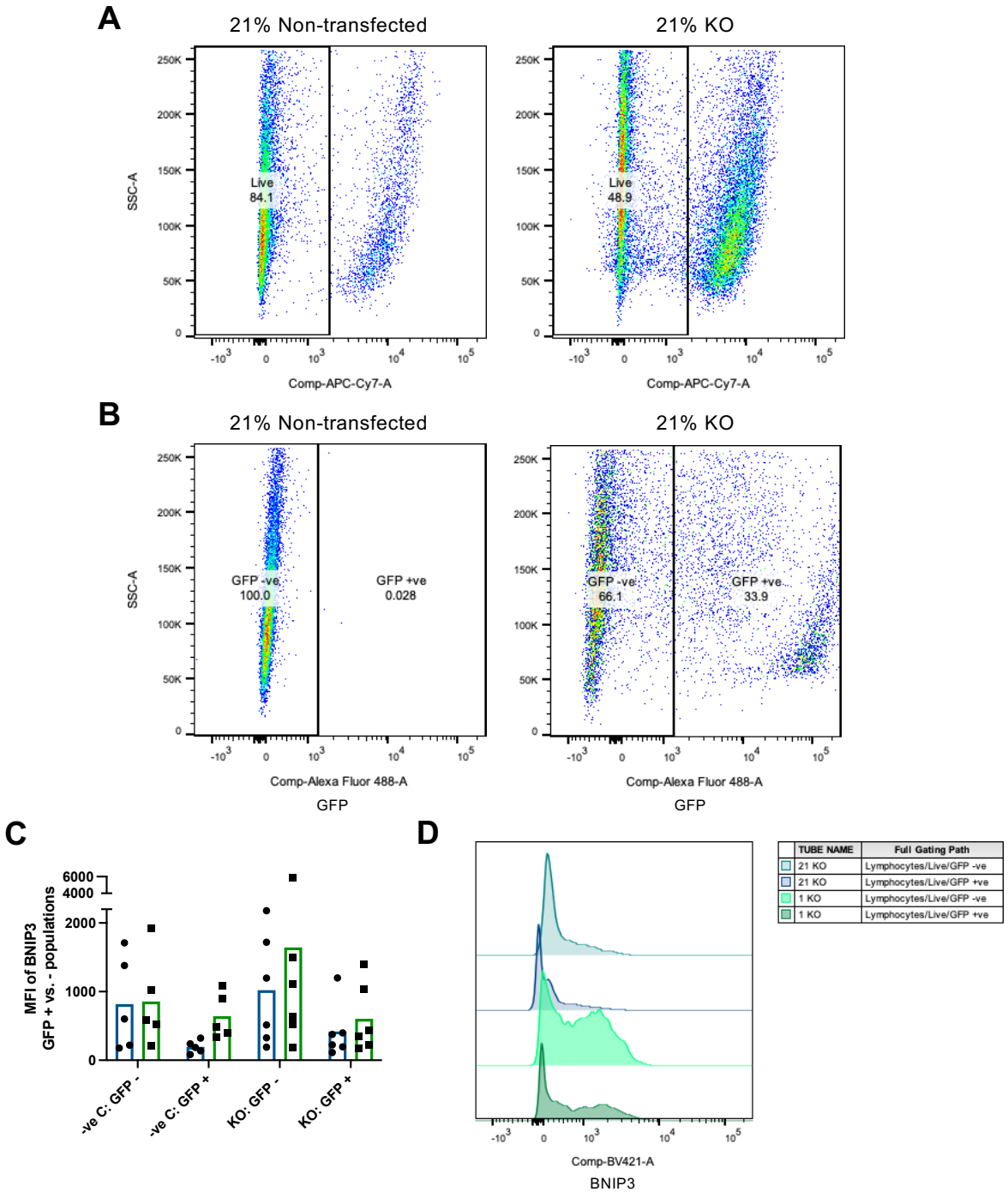

Figure 5.6. CRISPR-Cas9 knockout (KO) of BNIP3 in human CD8$^+$ T cells and analysis for BNIP3 expression. Isolated CD8$^+$ T cells were rested in 21% O_2 for 48 hours in 50 ng/ml IL-7 and IL-15 before transfection with a negative control (-ve C) or KO duplex RNA and a GFP Cas9 nuclease. Cells were rested overnight before a media change and activation with anti-CD3/CD28 the following morning. Transfected activated CD8$^+$ T cells were cultured in 21% or 1% O_2 for 72 hours prior to staining or restimulation as indicated. A) Example of APC-Cy7 (live cells) staining in 21% non-transfected and KO samples, n = 1; B) Example of GFP staining (transfection efficiency) in 21% non-transfected and KO samples, n = 1; C) MFI of BNIP3 in -ve C and KO populations comparing GFP + and - cells in 21% A and 1% A CD8$^+$ T cells, n = 6; D) Example histogram overlay of BNIP3 staining

in 21% and 1% KO samples comparing GFP + and - populations, n = 1. Blue bars = 21% O_2; Green bars = 1% O_2. Data analysed by (C left) multiple unpaired t-tests with two-stage linear step-up procedure of Benjamin, Krieger and Yekutieli post-hoc test, (C right) ordinary two-way ANOVA with Sidak's multiple comparisons post-hoc test, with a single pooled variance. * $p < 0.05$, ** $p < 0.005$, *** $p < 0.005$, or p values shown; ns = non-significant or 'blank', $p > 0.05$.

According to the hypothesis discussed above, HIF-1α-dependent upregulation of BNIP3 in hypoxia drives the suppression of mTOR observed previously ('**4. Results Chapter 2**'). Therefore, KO of BNIP3 should rescue the phosphorylation of mTOR in hypoxia. Interestingly, as with BNIP3, in the -ve C samples, a decrease in the MFI of phospho-mTOR was observed in the GFP^+ vs. GFP^- cells. Addition of the KO duplex RNA similarly reduced the MFI of phospho-mTOR in both GFP^+ and GFP^- cells in 21% O_2, without changing in 1% O_2 **(Figure 5.7A)**. Moreover, the consistent mTOR suppression of $CD8^+$ T cells in 1% O_2 observed in **4. Results Chapter 2**' was not reproduced in the transfected cells, suggesting again this may be altered by electroporation **(Figure 5.7A)**. Similar conflicting results were observed in CD25 and CD69 expression as measures of activation, as well as the MFI of c-Myc as a marker of metabolic reprogramming **(Figures 5.7B and 5.7C)**. Following culture for 72 hours in 21% and 1% O_2, $CD8^+$ T cells were restimulated for 4 hours with anti-CD3/CD28 alongside brefeldin A for intracellular cytokine staining. As with surface markers, the previously observed reduction in IFN-γ production in $CD8^+$ T cells in hypoxia ('**3. Results Chapter 1**') was not replicated here and BNIP3 KO in GFP^+ cells had no striking difference on IFN-γ and TNF-α production **(Figures 5.7D and 5.7E)**. Overall, no consistent conclusions can be drawn from this data as transfection alone appears to significantly impact cell function such that baseline observations are no longer reproduced.

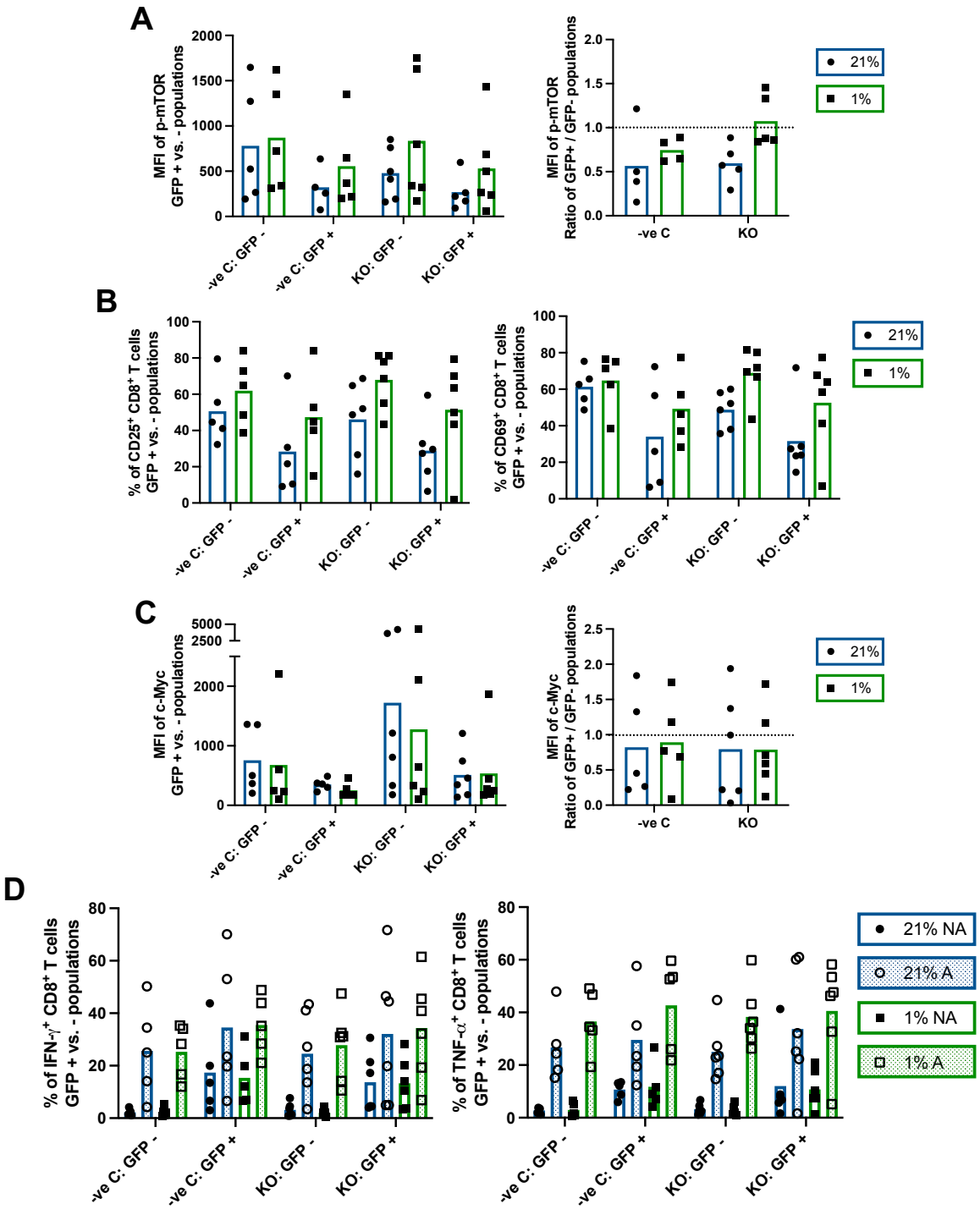

Figure 5.7. CRISPR-Cas9 knockout (KO) of BNIP3 in human CD8$^+$ T cells and analysis for expression of phosho- (p-) mTOR, c-Myc, activation status and cytokine production in hypoxia vs. normoxia. Isolated CD8$^+$ T cells were rested in 21% O_2 for 48 hours in 50 ng/ml IL-7 and IL-15 before transfection with a negative control (-ve C) or KO duplex RNA and a GFP Cas9 nuclease. Cells were rested overnight before a media change and activation with anti-CD3/CD28 the following morning. Transfected activated CD8$^+$ T cells were cultured in 21% or 1% O_2 for 72 hours prior to staining or restimulation as indicated. A) MFI of p-mTOR in -ve C and KO comparing GFP + and - cells in 21% A and 1% A CD8$^+$ T cells, n = 6, and MFI of p-mTOR in -ve C and KO samples as

a ratio of GFP+ / GFP- populations in 21% A and 1% A $CD8^+$ T cells, n = 6; C) Percentage of $CD25^+$ or $CD69^+$ live $CD8^+$ T cells in -ve C and KO comparing GFP + and - cells in 21% A and 1% A shown, n = 6; C) MFI of c-Myc in -ve C and KO comparing GFP + and - cells in 21% A and 1% A $CD8^+$ T cells, n = 6, and MFI of c-Myc in -ve C and KO samples as a ratio of GFP+ / GFP- populations in 21% A and 1% A $CD8^+$ T cells, n = 6; D) Percentage of IFN-γ^+ or TNF-α^+ live $CD8^+$ T cells in -ve C and KO comparing GFP + and - cells in 21% and 1% O_2, NA or A, addition of brefeldin A for stimulation, n = 6; E) Percentage of IFN-γ^+ or TNF-α^+ live $CD8^+$ T cells in KO populations comparing GFP + and - cells in 21% A and 1% A $CD8^+$ T cells, n = 6. Blue bars = 21% O_2; Green bars = 1% O_2. Data analysed by (A left, B, C left) multiple unpaired t-tests with two-stage linear step-up procedure of Benjamin, Krieger and Yekutieli post-hoc test. * $p < 0.05$, ** $p < 0.005$, *** $p < 0.005$, or p values shown; ns = non-significant or 'blank', $p > 0.05$.

5.4. Discussion

Upon stimulation, $CD8^+$ T cells up- and down-regulate many genes to coordinate effective T cell activation and responses. Whilst $CD8^+$ T cells activated in 21% and 1% O_2 had broad changes in gene expression compared to resting cells, bulk RNA-sequencing revealed key differences in genes expressed in each condition **(Figures 5.1 and 5.2)**. Interestingly, activated (A) $CD8^+$ T cells clustered well by O_2 tension compared to non-activated (NA) $CD8^+$ T cells which did not, demonstrating it is the activation of $CD8^+$ T cells in hypoxia that drives differences **(Figures 5.1 and 5.2)**. One key example is the upregulation of cell cycle genes in $CD8^+$ T cells activated in 21% O_2, which was not present in the 1% O_2 dataset **(Figures 5.1 and 5.2)**. This result is consistent with the defect I observe in $CD8^+$ T cell proliferation when activated and cultured in 1% O_2 for 6 days compared to those in 21% O_2 ('**3. Results Chapter 1, Figure 3.6**') and with previous literature using a similar protocol (Caldwell *et al.*, 2001; Liu *et al.*, 2020). Various metabolic pathways were also unique to $CD8^+$ T cells activated in 21% O_2, including fatty acid metabolism and degradation, and amino acid metabolism **(Figures 5.1 and 5.2)**. These results suggest that further metabolic differences from an increase in glycolysis exist in hypoxic activated cells, in agreement with data presented in '**4. Results Chapter 2**'.

Importantly, many genes upregulated in activated $CD8^+$ T cells in 1% compared to 21% O_2 were HIF-target genes, confirming the stabilisation of HIF-1α and the induction of its effects in my culture system **(Figure 5.2)**. These included genes involved in glycolysis and gluconeogenesis (enolase 1 (ENO1), glyceraldehyde-3-phosphate dehydrogenase (GAPDH), hexokinase 2 (HK2), phosphoglycerate kinase 1 (PGK1),

and triosephosphate isomerase 1 (TPI1)) (Hong, Lee and Kim, 2004) and the HIF-signalling pathway (EGLN1, PLCG1, PDK1, signal transducer and activator of transcription 3 (STAT3), VEGFA), among others **(Figure 5.2)**. Given the vast regulation of cellular function and metabolism driven by HIF-1α, it should be considered that the functional defects in A $CD8^+$ T cells in hypoxia also originate from HIF-1α. However, previous literature suggests that hypoxia-induced functional defects on T cells may be independent of HIF-1α stabilisation (Scharping *et al.*, 2021). Other pathways upregulated in 1% compared to 21% O_2 were metabolic systems, including the biosynthesis of amino acids and fructose and mannose metabolism suggesting hypoxia drives vast metabolic changes in A $CD8^+$ T cells **(Figure 5.2)**.

I also considered target genes upregulated in A $CD8^+$ T cells in 1% O_2 in my bulk RNA-sequencing dataset that may be driving the suppression of mTOR. REDD1, otherwise known as DDIT4, was upregulated in 1% O_2 A $CD8^+$ T cells vs. 21% O_2 A $CD8^+$ T cells **(Figure 5.2)**, and has been shown to inhibit mTOR in hypoxia (Brugarolas *et al.*, 2004; Vadysirisack and Ellisen, 2012). However, the expression of REDD1 protein in A $CD8^+$ T cells in 1% O_2 was not consistently altered **(Figure 5.3)**. Another significantly upregulated gene in 1% O_2 A $CD8^+$ T cells vs. 21% O_2 A $CD8^+$ T cells was BNIP3 **(Figure 5.2)**. The HIF-1α dependent BNIP3 is usually recognised as an autophagy gene (Zhang and Ney, 2009), but has also been shown to direct suppression of mTOR in hypoxia by interacting with and degrading an activator of mTOR, Rheb (Li *et al.*, 2007). BNIP3 protein expression was significantly upregulated in $CD8^+$ T cells activated in hypoxia, dependent on HIF-1α, and Rheb expression was reciprocally

decreased **(Figure 5.3)**. Therefore, I hypothesised that this mechanism may be causing the mTOR suppression observed in hypoxia.

To investigate this mechanism further, I attempted to KO BNIP3 with CRISPR-Cas9 in primary human $CD8^+$ T cells. Whilst some success was achieved with the knockout of BNIP3, the electroporation process appeared to alter the function of $CD8^+$ T cells independently of BNIP3 knockout and usual hypoxic responses were not reproduced for T cell activation (CD25, CD69), function (IFN-γ) or mTOR signalling (p-p70S6K, c-Myc) **(Figures 5.5, 5.6 and 5.7)**. Therefore, no definitive conclusions can be drawn regarding the presence of the BNIP3/Rheb/mTOR mechanism in $CD8^+$ T cells in hypoxia and other methods of knockdown, for example small interfering RNA (siRNA) or lipofectamine transfection, should be tried to optimise these experiments further. In addition, a direct interaction between BNIP3 and Rheb, which has been demonstrated in other cell types (Li *et al.*, 2007), could be interrogated in $CD8^+$ T cells by immunoprecipitation experiments.

Another interesting observation from the RNA-sequencing data was that the calcium signalling pathway was upregulated in 1% compared to 21% O_2 **(Figure 5.2)**. Given I observed a suppression in calcium influx upon T cell activation in hypoxia ('**3. Results Chapter 1**'), this may reflect cellular adaptation to this (Bootman and Bultynck, 2020). The intricate cytosolic Ca^{2+} signalling pathways have also been linked to the induction of autophagy (Bootman *et al.*, 2018), a well described recycling system of cellular components (Parzych and Klionsky, 2014), which is consistent with the upregulation of BNIP3 expression in hypoxic activated $CD8^+$ T cells.

Despite the reported role of AMPK in the cellular response to energetic stress (Corton, Gillespie and Hardie, 1994; Hawley *et al.*, 2010; Mungai *et al.*, 2011), investigation of the role of the AMPK pathway in $CD8^+$ T cells in hypoxia revealed that AMPK inhibition did not rescue the functional defect on IFN-γ release observed in hypoxia, although it may impact the release of cytokines in normoxia **(Figure 5.3)**. Similarly, analysis of the phosphorylation of AMPK in mouse $CD8^+$ T cells activated in normoxia and cultured in normoxia or hypoxia for 5 or 18 hours and treated with oligomycin to induce respiratory restriction, suggested that AMPK signalling is not associated with the inhibition of T cell function seen with respiratory restriction during early T cell activation (Saragovi *et al.*, 2020). Importantly, compound C, the AMPK inhibitor used in this thesis, has been shown to have various off-target effects (Saito *et al.*, 2012). For example, the inhibitor has been shown to inhibit vascular endothelial growth factor type II receptor (VEGFR2) (Saito *et al.*, 2012), the activation of HIF-1α independently of AMPK (Emerling *et al.*, 2007), and various other kinases with comparable potencies (Bain *et al.*, 2007). Therefore, conclusions taken from these data should be made cautiously.

NFκB activity is also reported to be altered in hypoxia (D'Ignazio and Rocha, 2016). Since this plays a key role in T cell signalling and activity, I began to explore this pathway in my culture system but observed no difference in staining of IκB in activated $CD8^+$ T cells in hypoxia. Therefore, it is likely not NF-κB or AMPK driving functional effects observed in hypoxia. Previous literature has also reported on the immunosuppressive effects of the accumulation of adenosine in the TME and shown that hypoxia increases this accumulation (Bruzzese *et al.*, 2014; Ohta *et al.*, 2014). However, the inhibitory effects of hypoxia on T cell function have been shown to be

independent from adenosine production and transient, whilst adenosine immunosuppression of T cells is persistent (Ohta *et al.*, 2014). The relationship between hypoxia and adenosine immunosuppression is thought to be regulated through the NF-κB pathway (Bruzzese *et al.*, 2014).

Finally, GAPDH expression increased in A $CD8^+$ T cells in hypoxia **(Figure 5.2)**. GAPDH has been shown to bind to the AU-rich region of the 3' untranslated region of IFN-γ mRNA to directly regulate levels of translation and production of IFN-γ in T cells (Chang *et al.*, 2013). Therefore, post-translational mechanisms of control should be considered when assessing $CD8^+$ T cell function in hypoxia and further work should be conducted to confirm the existence of this mechanism.

5.5. Conclusion

I have begun to explore potential mechanisms driving suppression of $CD8^+$ T cell IFN-γ production and release, proliferation, and activation in hypoxia via an unbiased method of gene analysis and targeted exploration of specific target genes. However, this work is inconclusive and whilst hypotheses exist, further experimentation is required to confirm or deny the presence of particular mechanisms and their impact on activated $CD8^+$ T cell function in hypoxia. It is likely that several complex mechanisms exist to impact $CD8^+$ T cell function in hypoxia and comprehensive work is required to understand these completely.

6. Results Chapter 4

Translating our knowledge of $CD8^+$ T cell function and metabolism in hypoxia to multiple myeloma (MM)

6. Results Chapter 4: Translating our knowledge of CD8$^+$ T cell function and metabolism in hypoxia to multiple myeloma (MM)

6.1. Introduction

Multiple myeloma (MM) is a haematological cancer that arises from the clonal proliferation of plasma cells in the bone marrow (BM) (Cowan *et al.*, 2022). Whilst significant improvements have been made in the management of MM, it remains an incurable disease (Ravi *et al.*, 2018). Current and emerging therapeutic options rely on the effective functioning of the immune system, in particular CD8$^+$ T cells. These include immunomodulatory drugs (IMiDs), monoclonal antibodies, CAR-T cells and bispecific antibodies. However, it is well known that components of the immune system, including CD8$^+$ T cells, are dysfunctional in the TME (Gudgeon *et al.*, 2023). For example, we have previously shown that CD8$^+$ T cells present in the BM produce less IFN-γ, TNF-α, IL-2 and granzyme-B, than those in the PB of MM patients (Gudgeon *et al.*, 2023). Therefore, understanding how and why CD8$^+$ T cells are dysfunctional in the MM TME is crucial to improve patient outcomes to therapies.

Previous literature has confirmed the MM TME hypoxic, with increased HIF-1α protein staining in the BM of MM patients vs. healthy controls and greater pimonidazole staining in a murine model of MM (Asosingh *et al.*, 2005; Colla *et al.*, 2010). In this thesis, I have shown that hypoxia impairs the efficient activation, IFN-γ cytokine production and release, proliferation, and metabolic reprogramming upon stimulation, of CD8$^+$ T cells in hypoxia ('**3. Results Chapter 1**' and '**4. Results Chapter 2**'). Thus, I hypothesise that the hypoxia present in the MM TME may contribute to the observed CD8$^+$ T cell dysfunction and potentially limit responses to immune-directed therapies.

6.2. Aims

$CD8^+$ T cells present in the MM TME are dysfunctional, and the BM MM TME is known to be hypoxic. Therefore, I investigated the hypothesis that hypoxia present in the MM TME contributes to $CD8^+$ T cell dysfunction and may potentially limit response to immune-directed therapies. The aims for this chapter include:

1. To investigate the impact of hypoxia on $CD8^+$ T cell responses to myeloma cell-targeting bispecific antibodies
2. To phenotype $CD8^+$ T cells present in the BM and PB of MM patients
3. To explore the function of $CD8^+$ T cells present in the BM and PB of MM patients and mechanistic links to hypoxic exposure

6.3. Results

6.3.1. $CD8^+$ T cells activated with a CD3xBCMA bispecific antibody in hypoxia have impaired activation and cytokine production, but are sufficient in killing

To investigate the killing capacity of $CD8^+$ T cells in hypoxia in the therapeutic context of MM, I co-cultured human $CD8^+$ T cells with MM cell lines in the presence of a laboratory-grade CD3xBCMA bispecific antibody. The three MM cell lines utilised in these experiments were JJN3, AMO, and L363, which all express B cell maturation antigen (BCMA). Importantly, BCMA is also highly expressed by primary MM plasma cells (Bataille *et al.*, 2006). A diagram to show how these experiments work is shown in **Figure 6.1A** and a diagram of the experiment timeline is shown in **Figure 6.1B**. The addition of the CD3xBCMA bispecific antibody engages the MM plasma cells (cell lines) via BCMA and stimulates the $CD8^+$ T cells via CD3 to release perforin and granzyme B and kill the target plasma cell (cell lines) **(Figure 6.1A and 6.1B)**. The target cell lines are labelled with cell trace violet (CTV) prior to culture so they can be identified by flow cytometry (i.e., cells staining positive for CTV) and stained with a live/dead probe to determine the percentage killed by $CD8^+$ T cells **(Figure 6.1C)**. In a separate well, brefeldin A and monensin are added, in order to be able to stain the $CD8^+$ T cells for intracellular cytokines and CD107a degranulation, as performed in '**3. Results Chapter 1**' **(Figure 6.1A and 6.1B)**. Optimisation of methods for this protocol was conducted by Dr Nancy Gudgeon in our laboratory.

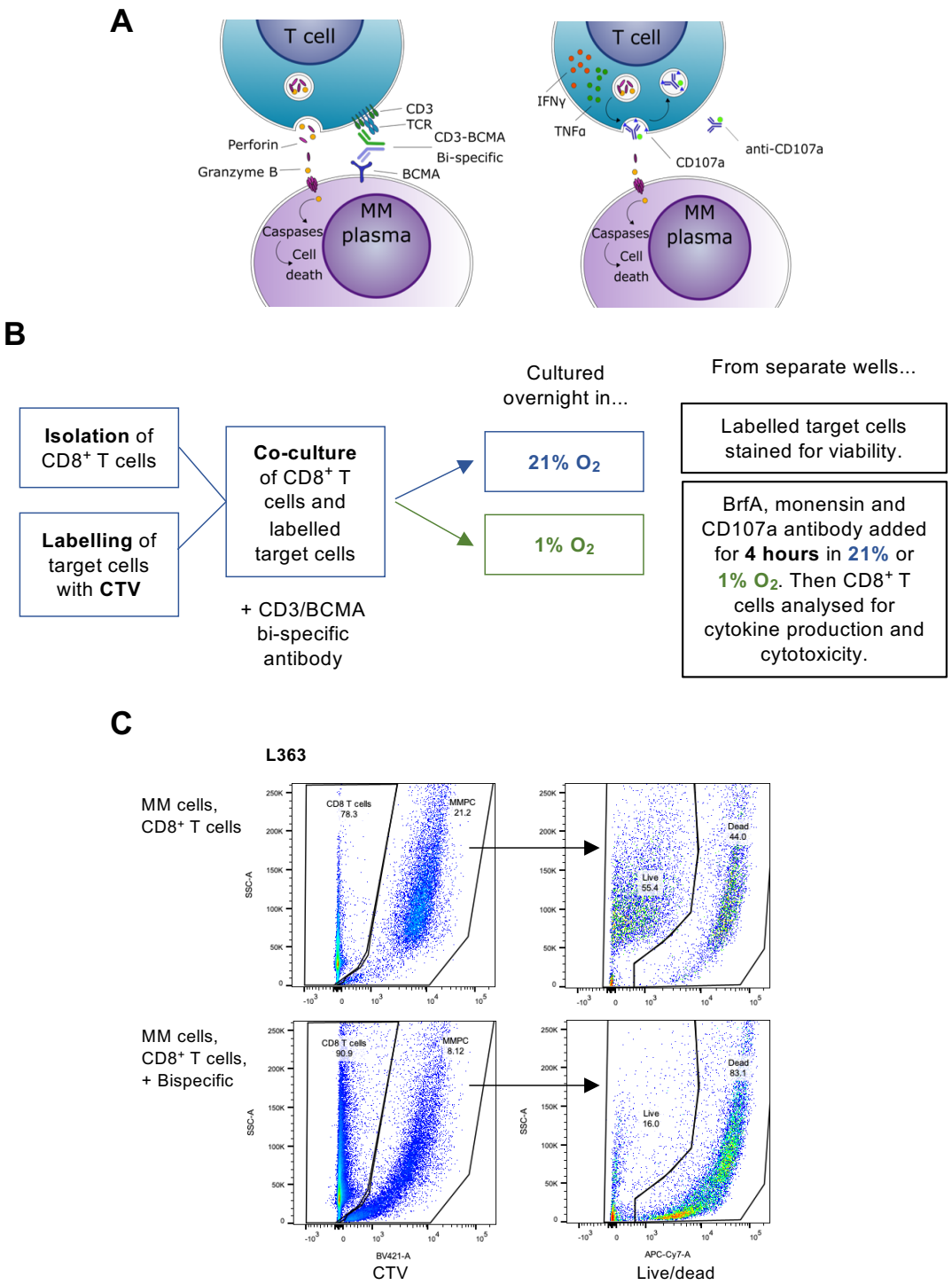

Figure 6.1. CD8+ T cell and MM cell line +/- CD3xBCMA bispecific antibody co-culture experiments to assess cytotoxicity and CD8+ T cell function in hypoxia vs. normoxia. A) Diagram to demonstrate how the CD8+ T cell and MM cell line +/- CD3xBCMA bispecific antibody co-culture experiments assess cytotoxicity and CD8+ T cell function. Diagram courtesy of Dr Nancy Gudgeon; B) Diagram of experiment set-up; C) Example dot plots to demonstrate how MM cell lines (MM plasma cells, MMPC) are labelled with CTV for identification by flow cytometry and killing capacity of CD8+ T cells assessed by live/dead staining of MMPC. Shown is example with and without addition of the CD3xBCMA bispecific antibody.

JJN3 has the highest expression of BCMA, followed by L363, and AMO has the lowest expression of BCMA **(Figure 6.2A)**. I cultured $CD8^+$ T cells with each target cell line in increasing effector : target cell ratios, with or without the presence of the CD3xBCMA bispecific antibody. Addition of the bispecific antibody increased the percentage of dead JJN3 target cells, which associated with effector : target cell ratios **(Figure 6.2B)**. Similarly, addition of the bispecific antibody tended to increase killing of AMO and L363 target cell lines by $CD8^+$ T cells **(Figures 6.2B)**, however the increase compared to control was less for AMO target cells, which may relate to their lower expression of BCMA **(Figure 6.2B)**. When tested under hypoxia, there was no difference in the amount of killing of JJN3, AMO and L363 target cells by $CD8^+$ T cells compared to 21% O_2 **(Figure 6.2B)**. These data are in agreement with those from previous experiments demonstrating little effect of hypoxia on $CD8^+$ T cell cytotoxic granule expression or degranulation when stimulated with anti-CD3/CD28 ('**3. Results Chapter 1, Figure 3.5**').

In accordance with the reduction of CD25 expression observed on $CD8^+$ T cells activated via CD3/CD28 in hypoxia ('**3. Results Chapter 1, Figure 3.1**'), $CD8^+$ T cells activated by a CD3xBCMA bispecific antibody and co-cultured with MM cell lines (JJN3, AMO, and L363) had significantly fewer $CD25^+$ $CD8^+$ T cells in 1% O_2 compared to those stimulated in 21% O_2 **(Figures 6.2C and 6.2D)**. There was no difference, or a slight increase, in the percentage of $CD69^+$ $CD8^+$ T cells in 1% vs 21% O_2 with bispecific antibody activation when co-cultured with JJN3, AMO or L363 MM cell lines **(Figures 6.2C and 6.2E)**. A significantly reduced percentage of $CD25^+$ $CD69^+$ $CD8^+$ T cells were present in 1% vs. 21% O_2 when co-cultured with AMO, but no difference

with JJN3 or L363 **(Figures 6.2C and 6.2F)**. HIF-1α drives CD69 expression and thus, it is an unreliable marker of T cell activation in hypoxia ('**3. Results Chapter 1, Figure 3.1**'), the reduction in percentage of $CD25^+$ $CD8^+$ T cells in hypoxia suggests impaired activation of $CD8^+$ T cells stimulated via a bispecific antibody.

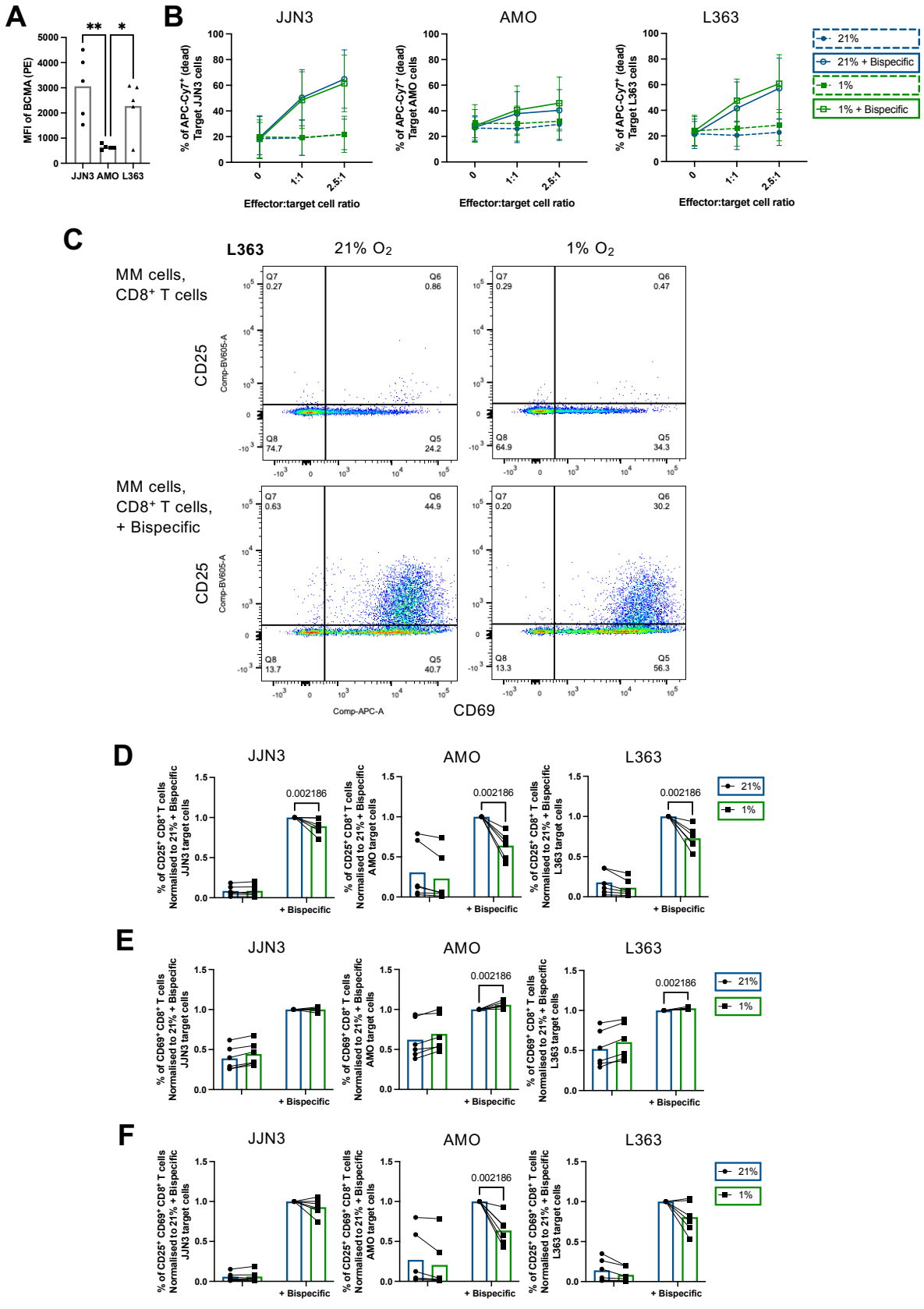
A
B
C
D
E
F
JJN3
AMO
L363
21%
21% + Bispecific
1%
1% + Bispecific
Effector:target cell ratio
MM cells, CD8+ T cells
MM cells, CD8+ T cells, + Bispecific
21% O2
1% O2
CD25
CD69
0.002186
+ Bispecific

Figure 6.2. $CD8^+$ T cell and MM cell line +/- CD3xBCMA bispecific antibody co-culture experiments and assessment of killing capacity and $CD8^+$ T cell activation status in hypoxia vs. normoxia. A) MFI of BCMA expression in three MM cell lines: JJN3, AMO and L363, n = 5; B) Percentage of APC-$Cy7^+$ (Dead) target JJN3, AMO and L363 cells, n = 5, median and SD bars shown; C) Example histograms of CD25 (BV605) and CD69 (APC) staining in $CD8^+$ T cells cultured with MM target cell lines (L363) +/- CD3xBCMA bispecific antibody in 21% or 1% O_2, n = 1; D) Percentage of $CD25^+$ $CD8^+$ T cells when cultured with MM target cell lines (JJN3, AMO, or L363) +/- CD3xBCMA bispecific antibody, n = 6, normalised to 21% + Bispecific; F) Percentage of $CD69^+$ $CD8^+$ T cells when cultured with MM target cell lines (JJN3, AMO, or L363) +/- CD3xBCMA bispecific antibody, n = 6, normalised to 21% + Bispecific; G) Percentage of $CD25^+$ $CD69^+$ $CD8^+$ T cells when cultured with MM target cell lines (JJN3, AMO, or L363) +/- CD3xBCMA bispecific antibody, n = 6, normalised to 21% + Bispecific. Blue bars = 21% O_2; Green bars = 1% O_2. Data were analysed by (A) ordinary one-way ANOVA with Tukey's multiple comparisons post-hoc test, with a single pooled variance, (D, E, F) Multiple Mann-Whitney tests with two-stage linear step-up procedure of Benjamini, Krieger and Yekutieli. * $p < 0.05$, ** $p < 0.005$, *** $p < 0.005$, or p-values shown, ns = non-significant or 'blank', $p > 0.05$.

Investigation of IFN-γ and TNF-α cytokine production via intracellular cytokine staining on $CD8^+$ T cells revealed IFN-γ production, by the percentage of IFN-γ^+ $CD8^+$ T cells, to be significantly reduced in $CD8^+$ T cells stimulated by a CD3xBCMA bispecific antibody in 1% vs. 21% O_2 and co-cultured with AMO and L363 MM cell lines, and trending towards a reduction with JJN3 target cells **(Figures 6.3A and 6.3B)**. Interestingly, and unlike observations with anti-CD3/CD28 stimulation ('**3. Results Chapter 1, Figure 3.3**'), TNF-α production, by the percentage of TNF-α^+ $CD8^+$ T cells, was significantly reduced in $CD8^+$ T cells stimulated in 1% vs. 21% O_2 via a CD3xBCMA bispecific antibody co-cultured with AMO and L636 MM cell lines, but unchanged with JJN3 target cells **(Figures 6.3A and 6.3C)**. Thus, TNF-α production may be slightly more susceptible to dysfunction in hypoxia via CD3xBCMA bispecific stimulation. The percentage of IFN-γ^+ TNF-α^+ $CD8^+$ T cells was also significantly reduced in $CD8^+$ T cells stimulated in 1% vs. 21% O_2 via a CD3xBCMA bispecific antibody co-cultured with AMO and L636 MM cell lines, but unchanged with JJN3 target cells **(Figures 6.3A and 6.3D)**.

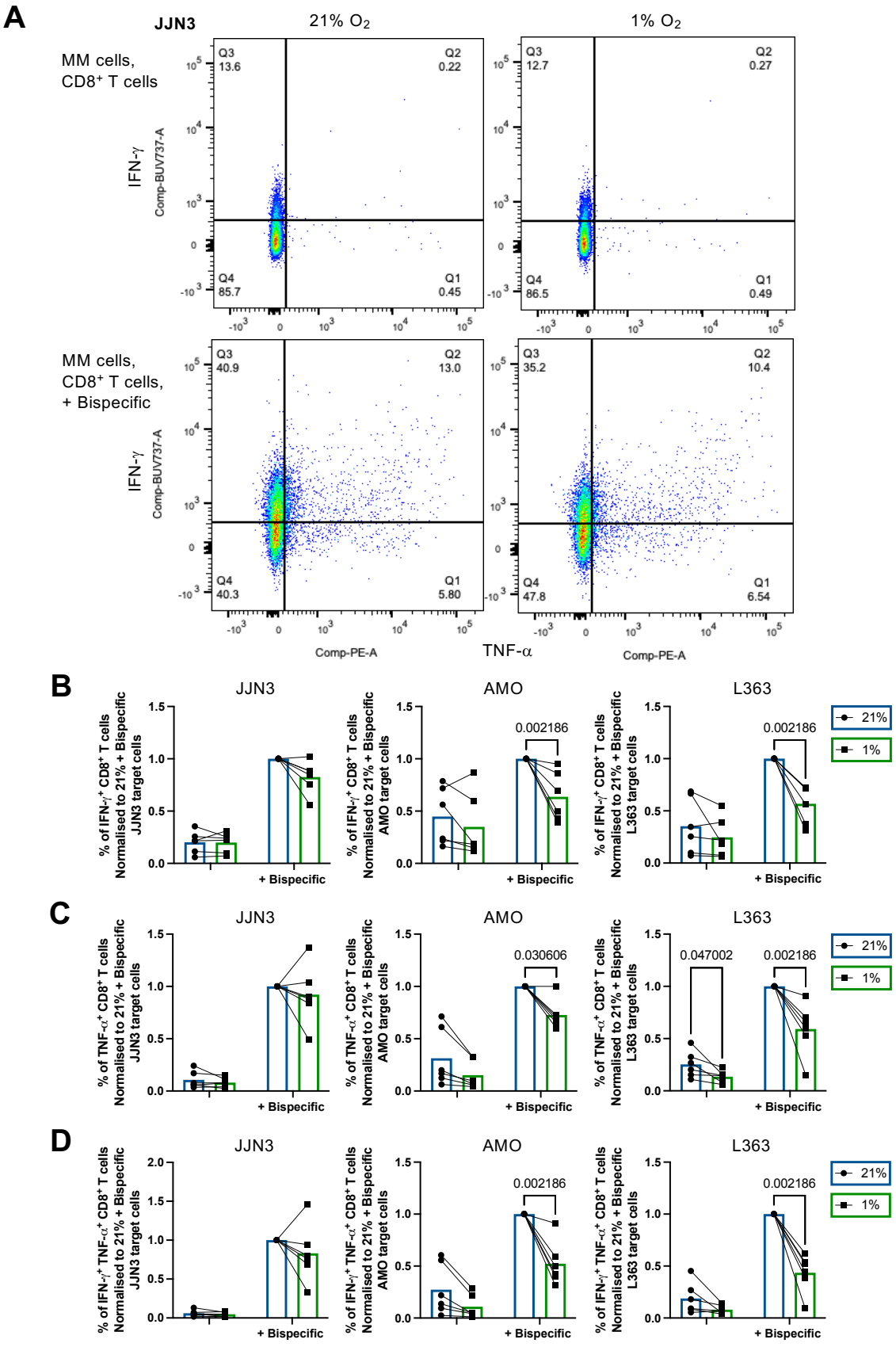
A
JJN3
21% O2
1% O2
MM cells, CD8+ T cells
MM cells, CD8+ T cells, + Bispecific
IFN-γ
Comp-BUV737-A
Comp-PE-A
TNF-α
Q3 13.6
Q2 0.22
Q4 85.7
Q1 0.45
Q3 12.7
Q2 0.27
Q4 86.5
Q1 0.49
Q3 40.9
Q2 13.0
Q4 40.3
Q1 5.80
Q3 35.2
Q2 10.4
Q4 47.8
Q1 6.54
B
JJN3
AMO
L363
% of IFN-γ+ CD8+ T cells Normalised to 21% + Bispecific JJN3 target cells
% of IFN-γ+ CD8+ T cells Normalised to 21% + Bispecific AMO target cells
% of IFN-γ+ CD8+ T cells Normalised to 21% + Bispecific L363 target cells
0.002186
+ Bispecific
21%
1%
C
% of TNF-α+ CD8+ T cells Normalised to 21% + Bispecific JJN3 target cells
% of TNF-α+ CD8+ T cells Normalised to 21% + Bispecific AMO target cells
% of TNF-α+ CD8+ T cells Normalised to 21% + Bispecific L363 target cells
0.030606
0.047002
0.002186
D
% of IFN-γ+ TNF-α+ CD8+ T cells Normalised to 21% + Bispecific JJN3 target cells
% of IFN-γ+ TNF-α+ CD8+ T cells Normalised to 21% + Bispecific AMO target cells
% of IFN-γ+ TNF-α+ CD8+ T cells Normalised to 21% + Bispecific L363 target cells

Figure 6.3. $CD8^+$ T cell and MM cell line +/- CD3xBCMA bispecific antibody co-culture experiments and assessment of $CD8^+$ T cell cytokine production in hypoxia vs. normoxia. A) Example histograms of IFN-γ (BUV737) and TNF-α (PE) staining in $CD8^+$ T cells cultured with MM target cell lines (JJN3) +/- CD3xBCMA bispecific antibody in 21% or 1% O_2, n = 1; B) Percentage of IFN-γ^+ $CD8^+$ T cells when cultured with MM target cell lines (JJN3, AMO, or L363) +/- CD3xBCMA bispecific antibody, n = 6, normalised to 21% + Bispecific; C) Percentage of TNF-α^+ $CD8^+$ T cells shown when cultured with MM target cell lines (JJN3, AMO, or L363) +/- CD3xBCMA bispecific antibody, n = 6, normalised to 21% + Bispecific; D) Percentage of IFN-γ^+ TNF-α^+ $CD8^+$ T cells shown when cultured with MM target cell lines (JJN3, AMO, or L363) +/- CD3-BCMA bispecific antibody, n = 6, normalised to 21% + Bispecific. Blue bars = 21% O_2; Green bars = 1% O_2. Data were analysed by (B, C, D) Multiple Mann-Whitney tests with two-stage linear step-up procedure of Benjamini, Krieger and Yekutieli. * $p < 0.05$, ** $p < 0.005$, *** $p < 0.005$, or p-values shown, ns = non-significant or 'blank', $p > 0.05$.

In agreement with the intact killing of $CD8^+$ T cells in 1% O_2 **(Figure 6.2B)**, the percentage of cytotoxic molecule positive $PrfA^+$ and $GzmB^+$ $CD8^+$ T cells activated by bispecific antibody activation in 1% O_2 was similar or only slightly altered compared to those in 21% O_2 **(Figure 6.4, Figures 6.5A and 6.5B)**. Furthermore, the percentage of $CD107a^+$ $CD8^+$ T cells, as a measure of degranulation activity, activated by bispecific antibody activation in 1% O_2 was similar or only slightly altered compared to those in 21% O_2 **(Figure 6.4 and Figure 6.5C)**. These results confirm findings from *in vitro* experiments with polyclonal anti-CD3/CD28 T cell stimulation ('**3. Results Chapter 1, Figure 3.5**') and bring my findings into a therapeutic context for MM.

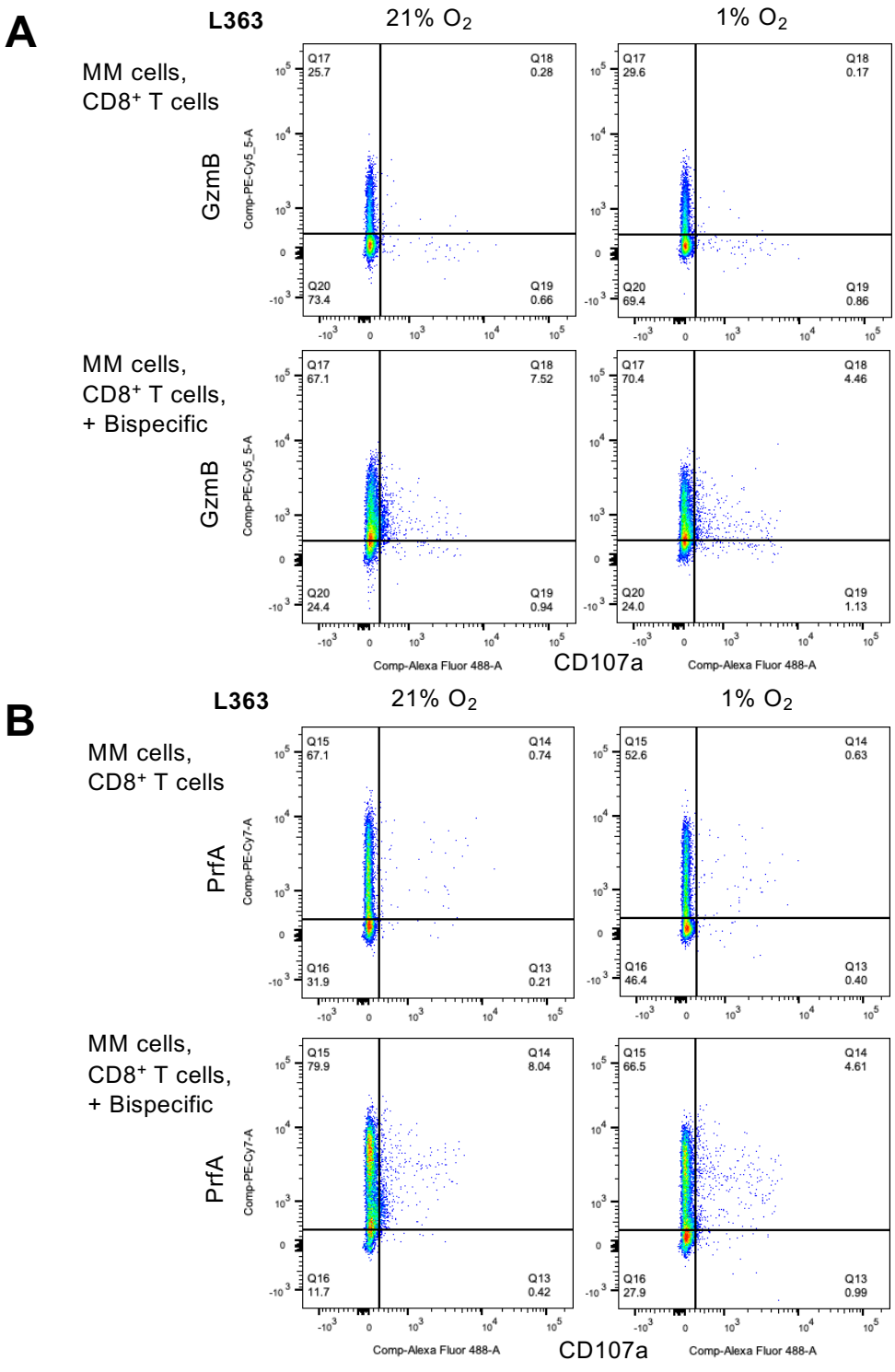

Figure 6.4. CD8+ T cell and MM cell line +/- CD3xBCMA bispecific antibody co-culture experiments and dot plot examples of CD8+ T cell cytotoxicity in hypoxia vs. normoxia. A) Example histograms of GzmB (Per-Cy5.5) and CD107a (AF488) staining in CD8+ T cells cultured with MM target cell lines (L363) +/- CD3xBCMA bispecific antibody in 21% or 1% O_2, n = 1; B) Example histograms of PrfA (PE-Cy7) and CD107a (AF488) staining in CD8+ T cells cultured with MM target cell lines (L363) +/- CD3xBCMA bispecific antibody in 21% or 1% O_2, n = 1.

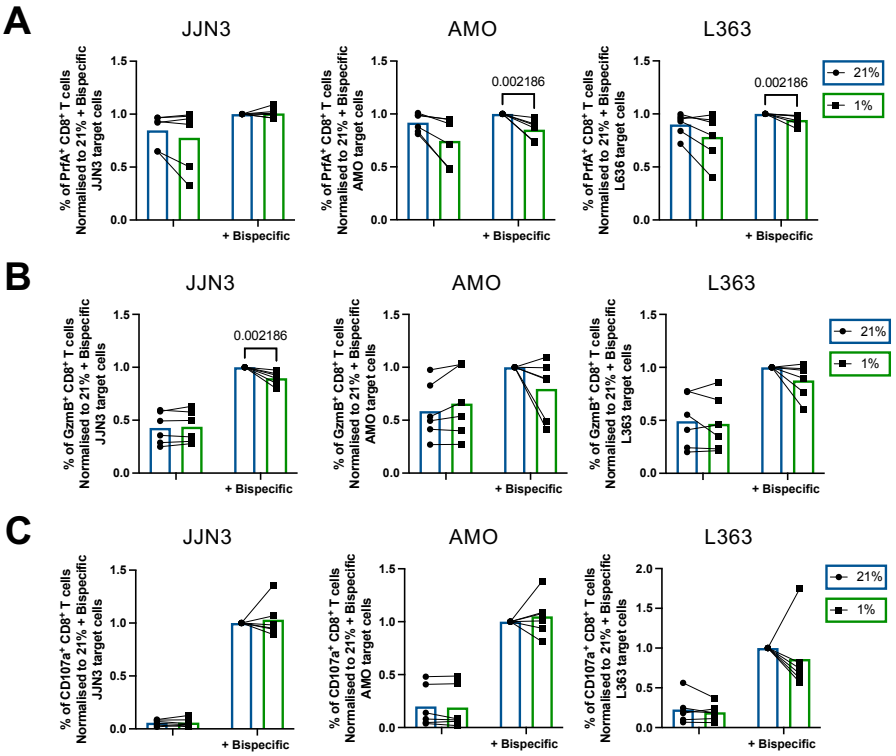

Figure 6.5. $CD8^+$ T cell and MM cell line +/- CD3xBCMA bispecific antibody co-culture experiments and assessment $CD8^+$ T cell cytotoxicity in hypoxia vs. normoxia. A) Percentage of $PrfA^+$ $CD8^+$ T cells when cultured with MM target cell lines (JJN3, AMO, or L363) +/- CD3xBCMA bispecific antibody, n = 6, normalised to 21% + Bispecific; C) Percentage of $GzmB^+$ $CD8^+$ T cells shown when cultured with MM target cell lines (JJN3, AMO, or L363) +/- CD3xBCMA bispecific antibody, n = 6, normalised to 21% + Bispecific; D) Percentage of $CD107a^+$ $CD8^+$ T cells shown when cultured with MM target cell lines (JJN3, AMO, or L363) +/- CD3-BCMA bispecific antibody, n = 6, normalised to 21% + Bispecific. Blue bars = 21% O_2; Green bars = 1% O_2. Data were analysed by (A, B, C) Multiple Mann-Whitney tests with two-stage linear step-up procedure of Benjamini, Krieger and Yekutieli. * $p < 0.05$, ** $p < 0.005$, *** $p < 0.005$, or p-values shown, ns = non-significant or 'blank', $p > 0.05$.

6.3.2. Phenotype of $CD8^+$ T cells isolated from the BM and PB of MM patients

To explore the phenotypic and functional differences of $CD8^+$ T cells present in the BM and PB of MM patients, paired BM aspirates and PB samples were collected from 8 individual newly diagnosed MM patients. BM mononuclear cells and PBMCs were isolated and either stained immediately for flow cytometric analysis or rested overnight in 21% or 1% O_2 and stained the following day. BM mononuclear cells and PBMCs were gated on lymphocytes and live cells, CD4 and CD8 surface expression and CD56 to remove NK cells and give a true $CD8^+$ T cell population **(Figures 6.6A and 6.6B)**. $CD4^+$ and true $CD8^+$ T cells were gated on CD45RA and CCR7 expression to split populations into naïve ($CD45RA^+$ $CCR7^+$), central memory (CM, $CD45RA^-$ $CCR7^+$), effector memory (EM, $CD45RA^-$ $CCR7^-$), and EMRA ($CD45RA^+$ $CCR7^-$) $CD8^+$ T cells **(Figure 6.6C)** and by programmed cell death protein 1 (PD-1) and T cell immunoreceptor with immunoglobulin and ITIM domain (TIGIT) status ($PD\text{-}1^-$ $TIGIT^-$, $PD\text{-}1^+$ $TIGIT^-$, $PD\text{-}1^-$ $TIGIT^+$, $PD\text{-}1^+$ $TIGIT^+$) **(Figure 6.6D)**. The expression of the checkpoints PD-1 and TIGIT are increased on the surface of T cells in MM patients compared to healthy controls (Benson *et al.*, 2010; Rosenblatt *et al.*, 2011; Yadav *et al.*, 2016), and compared with MGUS or SMM patients (Kwon *et al.*, 2020). Functionally, PD-1 engages with programmed death-ligand 1 (PD-L1) present on the myeloma plasma cells to regulate immune evasion (Tamura *et al.*, 2020), and TIGIT plays a role in $CD8^+$ T cell and NK cell dysfunction in MM (Guillerey *et al.*, 2018; Liu *et al.*, 2022). Given the importance of these checkpoints in the immune response to cancer, PD-1/TIGIT co-inhibition is being trialed for therapeutic use in MM (Chu *et al.*, 2023) and it is useful to use both PD-1 and TIGIT expression to phenotype $CD8^+$ T cells present in the MM environment.

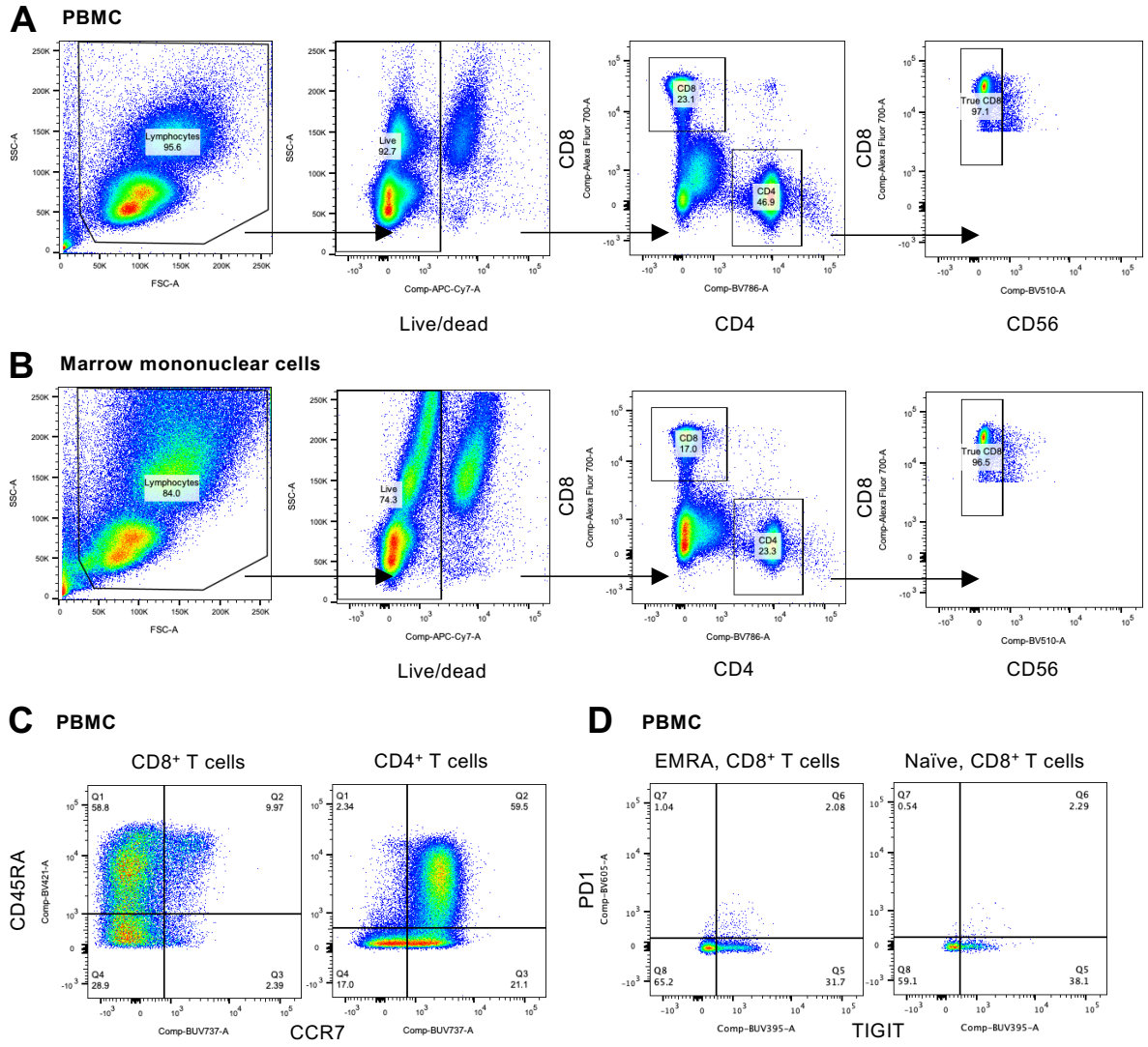

Figure 6.6. Gating strategy to analyse CD8⁺ T cells isolated from the PB and BM aspirates of MM patients. PBMCs and mononuclear cells were isolated from PB and BM aspirates, respectively, of MM patients, and stained immediately *ex vivo* or after freezing for surface markers. A) Example of flow cytometry gating strategy in PBMC's: lymphocytes -> live cells -> CD4⁺ and CD8⁺ -> true CD8⁺ (remove NK cells), n = 1; B) Example of gating strategy in marrow mononuclear cells for flow cytometry: lymphocytes -> live cells -> CD4⁺ and CD8⁺ -> true CD8⁺ (remove NK cells), n = 1; C) Example of gating strategy for CD4⁺ and CD8⁺ T cells into subsets: naïve (CD45RA⁺ CCR7⁺), central memory (CM, CD45RA⁻ CCR7⁺), effector memory (EM, CD45RA⁻ CCR7⁻), and EMRA (CD45RA⁺ CCR7⁻), shown is blood sample, n = 1; D) Example of gating strategy for CD8⁺ T cells subsets into PD-1 and TIGIT status (e.g., PD-1⁻ TIGIT⁻, PD-1⁺ TIGIT⁻, PD-1⁻ TIGIT⁺, PD-1⁺ TIGIT⁺), shown is EMRA and naïve CD8⁺ T cells, n = 1.

There were similar proportions of $CD4^+$ and $CD8^+$ T cells in each sample, with a non-significant trend towards slightly fewer $CD4^+$ and $CD8^+$ T cells in the marrow compared to the blood **(Figure 6.7A)**. A large proportion of $CD8^+$ T cells were EM and EMRA which is consistent with the age of the cohort and with that previously reported **(Table 2.1)** (Gudgeon *et al.*, 2023) **(Figure 6.7B)**. For $CD4^+$ T cells, there was a greater proportion of EM and naïve subsets **(Figure 6.7B)**. Naïve $CD8^+$ T cells were generally PD-1^- $TIGIT^-$, which is concordant with a lack of antigen encounter **(Figure 6.7C)**. CM and EM $CD8^+$ T cells had a mix of PD-1 and TIGIT status but with the presence of PD-1^+ $TIGIT^+$ cells **(Figure 6.7C)**. EMRA $CD8^+$ T cells had fewer double positives and greater proportions of double negatives and PD-1^- $TIGIT^+$ in accordance with recent reports (Brauneck *et al.*, 2021; Heiduk *et al.*, 2023) **(Figure 6.7C)**. The PD-1 and TIGIT status of $CD4^+$ subsets were similar to $CD8^+$ T cells, except from the presence of fewer double positive PD-1^+ $TIGIT^+$ cells **(Figure 6.7D)**. On the whole, frequencies of different populations by memory or checkpoint expression status were very similar between PB and BM samples, indicating no enrichment of specific populations within the BM environment.

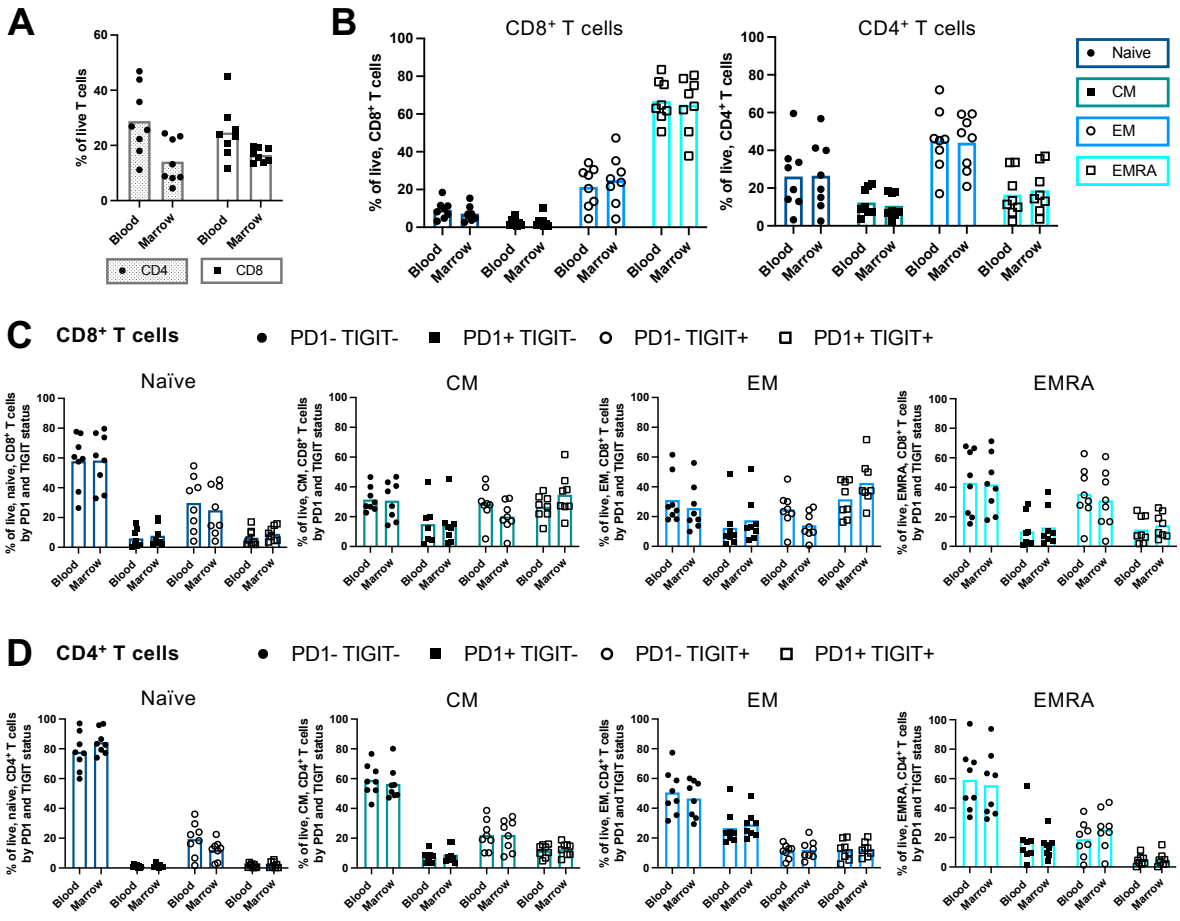

Figure 6.7. Phenotype of CD8$^+$ and CD4$^+$ T cells isolated from the PB and BM aspirates of MM patients. PBMCs and mononuclear cells were isolated from peripheral blood and bone marrow aspirates, respectively, of MM patients, and stained immediately *ex vivo* or after freezing for surface and functional markers. A) Percentage of live true CD8$^+$ and CD4$^+$ T cells in the blood and marrow, n = 8; F) Percentage of live, CD8$^+$ (left) and CD4$^+$ (right) T cells in each subset in the blood or marrow: naïve, CM, EM, and EMRA, n = 8; G) Percentage of live, naïve, CM, EM, or EMRA CD8$^+$ T cells by PD-1 and TIGIT status, n = 8; H) Percentage of live, naïve, CM, EM, or EMRA CD4$^+$ T cells by PD-1 and TIGIT status, n = 8. Dark blue = Naïve, Teal = CM, Aqua = EM, Turquoise = EMRA, CD4$^+$ or CD8$^+$ T cells. Data were analysed by (A) ordinary two-way ANOVA with Sidak's multiple comparisons post-hoc test, with a single pooled variance. * $p < 0.05$, ** $p < 0.005$, *** $p < 0.005$, or p values shown; ns = non-significant or 'blank', $p > 0.05$.

6.3.3. BNIP3 staining was not useful as a marker of hypoxia in the BM and Rheb expression decreased in CD8$^+$ T cells in BM vs. PB

In '**5. Results Chapter 3**' the HIF-dependent upregulation of BNIP3 was identified as a marker of hypoxia and I began to investigate a mechanism of mTOR suppression via the interaction of BNIP3 and Rheb. Therefore, I explored using BNIP3 as a marker of hypoxia in our paired MM BM and PB samples with the hypothesis that the expression of BNIP3 would be greater in the BM, where we expect it to be more hypoxic, than the PB. Interestingly, the reverse was observed and decreased BNIP3 expression was observed in the BM vs. the PB **(Figure 6.8A)**. A trend towards a decrease in BNIP3 expression in the BM vs. the PB was also observed in each individual CD8$^+$ T cell subset excluding CM where no change was seen **(Figure 6.8B)**. Since the decrease in BNIP3 in the BM appeared to be greatest in EMRA CD8$^+$ T cells and EMRA were the largest subset this may partially explain the overall reduction in the whole CD8$^+$ T cell population **(Figures 6.8A and 6.8B)**. The decrease of BNIP3 expression in the BM was observed across all PD-1/TIGIT populations **(Figure 6.8C)**.

Since BNIP3 is upregulated and maintained by exposure to hypoxia, I wanted to understand if processing of BM samples in normal atmospheric conditions was driving the degradation of BNIP3 protein and lowering the BNIP3 abundance in the 'hypoxic' BM. To explore this, PBMC were isolated from healthy leucocyte cones, pre-conditioned overnight in 21% or 1% O_2, and activated the following morning via CD3/CD28 for 24 hours in the respective O_2 condition. Cells were stained at baseline for expression of BNIP3 or moved from 1% O_2 back to 21% O_2 for a total of 8 hours and stained at roughly 1-2-hour intervals within this time period. Activated (A) CD8$^+$ T

cells had higher expression of BNIP3 than non-activated (NA) $CD8^+$ T cells at all time points **(Figure 6.8D)**. However, $CD8^+$ T cells moved from 1% to 21% O_2 quickly degraded BNIP3 protein within 5-7 hours **(Figure 6.8D)**. Therefore, patient samples processed in atmospheric O_2 (collection, transfer and isolation usually taking 5-6 hours) would likely have degraded BNIP3 protein prior to staining and analysis. BNIP3 may therefore not be a good marker of hypoxic exposure in these MM patient samples.

The MFI of Rheb appeared to be slightly decreased in $CD8^+$ T cells in the BM compared to the PB **(Figure 6.8E)**. More specifically, this was observed in EM and EMRA $CD8^+$ T cell subsets in the BM vs. PB but did not change and tended to increase in naïve and CM $CD8^+$ T cell subsets in the BM vs. PB, respectively **(Figure 6.8F)**. There was little change in Rheb expression across PD-1/TIGIT statuses in the BM vs. PB **(Figure 6.8G)**. Therefore, Rheb staining overall in $CD8^+$ T cells in the BM vs. PB may reflect that seen in previous *in vitro* experiments, however this is not consistent when gated into subset or PD-1/TIGIT status.

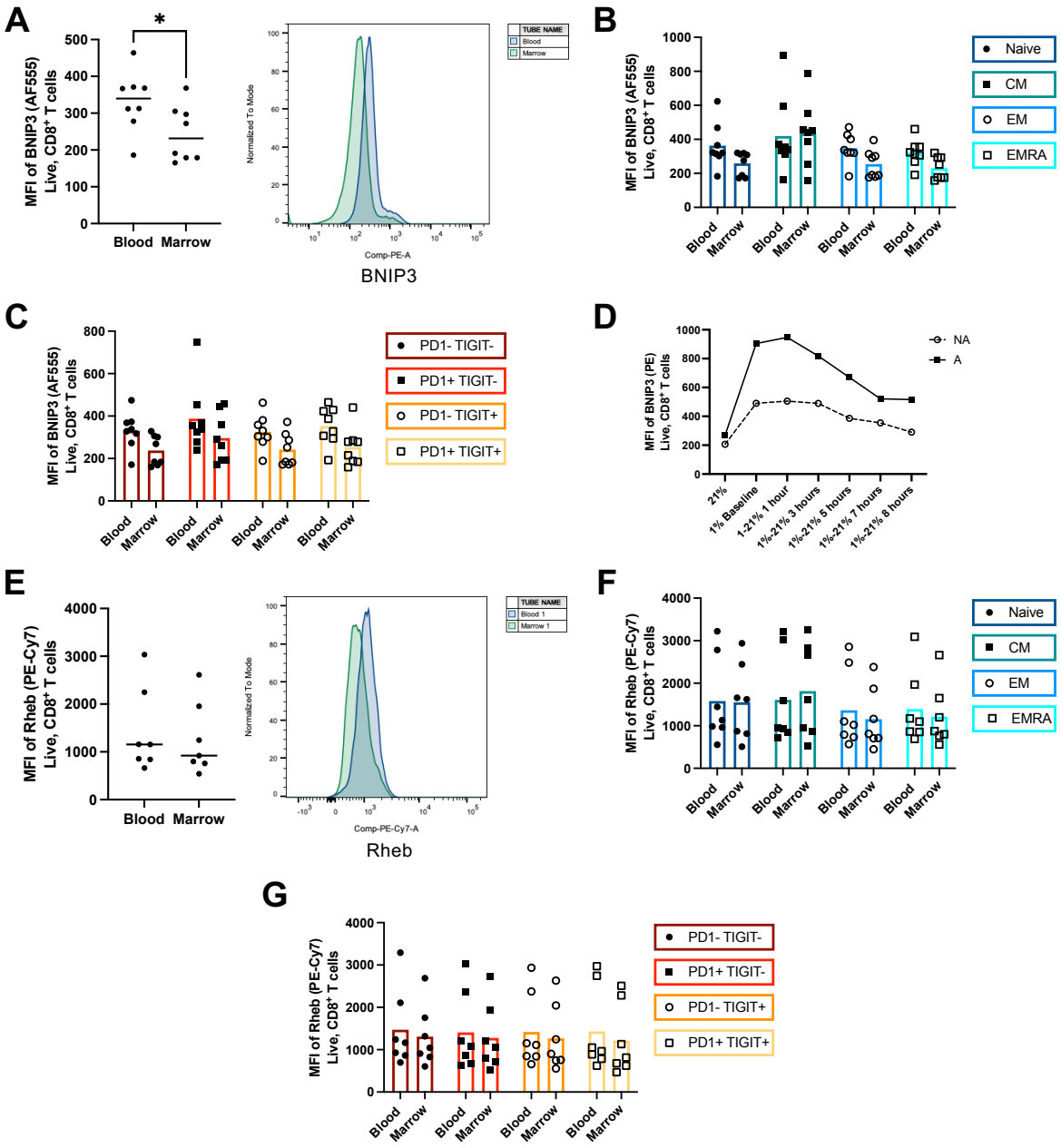

Figure 6.8. Expression of BNIP3 and Rheb in CD8$^+$ T cells isolated from the PB and BM of MM patients. PBMCs and mononuclear cells were isolated from PB and BM aspirates, respectively, of MM patients, and stained and fixed immediately *ex vivo* or after freezing for intracellular proteins. A) MFI of BNIP3 (AF555, PE) in live, CD8$^+$ T cells from blood or marrow, n = 8, and example histogram shown, n = 1; B) MFI of BNIP3 in live, CD8$^+$ T cells from blood or marrow in the various subsets: Naïve (BUV737$^+$ BV421$^+$), central memory (CM, BUV737$^+$ BV421$^-$), effector memory (EM, BUV737$^-$ BV421$^-$), and EMRA (BUV737$^-$ BV421$^+$), n = 8; C) MFI of BNIP3 in live, CD8$^+$ T cells from blood or marrow by PD-1 and TIGIT status (e.g., PD-1$^-$ TIGIT$^-$, PD-1$^+$ TIGIT$^-$, PD-1$^-$ TIGIT$^+$, PD-1$^+$ TIGIT$^+$), n = 8; D) PBMCs were pre-conditioned overnight in 21% or 1% O_2 and activated the following morning with anti-CD3/CD28. Cells were harvested at various time points as indicated and returned to 1% O_2 prior to staining of BNIP3, MFI of BNIP3 in CD8$^+$ T cells shown, n = 3; E) MFI of Rheb (PE-Cy7) in live, CD8$^+$ T cells from blood or marrow, n = 8, and

example histogram shown, n = 1; F) MFI Rheb in live, $CD8^+$ T cells from blood or marrow in the various subsets: Naïve, CM, EM, and EMRA, n = 8; G) MFI of Rheb in live, $CD8^+$ T cells from blood or marrow by PD-1 and TIGIT status, n = 8. Dark blue = Naïve, Teal = CM, Aqua = EM, Turquoise = EMRA, $CD8^+$ T cells. PD-1/TIGIT status colours as indicated. Data were analysed by (A, E) paired t test, (B, C, F, G) ordinary two-way ANOVA with Sidak's multiple comparisons test, with a single pooled variance * $p < 0.05$, ** $p < 0.005$, *** $p < 0.005$, or p values shown; ns = non-significant or 'blank', $p > 0.05$.

6.3.4. Production of intracellular cytokines (IFN-γ and TNF-α) did not appear to change between $CD8^+$ T cells in the BM and PB

To investigate the capacity of $CD8^+$ T cells from the BM and PB to produce cytokines in 21% and 1% O_2, PBMCs and BM mononuclear cells were pre-conditioned overnight in 21% and 1% O_2, activated the following morning with anti-CD3/CD28 for 4 hours with the addition of brefeldin A in the same O_2 conditions, and stained for intracellular cytokines. As with immediate *ex vivo* or after freezing staining, the percentage of EMRA $CD8^+$ T cells was highest across PB and BM in 21% and 1% O_2, followed by EM, and naïve and CM the lowest percentage **(Figure 6.9A)**. **Figure 6.9B** demonstrates IFN-γ and TNF-α staining in PB and BM $CD8^+$ T cells in 21% and 1% O_2, as indicated. The production of IFN-γ, measured by the percentage of IFN-γ^+ $CD8^+$ T cells, may trend towards a slight reduction in the BM vs. PB in 21% O_2, but was similar between the BM vs. PB in 1% O_2 **(Figures 6.9B and 6.9C)**. Similarly, the percentage of TNF-α^+ $CD8^+$ T cells in the BM vs. PB in 21% O_2 may also trend towards a reduction but did not change in 1% O_2 **(Figures 6.9B and 6.9C)**. Little difference was observed in the percentage of IFN-γ^+ TNF-α^+ $CD8^+$ T cells in the BM and PB in the two O_2 conditions **(Figures 6.9B and 6.9C)**. Gating total $CD8^+$ T cells into the various subsets (naïve, CM, EM, and EMRA) revealed EM and EMRA $CD8^+$ T cells to produce the highest amount of IFN-γ and TNF-α (measured per percentage of IFN-γ^+ and TNF-α^+ $CD8^+$ T cells), and naïve $CD8^+$ T cells to produce the least **(Figures 6.10A-6.10D)**.

There was little change across the PB and BM and the two O_2 conditions for production of either cytokine in naïve $CD8^+$ cells, however BM naïve $CD8^+$ T cells in 1% O_2 may have the least capacity to produce IFN-γ **(Figure 6.10A)**. PB CM $CD8^+$ T cells may have less capacity to produce IFN-γ in 1% vs 21% O_2, but this was not seen in BM $CD8^+$ T cells, and BM EM $CD8^+$ T cells in 1% O_2 may have the least capacity to produce IFN-γ **(Figures 6.10B and 6.10C)**. PB and BM EMRA $CD8^+$ T cells may reduce production of IFN-γ and TNF-α when activated in 1% vs. 21% O_2 **(Figure 6.10D)**. With the small number of patients and the substantial inter-patient variability observed here, none of these results reached statistical significance in these experiments, but overall trends are in agreement with our previously published findings in a much larger patient cohort (Gudgeon *et al.*, 2023).

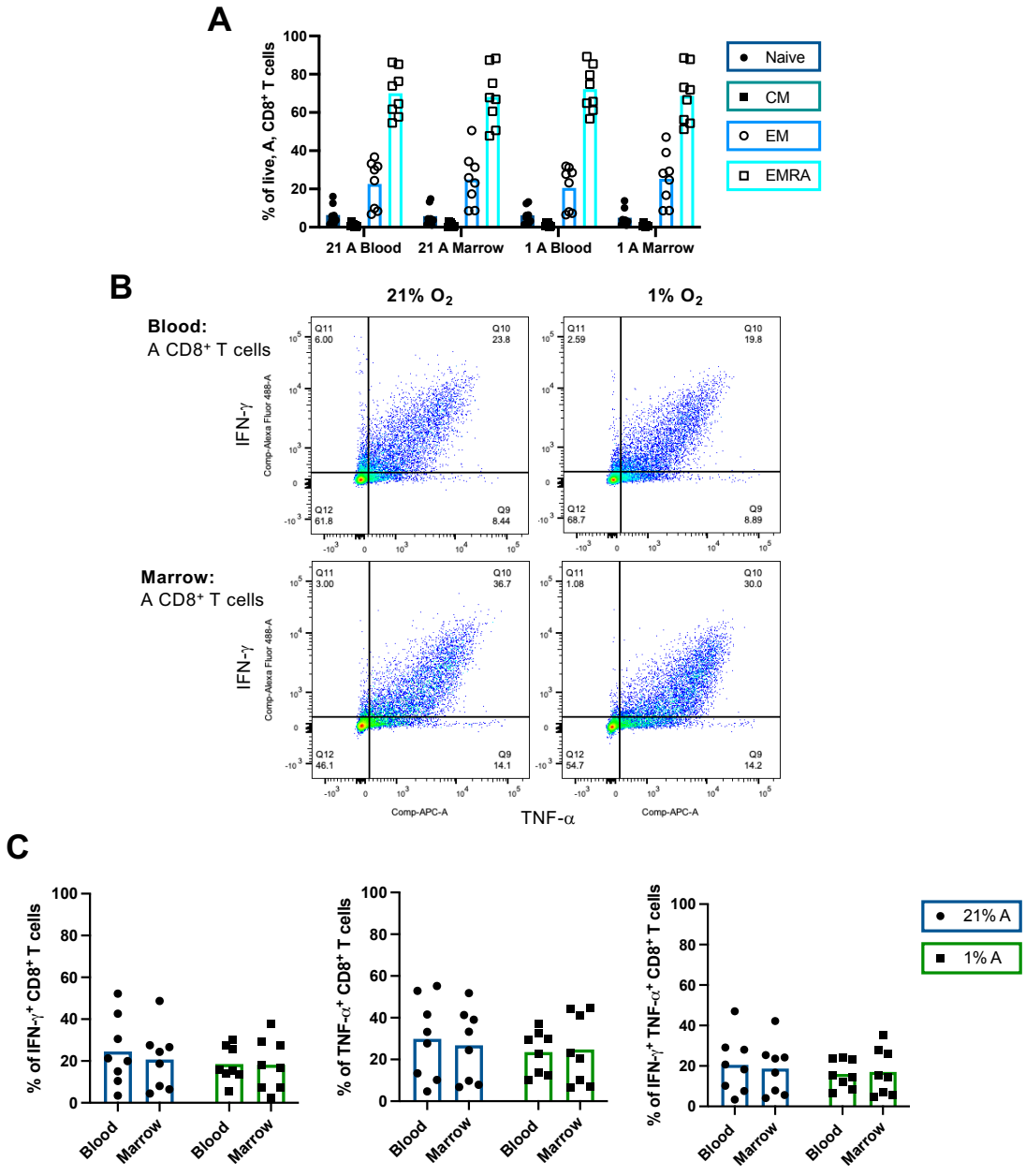

Figure 6.9. Production of cytokines in $CD8^+$ T cells isolated from the PB and BM of MM patients cultured in hypoxia vs. normoxia. PBMCs and mononuclear cells were isolated from PB and BM aspirates, respectively, of MM patients, pre-conditioned overnight in 21% or 1% O_2, and activated the following morning with anti-CD3/CD28 + brefeldin A for 4 hours for intracellular cytokine staining. A) Percentage of live, $CD8^+$ T cells in each subset in the blood or marrow in 21% or 1% O_2: Naïve ($BUV737^+$ $BV421^+$), central memory (CM, $BUV737^+$ $BV421^-$), effector memory (EM, $BUV737^-$ $BV421^-$), and EMRA ($BUV737^-$ $BV421^+$), n = 8; B) Examples histograms of IFN-γ (AF488) and TNF-a (APC) staining in BM and PB $CD8^+$ T cells cultured and activated in 21% and 1% O_2, n = 1; C) Percentage of IFN-γ^+, TNF-α^+, or IFN-γ^+ TNF-α^+ Live A $CD8^+$ T cells shown, n = 8. Dark blue = Naïve, Teal = CM, Aqua = EM, Turquoise = EMRA, $CD8^+$ T cells. Blue bars = 21% O_2; Green bars = 1% O_2. Data analysed by (C) ordinary two-way ANOVA with Tukey's multiple comparisons post-hoc test, with a single pooled variance. * $p < 0.05$, ** $p < 0.005$, *** $p < 0.005$, or p-values shown, ns = non-significant or 'blank', $p > 0.05$.

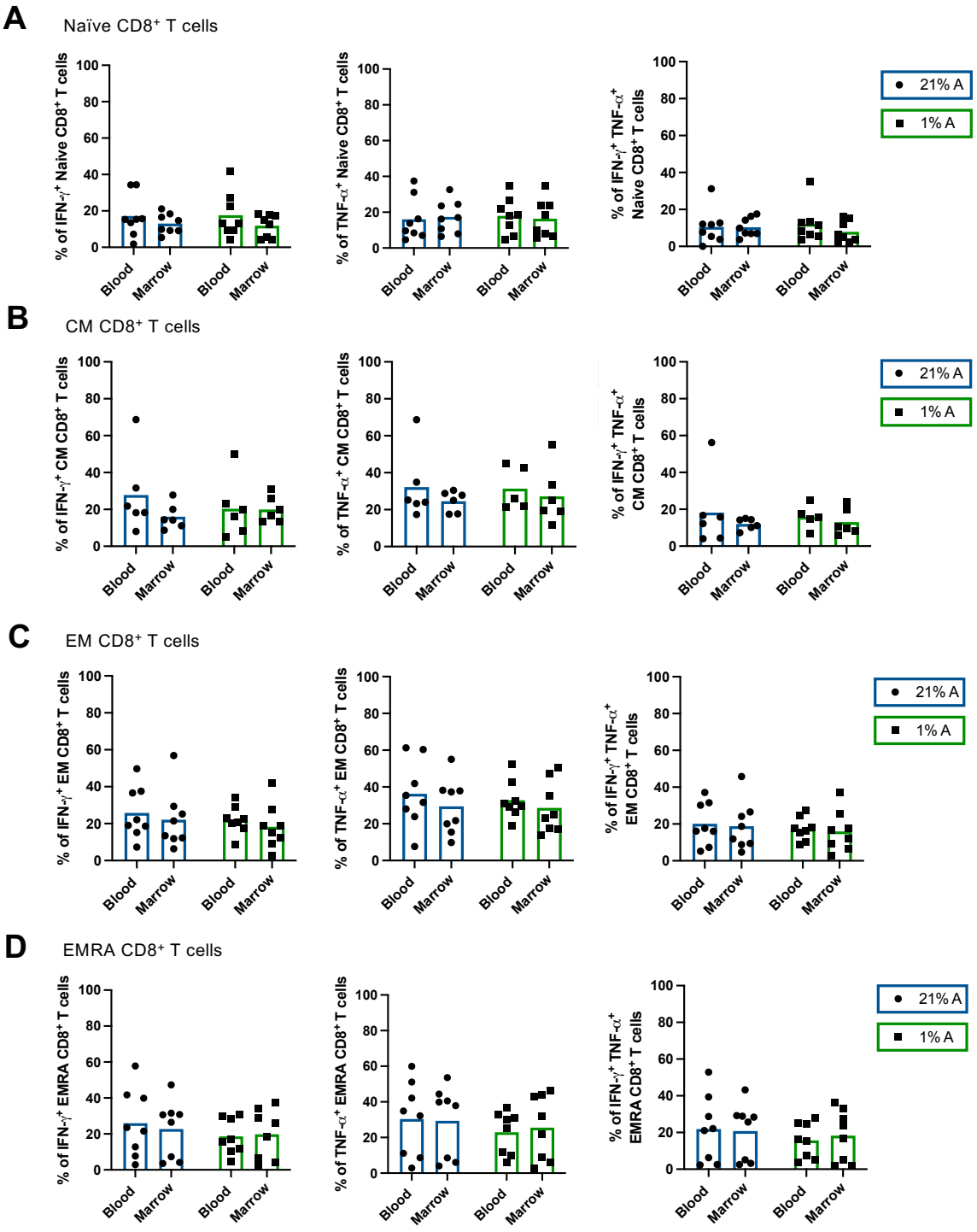

Figure 6.10. Production of cytokines in naïve, CM, EM and EMRA CD8$^+$ T cells isolated from the PB and BM of MM patients cultured in hypoxia vs. normoxia. PBMCs and mononuclear cells were isolated from PB and BM aspirates, respectively, of MM patients, pre-conditioned overnight in 21% or 1% O_2, and activated the following morning with anti-CD3/CD28 + brefeldin A for 4 hours for intracellular cytokine staining. CD8$^+$ T cells gated into various subsets: Naïve (BUV737$^+$ BV421$^+$), central memory (CM, BUV737$^+$ BV421$^-$), effector memory (EM, BUV737$^-$ BV421$^-$), and EMRA (BUV737$^-$ BV421$^+$). A-D) Percentage of IFN-γ^+, TNF-α^+, or IFN-γ^+ TNF-α^+, A) Live A Naïve CD8$^+$ T cells, B) Live A CM CD8$^+$ T cells, C) Live A EM CD8$^+$ T cells, D) Live A EMRA CD8$^+$ T

cells, n = 8. Dark blue = Naïve, Teal = CM, Aqua = EM, Turquoise = EMRA, $CD8^+$ T cells. Blue bars = 21% O_2; Green bars = 1% O_2. Data analysed by (A, B, C, D) ordinary two-way ANOVA with Tukey's multiple comparisons post-hoc test, with a single pooled variance. * $p < 0.05$, ** $p < 0.005$, *** $p < 0.005$, or p-values shown, ns = non-significant or 'blank', $p > 0.05$.

6.3.5. Proliferation of $CD8^+$ T cells in the BM is impaired compared to $CD8^+$ T cells in the PB of MM patients

To measure the proliferation of $CD8^+$ T cells in the BM and PB, PBMCs and marrow mononuclear cells were stained with the well-recognised proliferation marker Ki67 (Sun and Kaufman, 2018). $CD8^+$ T cells present in the BM had reduced Ki67 staining, and thus proliferation, compared to those in the PB **(Figure 6.11A)**. Ki67 staining tended to be highest in CM and EM subsets of $CD8^+$ T cells, and lowest in naïve and EMRA $CD8^+$ T cells **(Figure 6.11B)**, consistent with the expected rates of proliferation (Sallusto, Geginat and Lanzavecchia, 2004; Willinger *et al.*, 2005; Larbi and Fulop, 2014). The trend for a reduction in Ki67 staining was consistent across all subsets of $CD8^+$ T cells in the BM compared to PB (Naïve, CM, EM, and EMRA) and PD-1/TIGIT statuses **(Figures 6.11B and 6.11C)**. Overall, proliferation of $CD8^+$ T cells present in the BM of MM patients was impaired compared to $CD8^+$ T cells present in the PB of MM patients.

6.3.6. $CD8^+$ T cells in the BM have a reduced c-Myc expression compared to $CD8^+$ T cells in the PB of MM patients

To investigate metabolic capacity in $CD8^+$ T cells in MM, expression of c-Myc, a well-known marker of T cell metabolic reprogramming capacity (Wang *et al.*, 2011), was assessed in $CD8^+$ T cells and compared between the BM and PB. c-Myc expression was significantly reduced in $CD8^+$ T cells in the BM compared to those in the PB

(Figure 6.11D). This trend was consistent across all $CD8^+$ T cell subsets and PD-1/TIGIT statuses, and significant in CM and EM $CD8^+$ T cell subsets and $PD1^-$ $TIGIT^-$ $CD8^+$ T cells **(Figures 6.11E and 6.11F)**. Therefore, the metabolic capacity of $CD8^+$ T cells present in the BM of MM patients may also be impaired compared to $CD8^+$ T cells present in the PB of MM patients.

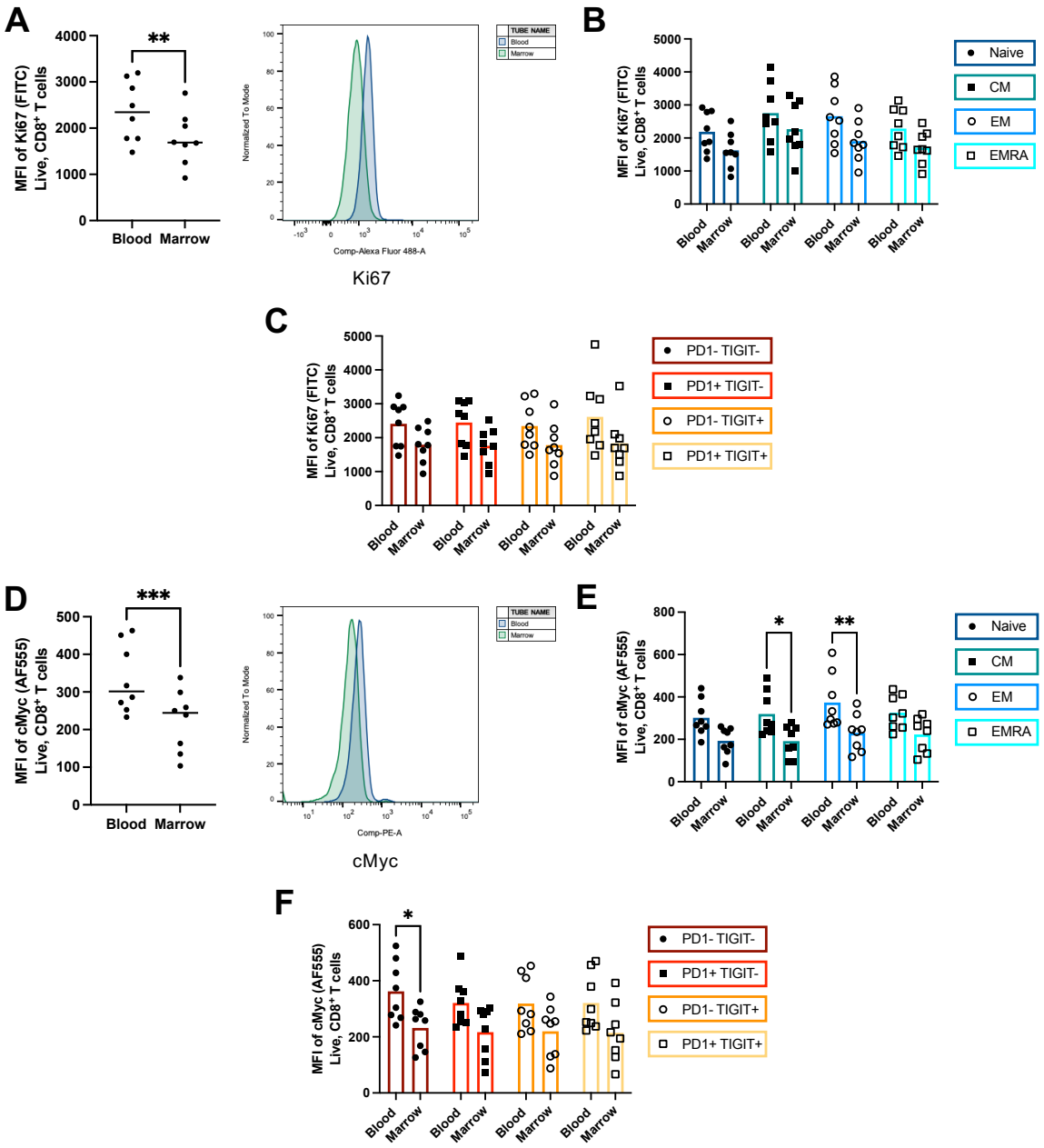

Figure 6.11. Proliferation and expression of c-Myc in $CD8^+$ T cells isolated from the PB and BM of MM patients. PBMCs and mononuclear cells were isolated from PB and BM aspirates, respectively, of MM patients, and stained immediately *ex vivo* or after freezing for functional markers. A) MFI of Ki67 (FITC, AF488) in live, $CD8^+$ T cells from blood or marrow, n = 8, and example histogram shown, n = 1; B) MFI of Ki67 in live, $CD8^+$ T cells from blood or marrow in the various subsets: Naïve ($BUV737^+$ $BV421^+$), central memory (CM, $BUV737^+$ $BV421^-$), effector memory (EM, $BUV737^-$ $BV421^-$), and EMRA ($BUV737^-$ $BV421^+$), n = 8; C) MFI of Ki67 in live, $CD8^+$ T cells from blood or marrow by PD-1 and TIGIT status (e.g., PD-1^- $TIGIT^-$, PD-1^+ $TIGIT^-$, PD-1^- $TIGIT^+$, PD-1^+ $TIGIT^+$), n = 8; D) MFI of c-Myc (AF555, PE) in live, $CD8^+$ T cells from blood or marrow, n = 8, and example histogram shown, n = 1; E) MFI of c-Myc in live, $CD8^+$ T cells from blood or marrow in the various subsets: Naïve, CM, EM, and EMRA, n = 8; F) MFI of c-Myc in live, $CD8^+$ T cells from blood or marrow by PD-1 and TIGIT status, n = 8. Dark blue = Naïve, Teal = CM, Aqua =

EM, Turquoise = EMRA, $CD8^+$ T cells. Data analysed by (A, D) paired t-test, (B, C, E, F) ordinary two-way ANOVA with Sidak's multiple comparisons test, with a single pooled variance. * $p < 0.05$, ** $p < 0.005$, *** $p < 0.005$, or p-values shown, ns = non-significant or 'blank', $p > 0.05$.

6.3.7. Activation and culture of MM PB $CD8^+$ T cells in 1% O_2 increases mitochondrial mass compared to those activated and cultured in 21% O_2

To further investigate the mitochondrial content and function of $CD8^+$ T cells in the BM and PB of MM patients, PBMCs and mononuclear cells were thawed then cultured overnight in 21% and 1% O_2 and stained for mitochondrial mass (MVG) and membrane potential (MSO) as before ('**4. Results Chapter 2, Figure 4.9**'). We have previously determined that frozen cells need to be rested for several hours to recover pre-freezing staining with these mitochondrial probes, and therefore conducted this at both 21% and 1% O_2 in order to replicate peripheral and BM environmental O_2 tensions as best as possible. No difference was observed between the mitochondrial mass, as per MVG staining, of the BM and PB $CD8^+$ T cells, at either 21% or 1% O_2 **(Figure 6.12A)**. However, culture of $CD8^+$ T cells from the PB of MM patients in 1% O_2 significantly increased their mitochondrial mass compared to those cultured in 21% O_2, as observed with healthy donor PB $CD8^+$ T cells **(4. Chapter 2, Figure 4.9)**. A similar trend was observed for BM $CD8^+$ T cells from MM patients, albeit not to the same extent, perhaps indicating less capacity to increase mitochondrial capacity under hypoxia, consistent with reduced c-Myc **(Figure 6.12A)**. No change in the mitochondrial membrane potential was observed between $CD8^+$ T cells from the BM and PB of MM patients and between the two O_2 conditions, which is inconsistent with previous findings in stimulated, healthy donor PB $CD8^+$ T cells **(4. Chapter 2, Figure 4.9)**, albeit culture duration is different here and cells are not stimulated **(Figure**

6.12B). Similarly, when total $CD8^+$ T cells were gated by subsets (Naïve, CM, EM, and EMRA), mitochondrial mass appeared to increase in PB and BM $CD8^+$ T cells cultured in 1% vs. 21% O_2 but may trend towards a slight reduction of BM vs. PB in 1% O_2, for all $CD8^+$ T cell subsets **(Figure 6.12C)**. Mitochondrial membrane potential appeared largely unchanged depending on the origin of $CD8^+$ T cell from MM patients (PB or BM) or by O_2 condition **(Figure 6.12C)**. A similar pattern to that observed in subsets was observed when gating total $CD8^+$ T cells by PD-1/TIGIT status **(Figure 6.12D)**. Overall, whilst no difference in mitochondrial mass is observed between $CD8^+$ T cells from the PB and BM of MM patients, when cultured in 1% O_2, all $CD8^+$ T cells appear to increase mitochondrial mass. No change is observed for mitochondrial membrane potential in all conditions. Of note, in future experiments, it would be important to include age-matched controls from healthy BM and PB samples before interpreting findings from MM patients. This is because MM patients may have system-wide effects on their immune system and $CD8^+$ T cells that are not seen in healthy controls. These samples may be collected from older patients undergoing hip transplants or hip surgery.

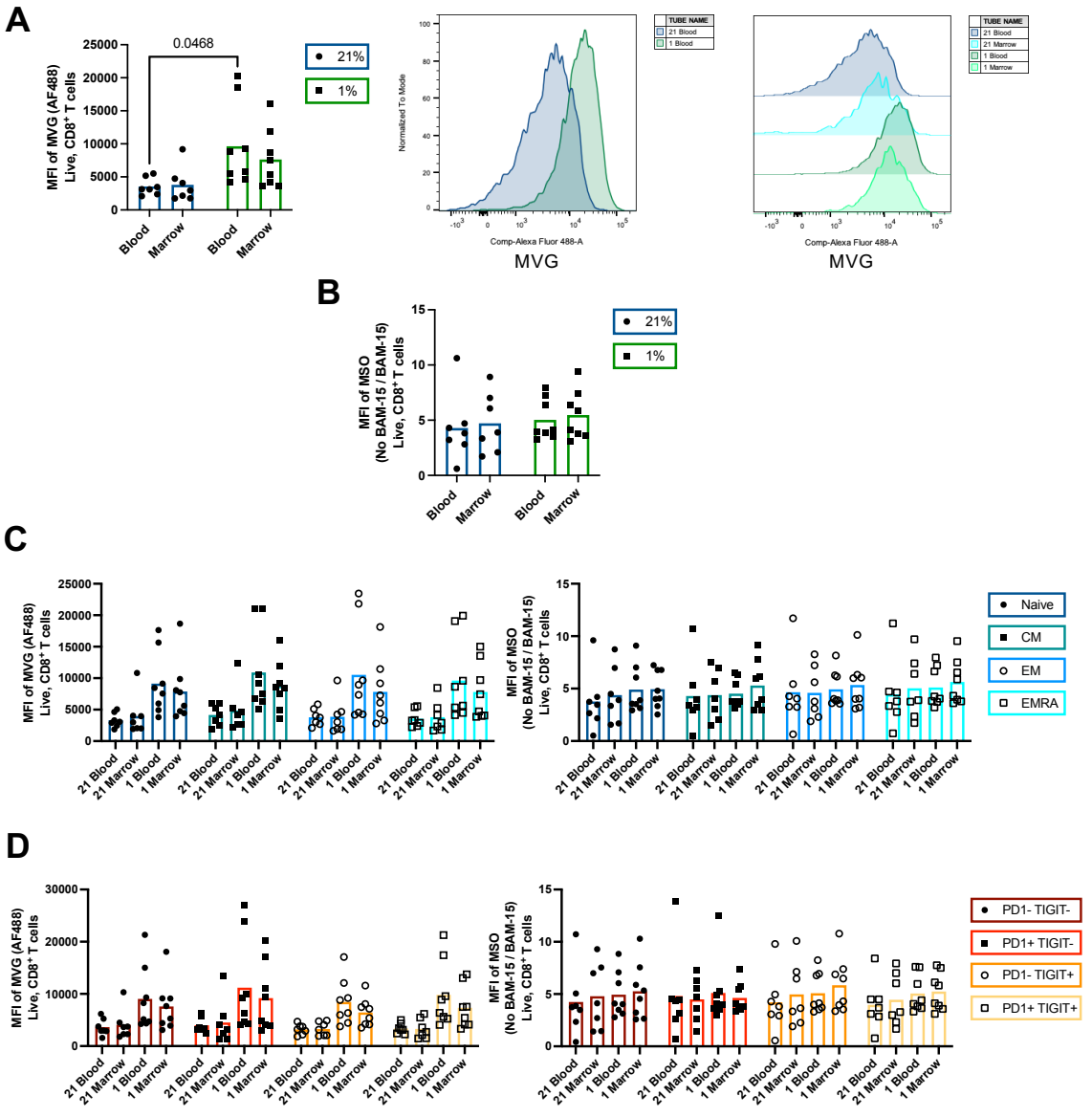

Figure 6.12. Mitochondrial membrane potential and mass of CD8$^+$ T cells isolated from the PB and BM of MM patients cultured in hypoxia vs. normoxia. PBMCs and mononuclear cells were isolated from PB and BM aspirates, respectively, of MM patients, pre-conditioned overnight in 21% or 1% O_2, and analysed the following morning. A) MFI of MVG (mitochondrial mass, AF488) of live, CD8$^+$ T cells in PB or BM cultured overnight in 21% or 1% O_2, n = 8, example histograms shown for MVG of PB samples in 21% vs. 1% O_2 and PB vs. BM in 21% vs 1% O_2, n = 1; B) MFI of MSO (mitochondrial membrane potential, BAM15 / BAM15) of live, CD8$^+$ T cells in PB or BM cultured overnight in 21% or 1% O_2, n = 8; C) MFI of MVG and MSO of live, CD8$^+$ T cells in various subsets: Naïve (BUV737$^+$ BV421$^+$), central memory (CM, BUV737$^+$ BV421$^-$), effector memory (EM, BUV737$^-$ BV421$^-$), and EMRA (BUV737$^-$ BV421$^+$), in PB or BM cultured overnight in 21% or 1% O_2, n = 8; D) MFI of MVG and MSO of live, CD8$^+$ T cells in blood or marrow by PD-1 and TIGIT status (e.g., PD-1$^-$ TIGIT$^-$, PD-1$^+$ TIGIT$^-$, PD-1$^-$ TIGIT$^+$, PD-1$^+$ TIGIT$^+$), cultured overnight in 21% or 1% O_2, n = 8. Dark blue = Naïve, Teal = CM, Aqua = EM, Turquoise = EMRA, CD8$^+$ T cells. Blue bars = 21% O_2; Green bars = 1% O_2. Data analysed by (A, B) ordinary two-way ANOVA with Tukey's multiple comparisons post-hoc test, with a single pooled variance. * $p < 0.05$, ** $p < 0.005$, *** $p < 0.005$, or p-values shown, ns = non-significant or 'blank', $p > 0.05$.

6.4. Discussion

$CD8^+$ T cells present in the MM TME are known to be dysfunctional (Gudgeon *et al.*, 2023). For example, our laboratory has shown that the function of $CD8^+$ T cells from MM patients is decreased compared to healthy controls and BM $CD8^+$ T cells produce less IFN-γ, TNF-α, IL-2 and granzyme-B than PB $CD8^+$ T cells of MM patients (Gudgeon *et al.*, 2023). $CD8^+$ T cells from the BM of MM patients have decreased mitochondrial mass and increase uptake of long-chain fatty acids compared to those from the PB (Gudgeon *et al.*, 2023). Importantly, analysis of MM patients who were responsive to treatment revealed a restoration of metabolic and functional $CD8^+$ T cell dysfunction compared to those patients who were not responsive to treatment (Gudgeon *et al.*, 2023). Previous literature has also reported that the MM TME is hypoxic (Asosingh *et al.*, 2005; Colla *et al.*, 2010; Li *et al.*, 2022). Since earlier chapters in this thesis revealed specific impairments on $CD8^+$ T cell effector function and metabolic reprogramming by hypoxia ('**3. Results Chapter 1**' and '**4. Results Chapter 2**'), I hypothesised that the $CD8^+$ T cell dysfunction observed in MM may partially be due to the hypoxic nature of the TME.

One novel therapeutic approach being trialled for use in MM are bispecific antibodies, or BiTEs, for example those which engage CD3 on the T cell and BCMA on the malignant MM plasma cell (Hipp *et al.*, 2017; Cohen, 2019; Shah and Mailankody, 2020; Topp *et al.*, 2020). I first wanted to understand how activation via a CD3xBCMA bispecific antibody would impact the killing capacity and production of cytokines of $CD8^+$ T cells co-cultured with a MM cell line expressing BCMA. These experiments revealed a striking increase in killing by $CD8^+$ T cells of the MM target cells when the

bispecific antibody was added to culture, compared to when the bispecific was not added **(Figures 6.1 and 6.2)**, confirming the pre-clinical efficacy of these antibodies observed previously (Hipp *et al.*, 2017). Killing of target cells was consistent with increased release of perforin A and granzyme B cytolytic granules on activation with the bispecific, as well as expression of the degranulation marker, CD107a **(Figures 6.2, 6.4 and 6.5)**. Culture with the bispecific antibody also upregulated activation markers on the $CD8^+$ T cells, including the early activation marker, CD69 and the late marker, CD25 **(Figure 6.2)**, consistent with earlier reports (Hipp *et al.*, 2017). Therefore, our work is consistent with the previously reported therapeutic efficacy of bispecific antibodies.

To understand how well bispecific antibodies work in hypoxia, which is important in the MM TME, I conducted the same experiments performed at atmospheric O_2 in hypoxia. Consistent with that shown in '**3. Results Chapter 1**' with anti-CD3/CD28 stimulation, $CD8^+$ T cells activated in hypoxia via a CD3xBCMA bispecific antibody demonstrated decreased surface expression of CD25 and production of IFN-γ compared to those activated in normoxia **(Figures 6.2 and 6.3)**. Interestingly, $CD8^+$ T cells activated in hypoxia with the bispecific antibody also demonstrated decreased production of TNF-α compared to $CD8^+$ T cells activated in normoxia **(Figure 6.3)**; an effect not observed with anti-CD3/CD28 stimulation ('**3. Results Chapter 1, Figure 3.3**'). Stimulation with the CD3xBCMA bispecific antibody does not provide a CD28 signal to the $CD8^+$ T cell, unlike with anti-CD3/CD28 stimulation, thus it may be the lack of this signal driving the different response to hypoxia on TNF-α production. However, effector $CD8^+$ T cells with a knockout of CD28 and stimulated with anti-CD3/CD28 reduced the percentage

of IFN-γ, TNF-α, and granzyme B positive cells compared to those with wildtype CD28 (Lai *et al.*, 2021). Thus, further investigation is required on the impact of hypoxia when $CD8^+$ T cells receive different activation signals. The impact on TNF-α may suggest that stimulation with anti-CD3/CD28 or a CD3xBCMA bispecific antibody drive slightly different signalling pathways or have different dependencies upon TNF-α production but work should be conducted to clarify this.

Interestingly, the defect on cytokine production in hypoxia on $CD8^+$ T cells was more apparent when target cells had a reduced BCMA expression level. For instance, AMO target cell lines had the lowest expression of BCMA, and JJN3 target cell lines the greatest expression (**Figure 6.2**). This corresponded with a greater defect on IFN-γ and TNF-α production in hypoxia with CD3xBCMA bispecific antibody stimulation when cells were cultured with AMO target cells compared to JJN3 (**Figure 6.3**). A similar effect was observed in CD25 expression (**Figure 6.1**). This finding may suggest that a higher expression of BCMA helps to overcome the hypoxia-induced defects on $CD8^+$ T cell function.

Killing of MM target cells by $CD8^+$ T cells with CD3xBCMA bispecific antibody activation, as well as the release of cytotoxic granules, perforin A and granzyme B and expression of degranulation marker, CD107a, were similar between $CD8^+$ T cells cultured and activated in hypoxia and normoxia **(Figures 6.2, 6.4 and 6.5)**. These results agree with those from the assays of $CD8^+$ T cell cytotoxic potential in hypoxia performed in '**3. Results Chapter 1, Figure 3.5**'. This data may also be reassuring to those working with bispecific antibodies in the MM clinical context, as it suggests that

initial killing of the malignant plasma cells by T cell engagement won't be impaired by the hypoxic TME. Of course, other factors, such as metabolic limitation or accumulation, may impair the efficacy of T cell killing with bispecific antibody activation, and should be investigated with further exploration. Furthermore, it may be that no defect is evident in the initial killing by $CD8^+$ T cells in hypoxia as perforin and granzyme-B exist as pre-stored granules within the cell. In future experiments, investigation of serial killing of target cells by $CD8^+$ T cells may reveal defects in hypoxia not observed in the initial killing. Here, the cells may release their pre-stored granules for the initial killing but have reduced capacity in hypoxia to produce and release further cytotoxic granules for serial killings. These experiments may be conducted by replacing target cells in culture after each killing and carrying out several assays back-to-back. In this case, these $CD8^+$ T cells may have dysfunctional killing and impair the efficacy of bispecific antibodies, however, further experiments are required to prove this hypothesis.

To expand our healthy human $CD8^+$ T cell work into the MM disease context, we recruited a total of 8 newly diagnosed MM patients and stored paired PB and BM aspirate samples. Using three flow cytometry panels I formed an extensive understanding of the phenotype, function, and metabolic capacity of $CD8^+$ T cells present in the MM PB and BM. Since the MM BM environment is known to be immunosuppressive and hypoxic, I hypothesised that the function and metabolic capacity of $CD8^+$ T cells present in the BM would be impaired compared to $CD8^+$ T cells in the PB of MM patients. As expected, given the older age of the cohort **(Table 2.1)** and previous literature (Gudgeon *et al.*, 2023), a large proportion of $CD8^+$ T cells

present in both the BM and PB samples of MM patients were EMRA $CD8^+$ T cells **(Figure 6.7)**. Naïve $CD8^+$ T cells were generally PD-1/TIGIT double negative, indicative of their lack of antigen encounter, whilst memory subsets began to express PD-1 and/or TIGIT **(Figure 6.7)**. There was no apparent difference in PD-1 and TIGIT status between the BM and PB of MM patients **(Figure 6.7)**, which contrasts previous studies which show a greater percentage of PD-1^+ $CD8^+$ T cells in the BM vs. PB of MM patients (Tan *et al.*, 2018).

Since I determined BNIP3 as a good marker of hypoxia in '**5. Results Chapter 3**', I thought to determine the presence of hypoxia in our MM samples by staining for BNIP3 expression. Whilst we expected a greater BNIP3 expression in the BM, where it is thought to be hypoxic, the opposite was observed and BNIP3 expression was decreased in the BM compared to the PB of MM patients **(Figure 6.8)**. A degradation assay confirmed that within 5-7 hours of returning a sample to normoxic conditions, BNIP3 protein begins to degrade **(Figure 6.8)**. Since all of the MM patient samples had been processed and stored within atmospheric conditions, often with no time urgency, this may explain the lack of BNIP3 upregulation in the BM of MM patients. It would be interesting to determine the hypoxic status of the MM BM through different means. For example, confocal staining of BM trephines with hypoxic or HIF-dependent markers, such as BNIP3 or REDD1/DDIT4, that are fixed and stored immediately after the procedure. BNIP3 is also a key driver of autophagy, so it would be interesting to determine the activity of autophagy pathways on return to atmospheric O_2 of hypoxic samples. For example, with the measurement of microtubule associated protein 1 light chain 3 alpha (MAP1LC3A, or LC3) expression with flow cytometry (Yoshii and

Mizushima, 2017). The mechanism of BNIP3-Rheb interaction driving mTOR suppression ('**5. Results Chapter 3**') was also difficult to assess in these MM samples **(Figure 6.8)**. It is likely that re-oxygenation of samples quickly alters the regulation of this mechanism given the importance of mTOR in energetic stress.

For functional analysis, it was difficult to determine where best to rest $CD8^+$ T cells overnight. Culture at atmospheric levels will potentially rescue any hypoxic impairments on function that were present within the hypoxic BM, but culture overnight within hypoxia may falsely produce hypoxic functional effects. Therefore, for these experiments I cultured the PB and BM samples both overnight in 21% and 1% O_2 prior to mitochondrial assessment or restimulation for intracellular cytokine analysis the following day **(Figures 6.9, 6.10 and 6.12)**. I hoped this would give us a general idea of what may be happening within the hypoxic BM TME on $CD8^+$ T cell function. Whilst I saw a trend for impaired $CD8^+$ T cell cytokine production in the BM compared to the PB, this did not reach significance as per our previous studies **(Figure 6.9)** (Gudgeon *et al.*, 2023). This is likely due to the limited number of patients recruited, compared to the larger number in our previous report (Gudgeon *et al.*, 2023). The effect of hypoxia was also not clear when PB and BM samples were cultured and activated the following morning in low O_2 conditions **(Figure 6.9)**, compared to that seen in '**3. Results Chapter 1**'. Importantly, the period used for activation for these experiments (4 hours) was much shorter than that used in '**3. Results Chapter 1**' (48 hours), and cells were not re-activated after an initial activation period. $CD8^+$ T cells were also only around 20% cytokine positive, suggesting they had not produced much cytokine as of yet. Therefore, a longer incubation period and perhaps a re-stimulation would have made

the effect size in cytokine assessment clearer. It may also be relevant to culture patient samples at 5% O_2 as a true representation of physiological oxygen levels, especially in the context of bispecific antibody activity.

In contrast, proliferation of $CD8^+$ T cells present in the BM of MM patients was consistently impaired compared to the PB **(Figure 6.11)**. These results are in line with the defect on $CD8^+$ T cell proliferation in hypoxia observed in '**3. Results Chapter 1, Figure 3.6**'. Furthermore, c-Myc staining, as a measure of metabolic reprogramming, was also impaired in $CD8^+$ T cells in the BM compared to the PB of MM patients **(Figure 6.11)**, an effect observed in '**4. Results Chapter 2, Figure 4.6**' with assessment of $CD8^+$ T cell metabolic reprogramming upon activation in hypoxia. Of course, other potential drivers exist which may also be responsible for the decreased c-Myc expression observed in the BM compared to the PB of MM patients. For example, studies have demonstrated that increased lipid uptake suppresses NK cell effector and metabolic capacity, including the expression of c-Myc (Michelet *et al.*, 2018), and reduces effector and metabolic functionality of $CD8^+$ T cells (Manzo *et al.*, 2020; Ma *et al.*, 2021; Xu *et al.*, 2021). Given that previous work in our laboratory has shown that the BM environment of MM demonstrates elevated uptake of long-chain fatty acids (Gudgeon *et al.*, 2023), the decrease of c-Myc expression in the BM of MM patients may be a consequence of lipid accumulation, in combination with the impact of hypoxia. Furthermore, PB $CD8^+$ T cells from MM patients increase their mitochondrial mass upon hypoxic exposure **(Figure 6.12)**, as seen in healthy $CD8^+$ T cells activated and cultured in hypoxia ('**4. Results Chapter 2, Figure 4.9**'), however BM $CD8^+$ T cells demonstrate less capacity to do this **(Figure 6.12)**. This effect may

be related to the decreased c-Myc expression observed in BM $CD8^+$ T cells **(Figure 6.11)**. Therefore, whilst we can't directly confirm the presence of a hypoxic environment in the BM, similar functional and metabolic reprogramming effects are observed.

6.5. Conclusion

Overall, the experiments in this chapter have confirmed my previous findings within a therapeutic context with bispecific antibody engagement of $CD8^+$ T cells and MM plasma cells. The results suggest that the hypoxic environment will not impair killing of target cells by $CD8^+$ T cells but will impair their activation and production of IFN-γ and TNF-α. Analysis of matched BM and PB samples from MM patients revealed an impairment of proliferation and reduced c-Myc expression in the BM compared to the PB of MM patients. These effects have previously been observed in $CD8^+$ T cells activated and cultured in hypoxia. Further work is required to clarify the hypoxic nature of the MM TME and bring into the context of potential mechanisms (e.g., BNIP3-Rheb-mTOR interaction) identified in '**5. Results Chapter 3**'.

7. Discussion

7. Discussion

7.1. Discussion of Results Chapters 1-4

The impact of the hypoxic TME on $CD8^+$ T cell activation is incompletely understood. Here, I have conducted *in vitro* functional and metabolic assays on healthy human $CD8^+$ T cells pre-conditioned and activated via anti-CD3/CD28 in atmospheric (21% O_2), physiological (5% O_2), and hypoxic (1% O_2) conditions. The underlying mechanisms driving the impaired response of specific effector functions of $CD8^+$ T cells in hypoxia were explored through unbiased analyses with bulk RNA-sequencing and targeted analyses with CRISPR-Cas9 on primary cells. To bring the *in vitro* findings and mechanistic analysis into the disease context, $CD8^+$ T cells from matched peripheral blood (PB) and bone marrow (BM) samples of newly diagnosed multiple myeloma patients (MM) were analysed for functional and phenotypic characteristics.

Previously, studies exploring $CD8^+$ T cell function in hypoxia have been contradictory. Effects of hypoxia on $CD8^+$ T cell function is impacted by the protocol used for culture and activation in hypoxia, for example, the species of origin, the differentiation state, and how and when $CD8^+$ T cells are activated. Since it has recently been shown that $CD8^+$ T cells must be re-activated within the tumour site to acquire effector functions (Prokhnevska *et al.*, 2023), our experimental set-up aimed to interrogate $CD8^+$ T cell activation, function and metabolism when stimulated in hypoxia. To do this $CD8^+$ T cells were freshly isolated from human PBMC, pre-conditioned overnight in 21%, 5% or 1% O_2, and activated the following morning with anti-CD3/CD28 in the same O_2 conditions prior to functional analyses. Studies utilising a similar protocol have demonstrated that freshly isolated $CD8^+$ T cells activated in hypoxia may have

impaired proliferation and cytokine production compared to $CD8^+$ T cells activated in normoxia. In mice, CTLs differentiated in hypoxia had impaired IFN-γ and IL-2 production and proliferation, compared to CTLs differentiated in normoxia (Caldwell *et al.*, 2001). However, the effects on cytokine production depend on method of T cell activation as PHA or concanavalin A stimulation of PBMC contrasted these results (Krieger, Landsiedel and Lawrence, 1996; Naldini *et al.*, 1997; Atkuri, Herzenberg and Herzenberg, 2005). Human T cells activated in hypoxia demonstrated impaired proliferation compared to those activated in normoxia (Atkuri, Herzenberg and Herzenberg, 2005; Larbi *et al.*, 2010). PBMC activated via PHA in hypoxia have been reported to accumulate in the G1 and G2 phases of the cell cycle and not to progress to the S and M phases efficiently, which ultimately inhibits their division and proliferation (Naldini and Carraro, 1999). In '**3. Results Chapter 1**', we demonstrate that healthy human $CD8^+$ T cells pre-conditioned and stimulated by anti-CD3/CD28 in hypoxia have impaired proliferation, and release and production of the cytokine IFN-γ compared to $CD8^+$ T cells stimulated in normoxia. Importantly, re-stimulation with PMA and ionomycin rescued the hypoxic-induced effect on IFN-γ production, indicating signalling impairments. A graphical abstract demonstrating the functional impacts of hypoxia on activated $CD8^+$ T cells is shown in **Figure 7.1.** The effect of hypoxia on $CD8^+$ T cell cytotoxicity and activation efficacy in previous literature has also not been clear. For example, CTLs differentiated in hypoxia had improved cytolytic capacity over those differentiated in normoxia, but no impact on Fas ligand or perforin was seen (Caldwell *et al.*, 2001). Furthermore, activation of CTLs appeared to be inhibited by hypoxia at the population level, but on an individual cell-cell basis, CTLs had an improved activation status in hypoxia vs. normoxia (Caldwell *et al.*, 2001). In our work,

the cytotoxic capacity and production and release of the cytokine TNF-α of $CD8^+$ T cells was not impaired by anti-CD3/CD28 stimulation in hypoxia **(Figure 7.1)**. However, the activation of $CD8^+$ T cells pre-conditioned and stimulated by anti-CD3/CD28 in hypoxia was impaired compared to those stimulated in normoxia **(Figure 7.1)**. Therefore, we are able to reproduce previous findings from other studies and expand knowledge to the impact of hypoxia on $CD8^+$ T cell cytokine production and release, cytotoxicity and activation.

We observed these same functional results in '**6. Results Chapter 4**' but with stimulation of $CD8^+$ T cells with a CD3xBCMA bispecific antibody and BCMA-expressing MM cell lines **(Figure 7.1)**. Bispecific antibodies, or BiTEs, which engage CD3 on the T cell and BCMA on the malignant plasma cell, are being tested in clinical trials for MM (Hipp *et al.*, 2017; Cohen, 2019; Shah and Mailankody, S, 2020; Topp *et al.*, 2020). We confirmed previously reported pre-clinical efficacy of the CD3xBCMA bispecific antibody with an increase in MM target cell death, release of perforin A and granzyme B, and upregulation of CD25 and CD69, with addition of the antibody (Hipp *et al.*, 2017) **(Figure 7.1)**. Cytotoxic capacity and killing ability of $CD8^+$ T cells was not impaired upon activation with the CD3xBCMA bispecific antibody in hypoxia, consistent with our earlier work with healthy human $CD8^+$ T cells in '**3. Results Chapter 1**' **(Figure 7.1)**. However, unlike with anti-CD3/CD28 stimulation, TNF-α production and release were impaired in hypoxia ('**6. Results Chapter 4**'). Thus, in a therapeutic context for MM, bispecific antibody activation may drive different signalling pathways or have a greater impact on the range $CD8^+$ T cell functions impaired in hypoxia, but further work is required to confirm this.

Intracellular cytokine experiments in '**3. Results Chapter 1**' revealed PMA/ionomycin stimulation to rescue the impairment on IFN-γ cytokine production by hypoxia compared to anti-CD3/CD28 stimulation. Since PMA/ionomycin stimulation bypasses T cell signalling pathways (Ai *et al.*, 2013), we next explored the impact of hypoxia on activation-induced $CD8^+$ T cell signalling in hypoxia. Upstream TCR (i.e., phosphorylation of Lck and ERK) and CD28 signalling (i.e., phosphorylation of AKT) appeared to be intact in $CD8^+$ T cells activated in hypoxia, however, downstream mTOR and NFAT signalling was impaired ('**4. Results Chapter 2**') **(Figure 7.1)**. The defect in NFAT signalling was consistent with an impairment of calcium flux across the membrane and confirmed utilising two murine reporter systems (Nr4a3-Tocky and Nur77-Tempo murine models) (Bending *et al.*, 2018; Elliot *et al.*, 2022). The alteration of calcium flux has been reported previously in $CD8^+$ T cells activated in hypoxia and suggested to be due to membrane depolarisation and inhibition of the voltage-dependent potassium ion (K^+) channel 3 (Kv1.3), which may contribute to the hypoxia-induced deficits on T cell activation (Robbins *et al.*, 2005; Szigligeti *et al.*, 2006). Future investigation could be conducted to confirm this theory in our experimental setting. The observation of reduced mTOR phosphorylation in $CD8^+$ T cells activated in hypoxia, together with reduced phosphorylation of its downstream effector p70S6K, has not been previously reported, therefore this knowledge is able to expand on the field.

mTOR is a key player in the metabolic reprogramming of $CD8^+$ T cells (Chapman and Chi, 2015), whereby resting cells upregulate aerobic glycolysis and to a lesser extent, oxidative metabolism, upon activation (Fox, Hammerman and Thompson, 2005; Gerriets and Rathmell, 2012). This enables the rapid increase in energy and biomass

required for their effector functions (Fox, Hammerman and Thompson, 2005; Gerriets and Rathmell, 2012). Expression of the transcription factor c-Myc, also responsible for directing $CD8^+$ T cell activation-induced metabolic reprogramming, was also downregulated in expression in hypoxia ('**4. Results Chapter 2**') (Wang *et al.*, 2011). Interestingly, we did not observe an increase in glucose uptake or lactate production of $CD8^+$ T cells activated in hypoxia, suggesting no increase in glycolysis as would be expected, which relates to the impairment in mTOR signalling observed ('**4. Results Chapter 2**'). However, bulk RNA-sequencing revealed the expression of glycolytic genes in $CD8^+$ T cells activated hypoxia to increase which contrasts with the suppression of mTOR signalling in hypoxia ('**5. Results Chapter 3**'). It would be interesting to follow up the mechanisms driving these findings.

To understand how the defect observed in mTOR signalling and c-Myc expression in hypoxia may alter $CD8^+$ T cell metabolic reprogramming we conducted ^{13}C-stable isotype tracing ('**4. Results Chapter 2**'). ^{13}C-glucose and -glutamine labelling into TCA cycle metabolites of $CD8^+$ T cells activated in hypoxia was significantly impaired compared to those activated in normoxia, albeit glucose to a lesser extent. Labelling into TCA cycle intermediates with ^{13}C-glutamine was greater than with ^{13}C-glucose, consistent with previous studies (Blagih *et al.*, 2015; Matheson *et al.*, 2022). ^{13}C-glutamine tracing also revealed the presence of the well-characterised hypoxic response, reductive carboxylation of α-KG to citrate, which is thought to be beneficial for lipid synthesis in hypoxia (Metallo *et al.*, 2011; Eales, Hollinshead and Tennant, 2016; Yoo *et al.*, 2020). The impact of hypoxia on $CD8^+$ T cell activation-induced glutaminolysis and glycolysis were consistent with a decrease in mitochondrial

membrane potential in hypoxia, as observed in previous studies (Zhang *et al.*, 2017). In contrast, whilst we observed a decrease in the production of mitochondrial ROS in $CD8^+$ T cells activated in hypoxia, the majority of other cell types increase the production of ROS in hypoxia (Hamanaka and Chandel, 2009; Zhang *et al.*, 2017). ROS are well known modulators of T cell signalling and the decrease in ROS production observed may be related to the impaired NFAT signalling of $CD8^+$ T cells in hypoxia (Sena *et al.*, 2013), however further experiments are required to confirm this. Overall, impairments in activation-induced glycolysis and glutaminolysis, and reductive carboxylation of α-KG to citrate, were observed in $CD8^+$ T cells stimulated in hypoxia **(Figure 7.1)**.

To explore the mechanistic basis for the functional and metabolic effects observed in $CD8^+$ T cells activated in hypoxia, we performed unbiased bulk RNA-sequencing to explore differentially expressed genes (DEGs) between non-activated and activated $CD8^+$ T cells in 21% and 1% O_2 ('**5. Results Chapter 3**'). Initially, we confirmed the significant changes in gene expression upon activation in $CD8^+$ T cells in hypoxia and normoxia. Interestingly, genes related to the cell cycle were upregulated in $CD8^+$ T cells activated in normoxia but not in hypoxia, consistent with the defect observed in proliferation in '**3. Results Chapter 1**'. DEGs between activated $CD8^+$ T cells in hypoxia and normoxia included various HIF-1α targets which were upregulated in hypoxia, as expected. These include genes for glycolysis and gluconeogenesis and those in the HIF-signalling pathway. Importantly, we identified DEGs upregulated in $CD8^+$ T cells in hypoxia that may be responsible for driving the suppression of mTOR. One gene of interest was BNIP3, encoding the protein BNIP3, which has been shown

to interact with and degrade an activator of mTOR, Rheb, in hypoxia, thus inhibiting mTOR activity (Li *et al.*, 2007; Zhang and Ney, 2009). BNIP3 expression was significantly upregulated in $CD8^+$ T cells activated in hypoxia, dependent on HIF-1α, and Rheb expression reciprocally reduced. To explore this mechanism further, we began to optimise a CRISPR-Cas9 system to knock down BNIP3 in primary human $CD8^+$ T cells and explore the functional effects in hypoxia and normoxia ('**5. Results Chapter 3**'). However, the electroporation process of the CRISPR-Cas9 system appeared to impact the function of normoxic cells and the usual impact of hypoxia on $CD8^+$ T cell function was not observed. Therefore, further optimisation of these systems is required to draw conclusions regarding the impact of BNIP3 upregulation on mTOR suppression in hypoxia.

To extend our work to a translational and clinical context, in '**6. Results Chapter 4**' we describe how we isolate $CD8^+$ T cells from matched PB and BM samples from newly diagnosed MM patients for analysis of functional and phenotypic markers. The MM BM TME is reported to be hypoxic (Asosingh *et al.*, 2005; Colla *et al.*, 2010), and it is also described that the BM environment of MM is suppressive for $CD8^+$ T cells (Gudgeon *et al.*, 2023). Thus, we wanted to understand if the hypoxic nature of the MM BM (compared to the PB) may contribute to this. This work is important since many immune-directed therapies being employed for use in MM rely on the effective functioning of $CD8^+$ T cells in the MM BM environment, for example with bispecific antibodies or CAR-T cells. With phenotypic analysis, we demonstrated a high proportion of EMRA $CD8^+$ T cells present in the PB and BM which is indicative of the patient age range in MM **(Table 2.1)** (Gudgeon *et al.*, 2023). However, it was difficult

to confirm that the BM had greater levels of hypoxia than the PB, based on expression of our hypoxic marker, BNIP3. Despite being a good marker of hypoxia, BNIP3 degrades quickly on return to normoxia, making it unsuitable for a read-out of hypoxia in patient samples that had been processed within atmospheric conditions.

The small number of patients recruited to this study also limited the statistical tests performed, however previous work from our laboratory has demonstrated a reduction in the production of IFN-γ and TNF-α in the BM compared to the PB of MM patients (Gudgeon *et al.*, 2023). However, notable findings of the analysis performed here are a reduction of c-Myc expression and Ki67 staining, or proliferation, of $CD8^+$ T cells present in the BM compared to the PB of MM patients. These effects are consistent with that observed in our *in vitro* experiments of healthy human $CD8^+$ T cells activated in hypoxia in '**3. Results Chapter 1**'. A reduction in mitochondrial membrane potential of $CD8^+$ T cells present in the BM compared to the PB of MM patients was also observed, consistent with that observed in '**4. Results Chapter 2**' with healthy human $CD8^+$ T cells activated in hypoxia. Therefore, whilst we are unable to directly prove the existence of a hypoxic environment in the BM of MM patients, similar functional and metabolic impairments are observed in the $CD8^+$ T cells present in the BM compared to the PB to what we see with healthy human $CD8^+$ T cells activated in hypoxia. It should be noted however that the TME is highly complex and other nutritional deficiencies or competition with other cell types may be responsible for driving similar effects, for example a lack of glucose or accumulation of lactate.

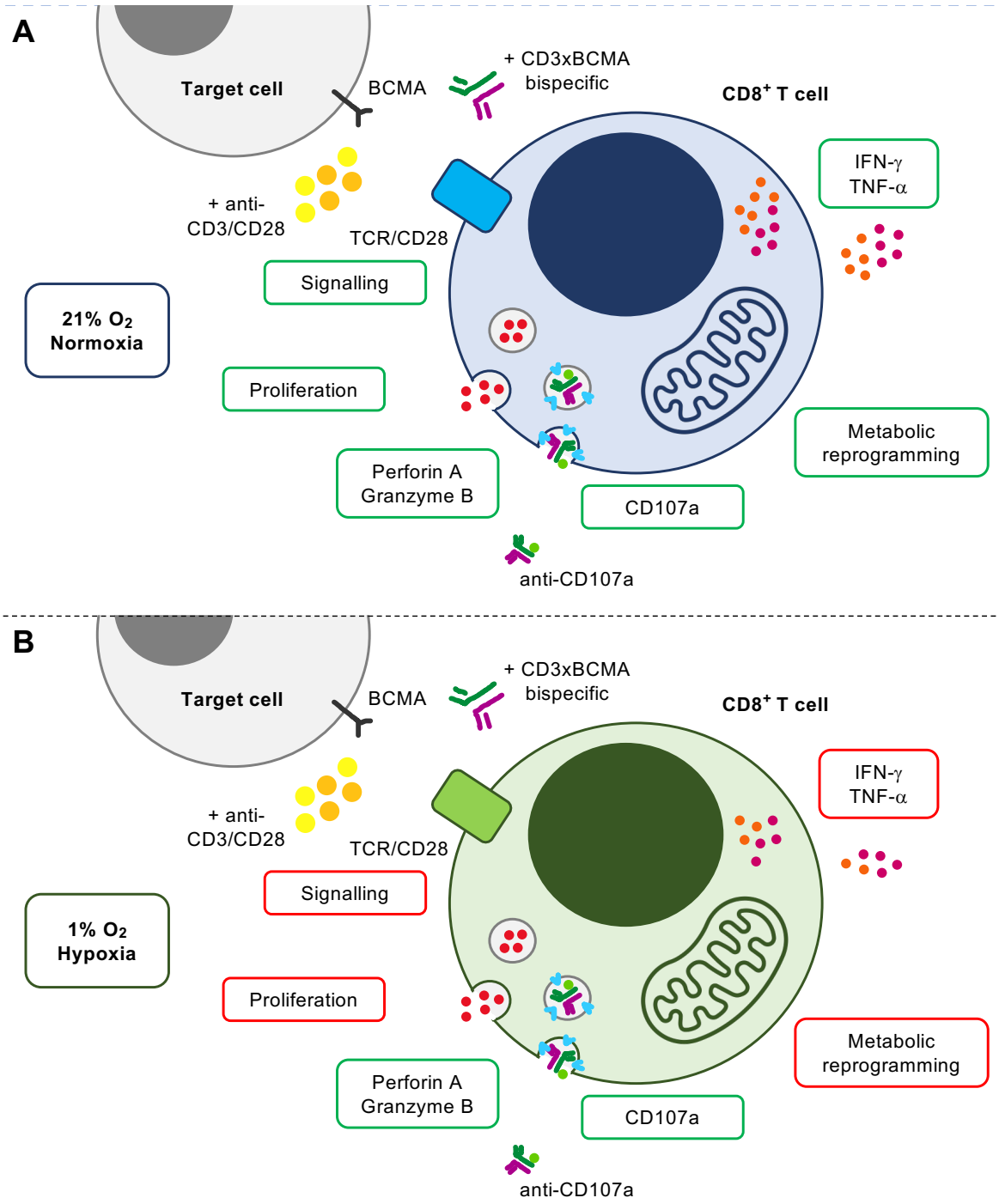

Figure 7.1. Graphical diagram to demonstrate the functional and metabolic impacts of hypoxia on activated $CD8^+$ T cells. A) $CD8^+$ T cell in 21% O_2 activated by anti-CD3/CD28 or a CD3xBCMA bispecific antibody. The cell is functionally able to proliferate, engage signalling pathways, kill target cells, release cytolytic granules perforin A and granzyme B, express the degranulation marker CD107a, produce and release IFN-γ and TNF-α cytokines and metabolically reprogram; B) $CD8^+$ T cell in 1% O_2 activated by anti-CD3/CD28 or a CD3xBCMA bispecific antibody. Impairments exist in proliferation, engaging signalling pathways (at the level of mTOR and NFAT), production and release of IFN-γ and TNF-α cytokines and metabolic reprogramming. The cell is functionally able to kill target cells, release cytolytic granules perforin A and granzyme B and express CD107a.

7.2. Future experiments:

Several future experiments could be performed to expand on the work conducted in this thesis. These will be structured according to their relevant chapter below.

3. Results Chapter 1: To expand on the work conducted in '**3. Results Chapter 1**' it would be useful to determine the response of $CD8^+$ T cells activated in hypoxia via an antigen-specific stimulation. This is relevant as activation of T cells in the cancer setting would be against a particular antigen and not in a polyclonal manner, as with anti-CD3/CD28 stimulation used in this thesis. We began exploring this using a mix of tetramers against Epstein Barr Virus (EBV) antigens, to which the majority of healthy donors should respond. However, the percentage of cells responding to the EBV tetramer mix was very small (< 1% of cells) and did not allow for robust conclusions to be made. It would be interesting to continue this work using enzyme-linked immunosorbent spot (ELISpot) assays to observe the amount of cytokine produced by EBV antigen-specific $CD8^+$ T cells in hypoxia compared to normoxia.

Given the differences observed in hypoxia between individual cytokines and with various stimulation methods, it may be interesting to explore the differences in regulation between IFN-γ and TNF-α release and production. For example, understanding why TNF-α is not impacted in hypoxia with anti-CD3/CD28 stimulation but is impacted in hypoxia with CD3xBCMA bispecific antibody stimulation of $CD8^+$ T cells. This may be done through the inhibition of different signalling pathways and metabolic processes. It may also be interesting to understand which stage of the cell cycle is blocked in $CD8^+$ T cells activated in hypoxia and subsequently inhibiting their

proliferation. This may be done with the use of fluorescent dyes and flow cytometric analysis.

4. Results Chapter 2: It may be interesting to build upon the exploration of $CD8^+$ T cell signalling in hypoxia in '**4. Results Chapter 2**' by understanding how the deficit in ROS production contributes to impaired T cell signalling in hypoxia. Experiments to induce ROS were trialled for use by employing mitoparaquat and DMNQ, however these did not successfully increase the levels of ROS production. If ROS levels were to be rescued, the function of $CD8^+$ T cells in hypoxia could be assessed to determine their relationship.

The metabolic work conducted in this thesis could also be expanded through use of unbiased approaches, such as proteomic and metabolomic analysis. This would provide a wide understanding to the alterations in metabolic networks when $CD8^+$ T cells are activated in hypoxia. Targeted analysis, for example with LC-MS, could provide more in-depth understanding of how lipid metabolism is altered in $CD8^+$ T cells activated in hypoxia and how this relates to the induction of reductive carboxylation. We also began exploring the Single Cell ENergetIc metabolism by profiling Translation inhibition (SCENITH) assay for use in $CD8^+$ T cells activated in hypoxia, however several of the inhibitors did not work as expected and further optimisation would be required to use this technique for metabolic analysis in our experimental setting. Finally, use of the Seahorse assay would be useful to determine oxygen consumption rate and extracellular acidification rate (as a measure of glycolysis) in $CD8^+$ T cells activated in hypoxia. However, this would require access to a Seahorse machine

located within an atmospheric controlled chamber to alter the oxygen status, and hypoxic and normoxic $CD8^+$ T cells could not be analysed in parallel.

5. Results Chapter 3: To further explore the mechanism behind mTOR suppression of $CD8^+$ T cells activated in hypoxia it would be useful to optimise the CRISPR-Cas9 system for knock out of BNIP3 in primary human T cells. This would provide an answer as to why normoxic cells appear to be impacted by electroporation and the usual hypoxic effects are not observed. Due to access issues, the recommended machine was not used for these initial CRISPR-Cas9 experiments. Therefore, we would first correct for this. If further exploration with the CRISPR-Cas9 system and electroporation for transfection proved inconclusive, we could trial lipofectamine transfection or siRNA knock-down as alternative methods to knock out BNIP3 in primary human T cells.

It would also be important to consider other mechanisms potentially responsible for the effects of hypoxia. For example, detailed interrogation of the AMPK or the NF-κB pathways with inhibition or gene knock-down/over-expression to help understand the effects of hypoxia on function and metabolism of $CD8^+$ T cells.

Since we observed BNIP3 as a key upregulated DEG in hypoxic activated $CD8^+$ T cells, it would also be useful to measure the levels of autophagy in $CD8^+$ T cells activated in hypoxia. For example, measurement of the levels of LC3 by flow cytometry in $CD8^+$ T cells in hypoxia compared to normoxia would provide a read-out of autophagy. This knowledge may also help us understand the degradation of BNIP3 on return to normoxia when analysing patient samples in '**6. Results Chapter 4**'.

6. Results Chapter 4: Initially, to extend work conducted in '**6. Results Chapter 4**', it would be important to increase the number of MM patients included in the phenotypic and functional analysis to observe more consistent effects and reach greater statistical power. To confirm existence of a hypoxic environment in the BM of MM patients we could stain with other well-recognised, potentially more stable, markers of hypoxia, for example LDHA. When the BM aspirates are collected from patients a BM trephine sample is also collected, immediately fixed and stored. Analysis of these samples would thus increase the chance of observing markers susceptible to degradation. Therefore, we could conduct confocal staining of these BM trephines of MM patients for hypoxic markers, such as BNIP3, REDD1 or LDHA, to help confirm the existence of a hypoxic environment in the BM.

Finally, future experiments could administer the hypoxic stain, pimonidazole, to MM patients prior to BM aspirate/trephine collection. This would stain hypoxic regions present in the BM and enable direct visualisation of cells exposed to hypoxia by multi-colour flow cytometry panels. The anti-pimonidazole antibody could be combined with phenotypic and functional markers of T cells, as well as other relevant immune cells, to give a detailed view of the relationship between hypoxia and the immune system in MM. Since this is *in vivo* work within patients, the suitable and relevant ethics application would have to be completed in order to conduct this work.

8. Conclusion

8. Conclusion

In this thesis I have shown that $CD8^+$ T cells pre-conditioned and activated in hypoxia have impaired activation, proliferation, and IFN-γ cytokine production and release. $CD8^+$ T cell cytotoxic capacity and TNF-α cytokine production and release are intact in hypoxia. A defect in activation-induced signalling in $CD8^+$ T cells in hypoxia exists at the level of NFAT and mTOR. $CD8^+$ T cells in hypoxia have impaired activation-induced upregulation of glutaminolysis and glycolysis required for the increased energy and biomass for their effector response, which is consistent with reduced c-Myc expression, mitochondrial membrane potential, and production of ROS. A potential BNIP3-Rheb interaction suppressing mTOR was explored with CRISPR-Cas9, however no direct conclusions on the mechanism can be drawn. To bring this work to a therapeutic context, $CD8^+$ T cells cultured with MM cell lines and a CD3xBCMA bispecific antibody demonstrated similar functional effects in hypoxia as with polyclonal stimulation. BM samples of MM patients were also analysed, identifying decreased proliferation and c-Myc expression compared to PB counterparts. This work has built on prior understanding in the field to show that the $CD8^+$ T cell dysfunction in hypoxia occurs at the level of mTOR and NFAT and extends to a defect in activation-induced metabolic reprogramming. The work in this thesis unifies past disparate findings within the literature by reproducing functional impacts on $CD8^+$ T cells activated in hypoxia. I have also highlighted the importance of the conditions of hypoxic exposure on downstream effects, which should be taken into account for future research in the field. Given the hypoxic nature of the TME, including in MM, this work could be instrumental in understanding the limitations of response with immune-directed therapies, which ultimately, may improve overall patient outcomes.

List of references

List of references

Aguilera, K.Y. and Brekken, R.A. (2014) 'Hypoxia Studies with Pimonidazole *in vivo*', *Bio-protocol,* 4 (10): pp. e1254. doi: 10.21769/bioprotoc.1254.

Ai, W., Li, H., Song, N., Li, L. and Chen, H. (2013) 'Optimal Method to Stimulate Cytokine Production and Its Use in Immunotoxicity Assessment', *International Journal of Environmental Research and Public Health,* 10 (9): pp. 3834-3842. doi: 10.3390/ijerph10093834.

Aktas, E., Kucuksezer, U.C., Bilgic, S., Erten, G. and Deniz, G. (2009) 'Relationship between CD107a expression and cytotoxic activity', *Cellular Immunology,* 254 (2): pp. 149-154. doi: 10.1016/j.cellimm.2008.08.007.

Alabduladhem, T.O. and Bordoni, B. (2022) 'Physiology, Krebs Cycle', in StatPearls. StatPearls Publishing. Available at: https://www.ncbi.nlm.nih.gov/books/NBK556032/ (Accessed: 22 March 2024)

Albagoush, S.A., Shumway, C. and Azevedo, A.M. (2023) 'Multiple Myeloma', in StatPearls. StatPearls Publishing. Available at: https://www.ncbi.nlm.nih.gov/books/NBK534764/ (Accessed: 8 February 2024)

Alberts, B., Johnson, A., Lewis, J., Raff, M., Roberts, K. and Walter, P. (2002) 'The adaptive immune system', in *Molecular Biology of the Cell*. 4th edition. Garland Science. Available at: https://www.ncbi.nlm.nih.gov/books/NBK21070/ (Accessed: 24 January 2024)

Al-Khami, A.A., Rodriguez, P.C. and Ochoa, A.C. (2017) 'Energy metabolic pathways control the fate and function of myeloid immune cells', *Journal of Leukocyte Biology,* 102 (2): pp. 369-380. doi: 10.1189/jlb.1VMR1216-535R.

Anders, S., Pyl, P.T. and Huber, W. (2015) 'HT-Seq - a Python framework to work with high-throughput sequencing data', *Bioinformatics,* 31 (2): pp. 166-169. doi: 10.1093/bioinformatics/btu638.

Andrews, S. (2010) 'Babraham Bioinformatics – FastQC A Quality Control tool for High Throughput Sequence Data'. (Version 0.11.6) [Computer programme]. Available at: https://www.bioinformatics.babraham.ac.uk/projects/fastqc/.

Argüello, R.J., Combes, A.J., Char, R., Gigan, J-P., Baaziz, A.I., Bousiquot, E., Camosseto, V., Samad, B., Tsui, J., Yan, P., Boissonneau, S., Figarella-Branger, D., Gatti, E., Tabouret, E., Krummel, M.F. and Pierre, P. (2020) 'SCENITH: A flow cytometry based method to functionally profile

energy metabolism with single cell resolution', *Cell Metabolism,* 32 (6): pp. 1063-1075.e7. doi: 10.1016/j.cmet.2020.11.007.

Arnold, P.K. and Finley, L.W.S. (2023) 'Regulation and function of the mammalian tricarboxylic acid cycle', *Journal of Biological Chemistry,* 299 (2): pp. 102838. doi: 10.1016/j.jbc.2022.102838.

Asosingh, K., De Raeve, H., De Ridder, M., Storme, G.A., Willems, A., Riet, I.V., Camp, B.V. and Vanderkerken, K. (2005) 'Role of the hypoxic bone marrow microenvironment in 5T2MM murine myeloma tumor progression', *Haematologica,* 90 (6): pp. 810-817. Available at: https://pubmed.ncbi.nlm.nih.gov/15951294/ (Accessed 22 April 2024)

Atkuri, K.R., Herzenberg, L.A. and Herzenberg, L.A. (2005) 'Culturing at atmospheric oxygen levels impacts lymphocyte function', *Proceedings of the National Academy of Sciences of the United States of America,* 102 (10): pp. 3756-3759. doi: 10.1073/pnas.0409910102.

Atkuri, K.R., Herzenberg, L.A., Niemi, A-K., Cowan, T. and Herzenberg, L.A. (2007) 'Importance of culturing primary lymphocytes at physiological oxygen levels', *Proceedings of the National Academy of Sciences of the United States of America,* 104 (11): pp. 4547-4552. doi: 10.1073/pnas.0611732104.

Atsaves, V., Leventaki, V., Rassidakis, G.Z. and Claret, F.X. (2019) 'AP-1 Transcription Factors as Regulators of Immune Responses in Cancer', *Cancers (Basel),* 11 (7): pp. 1037. doi: 10.3390/cancers11071037.

Aviner, R. (2020) 'The science of puromycin: From studies of ribosome function to applications in biotechnology', *Computational and Structural Biotechnology Journal,* 18: pp. 1074-1083. doi: 10.1016/j.csbj.2020.04.014.

Bain, J., Plater, L., Elliott, M., Shpiro, N., Hastie, C.J., McLauchlan, H., Klevernic, I., Arthur, J.S.C., Alessi, D.R. and Cohen, P. (2007) 'The selectivity of protein kinase inhibitors: a further update', *Biochemical Journal,* 408 (3): pp. 297-315. doi: 10.1042/BJ20070797.

Bandyopadhyay, R.S., Phelan, M. and Faller, D.V. (1995) 'Hypoxia induces AP-1 regulated genes and AP-1 transcription factor binding in human endothelial and other cell types', *Biochimica et Biphysica Acta,* 1264 (1): pp. 72-78. doi: 10.1016/0167-4781(95)00116-x-.

Barnes, S.E., Wang, Y., Chen, L., Molinero, L.L., Gajewski, T.F., Evaristo, C. and Alegre, M-L. (2015) 'T cell-NF-kB activation is required for tumour control *in vivo*', *The Journal for ImmunoTherapy of Cancer,* 3: pp. 1. doi: 10.1186/s40425-014-0045-x.

Bataille, R., Jégo, G., Robillard, N., Barillé-Nion, S., Harousseau, J-L., Moreau, P., Amiot, M. and Pellat-Deceunynck, C. (2006) 'The phenotype of normal, reactive and malignant plasma cells. Identification of "many and multiple myelomas" and of new targets for myeloma therapy', *Haematologica,* 91 (9): pp. 1234-1240. Available at: https://pubmed.ncbi.nlm.nih.gov/16956823/ (Accessed 19 April 2024)

Bauer, D.E., Harris, M.H., Plas, D.R., Lum, J.J., Hammerman, P.S., Rathmell, J.C., Riley, J.L. and Thompson, C.B. (2004) 'Cytokine stimulation of aerobic glycolysis in haematopoietic cells exceeds proliferative demand', *The FASEB Journal,* 18 (11): pp. 1303-1305. doi: 10.1096/fj.03-1001fje.

Beach, D., Gonen, R., Bogin, Y., Reischl, I.G. and Yablonski, D. (2007) 'Dual role of SLP-76 in mediating T cell receptor-induced activation of phospholipase C-gamma 1', *Journal of Biological Chemistry,* 282 (5): pp. 2937-2946. doi: 10.1074/jbc.M606697200.

Bending, D., Martin, P.P., Paduraru, A., Ducker, C., Marzaganov, E., Laviron, M., Kitano, S., Miyachi, H., Crompton, T. and Ono, M. (2018) 'A timer for analyzing temporally dynamic changes in transcription during differentiation in vivo', *Journal of Cell Biology,* 217 (8): pp. 2931-2950. doi: 10.1083/jcb.201711048.

Benjamini, Y., Krieger, A.M. and Yekutieli, D. (2006) 'Adaptive linear step-up procedures that control the false discovery rate', *Biometrika,* 93 (3): pp. 491-507. doi: 10.1093/biomet/93.3.491.

Benson Jr., D.M., Bakan, C.E., Mishra, A., Hofmeister, C.C., Efebera, Y., Becknell, B., Baiocchi, R.A., Zhang, J., Yu, J., Smith, M.K., Greenfield, C.N., Porcu, P., Devine, S.M., Rotem-Yehudar, R., Lozanski, G., Byrd, J.C. and Caligiuri, M.A. (2010) 'The PD-1/PD-L1 axis modulates the natural killer cell versus multiple myeloma effect: a therapeutic target for CT-011, a novel monoclonal anti-PD-1 antibody', *Blood,* 116 (13): pp. 2286-2294. doi: 10.1182/blood-2010-02-271874.

Berridge, M.J. (2009) 'Inositol triphosphate and calcium signalling mechanisms', *Biochimica et Biophysica Acta,* 1793 (6): pp. 933-940. doi: 10.1016/j.bbamcr.2008.10.005.

Bird, S.A. and Boyd, K. (2019) 'Multiple myeloma: an overview of management', *Palliative Care and Social Practice,* 13: pp. 1178224219868235. doi: 10.1177/1178224219868235.

Bishop, E.L. (2023) 'Interrogating a role for tumour necrosis factor alpha in $CD4^+$ T cell metabolism in health and inflammatory disease', University of Birmingham. Ph.D. Available from: http://etheses.bham.ac.uk/id/eprint/13651.

Blagih, J., Coulombe, F., Vincent, E.E., Dupuy, F., Galicia-Vazquez, G., Yurchenko, E., Rassi, T.C., van der Windt, G.J.W., Viollet, B., Pearce, E.L., Pelletier, J., Piccirillo, C.A., Krawczyk, C.M., Divangahi, M. and Jones, R.G. (2015) 'The energy sensor AMPK regulates T cell metabolic adaptation and effector responses in vivo', *Immunity,* 42 (1): pp. 41-54. doi: 10.1016/j.immuni.2014.12.030.

Bommhardt, U., Schraven, B. and Simeoni, L. (2019) 'Beyond TCR Signaling: Emerging Functions of Lck in Cancer and Immunotherapy', *International Journal of Molecular Sciences,* 20 (14): pp. 3500. doi: 10.3390/ijms20143500.

Bootman, M.D., Chehab, T., Bultynck, G., Parys, J.B. and Rietdorf, K. (2018) 'The regulation of autophagy by calcium signals: Do we have a consensus?', *Cell Calcium,* 70: pp. 32-46. doi: 10.1016/j.ceca.2017.08.005.

Bootman, M.D. and Bultynck, G. (2020) 'Fundamentals of Cellular Calcium Signaling: A Primer', *Cold Spring Harbor Perspectives in Biology,* 12 (1): pp. a038802.

Brauneck, F., Haag, F., Woost, R., Wildner, N., Tolosa, E., Rissiek, A., Vohwinkel, G., Wellbrock, J., Bokemeyer, C., Schulze zur Wiesch, J., Ackermann, C. and Fiedler, W. (2021) 'Increased frequency of $TIGIT^+CD73\text{-}CD8^+$ T cells with a $TOX^+TCF\text{-}1low$ profile in patients with newly diagnosed and relapsed AML', *Oncoimmunology,* 10 (1): pp. 1930391. doi: 10.1080/2162402X.2021.1930391.

Brehm, M.A., Daniels, K.A. and Welsh, R.M. (2005) 'Rapid production of TNF-alpha following TCR engagement of naïve CD8 T cells', *The Journal of Immunology,* 175 (8): pp. 5043-5049. doi: 10.4049/jimmunol.175.8.5043.

Brown, R.D., Pope, B., Yuen, E., Gibson, J. and Joshua, D.E. (1998) 'The expression of T cell related costimulatory molecules in multiple myeloma', *Leukemia and Lymphoma,* 31 (3-4): pp. 379-384. doi: 10.3109/10428199809059231.

Brugarolas, J., Lei, K., Hurley, R.L., Manning, B.D., Reiling, J.H., Hafen, E., Witters, L.A., Ellisen, L.W. and Kaelin Jr, W.G. (2004) 'Regulation of mTOR function in response to hypoxia by REDD1 and the TSC1/TSC2 tumor suppressor complex', *Genes and Development,* 18 (23): pp. 2893-2904. doi: 10.1101/gad.1256804.

Bruzzese, L., Fromonot, J., By, Y., Durand-Gorde, J-M., Condo, J., Kipson, N., Guieu, R., Fenouillet, E. and Ruf, J. (2014) 'NF-κB enhanced hypoxia-driven T-cell immunosuppression via upregulation of adenosine A(2A) receptors', *Cellular Signalling,* 26 (5): pp. 1060-1067. doi: 10.1016/j.cellsig.2014.01.024.

Bushnell, B. (2014) 'BBMap: A Fast, Accurate, Splice-Aware Aligner'. (Version 37.99) [Computer Programme]. Available at: https://sourceforge.net/projects/bbmap/.

Busuttil, V., Droin, N., McCormick, L., Bernassola, F., Candi, E., Melino, G. and Green, D.R. (2010) 'NF-κB inhibits T-cell activation-induced, p73-dependent cell death by induction of MDM2', *Proceedings of the National Academy of Sciences of the United States of America,* 107 (42): pp. 18061-18066. doi: 10.1073/pnas.1006163107.

Caldwell, C.C., Kojima, H., Lukashev, D., Armstrong, J., Farber, M., Apasov, S.G. and Sitkovsky, M.V. (2001) 'Differential effects of physiologically relevant hypoxic conditions on T lymphocyte development and effector functions', *The Journal of Immunology,* 167 (11): pp. 6140-6149. doi: 10.4049/jimmunol.167.11.6140.

Cancer Research UK. (2015) *Cancer Statistics for the UK*. Available at: https://www.cancerresearchuk.org/health-professional/cancer-statistics-for-the-uk (Accessed: 9 May 2023)

Cancer Research UK. (2015) *Myeloma statistics.* Available at: https://www.cancerresearchuk.org/health-professional/cancer-statistics/statistics-by-cancer-type/myeloma (Accessed 8 February 2024)

Carlson, M. (2019) 'org.Hs.eg.db'. (R package version 3.12.0) [Computer programme]. Available at: https://bioconductor.org/packages/org.Hs.eg.db/.

Carr, E.L., Kelman, A., Wu, G.S., Gopaul, R., Senkevitch, E., Aghvanyan, A., Turay, A.M. and Frauwirth, K.A. (2010) 'Glutamine uptake and metabolism are coordinately regulated by ERK/MAPK during

T lymphocyte activation', *The Journal of Immunology,* 185 (2): pp. 1037-1044. doi: 10.4049/jimmunol.0903586.

Cham, C.M. and Gajewski, T.F. (2005) 'Glucose availability regulates IFN-gamma production and p70S6 kinase activation in CD8+ effector T cells', *The Journal of Immunology,* 174 (8): pp. 4670-4677. doi: 10.4049/jimmunol.174.8.4670.

Cham, C.M., Driessens, G., O'Keefe, J.P. and Gajewski, T.F. (2008) 'Glucose Deprivation Inhibits Multiple Key Gene Expression Events and Effector Functions in $CD8^+$ T Cells', *European Journal of Immunology,* 38 (9): pp. 2438-2450. doi: 10.1002/eji.200838289.

Chang, C.H., Curtis, J.D., Maggi, L.B., Faubert, B., Villarino, A.V., O'Sullivan, D., Huang, S.C-C., van der Windt, G.J.W., Blagih, J., Qiu, J., Weber, J.D., Pearce, E.J., Jones, R.G. and Pearce, E.L. (2013) 'Posttranscriptional control of T cell effector function by aerobic glycolysis', *Cell,* 153 (6): pp. 1239-1251. doi: 10.1016/j.cell.2013.05.016.

Chapman, N.M. and Chi, H. (2015) 'mTOR Links Environmental Signals to T Cell Fate Decisions', *Frontiers in Immunology,* 5: pp. 686. doi: 10.3389/fimmu.2014.00686.

Chee, N.T., Lohse, I. and Brothers, S.P. (2019) 'mRNA-to-protein translation in hypoxia', *Molecular Cancer,* 18 (1): pp. 49. doi: 10.1186/s12943-019-0968-4.

Chi, H. (2012) 'Regulation and function of mTOR signalling in T cell fate decision', *Nature Reviews Immunology,* 12 (5): pp. 325-338. doi: 10.1038/nri3198.

Chong, H., Vikis, H.G. and Guan, K-L. (2003) 'Mechanisms of regulating the Raf kinase family', *Cellular Signalling,* 15 (5): pp. 463-469. doi: 10.1016/s0898-6568(02)00139-0.

Chopp, L., Redmond, C., O'Shea, J.J. and Schwartz, D.M. (2023) 'From thymus to tissues and tumours: A review of T-cell biology', *The Journal of Allergy and Clinical Immunology,* 151 (1): pp. 81-97. doi: 10.1016/j.jaci.2022.10.011.

Chow, D.C., Wenning, L.A., Miller, W.M. and Papoutsakis, E.T. (2001) 'Modeling pO(2) distributions in the bone marrow hematopoietic compartment. I. Krogh's model', *Biophysical Journal,* 81 (2): pp. 675-684. doi: 10.1016/S0006-3495(01)75732-3.

Chu, X., Tian, W., Wang, Z., Zhang, J. and Zhou, R. (2023) 'Co-inhibition of TIGIT and PD-1/PD-L1 in Cancer Immunotherapy: Mechanisms and Clinical Trials', *Molecular Cancer,* 22 (1): pp. 93. doi: 10.1186/s12943-023-01800-3.

Clever, D., Roychoudhuri, R., Constantinides, M.G., Askenase, M.H., Sukumar, M., Klebanoff, C.A., Eil, R.L., Hickman, H.D., Yu, Z., Pan, J.H., Palmer, D.C., Phan, A.T., Goulding, J., Gattinoni, L., Goldrath, A.W., Belkaid, Y. and Restifo, N.P. (2016) 'Oxygen Sensing by T Cells Establishes an Immunologically Tolerant Metastatic Niche', *Cell,* 166 (5): pp. 1117-1131. doi: 10.1016/j.cell.2016.07.032.

Cohen, A.D. (2019) 'Myeloma: next generation immunotherapy', *Hematology the American Society of Hematology Education Program',* 2019 (1): pp. 266-272. doi: 10.1182/hematology.2019000068.

Colla, S., Storti, P., Donofrio, G., Todoerti, K., Bolzoni, M., Lazzaretti, M., Abeltino, M., Ippolito, L., Neri, A., Ribatti, D., Rizzoli, V., Martella, E. and Giuliani, N. (2010) 'Low bone marrow oxygen tension and hypoxia-inducible factor-1α overexpression characterize patients with multiple myeloma: role on the transcriptional and proangiogenic profiles of CD138(+) cells', *Leukemia,* 24 (11): pp. 1967-1970. doi: 10.1038/leu.2010.193.

Colombani, T., Rogers, Z.J., Bhatt, K., Sinoimeri, J., Gerbereux, L., Hamrangsekachaee, M. and Bencherif, S.A. (2023) 'Hypoxia-inducing cryogels uncover key cancer-immune cell interactions in an oxygen-deficient tumor microenvironment', *Bioactive Materials,* 29: pp. 279-295. doi: 10.1016/j.bioactmat.2023.06.021.

Copland, A., Mackie, G.M., Scarfe, L., Lecky, D.A.J., Gudgeon, N., McQuade, R., Ono, M., Barthel, M., Hardt, W-D., Ohno, H., Dimeloe, S., Bending, D. and Maslowski, K.M. (2023) '*Salmonella* cancer therapy metabolically disrupts tumours at the collateral cost of T cell immunity' [Pre-print] (Accessed 14 July 2024). doi: 10.1101/2023.01.12.523780.

Corral, L.G., Haslett, P.A., Muller, G.W., Chen, R., Wong, L.M., Ocampo, C.J., Patterson, R.T., Stirling, D.I. and Kaplan, G. (1999) 'Differential cytokine modulation and T cell activation by two distinct classes of thalidomide analogues that are potent inhibitors of TNF-alpha', *The Journal of Immunology,* 163 (1): pp. 380-386. Available at: https://pubmed.ncbi.nlm.nih.gov/10384139/ (Accessed: 19 April 2024)

Corton, J.M., Gillespie, J.G. and Hardie, D.G. (1994) 'Role of the AMP-activated protein kinase in the cellular stress response', *Current Biology,* 4 (4): 315-324. doi: 10.1016/s0960-9822(00)00070-1.

Courtney, A.H., Lo, W-L. and Weiss, A. (2018) 'TCR Signaling: Mechanisms of Initiation and Propagation', *Trends in Biochemical Sciences,* 43 (2): pp. 108-123. doi: 10.1016/j.tibs.2017.11.008.

Cowan, A.J., Green, D.J., Kwok, M., Lee, S., Coffey, D.G., Holmberg, L.A., Tuazon, S., Gopal, A.K. and Libby, E.N. (2022) 'Diagnosis and Management of Multiple Myeloma: A Review', *JAMA,* 327 (5): pp. 464-477. doi: 10.1001/jama.2022.0003.

Curtsinger, J.M., Lins, D.C. and Mescher, M.F. (2003) 'Signal 3 determines tolerance versus full activation of naïve CD8 T cells: dissociating proliferation and development of effector function', *Journal of Experimental Medicine,* 197 (9): pp. 1141-1151. doi: 10.1084/jem.20021910.

de Almeida, P.E., Mak, J., Hernandez, G., Jesudason, R., Herault, A., Javinal, V., Borneo, J., Kim, J.M. and Walsh, K.B. (2020) 'Anti-VEGF Treatment Enhances $CD8^+$ T-cell Antitumor Activity by Amplifying Hypoxia', *Cancer Immunology Research,* 8 (6): pp. 806-818. doi: 10.1158/2326-6066.CIR-19-0360.

DeBerardinis, R.J. and Thompson, C.B. (2012) 'Cellular metabolism and disease: what do metabolic outliers teach us?', *Cell,* 148 (6): pp. 1132-1144. doi: 10.1016/j.cell.2012.02.032.

Delgoffe, G.M., Kole, T.P., Zheng, Y., Zarek, P.E., Matthews, K.L., Xiao, B., Worley, P.F., Kozma, S.C. and Powell, J.D. (2009) 'The mTOR kinase differentially regulates effector and regulatory T cell lineage commitment', *Immunity,* 30 (6): pp. 832-844. doi: 10.1016/j.immuni.2009.04.014.

Dengler, V.L., Galbraith, M. and Espinosa, J.M. (2014) 'Transcriptional regulation by hypoxia inducible factors', *Critical Reviews in Biochemistry and Molecular Biology,* 49 (1): pp. 1-15. doi: 10.3109/10409238.2013.838205.

De Ponte Conti, B., Miluzio, A., Grassi, F., Abrignani, S., Biffo, S. and Ricciardi, S. (2021) 'mTOR-dependent translation drives tumor infiltrating $CD8^+$ effector and $CD4^+$ Treg cells expansion', *ELife,* 10: pp. e69015. doi: 10.7554/eLife.69015.

Deshpande, O.A. and Mohiuddin, S.S. (2023) 'Biochemistry, Oxidative Phosphorylation', in StatPearls. StatPearls Publishing. Available at: https://www.ncbi.nlm.nih.gov/books/NBK553192/ (Accessed 17 May 2023)

Di Benedetto, S., Derhovanessian, E., Steinhagen-Thiessen, E., Goldeck, D., Müller, L. and Pawelec, G. (2015) 'Impact of age, sex and CMV-infection on peripheral T cell phenotypes: results from

the Berlin BASE-II Study', *Biogerontology,* 16 (5): pp. 631-643. doi: 10.1007/s10522-015-9563-2.

D'Ignazio, L. and Rocha, S. (2016) 'Hypoxia Induced NF-κB', *Cells,* 5 (1): pp. 10. doi: 10.3390/cells5010010.

Dimeloe, S., Burgener, A-V., Grählert, J. and Hess, C. (2017) 'T-cell metabolism governing activation, proliferation and differentiation; a modular view', *Immunology,* 150 (1): pp. 35-44. doi: 10.1111/imm.12655.

Dobin, A., Davis, C.A., Schlesinger, F., Drenkow, J., Zaleski, C., Jha, S., Batut, P., Chaisson, M. and Gingeras, T.R. (2013) 'STAR: ultrafast universal RNA-seq aligner', *Bioinformatics (Oxford England),* 29 (1): pp. 15-21. doi: 10.1093/bioinformatics/bts635.

Dodd, K.M., Yang, J., Shen, M.H., Sampson, J.R. and Tee, A.R. (2015) 'mTORC1 drives HIF-1α and VEGF-A signalling via multiple mechanisms involving 4E-BP1, S6K1 and STAT3', *Oncogene,* 34 (17): pp. 2239-2250. doi: 10.1038/onc.2014.164.

Doedens, A.L., Phan, A.T., Stradner, M.H., Fujimoto, J.K., Nguyen, J.V., Yang, E., Johnson, R.S. and Goldrath, A.W. (2013) 'Hypoxia-inducible factors enhance the effector responses of CD8(+) T cells to persistent antigen', *Nature Immunology,* 14 (11): pp. 1173-1182. doi: 10.1038/ni.2714.

Druker, J., Wilson, J.W., Child, F., Shakir, D., Fasanya, T. and Rocha, S. (2021) 'Role of Hypoxia in the Control of the Cell Cycle', *International Journal of Molecular Sciences',* 22 (9): pp. 4874. doi: 10.3390/ijms22094874.

Dustin, M.L. (2014) 'The immunological synapse', *Cancer Immunology Research,* 2 (11): pp. 1023-1033. doi: 10.1158/2326-6066.CIR-14-0161.

Eales, K.L., Hollinshead, K.E.R. and Tennant, D.A. (2016) 'Hypoxia and metabolic adaptation of cancer cells', *Oncogenesis,* 5 (1): pp. e190. doi: 10.1038/oncsis.2015.50.

Ebert, B.L. and Bunn, H.F. (1998) 'Regulation of transcription by hypoxia requires a multiprotein complex that includes hypoxia-inducible factor 1, an adjacent transcription factor, and p300/CREB binding protein', *Molecular and Cellular Biology,* 18 (7): pp. 4089-4096. doi: 10.1128/MCB.18.7.4089.

Ebinu, J.O., Bottorff, D.A., Chan, E.Y., Stang, S.L., Dunn, R.L. and Stone, J.C. (1998) 'RasGRP, a Ras guanyl nucleotide-releasing protein with calcium- and diacylglycerol-binding motifs', *Science,* 280 (5366): pp. 1082-1086. doi: 10.1126/science.280.5366.1082.

Edmead, C.E., Patel, Y.I., Wilson, A., Boulougouris, G., Hall, N.D., Ward, S.G. and Sansom, D.M. (1996) 'Induction of activator protein (AP)-1 and nuclear factor-kappa B by CD28 stimulation involves both phosphatidylinositol 3-kinase and acidic sphingomyelinase signals', *The Journal of Immunology,* 157 (8): pp. 3290-3297. Available at: https://pubmed.ncbi.nlm.nih.gov/8871623/

Egan, D.F., Shackelford, D.B., Mihaylova, M.M., Gelino, S., Kohnz, R.A., Mair, W., Vasquez, D.S., Joshi, A., Gwinn, D.A., Taylor, R., Asara, J.M., Fitzpatrick, J., Dillin, A., Viollet, B., Kundu, M., Hansen, M. and Shaw, R.J. (2011) 'Phosphorylation of ULK1 (hATG1) by AMP-activated protein kinase connects energy sensing to mitophagy', *Science,* 331 (6016): pp. 456-461. doi: 10.1126/science.1196371.

Elliot, T.A.E., Jennings, E.K., Lecky, D.A.J., Rouvray, S., Mackie, G.M., Scarfe, L., Sheriff, L., Ono, M., Maslowski, K.M. and Bending, D. (2022) 'Nur77-Tempo mice reveal T cell steady state antigen recognition', *Discovery Immunology,* 1 (1): pp. kyac009. doi: 10.1093/discim/kyac009.

Emerling, B.M., Viollet, B., Tormos, K.V. and Chandel, N.S. (2007) 'Compound C inhibits hypoxic activation of HIF-1 independent of AMPK', *FEBS Letters,* 581 (29): pp. 5727-5731. doi: 10.1016/j.febslet.2007.11.038.

Epstein, A.C., Gleadle, J.M., McNeill, L.A., Hewitson, K.S., O'Rourke, J., Mole, D.R., Mukherji, M., Metzen, E., Wilson, M.I., Dhanda, A., Tian, Y.M., Masson, N., Hamilton, D.L., Jaakkola, P., Barstead, R., Hodgkin, J., Maxwell, P.H., Pugh, C.W., Schofield, C.J. and Ratcliffe, P.J. (2001) 'C.elegans EGL-9 and mammalian homologs define a family of dioxygenases that regulate HIF by prolyl hydroxylation', *Cell,* 107 (1): pp. 43-54. doi: 10.1016/s0092-8674(01)00507-4.

Esensten, J.H., Helou, Y.A., Chopra, G., Weiss, A. and Bluestone, J.A. (2017) 'CD28 costimulation: from mechanism to therapy', *Immunity,* 44 (5): pp. 973-988. doi: 10.1016/j.immuni.2016.04.020.

Finlay, D.K., Rosenzweig, E., Sinclair, L.V., Feijoo-Carnero, C., Hukelmann, J.L., Rolf, J., Panteleyev, A.A., Okkenhaug, K. and Cantrell, D.A. (2012) 'PDK1 regulation of mTOR and hypoxia-inducible factor 1 integrate metabolism and migration of CD8+ T cells', *Journal of Experimental Medicine,* 209 (13): pp. 2441-2453. doi: 10.1084/jem.20112607.

Finley, L.W.S. (2023) 'What is cancer metabolism?', *Cell,* 186 (8): pp. 1670-1688. doi: 10.1016/j.cell.2023.01.038.

Fox, C.J., Hammerman, P.S. and Thompson, C.B. (2005) 'Fuel feeds function: energy metabolism and the T-cell response', *Nature Reviews Immunology,* 5 (11): pp. 844-852. doi: 10.1038/nri1710.

Fracchia, K.M., Pai, C.Y. and Walsh, C.M. (2013) 'Modulation of T Cell Metabolism and Function Through Calcium Signaling', *Frontiers in Immunology,* 4: pp. 324. doi: 10.3389/fimmu.2013.00324.

Frassanito, M.A., Cusmai, A. and Dammacco, F. (2001) 'Deregulated cytokine network and defective Th1 immune response in multiple myeloma', *Clinical and Experimental Immunology,* 125 (2): pp. 190-197. doi: 10.1046/j.1365-2249.2001.01582.x.

Fukuda, R., Zhang, H., Kim, J-W., Shimoda, L., Dang, C.V. and Semenza, G.L. (2007) 'HIF-1 regulates cytochrome oxidase subunits to optimize efficiency of respiration in hypoxic cells', *Cell,* 129 (1): pp. 111-122. doi: 10.1016/j.cell.2007.01.047.

Gallagher, M.P., Conley, J.M. and Berg, L.J. (2018) 'Peptide Antigen Concentration Modulates Digital NFAT1 Activation in Primary Mouse Naïve $CD8^+$ T Cells as Measured by Flow Cytometry of Isolated Cell Nuclei', *ImmunoHorizons,* 2 (7): pp. 208-215. doi: 10.4049/immunohorizons.1800032.

Georgiev, P., Belikoff, B.B., Hatfield, S., Ohta, A., Stikovsky, M.V. and Lukashev, D. (2013) 'Genetic deletion of the alternative isoform I.1 in HIF-1a in T cells enhances anti-bacterial immune response and improves survival in the model of bacterial peritonitis in mice', *European Journal of Immunology,* 43 (3): pp. 655-666. doi: 10.1002/eji.201242765.

Gerondakis, S., Fulford, T.S., Messina, N.L. and Grumont, R.J. (2014) 'NF-κB control of T cell development', *Nature Immunology,* 15 (1): pp. 15-25. doi: 10.1038/ni.2785.

Gerriets, V.A. and Rathmell, J.C. (2012) 'Metabolic pathways in T cell fate and function', *Trends in Immunology,* 33 (4): pp. 168-173. doi: 10.1016/j.it.2012.01.010.

Gertz, M.A. and Dingli, D. (2014) 'How we manage autologous stem cell transplantation for patients with multiple myeloma', *Blood,* 124 (6): pp. 882-890. doi: 10.1182/blood-2014-03-544759.

Giles, J.R., Globig, A-M., Kaech, S.M. and Wherry, E.J. (2023) '$CD8^+$ T cells in the cancer-immunity cycle', *Immunity,* 56 (10): pp. 2231-2253. doi: 10.1016/j.immuni.2023.09.005.

Gonzalez, H., Hagerling, C. and Werb Z. (2018) 'Roles of the immune system in cancer: from tumour initiation to metastatic progression', *Genes and Development,* 32 (19-20): pp. 1267-1284. doi: 10.1101/gad.314617.118.

Gorentla, B.K., Wan, C-K. and Zhong, X-P. (2011) 'Negative regulation of mTOR activation by diacylglycerol kinases', *Blood,* 117 (15): pp. 4022-4031. doi: 10.1182/blood-2010-08-300731.

Gräbnitz, F., Stark, D., Shlesinger, D., Petkidis, A., Borsa, M., Yermanos, A., Carr, A., Barandun, N., Wehling, A., Balaz, M., Schroeder, T. and Oxenius, A. (2023) 'Asymettric cell division safeguards memory CD8 T cell development', *Cell Reports,* 42 (5): pp. 112468. doi: 10.1016/j.celrep.2023.112468.

Groenewoud, M.J. and Zwartkruis, F.J.T. (2013) 'Rheb and Rags come together at the lysosome to activate mTORC1', *Biochemical Society Transactions,* 41 (4): pp. 951-955. doi: 10.1042/BST20130037.

Gropper, Y., Feferman, T., Shalit, T., Salame, T-M., Porat, Z. and Shakhar, G. (2017) 'Culturing CTLs under Hypoxic Conditions Enhances Their Cytolysis and Improves Their Anti-tumor Function', *Cell Reports,* 20 (11): pp. 2547-2555. doi: 10.1016/j.celrep.2017.08.071.

Gudgeon, N., Giles, H., Bishop, E.L., Fulton-Ward, T., Escribano-Gonzalez, C., Munford, H., James-Bott, A., Foster, K., Karim, F., Jayawardana, D., Mahmood, A., Cribbs, A.P., Tennant, D.A., Basu, S., Pratt, G. and Dimeloe, S. (2023) 'Uptake of long-chain fatty acids from the bone marrow suppresses CD8+ T-cell metabolism and function in multiple myeloma', *Blood Advances,* 7 (20): pp. 6035-6047. doi: 10.1182/bloodadvances.2023009890.

Guillerey, C., Harjunpää, H., Carrié, N., Kassem, S., Teo, T., Miles, K., Krumeich, S., Weulersse, M., Cuisinier, M., Stannard, K., Yu, Y., Minnie, S.A., Hill, G.R., Dougall, W.C., Avet-Loiseau, H., Teng, M.W.L., Nakamura, K., Martinet, L. and Smyth, M.J. (2018) 'TIGIT immune checkpoint blockade restores $CD8^+$ T-cell immunity against multiple myeloma', *Blood,* 132 (16): pp. 1689-1694. doi: 10.1182/blood-2018-01-825265.

Gupta, S.S., Wang, J. and Chen, M. (2020) 'Metabolic Reprogramming in $CD8^+$ T Cells During Acute Viral Infections', *Frontiers in Immunology,* 11: pp. 1013. doi: 10.3389/fimmu.2020.01013.

Hamanaka, R.B. and Chandel, N.S. (2009) 'Mitochondrial reactive oxygen species regulate hypoxic signaling', *Current Opinion in Cell Biology,* 21 (6): pp. 894-899. doi: 10.1016/j.ceb.2009.08.005.

Han, J., Khatwani, N., Searles, T.G., Turk, M.J. and Angeles, C.V. (2020) 'Memory $CD8^+$ T cell responses to cancer', *Seminars in Immunology,* 49: pp. 101435. doi: 10.1016/j.smim.2020.101435.

Hardie, D.G. and Ashford, M.L.J. (2014) 'AMPK: Regulating Energy Balance at the Cellular and Whole Body Levels', *Physiology,* 29 (2): pp. 99-107. doi: 10.1152/physiol.00050.2013.

Harrison, J.S., Rameshwar, P., Chang, V. and Bandari, P. (2002) 'Oxygen saturation in the bone marrow of healthy volunteers', *Blood,* 99 (1): pp. 394. doi: 10.1182/blood.v99.1.394.

Hasan, F., Chiu, Y., Shaw, R.M., Wang, J. and Yee, C. (2021) 'Hypoxia acts as an environmental cue for the human tissue-resident memory T cell differentiation program', *JCI Insight,* 6 (10): pp. e138970. doi: 10.1172/jci.insight.138970.

Haslett, P.A., Corral, L.G., Albert, M. and Kaplan, G. (1998) 'Thalidomide costimulates primary human T lymphocytes, preferentially inducing proliferation, cytokine production, and cytotoxic responses in the CD8+ subset', *Journal of Experimental Medicine,* 187 (11): pp. 1885-1892. doi: 10.1084/jem.187.11.1885.

Hawley, S.A., Pan, D.A., Mustard, K.J., Ross, L., Bain, J., Edelmann, A.M., Frenguelli, B.G. and Hardie, D.G. (2005) 'Calmodulin-dependent protein kinase kinase-beta is an alternative upstream kinase for AMP-activated protein kinase', *Cell Metabolism,* 2 (1): pp. 9-19. doi: 10.1016/j.cmet.2005.05.009.

Hawley, S.A., Ross, F.A., Chevtzoff, C., Green, K.A., Evans, A., Fogarty, S., Towler, M.C., Brown, L.J., Ogunbayo, O.A., Evans, A.M. and Hardie, D.G. (2010) 'Use of Cells Expressing γ Subunit Variants to Identify Diverse Mechanisms of AMPK Activation', *Cell Metabolism,* 11 (6): pp. 554-565. doi: 10.1016/j.cmet.2010.04.001.

Heiduck, M., Klimova, A., Reiche, C., Digomann, D., Beer, C., Aust, D.E., Distler, M., Weitz, J., Seifert, A.M. and Seifert, L. (2023) 'TIGIT Expression Delineates T-cell Populations with Distinct Functional and Prognostic Impact in Pancreatic Cancer', *Clinical Cancer Research,* 29 (14): pp. 2638-2650. doi: 10.1158/1078-0432.CCR-23-0258.

Hipp, S., Tai, Y-T., Blanset, D., Deegen, P., Wahl, J., Thomas, O., Rattel, B., Adam, P.J., Anderson, K.C. and Friedrich, M. (2017) 'A novel BCMA/CD3 bispecific T-cell engager for the treatment of

multiple myeloma induces selective lysis in vitro and in vivo', *Leukemia,* 31 (8): pp. 1743-1751. doi: 10.1038/leu.2016.388.

Hochachka, P.W., Buck, L.T., Doll, C.J. and Land, S.C. (1996) 'Unifying theory of hypoxia tolerance: molecular/metabolic defense and rescue mechanisms for surviving oxygen lack', *Proceedings of the National Academy of Sciences of the United States of America,* 93 (18): pp. 9493-9498. doi: 10.1073/pnas.93.18.9493.

Hodgson, R., Xu, X., Anzilotti, C., Deobagkar-Lele, M., Crockford, T.L., Kepple, J.D., Cawthorne, E., Bhandari, A., Cabrian-Serrano, A., Wilcock, M.J., Davies, B., Cornall, R.J. and Bull, K.R. (2022) 'NDRG1 is induced by antigen-receptor signaling but dispensable for B and T cell self-tolerance', *Communications Biology,* 5: pp. 1216. doi: 10.1038/s42003-022-04118-w.

Hong, S-S., Lee, H. and Kim, K-W. (2004) 'HIF-1α: a Valid Therapeutic Target for Tumor Therapy', *Cancer Research and Treatment,* 36 (6): pp. 343-353. doi: 10.4143/crt.2004.36.6.343.

Howell, D., Smith, A., Appleton, S., Bagguley, T., Macleod, U., Cook, G., Patmore, R. and Roman, E. (2017) 'Multiple myeloma: routes to diagnosis, clinical characteristics and survival – findings from a UK population-based study', *British Journal of Haematology,* 177 (1): pp. 67-71. doi: 10.1111/bjh.14513.

Ikeda, S. and Tagawa, H. (2021) 'Impact of hypoxia on the pathogenesis and therapy resistance in multiple myeloma', *Cancer Science,* 112 (10): pp. 3995-4004. doi: 10.1111/cas.15087.

Institute for Quality and Efficiency in Health Care. (2020) 'The innate and adaptive immune systems', in *Informed Health.org*. Cologne, Germany: Institute for Quality and Efficiency in Health Care (IQWiG). Available at: https://www.ncbi.nlm.nih.gov/books/NBK279396/ (Accessed: 24 January 2024)

Isakov, N., Wange, R.L., Burgess, W.H., Watts, J.D., Aebersold, R. and Samelson, L.E. (1995) 'ZAP-70 binding specificity to T cell receptor tyrosine-based activation motifs: the tandem SH2 domains of ZAP-70 bind distinct tyrosine-based activation motifs with varying affinity', *Journal of Experimental Medicine,* 181 (1): pp. 375-380. doi: 10.1084/jem.181.1.375.

Ivanova, I.G., Park, C.V. and Kenneth, N.S. (2019) 'Translating the Hypoxic Response – The Role of HIF Protein Translation in the Cellular Response to Low Oxygen', *Cells,* 8 (2): pp. 114. doi: 10.3390/cells8020114.

Iwashima, M., Irving, B.A., van Oers, N.S., Chan, A.C. and Weiss, A. (1994) 'Sequential interactions of the TCR with two distinct cytoplasmic tyrosine kinases', *Science,* 263 (5150): pp. 1136-1139. doi: 10.1126/science.7509083.

Jaakkola, P., Mole, D.R., Tian, Y.M., Wilson, M.I., Gielbert, J., Gaskell, S.J., von Kriegsheim, A., Hebestreit, H.F., Mukherji, M., Schofield, C.J., Maxwell, P.H., Pugh, C.W. and Ratcliffe, P.J. (2001) 'Targeting of HIF-alpha to the von Hippel-Lindau ubiquitylation complex by O2-regulated prolyl hydroxylation', *Science,* 292 (5516): pp. 468-472. doi: 10.1126/science.1059796.

Jornayvaz, F.R. and Shulman, G.I. (2010) 'Regulation of mitochondrial biogenesis', *Essays in Biochemistry,* 47: pp. 69-84. doi: 10.1042/bse0470069.

Kanatous, S.B., Mammen, P.P.A., Rosenberg, P.B., Martin, C.M., White, M.D., Dimaio, J.M., Huang, G., Muallem, S. and Garry D.J. (2009) 'Hypoxia reprograms calcium signaling and regulates myoglobin expression', *American Journal of Physiology – Cell Physiology,* 296 (3): pp. C393-402. doi: 10.1152/ajpcell.00428.2008.

Kania, E., Roest, G., Vervliet, T., Parys, J.B. and Bultynck, G. (2017) 'IP_3 Receptor-Mediated Calcium Signaling and Its Role in Autophagy in Cancer', *Frontiers in Oncology,* 7: pp. 140. doi: 10.3389/fonc.2017.00140.

Kay, N.E., Leong, T.L., Bone, N., Vesole, D.H., Greipp, P.R., Van Ness, B., Oken, M.M. and Kyle, R.A. (2001) 'Blood levels of immune cells predict survival in myeloma patients: results of an Eastern Cooperative Oncology Group phase 3 trial for newly diagnosed multiple myeloma patients', *Blood,* 98 (1): pp. 23-28. doi: 10.1182/blood.v98.1.23.

Kazandjian, D., Mailankody, S., Korde, N. and Landgren, O. (2014) 'Smoldering multiple myeloma: pathophysiologic insights, novel diagnostics, clinical risk models, and treatment strategies', *Clinical Advances in Hematology and Oncology,* 12 (9): pp. 578-587. Available at: https://pubmed.ncbi.nlm.nih.gov/25654479/ (Accessed 19 April 2024)

Kazandjian, D. (2016) 'Multiple myeloma epidemiology and survival: A unique malignancy', *Seminars in Oncology,* 43 (6): pp. 676-681. doi: 10.1053/j.seminoncol.2016.11.004.

Keppler, S.J., Rosenits, K., Koegl, T., Vucikuja, S. and Aichele, P. (2012) 'Signal 3 cytokines as modulators of primary immune responses during infections: the interplay of type I IFN and IL-12 in CD8 T cell responses', *PLoS One,* 7 (7): e40865. doi: 10.1371/journal.pone.0040865.

Kierans, S.J. and Taylor, C.T. (2021) 'Regulation of glycolysis by the hypoxia-inducible factor (HIF): implications for cellular physiology', *The Journal of Physiology,* 599 (1): pp. 23-37. doi: 10.1113/JP280572.

Kim, J., Kundu, M., Viollet, B. and Guan, K-L. (2011) 'AMPK and mTOR regulate autophagy through direct phosphorylation of Ulk1', *Nature Cell Biology,* 13 (2): pp. 132-141. doi: 10.1038/ncb2152.

Kim, J-W., Tchernyschyov, I., Semenza, G.L. and Dang, C.V. (2006) 'HIF-1-mediated expression of pyruvate dehydrogenase kinase: a metabolic switch required for cellular adaptation to hypoxia', *Cell Metabolism,* 3 (3): pp. 177-185. doi: 10.1016/j.cmet.2006.02.002.

Klein-Hessling, S., Muhammad, K., Klein, M., Pusch, T., Rudolf, R., Flöter, J., Qureischi, M., Beilhack, A., Vaeth, M., Kummerow, C., Backes, C., Schoppmeyer, R., Hahn, U., Hoth, M., Bopp, T., Berberich-Siebelt, F., Patra, A., Avots, A., Müller, N., Schulze, A. and Serfling, E. (2017) 'NFATc1 controls the cytotoxicity of $CD8^{+}$ T cells', *Nature Communications,* 8 (1): pp. 511. doi: 10.1038/s41467-017-00612-6.

Koshiji, M., Kageyama, Y., Pete, E.A., Horikawa, I., Barrett, J.C. and Huang, L.E. (2004) 'HIF-1 alpha induces cell cycle arrest by functionally counteracting Myc', *The EMBO Journal,* 23 (9): pp. 1949-1956. doi: 10.1038/sj.emboj.7600196.

Koumenis, C., Naczki, C., Koritzinksy, M., Rastani, S., Diehl, A., Sonenberg, N., Koromilas, A. and Wouters, B.G. (2002) 'Regulation of protein synthesis by hypoxia via activation of the endoplasmic reticulum kinase PERK and phosphorylation of the translation initiation factor eIF2alpha', *Molecular and Cellular Biology,* 22 (21): pp. 7405-7416. doi: 10.1128/MCB.22.21.7405-7416.2002.

Krejcik, J., Casneuf, T., Nijhof, I.S., Verbist, B., Bald, J., Plesner, T., Syed, K., Liu, K., van de Donk, N.W.C.J., Weiss, B.M., Ahmadi, T., Lokhorst, H.M., Mutis, T. and Sasser, A.K. (2016) 'Daratumumab depletes CD38+ immune regulatory cells, promotes T-cell expansion, and skews T-cell repertoire in multiple myeloma', *Blood,* 128 (3): pp. 384-394. doi: 10.1182/blood-2015-12-687749.

Krieger, J.A., Landsiedel, J.C. and Lawrence, D.A. (1996) 'Differential in vitro effects of physiological and atmospheric oxygen tension on normal human peripheral blood mononuclear cell

proliferation, cytokine and immunoglobulin production', *International Immunopharmacology,* 18 (10): pp. 545-552. doi: 10.1016/s0192-0561(96)00057-4.

Kumar, B.V., Connors, T. and Farber, D.L. (2018) 'Human T cell development, localization, and function throughout life', *Immunity,* 48 (2): pp. 202-213. doi: 10.1016/j.immuni.2018.01.007.

Kung, C., Pingel, J.T., Heikinheimo, M., Klemola, T., Varkila, K., Yoo, L.I., Vuopala, K., Poyhonen, M., Uhari, M., Rogers, M., Speck, S.H., Chatila, T. and Thomas, M.L. (2000) 'Mutations in the tyrosine phosphatase CD45 gene in a child with severe combined immunodeficiency disease', *Nature Medicine,* 6 (3): pp. 343-345. doi: 10.1038/73208.

Kwon, M., Kim, C.G., Lee, H., Cho, H., Kim, Y., Lee, E.C., Choi, S.J., Park, J., Seo, I-H., Bogen, B., Song, I-K., Jo, D-Y., Kim, J.S., Park, S-H., Choi, I., Choi, Y.S. and Shin, E-C. (2020) 'PD-1 Blockade Reinvigorates Bone Marrow $CD8^+$ T Cells from Patients with Multiple Myeloma in the Presence of TGFβ Inhibitors', *Clinical Cancer Research,* 26 (7): pp. 1644-1655. doi: 10.1158/1078-0432.CCR-19-0267.

Kyle, R.A., Therneau, T.M., Rajkumar, S.V., Larson, D.R., Plevak, M.F. and Melton 3rd, L.J. (2004) 'Long-term follow-up of 241 patients with monoclonal gammopathy of undetermined significance: the original Mayo Clinic series 25 years later', *Mayo Clinic Proceedings,* 79 (7): pp. 859-866. doi: 10.4065/79.7.859.

Labiano, S., Meléndez-Rodríguez, F., Palazón, A., Teijeira, Á., Garasa, S., Etxeberria, I., Aznar, M.Á., Sánchez-Paulete, A.R., Azpilikueta, A., Bolaños, E., Molina, C., de la Fuente, H., Maiso, P., Sánchez-Madrid, F., de Landázuri, M.O., Aragonés, J. and Melero, I. (2017) 'CD69 is a direct HIF-1α target gene in hypoxia as a mechanism enhancing expression on tumor-infiltrating T lymphocytes', *Oncoimmunology,* 6 (4): pp. e1283468. doi: 10.1080/2162402X.2017.1283468.

Lai, Y.P., Kuo, L-C., Lin, B-R., Lin, H-J., Lin, C-Y., Chen, Y-T., Hsiao, P-W., Chang, H-T., Ko, P.C-I., Chen, H-C., Chang, H-Y., Lu, J., Ho, H-N., Wu-Hsieh, B.A., Kung, J.T. and Chen, S-C. (2021) 'CD28 engagement inhibits CD73-mediated regulatory activity of $CD8^+$ T cells', *Communications Biology,* 4 (1): pp. 595. doi: 10.1038/s42003-021-02119-9.

Landgren, O., Kyle, R.A., Pfeiffer, R.M., Katzmann, J.A., Caporaso, N.E., Hayes, R.B., Dispenzieri, A., Kumar, S., Clark, R.J., Baris, D., Hoover, R. and Rajkumar, S.V. (2009) 'Monoclonal

gammopathy of undetermined significance (MGUS) consistently precedes multiple myeloma: a prospective study', *Blood,* 113 (22): pp. 5412-5417. doi: 10.1182/blood-2008-12-194241.

Lang, F. and Föller, M. (2014) 'Regulation of ion channels and transporters by AMP-activated kinase (AMPK)', *Channels,* 8 (1): pp. 20-28. doi: 10.4161/chan.27423.

Larbi, A., Zelba, H., Goldeck, D. and Pawelec, G. (2010) 'Induction of HIF-1alpha and the glycolytic pathway alters apoptotic and differentiation profiles of activated human T cells', *Journal of Leukocyte Biology,* 87 (2): pp. 265-273. doi: 10.1189/jlb.0509304.

Larbi, A. and Fulop, T. (2014) 'From "truly naïve" to "exhausted senescent" T cells: when markers predict functionality' *Cytometry Part A,* 85 (1): pp. 25-35. doi: 10.1002/cyto.a.22351.

Leahy, D.J. (1995) 'A structural view of CD4 and CD8', *The FASEB Journal,* 9 (1): pp. 17-25. doi: 10.1096/fasebj.9.1.7821755.

Li, W., Yuan, P., Liu, W., Xiao, L., Xu, C., Mo, Q., Xu, S., He, Y., Jiang, D. and Wang, X. (2022) 'Hypoxia-Immune-Related Gene SLC19A1 Serves as a Potential Biomarker for Prognosis in Multiple Myeloma', *Frontiers in Immunology,* 13: pp. 843369. doi: 10.3389/fimmu.2022.843369.

Li, Y., Wang, Y., Kim, E., Beemiller, P., Wang, C-Y., Swanson, J., You, M. and Guan, K-L. (2007) 'Bnip3 mediates the hypoxia-induced inhibition on mammalian target of rapamycin by interacting with Rheb', *Journal of Biological Chemistry,* 282 (49): pp. 35803-35813. doi: 10.1074/jbc.M705231200.

Li, Y., Zhao, L. and Li, X-F. (2021) 'Hypoxia and the Tumour Microenvironment', *Technology in Cancer Research and Treatment,* 20: pp. 15330338211036304. doi: 10.1177/15330338211036304.

Liberti, M.V. and Locasale, J.W. (2016) 'The Warburg Effect: How Does it Benefit Cancer Cells?', *Trends in Biochemical Sciences,* 41 (3): pp. 211-218. doi: 10.1016/j.tibs.2015.12.001.

Liikanen, I., Lauhan, C., Quon, S., Omilusik, K., Phan, A.T., Bartrolí, L.B., Ferry, A., Goulding, J., Chen, J., Scott-Browne, J.P., Yustein, J.T., Scharping, N.E., Witherden, D.A. and Goldrath, A.W. (2021) 'Hypoxia-inducible factor activity promotes antitumor effector function and tissue residency by CD8+ T cells', *Journal of Clinical Investigation,* 131 (7): pp. e143729. doi: 10.1172/JCI143729.

Lim, J-H., Park, J-W., Kim, M-S., Park, S-K., Johnson, R.S. and Chun, Y-S. (2006) 'Bafilomycin induces the p21-mediated growth inhibition of cancer cells under hypoxic conditions by expressing

hypoxia-inducible factor-1 alpha', *Molecular Pharmacology,* 70 (6): pp. 1856-1865. doi: 10.1124/mol.106.028076.

Liu, L. and Simon, M.C. (2004) 'Regulation of transcription and translation by hypoxia', *Cancer Biology and Therapy,* 3 (6): pp. 492-497. doi: 10.4161/cbt.3.6.1010.

Liu, T., Zhang, L., Joo, D. and Sun, S-C. (2017) 'NF-κB signaling in inflammation', *Signal Transduction and Targeted Therapy,* 2 (1): pp. 1-9. doi: 10.1038/sigtrans.2017.23.

Liu, Y-N., Yang, J-F., Huang, D-J., Ni, H-N., Zhang, C-X., Zhang, L., He, J., Gu, J-M., Chen, H-X., Mai, H-Q., Chen, Q-Y., Zhang, X-S., Gao, S. and Li, J. (2020) 'Hypoxia Induces Mitochondrial Defect That Promotes T Cell Exhaustion in Tumor Microenvironment Through MYC-Regulated Pathways', *Frontiers in Immunology,* 21 (11): pp. 1906. doi: 10.3389/fimmu.2020.01906.

Liu, Z-Y., Deng, L., Jia, Y., Liu, H., Ding, K., Wang, W., Zhang, H. and Fu, R. (2022) 'CD155/TIGIT signalling plays a vital role in the regulation of bone marrow mesenchymal stem cell-induced natural killer-cell exhaustion in multiple myeloma', *Clinical and Translational Medicine,* 12 (7): pp. e861. doi: 10.1002/ctm2.861.

Long, X., Ortiz-Vega, S., Lin, Y. and Avruch, J. (2005) 'Rheb binding to mammalian target of rapamycin (mTOR) is regulated by amino acid sufficiency', *Journal of Biological Chemistry,* 280 (25): pp. 23433-23436. doi: 10.1074/jbc.C500169200.

Lopez-Girona, A., Mendy, D., Ito, T., Miller, K., Gandhi, A.K., Kang, J., Karasawa, S., Carmel, G., Jackson, P., Abbasian, M., Mahmoudi, A., Cathers, B., Rychak, E., Gaidarova, S., Chen, R., Schafer, P.H., Handa, H., Daniel, T.O., Evans, J.F. and Chopra, R. (2012) 'Cereblon is a direct protein target for immunomodulatory and antiproliferative activities of lenalidomide and pomalidomide', *Leukemia,* 26 (11): pp. 2326-2335. doi: 10.1038/leu.2012.119

Love, M.I., Huber, W. and Anders, S. (2014) 'Moderated estimation of fold change and dispersion for RNA-seq data with DESeq2', *Genome Biology,* 15 (12): pp. 550. doi: 10.1186/s13059-014-0550-8.

Luckheeram, R.V., Zhou, R., Verma, A.D. and Xia, B. (2012) 'CD4$^+$ T Cells: Differentiation and Functions', *Clinical and Developmental Immunology,* 2012: 925135. doi: 10.1155/2012/925135.

Lukashev, D., Klebanov, B., Kojima, H., Grinberg, A., Ohta, A., Berenfeld, L., Wenger, R.H., Ohta, A. and Stikovsky, M. (2006) 'Cutting edge: hypoxia-inducible factor 1alpha and its activation-

inducible short isoform I.1 negatively regulate functions of $CD4^+$ and $CD8^+$ T lymphocytes', *The Journal of Immunology,* 177 (8): pp. 4962-4965. doi: 10.4049/jimmunol.177.8.4962.

Lukashev, D. and Sitkovsky, M. (2008) 'Preferential expression of the novel alternative isoform I.3 of hypoxia-inducible factor 1 alpha in activated human T lymphocytes', *Human Immunology,* 69 (7): pp. 421-425. doi: 10.1016/j.humimm.2008.05.004.

Ma, E.H., Poffenberger, M.C., Wong, A.H-T. and Jones, R.G. (2017) 'The role of AMPK in T cell metabolism and function', *Current Opinion in Immunology,* 46: pp. 45-52. doi: 10.1016/j.coi.2017.04.004.

Ma, J., Mo, Y., Tang, M., Shen, J., Qi, Y., Zhao, W., Huang, Y., Xu, Y. and Qian, C. (2021) 'Bispecific Antibodies: From Research to Clinical Application', *Frontiers in Immunology,* 12: pp. 626616. doi: 10.3389/fimmu.2021.626616.

Ma, X., Xiao, L., Liu, L., Ye, L., Su, P., Bi, E., Wang, Q., Yang, M., Qian, J. and Yi, Q. (2021) 'CD36-mediated ferroptosis dampens intratumoral $CD8^+$ T cell effector function and impairs their antitumor ability', *Cell Metabolism,* 33 (5): pp. 1001-1012.e5. doi: 10.1016/j.cmet.2021.02.015.

Macián, F., López-Rodríguez, C. and Rao, A. (2001) 'Partners in transcription: NFAT and AP-1', *Oncogene,* 20 (19): pp. 2476-2489. doi: 10.1038/sj.onc.1204386.

Macián, F., García-Cózar, F., Im, S-H., Horton, H.F., Byrne, M.C. and Rao, A. (2002) 'Transcriptional mechanisms underlying lymphocyte tolerance', *Cell,* 109 (6): pp. 719-731. doi: 10.1016/s0092-8674(02)00767-5.

Macian, F. (2005) 'NFAT proteins: key regulators of T-cell development and function', *Nature Reviews Immunology,* 5 (6): pp. 472-484. doi: 10.1038/nri1632.

Makino, Y., Nakamura, H., Ikeda, E., Ohnuma, K., Yamauchi, K., Yabe, Y., Poellinger, L., Okada, Y., Morimoto, C. and Tanaka, H. (2003) 'Hypoxia-inducible factor regulates survival of antigen receptor-driven T cells', *The Journal of Immunology,* 171 (12): pp. 6534-6540. doi: 10.4049/jimmunol.171.12.6534.

Marraco, S.A.F., Neubert, N.J., Verdeil, G. and Speiser, D.E. (2015) 'Inhibitory Receptors Beyond T Cell Exhaustion', *Frontiers in Immunology,* 6: pp. 310. doi: 10.3389/fimmu.2015.00310.

Marriott, J.B., Clarke, I.A., Dredge, K., Muller, G., Stirling, D. and Dalgleish, A.G. (2002) 'Thalidomide and its analogues have distinct and opposing effects on TNF-alpha and TNFR2 during co-

stimulation of both CD4(+) and CD8(+) T cells', *Clinical and Experimental Immunology,* 130 (1): pp. 75-84. doi: 10.1046/j.1365-2249.2002.01954.x.

Martinez, G.J., Pereira, R.M., Äijö, T., Kim, E.Y., Marangoni, F., Pipkin, M.E., Togher, S., Heissmeyer, V., Zhang, Y.C., Crotty, S., Lamperti, E.D., Ansel, K.M., Mempel, T.R., Lähdesmäki, H., Hogan, P.G. and Rao, A. (2015) 'The transcription factor NFAT promotes exhaustion of activated $CD8^+$ T cells', *Immunity,* 42 (2): pp. 265-278. doi: 10.1016/j.immuni.2015.01.006.

Matheson, L.S., Petkau, G., Sáenz-Narciso, B., D'Angeli, V., McHugh, J., Newman, R., Munford, H., West, J., Chakraborty, K., Roberts, J., Lukasiak, S., Díaz-Munoz, M.D., Bell, S.E., Dimeloe, S. and Turner, M. (2022) 'Multiomics analysis couples mRNA turnover and translational control of glutamine metabolism to the differentiation of the activated $CD4^+$ T cell', *Scientific Reports,* 12 (1): pp. 19657. doi: 10.1038/s41598-022-24132-6.

Matsumoto, R., Wang, D., Blonska, M., Li, H., Kobayashi, M., Pappu, B., Chen, Y., Wang, D. and Lin, X. (2005) 'Phosphorylation of CARMA1 plays a critical role in T cell receptor-mediated NF-kappa B activation', *Immunity,* 23 (6): pp. 575-585. doi: 10.1016/j.immuni.2005.10.007.

Maude, S.L., Laetsch, T.W., Buechner, J., Rives, S., Boyer, M., Bittencourt, H., Bader, P., Verneris, M.R., Stefanski, H.E., Myers, G.D., Qayed, M., De Moerloose, D., Hiramatsu, H., Schlis, K., Davis, K.L., Martin, P.L., Nemecek, E.R., Yanik, G.A., Peters, C., Baruchel, A., Boissel, N., Mechninaud, F., Balduzzi, A., Krueger, J., June, C.H., Levine, B.L., Wood, P., Taran, T., Leung, M., Mueller, K.T., Zhang, Y., Sen, K., Lebwohl, D., Pulsipher, M.A. and Grupp, S.A. (2018) 'Tisagenlecleucel in Children and Young Adults with B-Cell Lymphoblastic Leukemia', *The New England Journal of Medicine,* 387 (5): pp. 439-448. doi: 10.1056/NEJMoa1709866.

Manzo, T., Prentice, B.M., Anderson, K.G., Raman, A., Schalck, A., Codreanu, G.S., Lauson, C.B.N., Tiberti, S., Raimondi, A., Jones, M.A., Reyzer, M., Bates, B.M., Spraggins, J.M., Patterson, N.H., McLean, J.A., Rai, K., Tacchetti, C., Tucci, S., Wargo, J.A., Rodighiero, S., Clise-Dwyer, K., Sherrod, S.D., Kim, M., Navin, N.E., Caprioli, R.M., Greenberg, P.D., Draetta, G. and Nezi, L. (2020) 'Accumulation of long-chain fatty acids in the tumor microenvironment drives dysfunction in intrapancreatic $CD8^+$ T cells', *Journal of Experimental Medicine,* 217 (8): pp. e20191920. doi: 10.1084/jem.20191920.

Maxwell, P.H., Wiesener, M.S., Chang, G.W., Clifford, S.C., Vaux, E.C., Cockman, M.E., Wykoff, C.C., Pugh, C.W., Maher, E.R. and Ratcliffe P.J. (1999) 'The tumour suppressor protein VHL targets hypoxia-inducible factors for oxygen-dependent proteolysis', *Nature,* 399 (6733): pp. 271-275. doi: 10.1038/20459.

McKeown, S.R. (2014) 'Defining normoxia, physioxia and hypoxia in tumours – implications for treatment response', *The British Journal of Radiology,* 87 (1035): pp. 20130676. doi: 10.1259/bjr.20130676.

McNeill, L.A., Hewitson, K.S., Claridge, T.D., Seibel, J.F., Horsfall, L.E. and Schofield, C.J. (2002) 'Hypoxia-inducible factor asparaginyl hydroxylase (FIH-1) catalyses hydroxylation at the beta-carbon of asparagine-803', *Biochemical Journal,* 367 (Part 3): pp. 571-575. doi: 10.1042/BJ20021162.

McNeill, L., Salmond, R.J., Cooper, J.C., Carret, C.K., Cassady-Cain, R.L., Roche-Molina, M., Tandon, P., Holmes, N. and Alexander, D.R. (2007) 'The differential regulation of Lck kinase phosphorylation sites by CD45 is critical for T cell receptor signaling responses', *Immunity,* 27 (3): pp. 425-437. doi: 10.1016/j.immuni.2007.07.015.

Menk, A.V., Scharping, N.E., Moreci, R.S., Zeng, X., Guy, C., Salvatore, S., Bae, H., Xie, J., Young, H.A., Wendell, S.G. and Delgoffe, G.M. (2018) 'Early TCR Signaling Induces Rapid Aerobic Glycolysis Enabling Distinct Acute T Cell Effector Functions', *Cell Reports,* 22 (6): pp. 1509-1521. doi: 10.1016/j.celrep.2018.01.040.

Metallo, C.M., Gameiro, P.A., Bell, E.L., Mattaini, K.R., Yang, J., Hiller, K., Jewell, C.M., Johnson, Z.R., Irvine, D.J., Guarente, L., Kelleher, J.K., Vander Heiden, M.G., Iliopoulos, O. and Stephanopoulos, G. (2011) 'Reductive glutamine metabolism by IDH1 mediates lipogenesis under hypoxia', *Nature,* 481 (7381): pp. 380-384. doi: 10.1038/nature10602.

Metzen, E., Stiehl, D.P., Doege, K., Marxsen, J.H., Hellwig-Burgel, T. and Jelkmann, W. (2005) 'Regulation of the prolyl hydroxylase domain protein 2 (*phd2/egln-1*) gene: identification of a functional hypoxia-responsive element', *Biochemical Journal,* 387 (Part 3): pp. 711-717. doi: 10.1042/BJ20041736.

Miceli, M.C. and Parnes, J.R. (1991) 'The roles of CD4 and CD8 in T cell activation', *Seminars in Immunology*, 3 (3): pp. 133-141. Available at: https://pubmed.ncbi.nlm.nih.gov/1909592/ (Accessed: 17 April 2024)

Michalek, R.D., Gerriets, V.A., Nichols, A.G., Inoue, M., Kazmin, D., Chang, C-Y., Dwyer, M.A., Nelson, E.R., Pollizzi, K.N., Ilkayeva, O., Giguere, V., Zuercher, W.J., Powell, J.D., Shinohara, M.L., McDonnell, D.P. and Rathmell, J.C. (2011) 'Estrogen-related receptor-α is a metabolic regulator of effector T-cell activation and differentiation', *Proceedings of the National Academy of Sciences of the United States of America,* 108 (45): pp. 18348-18353. doi: 10.1073/pnas.1108856108.

Michelet, X., Dyck, L., Hogan, A., Loftus, R.M., Duquette, D., Wei, K., Beyaz, S., Tavakkoli, A., Foley, C., Donnelly, R., O'Farrelly, C., Raverdeau, M., Vernon, A., Pettee, W., O'Shea, D., Nikolajczyk, B.S., Mills, K.H.G., Brenner, M.B., Finlay, D. and Lynch, L. (2018) 'Metabolic reprogramming of natural killer cells in obesity limits antitumor responses', *Nature Immunology,* 19 (12): pp. 1330-1340. doi: 10.1038/s41590-018-0251.7.

Michie, C.A., McLean, A., Alcock, C. and Beverley, P.C. (1992) 'Lifespan of human lymphocyte subsets defined by CD45 isoforms', *Nature,* 360 (6401): pp. 264-265. doi: 10.1038/360264a0.

Michiels, C. (2004) 'Physiological and Pathological Responses to Hypoxia', *The American Journal of Pathology,* 164 (6): pp. 1875-1882. doi: 10.1016/S0002-9440(10)63747-9.

Mills, K.H. and Cawley, J.C. (1983) 'Abnormal monoclonal antibody-defined helper/suppressor T-cell subpopulations in multiple myeloma: relationship to treatment and clinical stage', *British Journal of Haematology,* 53 (2): pp. 271-275. doi: 10.1111/j.1365-2141.1983.tb02021.x.

Moulton, V.R. and Tsokos, G.C. (2015) 'T cell signaling abnormalities contribute to aberrant immune cell function and autoimmunity', *Journal of Clinical Investigation,* 125 (6): pp. 2220-2227. doi: 10.1172/JCI78087.

Mulero, M.C., Aubareda, A., Orzáez, M., Messeguer, J., Serrano-Candelas, E., Martínez-Hoyer, S., Messeguer, A., Pérez-Payá, E. and Pérez-Riba, M. (2009) 'Inhibiting the Calcineurin-NFAT (Nuclear Factor of Activated T Cells) Signaling Pathway with a Regulator of Calcineurin-derived Peptide without Affecting General Calcineurin Phosphatase Activity', *Journal of Biological Chemistry,* 284 (14): pp. 9394-9401. doi: 10.1074/jbc.M805889200.

Mungai, P.T., Waypa, G.B., Jairaman, A., Prakriya, M., Dokic, D., Ball, M.K. and Schumacker, P.T. (2011) 'Hypoxia triggers AMPK activation through reactive oxygen species-mediated activation of calcium release-activated calcium channels', *Molecular and Cellular Biology,* 31 (17): pp. 3531-3545. doi: 10.1128/MCB.05124-11.

Muz, B., de la Puente, P., Azab, F. and Azab, A.K. (2015) 'The role of hypoxia in cancer progression, angiogenesis, metastasis, and resistance to therapy', *Hypoxia,* 3: pp. 83-92. doi: 10.2147/HP.S93413.

Nakamura, H., Makino, Y., Okamoto, K., Poellinger, L., Ohnuma, K., Morimoto, C. and Tanaka, H. (2005) 'TCR engagement increases hypoxia-inducible-factor-1 alpha protein synthesis via rapamycin-sensitive pathway under hypoxic conditions in human peripheral T cells', *The Journal of Immunology,* 174 (12): pp. 7592-7599. doi: 10.4049/jimmunol.174.12.7592.

Naldini, A., Carraro, F., Silvestri, S. and Bocci, V. (1997) 'Hypoxia affects cytokine production and proliferative responses by human peripheral mononuclear cells', *Journal of Cellular Physiology,* 173 (3): pp. 335-342. doi: 10.1002/(SICI)1097-4652(199712)173:3<335::AID-JCP5>3.0.CO;2-O.

Naldini, A. and Carraro, F. (1999) 'Hypoxia modulates cyclin and cytokine expression and inhibits peripheral mononuclear cell proliferation', *Journal of Cellular Physiology,* 181 (3): pp. 448-454. doi: 10.1002/(SICI)1097-4652(199912)181:3<448::AID-JCP8>3.0.CO;2-F.

National Cancer Institute (2011). *Definition of Cancer – NCI Dictionary of Cancer Terms.* Available at: https://www.cancer.gov/publications/dictionaries/cancer-terms/def/cancer (Accessed: 9 May 2023)

National Cancer Institute (2015). *Immunotherapy for Cancer.* Available at: https://www.cancer.gov/about-cancer/treatment/types/immunotherapy (Accessed 24 January 2024)

National Institute for Health and Care Excellence (2018). *Myeloma: diagnosis and management.* Available at: https://www.nice.org.uk/guidance/ng35 (Accessed 8 February 2024)

Neelapu, S.S., Locke, F.L. Barlett, N.L., Lekakis, L.J., Miklos, D.B., Jacobson, C.A., Braunschweig, I., Oluwole, O.O., Siddiqi, T., Lin, Y., Timmerman, J.M., Stiff, P.J., Friedberg, J.W., Flinn, I.W., Goy, A., Hill, B.T., Smith, M.R., Deol, A., Farooq, U., McSweeney, P., Munoz, J., Avivi, I., Castro,

J.E., Westin, J.R., Chavez, J.C., Ghobadi, A., Komanduri, K.V., Levy, R., Jacobsen, E.D., Witzig, T.E., Reagen, P., Bot, A., Rossi, J., Navale, L., Jiang, Y., Aycock, J., Elias, M., Chang, D., Wiezorek, J. and Go, W.Y. (2017) 'Axicabtagene Ciloleucel CAR T-Cell Therapy in Refractory Large B-Cell Lymphoma', *The New England Journal of Medicine,* 377 (26): pp. 2531-2544. doi: 10.1056/NEJMoa1707447.

Noman, M.Z., Buart, S., Van Pelt, J., Richon, C., Hasmim, M., Leleu, N., Suchorska, W.M., Jalil, A., Lecluse, Y., El Hage, F., Giuliani, M., Pichon, C., Azzarone, B., Mazure, N., Romero, P., Mami-Chouaib, F. and Chouaib, S. (2009) 'The cooperative induction of hypoxia-inducible-factor-1 alpha and STAT3 during hypoxia induced an impairment of tumor susceptibility to CTL-mediated cell lysis', *The Journal of Immunology,* 182 (6): pp. 3510-3521. doi: 10.4049/jimmunol.0800854.

Oh, Y.M., Park, H.B., Shin, J.H., Lee, J.E., Park, H.Y., Kho, D.H., Lee, J.S., Choi, H., Okuda, T., Kokame, K., Miyata, T., Kim, I-H., Lee, S.H., Schwartz, R.H. and Choi, K. (2015) 'Ndrg1 is a T-cell clonal anergy factor negatively regulated by CD28 costimulation and interleukin-2', *Nature Communications,* 6: pp. 8698. doi: 10.1038/ncomms9698.

Ohta, A., Madasu, M., Subramanian, M., Kini, R., Jones, G., Choukèr, A., Ohta, A. and Sitkovsky, M. (2014) 'Hypoxia-induced and A2A adenosine receptor-independent T-cell suppression is short lived and easily reversible', *International Immunology,* 26 (2): pp. 83-91. doi: 10.1093/intimm/dxt045.

Ortiz-Prado, E., Dunn, J.F., Vasconez, J., Castillo, D. and Viscor, G. (2019) 'Partial pressure of oxygen in the human body: a general review', *American Journal of Blood Research,* 9 (1): pp. 1-14. Available at: https://www.ncbi.nlm.nih.gov/pmc/articles/PMC6420699/ (Accessed 22 April 2024)

Ortmann, B., Druker, J. and Rocha, S. (2014) 'Cell cycle progression in response to oxygen levels', *Cellular and Molecular Life Sciences,* 71 (18): pp. 3569-3582. doi: 10.1007/s00018-014-1645-9.

Pajak, B., Siwiak, E., Soltyka, M., Priebe, A., Zielinski, R., Fokt, I., Ziemniak, M., Jaskiewicz, A., Borowski, R., Domoradzki, T. and Priebe, W. (2020) '2-Deoxy-D-Glucose and Its Analogs: From Diagnostic to Therapeutic Agents', *International Journal of Molecular Sciences,* 21 (1): pp. 234. doi: 10.3390/ijms.21010234.

Palacios, E.H. and Weiss, A. (2004) 'Function of the Src-family kinases, Lck and Fyn, in T-cell development and activation', *Oncogene,* 23 (48): pp. 7990-8000. doi: 10.1038/sj.onc.1208074.

Palazon, A., Tyrakis, P.A., Macias, D., Veliça, P., Rundqvist, H., Fitzpatrick, S., Vojnovic, N., Phan, A.T., Loman, N., Hedenfalk, I., Hatschek, T., Lövrot, J., Foukakis, T., Goldrath, A.W., Bergh, J. and Johnson, R.S. (2017) 'An HIF-1α/VEGF-A Axis in Cytotoxic T Cells Regulates Tumor Progression', *Cancer Cell,* 32 (5): pp. 669-683.e5. doi: 10.1016/j.ccell.2017.10.003.

Papandreou, I., Cairns, R.A., Fontana, L., Lim, A.I. and Denko, N.C. (2006) 'HIF-1 mediates adaptation to hypoxia by actively downregulating mitochondrial oxygen consumption', *Cell Metabolism,* 3 (3): pp. 187-197. doi: 10.1016/j.cmet.2006.01.012.

Park, Y-J., Yoo, S-A., Kim, M. and Kim, W-U. (2020) 'The Role of Calcium-Calcineurin-NFAT Signaling Pathway in Health and Autoimmune Diseases', *Frontiers in Immunology,* 11: pp. 195. doi: 10.3389/fimmu.2020.00195.

Parzych, K.R. and Klionsky, D.J. (2014) 'An overview of autophagy: morphology, mechanism, and regulation', *Antioxidants and Redox Signaling,* 20 (3): pp. 460-473. doi: 10.1089/ars.2013.5371.

Paul, S. and Schaefer, B.C. (2013) 'A new look at T cell receptor signaling to nuclear factor-κB', *Trends in Immunology,* 34 (6): pp. 269-281. doi: 10.1016/j.it.2013.02.002.

Peng, Y., Tao, Y., Zhang, Y., Wang, J., Yang, J. and Wang, Y. (2023) 'CD25: A potential tumor therapeutic target', *International Journal of Cancer,* 152 (7): pp. 1290-1303. doi: 10.1002/ijc.34281.

Penna, A., Demuro, A., Yeromin, A.V., Zhang, S.L., Safrina, O., Parker, I. and Cahalan, M.D. (2008) 'The CRAC channel consists of a tetramer formed by Stim-induced dimerization of Orai dimers', *Nature,* 456 (7218): pp. 116-120. doi: 10.1038/nature07338.

Pescador, N., Cuevas, Y., Naranjo, S., Alcaide, M., Villar, D., Landázuri, M.O. and Peso, L.D. (2005) 'Identification of a functional hypoxia-responsive element that regulates the expression of the egl nine homologue 3 (egln3/phd3) gene', *Biochemical Journal,* 390 (Part 1): pp. 189-197. doi: 10.1042/BJ20042121.

Poyton, R.O., Ball, K.A. and Castello, P.R. (2009) 'Mitochondrial generation of free radicals and hypoxic signaling', *Trends in Endocrinology and Metabolism,* 20 (7): pp. 332-340. doi: 10.1016/j.tem.2009.04.001.

Pratt, G., Goodyear, O. and Moss, P. (2007) 'Immunodeficiency and immunotherapy in multiple myeloma', *British Journal of Haematology,* 138 (5): pp. 563-579. doi: 10.1111/j.1365-2141.2007.06705.x.

Prokhnevska, N., Cardenas, M.A., Valanparambil, R.M., Sobierajska, E., Barwick, B.G., Jansen, C., Moon, A.R., Gregorova, P., del Balzo, L., Greenwald, R., Bilen, M.A., Alemozaffar, M., Joshi, S., Cimmino, C., Larsen, C., Master, V., Sanda, M. and Kissick, H. (2023) 'CD8$^+$ T cell activation in cancer comprises an initial activation phase in lymph nodes followed by effector differentiation within the tumor', *Immunity,* 56 (1): pp. 107-124.e5. doi: 10.1016/j.immuni.2022.12.002.

Rajkumar, S.V. (2022) 'Multiple myeloma: 2022 update on diagnosis, risk stratification, and management', *American Journal of Hematology,* 97 (8): pp. 1086-1107. doi: 10.1002/ajh.26590.

Raleigh, J.A. and Koch, C.J. (1990) 'Importance of thiols in the reductive binding of 2-nitroimidazoles to macromolecules', *Biochemical Pharmacology,* 40 (11): pp. 2457-2464. doi: 10.1016/0006-2952(90)90086-z.

Raskov, H., Orhan, A., Christensen, J.P., Gögenur, I. (2021) 'Cytotoxic CD8$^+$ T cells in cancer and cancer immunotherapy', *British Journal of Cancer,* 124 (2): pp. 359-367. doi: 10.1038/s41416-020-01048-4.

Ravi, P., Kumar, S.K., Cerhan, J.R., Maurer, M.J., Dingli, D., Ansell, S.M. and Rajkumar, S.V. (2018) 'Defining cure in multiple myeloma: a comparative study of outcomes of young individuals with myeloma and curable hematologic malignancies', *Blood Cancer Journal,* 8 (3): pp. 26. doi: 10.1038/s41408-018-0065-8.

Reddy, M., Eirikis, E., Davis, C., Davis, H.M. and Prabhakar, U. (2004) 'Comparative analysis of lymphocyte activation marker expression and cytokine secretion profile in stimulated human peripheral blood mononuclear cell cultures: an in vitro model to monitor cellular immune function', *Journal of Immunological Methods,* 293 (1-2): pp. 127-142. doi: 10.1016/j.jim.2004.07.006.

Riha, P. and Rudd, C.E. (2010) 'CD28 co-signaling in the adaptive immune response', *Self/Nonself,* 1 (3): pp. 231-240. doi: 10.4161/self.1.3.12968.

Rivera, G.O.R., Knochelmann, H.M., Dwyer, C.J., Smith, A.S., Wyatt, M.M., Rivera-Reyes, A.M., Thaxton, J.E. and Paulos, C.M. (2021) 'Fundamentals of T Cell Metabolism and Strategies to

Enhance Cancer Immunotherapy', *Frontiers in Immunology,* 12: pp. 645242. doi: 10.3389/fimmu.2021.645242.

Robbins, J.R., Lee, S.M., Filipovich, A.H., Szigligeti, P., Neumeier, L., Petrovic, M. and Conforti, L. (2005) 'Hypoxia modulates early events in T cell receptor-mediated activation in human T lymphocytes via Kv1.3 channels', *The Journal of Physiology,* 564 (Part 1): pp. 131-143. doi: 10.1113/jphysiol.2004.081893.

Rocca, Y.D., Fonticoli, L., Rajan, T.S., Trubiani, O., Caputi, S., Diomede, F., Pizzicannella, J. and Marconi, G.D. (2022) 'Hypoxia: molecular pathophysiological mechanisms in human diseases', *Journal of Physiology and Biochemistry,* 78 (4): pp. 739-752. doi: 10.1007/s13105-022-00912-6.

Rosenblatt, J., Glotzbecker, B., Mills, H., Vasir, B., Tzachanis, D., Levine, J.D., Joyce, R.M., Wellenstein, K., Keefe, W., Schickler, M., Rotem-Yehudar, R., Kufe, D. and Avigan, D. (2011) 'PD-1 blockade by CT-011, anti PD-1 antibody, enhances ex-vivo T cell responses to autologous dendritic/myeloma fusion vaccine', *Journal of Immunotherapy,* 34 (5): pp. 409-418. doi: 10.1097/CJI.0b013e31821ca6ce.

Ross, S.H., Rollings, C.M. and Cantrell, D.A. (2021) 'Quantitative Analyses Reveal How Hypoxia Reconfigures the Proteome of Primary Cytotoxic T Lymphocytes', *Frontiers in Immunology,* 12: pp. 712402. doi. 10.3389/fimmu.2021.712402.

Rostamian, H., Khakpoor-Koosheh, M., Jafarzadeh, L., Masoumi, E., Fallah-Mehrjardi, K., Tavassolifar, M.J., Pawelek, J.M., Mirzaei, H.R. and Hadjati, J. (2022) 'Restricting tumor lactic acid metabolism using dichloroacetate improves T cell functions', *BMC Cancer,* 22 (1): pp. 39. doi: 10.1186/s12885-021-09151-2.

Saito, S., Furuno, A., Sakaurai, J., Park, H-R., Shin-ya, K. and Tomida, A. (2012) 'Compound C prevents the unfolded protein response during glucose deprivation through a mechanism independent of AMPK and BMP signaling', *PLoS One,* 7 (9): pp. e45845. doi: 10.1371/journal.pone.0045845.

Salerno, F., Paolini, N.A., Stark, R., von Lindern, M. and Wolkers, M.C. (2017) 'Distinct PKC-mediated posttranscriptional events set cytokine production kinetics in $CD8^+$ T cells', *Proceedings of the National Academy of Sciences of the United States of America,* 114 (36): pp. 9677-9682. doi: 10.1073/pnas.1704227114.

Sallusto, F., Lenig, D., Forster, R., Lipp, M. and Lanzavecchia, A. (1999) 'Two subsets of memory T lymphocytes with distinct homing potentials and effector functions', *Nature,* 401 (6574): pp. 708-712. doi: 10.1038/44385.

Sallusto, F., Geginat, J. and Lanzavecchia, A. (2004) 'Central memory and effector memory T cell subsets: function, generation, and maintenance', *Annual Review of Immunology,* 22: pp. 745-763. doi: 10.1146/annurev.immunol.22.012703.104702.

Samakai, E., Go, C. and Soboloff, J. (2018) 'Chapter 10: Defining the Roles of Ca2+ Signals during T Cell Activation', in Signaling Mechanisms Regulating T Cell Diversity and Function. Boca Raton (FL): CRC Press/Taylor & Francis. Available at: https://www.ncbi.nlm.nih.gov/books/NBK532321/ (Accessed: 7 February 2024)

Sanchez, L., Wang, Y., Siegel, D.S. and Wang, M.L. (2016) 'Daratumumab: a first-in-class CD38 monoclonal antibody for the treatment of multiple myeloma', *Journal of Hematology and Oncology,* 9 (1): pp. 51. doi: 10.1186/s13045-016-0283-0.

Saragovi, A., Abramovich, I., Omar, I., Arbib, E., Toker, O., Gottlieb, E. and Berger, M. (2020) 'Systemic hypoxia inhibits T cell response by limiting mitobiogenesis via matrix substrate-level phosphorylation arrest', *ELife,* 23 (9): pp. e56612. doi: 10.7554/eLife.56612.

Sawabe, T., Horiuchi, T., Nakamura, M., Tsukamoto, H., Nakahara, K., Harashima, S.I., Tsuchiya, T. and Nakano, S. (2001) 'Defect of lck in a patient with common variable immunodeficiency', *International Journal of Molecular Medicine,* 7 (6): pp. 609-614. doi: 10.3892/ijmm.7.6.609.

Scharping, N.E., Rivadeneira, D.B., Menk, A.V., Vignali, P.D.A., Ford, B.R., Rittenhouse, N.L., Peralta, R., Wang, Y., DePeaux, K., Poholek, A.C. and Delgoffe, G.M. (2021) 'Mitochondrial stress induced by continuous stimulation under hypoxia rapidly drives T cell exhaustion', *Nature Immunology,* 22 (2): pp. 205-215. doi: 10.1038/s41590-020-00834-9.

Schnell, A., Bod, L., Madi, A. and Kuchroo, V.K. (2020) 'The yin and yang of co-inhibitory receptors: toward anti-tumor immunity without autoimmunity', *Cell Research,* 30 (4): pp. 285-299. doi: 10.1038/s41422-020-0277-x.

Semenza, G.L., Jiang, B.H., Leung, S.W., Passantino, R., Concordet, J.P., Marie, P. and Giallongo, A. (1996) 'Hypoxia response elements in the aldolase A, enolase 1, and lactate dehydrogenase A

gene promotes contain essential binding sites for hypoxia-inducible factor 1', *Journal of Biological Chemistry,* 271 (51): pp. 32529-32537. doi: 10.1074/jbc.271.51.32529.

Semenza, G.L. (2010) 'Defining the role of hypoxia-inducible factor 1 in cancer biology and therapeutics', *Oncogene,* 29 (5): pp. 625-634. doi: 10.1038/onc.2009.441.

Sena, L.A., Li, S., Jairaman, A., Prakriya, M., Ezponda, T., Hildeman, D.A., Wang, C-R., Schumacker, P.T., Licht, J.D., Perlman, H., Bryce, P.J. and Chandel, N.S. (2013) 'Mitochondria are required for antigen-specific T cell activation through reactive oxygen species signaling', *Immunity,* 38 (2): pp. 225-236. doi: 10.1016/j.immuni.2012.10.020.

Setoguchi, R., Matsui, Y. and Mouri, K. (2015) 'mTOR signaling promotes a robust and continuous production of IFN-γ by human memory CD8+ T cells and their proliferation', *European Journal of Immunology,* 45 (3): pp. 893-902. doi: 10.1002/eji.201445086.

Shah, U.A. and Smith, E.L. (2019) 'Multiple Myeloma, Targeting B-Cell Maturation Antigen with Chimeric Antigen Receptor T-Cells', *Cancer,* 25 (3): pp. 208-216. doi: 10.1097/PPO.0000000000000379.

Shah, U.A. and Mailankody, S. (2020) 'Emerging immunotherapies in multiple myeloma', *BMJ,* 370: m3176. doi: 10.1136/bmj.m3176.

Shah, K., Al-Haidari, A., Sun, J. and Kazi, J.U. (2021) 'T cell receptor (TCR) signalling in health and disease', *Signal Transduction and Targeted Therapy,* 6 (412): pp. 1-26. doi: 10.1038/s41392-021-00823-w.

Shaw, R.J., Kosmatka, M., Bardeesy, N., Hurley, R.L., Witters, L.A., DePinho, R.A. and Cantley, L.C. (2004) 'The tumour suppressor LKB1 kinase directly activates AMP-activated kinase and regulates apoptosis in response to energy stress', *Proceedings of the National Academy of Sciences of the United States of America,* 101 (10): pp. 3329-3335. doi: 10.1073/pnas.0308061100.

Spencer, J.A., Ferraro, F., Roussakis, E., Klein, A., Wu, J., Runnels, J.M., Zaher, W., Mortensen, L.J., Alt, C., Turcotte, R., Yusuf, R., Côté, D., Vinogradov, S.A., Scadden, D.T. and Lin, C.P. (2014) 'Direct measurement of local oxygen concentration in the bone marrow of live animals', *Nature,* 508 (7495): pp. 269-273. doi: 10.1038/nature13034.

Sperandio, S., Fortin, J., Sasik, R., Robitaille, L., Corbeil, J. and de Belle, I. (2009) 'The transcription factor Egr1 regulates the HIF-1 alpha gene during hypoxia', *Molecular Carcinogenesis,* 48 (1): pp. 38-44. doi: 10.1002/mc.20454.

Stincone, A., Prigione, A., Cramer, T., Wamelink, M.M.C., Campbell, K., Cheung, E., Olin-Sandoval, V., Gruning, N-M., Krüger, A., Alam, M.T., Keller, M.A., Breitenbach, M., Brindle, K.M., Rabinowitz, J.D. and Ralser, M. (2015) 'The return of metabolism: biochemistry and physiology of the pentose phosphate pathway', *Biological Reviews Cambridge Philosophical Society,* 90 (3): pp. 927-963. doi: 10.1111/brv.12140.

Sullivan, D. (2019) 'The metabolic spectrum of memory T cells', *Immunology & Cell Biology,* 97 (7): pp. 636-646. doi: 10.1111/imcb.12274.

Sun, X. and Kaufman, P.D. (2018) 'Ki-67: more than a proliferation marker', *Chromosoma,* 127 (2): pp. 175-186. doi: 10.1007/s00412-018-0659-8.

Sun, Z. (2012) 'Intervention of PKC-θ as an immunosuppressive regimen', *Frontiers in Immunology,* 3: pp. 225. doi: 10.3389/fimmu.2012.00225.

Szigligeti, P., Neumeier, L., Duke, E., Chougnet, C., Takimoto, K., Lee, S.M., Filipovich, A.H. and Conforti, L. (2006) 'Signalling during hypoxia in human T lymphocytes – critical role of the src protein tyrosine kinase p56Lck in the O_2 sensitivity of Kv1.3 channels', *The Journal of Physiology,* 573 (Part 2): pp. 357-370. doi: 10.1113/jphysiol.2006.109967.

Tamura, H., Ishibashi, M., Sunakawa-Kil, M. and Inokuchi, K. (2020) 'PD-L1-PD-1 Pathway in the Pathophysiology of Multiple Myeloma', *Cancers (Basel),* 12 (4): pp. 924. doi: 10.3390/cancers12040924.

Tan, J., Chen, S., Huang, J., Chen, Y., Yang, L., Wang, C., Zhong, J., Lu, Y., Wang, L., Zhu, K. and Li, Y. (2018) 'Increased exhausted $CD8^+$ T cells with programmed death-1, T-cell immunoglobulin and mucin-domain-containing-3 phenotype in patients with multiple myeloma', *Asia-Pacific Journal of Clinical Oncology,* 14 (5): pp. e266-e274. doi: 10.1111/ajco.13033.

Thiel, M., Caldwell, C.C., Kreth, S., Kuboki, S., Chen, P., Smith, P., Ohta, A., Lentsch, A.B., Lukashev, D. and Sitkovsky, M.V. (2007) 'Targeted Deletion of HIF-1α Gene in T Cells Prevent their Inhibition in Hypoxic Inflamed Tissues and Improves Septic Mice Survival', *PLoS One,* 2 (9): pp. e853. doi: 10.1371/journal.pone.0000853.

Tian, Y., Babor, M., Lane, J., Schulten, V., Patil, V.S., Seumois, G., Rosales, S.L., Fu, Z., Picarda G., Burel, J., Zapardiel-Gonzaol, J., Tennekoon, R.N., De Silva, A.D., Premawansa, S., Premawansa, G., Wijewickrama, A., Greenbaum, J.A., Vijayanand, P., Weiskopf, D., Sette, A. and Peters, B. (2017) 'Unique phenotypes and clonal expansions of human CD4 effector memory T cells re-expressing CD45RA', *Nature Communications,* 8 (1): pp. 1473. doi: 10.1038/s41467-017-01728-5.

Topp, M.S., Duell, J., Zugmaier, G., Attal, M., Moreau, P., Langer, C., Krönke, J., Facon, T., Salnikov, A.V., Lesley, R., Beutner, K., Kalabus, J., Rasmussen, E., Riemann, K., Minella, A.C., Munzert, G. and Einsele, H. (2020) 'Anti-B-Cell-Maturation Antigen BiTE Molecule AMG 420 Induces Responses in Multiple Myeloma', *Journal of Clinical Oncology,* 38 (8): pp. 775-783. doi: 10.1200/JCO.19.02657.

Ullah, M.S., Davies, A.J. and Halestrap, A.P. (2006) 'The plasma membrane lactate transporter MCT4, but not MCT1, is up-regulated by hypoxia through a HIF-1 alpha-dependent mechanism', *Journal of Biological Chemistry,* 281 (14): pp. 9030-9037. doi: 10.1074/jbc.M511397200.

Van der Leun, A.M., Thommen, D.S. and Schumacher, T.N. (2020) '$CD8^+$ T cell states in human cancer: insights from single-cell analysis', *Nature Reviews Cancer,* 20 (4): pp. 218-232. doi: 10.1038/s41568-019-0235-4.

Vadysirisack, D.D. and Ellisen, L.W. (2012) 'mTOR activity under hypoxia', *Methods in Molecular Biology,* 821: pp. 45-58. doi: 10.1007/978-1-61779-430-8_4.

Veliça, P., Cunha, P.P., Vojnovic, N., Foskolou, I.P., Bargiela, D., Gojkovic, M., Rundqvist, H. and Johnson, R.S. (2021) 'Modified Hypoxia-Inducible Factor Expression in $CD8^+$ T Cells Increases Antitumor Efficacy', *Cancer Immunology Research,* 9 (4): pp. 401-414. doi: 10.1158/2326-6066.CIR-20-0561.

Vuilleyfroy de Silly, R., Ducimetiere, L., Maroun, C.Y., Dietrich, P-Y., Derouazi, M. and Walker, P.R. (2015) 'Phenotypic switch of $CD8^+$ T cells reactivated under hypoxia toward IL-10 secreting, poorly proliferative effector cells', *European Journal of Immunology,* 45 (8): pp. 2263-2275. doi: 10.1002/eji.201445284.

Wang, G.L. and Semenza, G.L. (1993) 'General involvement of hypoxia-inducible factor 1 in transcriptional responses to hypoxia', *Proceedings of the National Academy of Sciences of the United States of America,* 90 (9): pp. 4304-4308. doi: 10.1073/pnas.90.9.4304.

Wang, G.L., Jiang, B.H., Rue, E.A. and Semenza, G.L. (1995) 'Hypoxia-inducible factor 1 is a basic-helix-loop-helix-PAS heterodimer regulated by cellular O2 tension', *Proceedings of the National Academy of Sciences of the United States of America,* 92 (12): pp. 5510-5514. doi: 10.1073/pnas.92.12.5510.

Wang, R., Dillon, C.P., Shi, L.Z., Milasta, S., Carter, R., Finkelstein, D., McCormick, L.L., Fitzgerald, P., Chi, H., Munger, J. and Green, D.R. (2011) 'The transcription factor Myc controls metabolic reprogramming upon T lymphocyte activation', *Immunity,* 35 (6): pp. 871-882. doi: 10.1016/j.immuni.2011.09.021.

Wange, R.L. (2000) 'LAT, the linker for activation of T cells: a bridge between T-cell specific and general signaling pathways', *Science's Signal Transduction Knowledge Environment,* 2000 (63): re1. doi: 10.1126/stke.2000.63.re1.

Warburg, O. (1956) 'On respiratory impairment in cancer cells', *Science,* 124 (3215): pp. 269-270. Available at: https://pubmed.ncbi.nlm.nih.gov/13351639/ (Accessed 18 April 2024)

Wei, P., Kou, W., Riaz, F., Zhang, K., Fu, J. and Pan, F. (2023) 'Combination therapy of HIFα inhibitors and Treg depletion strengthen the anti-tumor immunity in mice', *European Journal of Immunology,* 53 (12): pp. e2250182. doi: 10.1002/eji.202250182.

Weidinger, C., Shaw, P.J. and Feske, S. (2013) 'STIM1 and STIM2-mediated Ca(2+) influx regulates antitumour immunity by CD8(+) T cells', *EMBO Molecular Medicine,* 5 (9): pp. 1311-1321. doi: 10.1002/emmm.201302989.

Weil, R. and Israël, A. (2006) 'Deciphering the pathway from the TCR to NF-kappa B', *Cell Death and Differentiation,* 13 (5): pp. 826-833. doi: 10.1038/sj.cdd.4401856.

Weiss, B.M., Abadie, J., Verma, P., Howard, R.S. and Kuehl, W.M. (2009) 'A monoclonal gammopathy precedes multiple myeloma in most patients', *Blood,* 113 (22): pp. 5418-5422. doi: 10.1182/blood-2008-12-195008.

Wheaton, W.W. and Chandel, N.S. (2011) 'Hypoxia. 2. Hypoxia regulates cellular metabolism', *American Journal of Physiology – Cell Physiology,* 300 (3): pp. C385-C393. doi: 10.1152/ajpcell.00485.2010.

Wherry, E.J. and Kurachi, M. (2015) 'Molecular and cellular insights into T cell exhaustion', *Nature Reviews Immunology,* 15 (8): pp. 486-499. doi: 10.1038/nri3862.

Wieczorek, M., Abualrous, E.T., Sticht, J., Álvaro-Benito, M., Stolzenberg, S., Noé, F. and Freund C. (2017) 'Major Histocomptability Complex (MHC) Class I and MHC Class II Proteins: Conformational Plasticity and Antigen Presentation', *Frontiers in Immunology,* 8: pp. 292. doi: 10.3389/fimmu.2017.00292.

Wickham, H., Chang, W., Henry, L., Pedersen, T.L., Takahashi, K., Wilke, C., Woo, K., Yutani, H. and Dunnington, D. (2016) 'ggplot2: Create Elegant Data Visualisations Using the Grammar of Graphics'. (R package version 3.3.5). [Computer programme]. Available at: https://CRAN.R-project.org/package=ggplot2.

Willinger, T., Freeman, T., Hasegawa, H., McMichael, A.J. and Callan, M.F.C. (2005) 'Molecular signatures distinguish human central memory from effector memory CD8 T cell subsets', *Journal of Immunology,* 175 (9): pp. 5895-5903. doi: 10.4049/jimmunol.175.9.5895.

Woods, A., Johnstone, S.R., Dickerson, K., Leiper, F.C., Fryer, L.G.D., Neumann, D., Schlattner, U., Wallimann, T., Carlson, M. and Carling, D. (2003) 'LKB1 is the upstream kinase in the AMP-activated protein kinase cascade', *Current Biology,* 13 (22): pp. 2004-2008. doi: 10.1016/j.cub.2003.10.031.

Woods, A., Dickerson, K., Heath, R., Hong, S-P., Momcilovic, M., Johnstone, S.R., Carlson, M. and Carling, D. (2005) 'Ca2+/calmodulin-dependent protein kinase kinase-beta acts upstream of AMP-activated protein kinase in mammalian cells', *Cell Metabolism,* 2 (1): pp. 21-33. doi: 10.1016/j.cmet.2005.06.005.

Xia, L., Oyang, L., Lin, J., Tan, S., Han, Y., Wu, N., Yi, P., Tang, L., Pan, Q., Rao, S., Liang, J., Tang, Y., Su, M., Luo, X., Yang, Y., Shi, Y., Wang, H., Zhou, Y. and Liao, Q. (2021) 'The cancer metabolic reprogramming and immune response', *Molecular Cancer,* 20 (28). doi: 10.1186/s12943-021-01316-8.

Xu, S., Chaudhary, O., Rodriguez-Morales, P., Sun, X., Chen, D., Zappasodi, R., Xu, Z., Pinto, A.F.M., Williams, A., Szhulze, I., Farsakoglu, Y., Varanasi, S.K., Low, J.S., Tang, W., Wang, H., McDonald, B., Tripple, V., Downes, M., Evans, R.M., Abumrad, N.A., Merghoub, T., Wolchok, J.D., Shokhirev, M.N., Ho, P-C., Witztum, J.L., Emu, B., Chi, G. and Kaech, S.M. (2021) 'Uptake of oxidized lipids by the scavenger receptor CD36 promotes lipid peroxidation and dysfunction in $CD8^+$ T cells in tumors', *Immunity,* 54 (7): pp. 1561-1577.e7. doi: 10.1016/j.immuni.2021.05.003.

Yadav, M., Green, C., Ma, C., Robert, A., Glibicky, A., Nakamura, R., Sumiyoshi, T., Meng, R., Chu, Y-W., Wu, J., Byon, J., Woodard, J., Adamkewicz, J., Grogan, J. and Venstrom, J.M. (2016) 'Tigit, CD226 and PD-L1/PD-1 Are Highly Expressed By Marrow-Infiltrating T Cells in Patients with Multiple Myeloma', *Blood,* 128 (22): pp. 2102. doi: 10.1182/blood.V128.22.2102.2102.

Yang, K., Shrestha, S., Zeng, H., Karmaus, P.W.F., Neale, G., Vogel, P., Guertin, D.A., Lamb, R.F. and Chi, H. (2013) 'T cell exit from quiescence and differentiation into Th2 cells depend on Raptor-mTORC1-mediated metabolic reprogramming', *Immunity,* 39 (6): pp. 1043-1056. doi: 10.1016/j.immuni.2013.09.015.

Yoo, H.C., Yu, Y.C., Sung, Y. and Han, J.M. (2020) 'Glutamine reliance in cell metabolism', *Experimental and Molecular Medicine,* 52 (9): pp. 1496-1516. doi: 10.1038/s12276-020-00504-8.

Yoshii, S.R. and Mizushima, N. (2017) 'Monitoring and Measuring Autophagy', *International Journal of Molecular Sciences,* 18 (9): pp. 1865. doi: 10.3390/ijms18091865.

Yu, G., Wang, L-G., Han, Y. and He, Q-Y. (2012) 'clusterProfiler: an R package for comparing biological themes among gene clusters', *Omics: A Journal of Integrative Biology,* 16 (5): pp. 284-287. doi: 10.1089/omi.2011.0118.

Zenewicz, L.A. (2017) 'Oxygen Levels and Immunological Studies', *Frontiers in Immunology,* 8: pp. 324. doi: 10.3389/fimmu.2017.00324.

Zhang, J. and Ney, P.A. (2009) 'Role of BNIP3 and NIX in cell death, autophagy, and mitophagy', *Cell Death and Differentiation,* 16 (7): pp. 939-946. doi: 10.1038/cdd.2009.16.

Zhang, N. and Bevan, M.J. (2011) 'CD8(+) T cells: foot soldiers of the immune system', *Immunity,* 35 (2): pp. 161-168. doi: 10.1016/j.immuni.2011.07.010.

Zhang, N., Yin, R., Zhou, P., Liu, X., Fan, P., Qian, L., Dong, L., Zhang, C., Zheng, X., Deng, S., Kuai, J., Liu, Z., Jiang, W., Wang, X., Wu, D. and Huang, Y. (2021) 'DLL1 orchestrates CD8+ T cells to induce long-term vascular normalization and tumor regression', *Proceedings of the National Academy of Sciences of the United States of America,* 118 (22): pp. e2020057118. doi: 10.1073/pnas.2020057118.

Zhang, P., Tchou-Wong, K-M. and Costa, M. (2007) 'Egr-1 mediates hypoxia-inducible transcription of the NDRG1 gene through an overlapping Egr-1/Sp1 binding site in the promoter', *Cancer Research,* 67 (19): pp. 9125-9133. doi: 10.1158/0008-5472.CAN-07-1525.

Zhang, Y., Kurupati, R., Liu, L., Zhou, X.Y., Zhang, G., Hudaihed, A., Filisio, F., Giles-Davis, W., Xu, X., Karakousis, G.C., Schuchter, L.M., Xu, W., Amaravadi, R., Xiao, M., Sadek, N., Krepler, C., Herlyn, M., Freeman, G.J., Rabinowitz, J.D. and Ertl, H.C.J. (2017) 'Enhancing $CD8^+$ T cell fatty acid catabolism within a metabolically challenging tumor microenvironment increases the efficacy of melanoma immunotherapy', *Cancer Cell,* 32 (3): pp. 377-391.e9. doi: 10.1016/j.ccell.2017.08.004.

Zhao, Y., Niu, C. and Cui, J. (2018) 'Gamma-delta ($\gamma\delta$) T cells: friend or foe in cancer development?', *Journal of Translational Medicine,* 16 (3). doi: 10.1186/s12967-017-1378-2.

Zhong, X-P., Guo, R., Zhou, H., Liu, C. and Wan, C-K. (2008) 'Diacylglycerol kinases in immune cell function and self-tolerance', *Immunological Reviews,* 224: pp. 249-264. doi: 10.1111/j.1600-065X.2008.00647.x.

Zhou, H., Wertz, I., O'Rourke, K., Ultsch, M., Seshagiri, S., Eby, M., Xiao, W. and Dixit, V.M. (2004) 'Bcl10 activates the NF-kappa B pathway through ubiquitination of NEMO', *Nature,* 427 (6970): pp. 167-171. doi: 10.1038/nature02273.

Zhu, Y.X., Braggio, E., Shi, C-X., Bruins, L.A., Schmidt, J.E., Van Wier, S., Chang, X-B., Bjorklund, C.C., Fonseca, R., Bergsagel, P.L., Orlowski, R.Z. and Stewart, A.K. (2011) 'Cereblon expression is required for the antimyeloma activity of lenalidomide and pomalidomide', *Blood,* 118 (18): pp. 4771-4779. doi: 10.1182/blood-2011-05-356063.

Zhu, Y.X., Kortuem, K.M. and Stewart, A.K. (2013) 'Molecular mechanism of action of immune-modulatory drugs thalidomide, lenalidomide and pomalidomide in multiple myeloma', *Leukemia and Lymphoma,* 54 (4): pp. 683-687. doi: 10.3109/10428194.2012.728597.

Zoncu, R., Efeyan, A. and Sabatini, D.M. (2011) ‘mTOR: from growth signal integration to cancer, diabetes and ageing’, *Nature Reviews Molecular Cell Biology,* 12 (1): pp. 21-35. doi: 10.1038/nrm3025.

Zumerle, S., Molon, B. and Viola, A. (2017) ‘Membrane Rafts in T Cell Activation: A Spotlight on CD28 Costimulation’, *Frontiers in Immunology,* 8: pp. 1467. doi: 10.3389/fimmu.2017.01467.

Supplementary 1: Table of individual MM patient information.

Background	**Sex**	**Age at time of sample** (years)	**Marrow trephine** (% PCs)	**Marrow aspirate (flow)** (% PCs)	**Marrow aspirate (morphology)** (% PCs)	**PP**	**PP type**	**FLC kappa**	**FLC lambda**	**FLC ratio**	**IgG**	**IgA**	**IgM**
New diagnosis myeloma	M	72	50	18	45	57	GK	2216.86	7.62	290.93	75.33	0.29	0.21
New diagnosis myeloma, also myelodysplasia	M	74	45	3	10	16.8	AK	94.65	21.26	4.45	8.64	20.57	0.22
New diagnosis myeloma	F	86	60	24	50	74.2	GK	15903.5	3.37	4719.14	69.22	0.23	0.07
New diagnosis myeloma	M	72	60	13	42	33.7	AK	4848.02	621.54	7.8	5.9	16.42	0.4
New diagnosis myeloma	M	81	50	10	14	None	K LC	1158.43	3.43	337.73	5.23	0.4	0.24
Diagnosis myeloma, previous MGUS	F	67	70	2.7	Inadequate sample	41.7	GK	164.17	8.47	19.38	51.24	0.18	0.2
New diagnosis myeloma	F	79	75	9.1	36	34.5	AL	11.34	249.14	0.05	6.69	35.71	0.33
New diagnosis myeloma	M	74	80	12.9	53	55.1	AK	595.97	2.47	241.28	2.44	38.48	0.11